OAR 69-0003
AD 686 100

Volume I

proceedings of the 1968 AIR FORCE SCIENCE & ENGINEERING SYMPOSIUM

AIR FORCE ACADEMY ★ 30-31 October • 1 November 1968

Office of Aerospace Research ★ Air Force Systems Command

PREFACE

The purpose of the Symposium was to review the science and engineering activities of the Air Force, and to reflect representative achievements in science, engineering and technical management. A concomitant aim was to provide a balanced program of maximum interest. Toward this end, the Program Committee selected papers which ran the full gamut of Air Force scientific effort.

The papers included here have four specific objectives:

a. To stimulate the involvement of scientific and engineering talent within the Air Force.

b. To demonstrate Air Force competence in research, development, and evaluation.

c. To provide a forum wherein Air Force personnel can demonstrate the full scope and depth of their current projects.

d. To promote the interchange of ideas among members of the Air Force science and engineering community.

In addition to these specific objectives, the Symposium was held to emphasize particularly the overall in-house capabilities of OAR and AFSC, and to illustrate the effectiveness of the Air Force laboratories.

TABLE OF CONTENTS

VOLUME I

SYMPOSIUM PAPERS

THE PRODUCTION OF RESTRICTED CHEMICAL LESIONS IN THE CNS BY CHEMICAL MEANS

By

Donald F. Buxton

Captain, USAF

6571st Aeromedical Research Laboratory

Aerospace Medical Division

Air Force Systems Command

Holloman Air Force Base, New Mexico

ABSTRACT

The need for a new technique of destroying nerve cells of the central nervous system is presented. The technique must kill the nerve cells in an area and leave intact the processes of remotely situated nerve cells which pass through the area. The ions of arsenical compounds are electrophoretically injected into the area to block the oxidative metabolism of the nerve cells and thus kill the cells. Both anatomical and physiological testing procedures are described to confirm the action of the chemical. The significance and potential importance of this technique for the military command, as well as for basic scientists, is discussed.

BIOGRAPHY

Donald Frederick Buxton was born in 1939 in Mansfield, Ohio. After graduation in 1957 from Murray High School, Murray, Kentucky, and after completion in 1959 of a pre-veterinary medicine curriculum at Murray State College, Murray, Kentucky, he entered the School of Veterinary Medicine at Auburn University, Auburn, Alabama, from which he received his Doctor of Veterinary Medicine degree in 1963. In September 1963 he entered the Department of Anatomical Sciences, College of Medicine, University of Florida, Gainesville, Florida as a graduate student and received the Doctor of Philosophy degree in Medical Sciences in 1966. He entered upon active duty as a first lieutenant in the USAF at the 6571st Aeromedical Research Laboratory, Holloman AFB, New Mexico, in October 1966. In April 1967 he was promoted to the temporary rank of captain. Dr. Buxton served as a neuroanatomist while stationed at Holloman and in June 1968 received an award certificate for scientific achievement based on his research conducted in that capacity.

Dr. Buxton is currently an Instructor in the Department of Anatomy, University of Arkansas Medical Center, Little Rock, Arkansas, and a member of the USAF inactive reserves.

THE PRODUCTION OF RESTRICTED CHEMICAL LESIONS IN THE CNS BY CHEMICAL MEANS

Donald F. Buxton, Captain, USAF
6571st Aeromedical Research Laboratory
Holloman Air Force Base, New Mexico 88330

The central nervous system, which includes the brain and spinal cord, performs and controls mental processes, both conscious and subconscious, physiological rhythms (such as the sleep-wakefulness cycle, hunger, thirst and other physiological drives), and motor activity. Thus, the central nervous system controls the total behavior of an individual. In order to understand and ultimately to be able to logically manipulate behavior, we must possess the knowledge of which brain cells control any individual portion of the total behavior. Psychologists and psychiatrists have made much progress in learning to control the mental process through the aid of environmental manipulation, treatment with drugs, and other means, although the physiological and anatomical bases for mental processes are not really understood. However, much more rapid progress could be made for the control of mental processes if these bases were known. Physiologists and anatomists have determined which brain cell groups control some physiological rhythms, including hunger, thirst and temperature regulation. However, the exact location of the brain cells controlling many other physiological rhythms, including the sleep-wakefulness cycle, respiration and cardiac rhythm, have eluded detection. Previous experimentation has somewhat localized the cells controlling these activities to the brain stem reticular formation, but their exact location is unknown.

Now let us quickly review some dynamic anatomy of brain cells, called neurons.

LIGHTS OFF - SLIDE 1

In this slide we see two neurons and a muscle. When neuron B is excited, an impulse will travel down the axon to the muscle and excite the muscle, thus causing a muscular contraction. Thousands or hundreds of thousands of these axons may be banded together outside the skull or vertebral column and called a nerve. Similarly, when the cell body of neuron A is excited an impulse will pass along its axon to neuron B and excite B.

SLIDE 2

Two general types of organization of these neurons are present in the central nervous system. In the phylogenetically newer portions of the nervous system, we have neurons grouped together in a cluster called a nucleus and the axons are emitted in a bundle called a nerve tract (outside the central nervous system it would be a nerve). The physiological actions resulting from manipulation of the brain nuclei are fairly well understood because the cell bodies are accessible and somewhat isolated from the neural tracts or axons. If we stimulate the cells of a nucleus or if we destroy the cells of a nucleus, we can feel fairly sure that the physiological effects which result are due to manipulation of the particular cell bodies of that nucleus and <u>not</u> due to the stimulation or destruction of axons which arise from neurons which do not belong to that nucleus.

On the other hand, the other portion of this slide depicts an alternative organization which also exists in the central nervous system. Here the cells are not grouped into definitive nuclei which orderly emit their axons but rather are in a loose knit organization in which the neurons are separated from each other by axons which have as their origin remotely placed neurons. This organization is more prominent in the phylogenetically older portion of the central nervous system which includes the brain stem reticular formation. If an electrode is placed in this type of organization and either stimulation or destruction by presently available technological methods is accomplished, the physiological effect from this area cannot be solely attributed to the neurons of that area because the transient axons arising from cell bodies in other areas would also be stimulated or destroyed. My research has thus centered about the development of a technique to kill the nerve cells in such a neural organization but leave the transient axons intact both physiologically and anatomically. With such a technique the relatively unexplored areas of reticular formation, and other brain areas, could be studied in exact detail to determine which cells control which physiological and mental activities.

In order to kill only the neurons in such an organization, a number of pitfalls must be avoided.

SLIDE 3

1. Destruction techniques presently available involve the indiscriminate coagulation of proteins either by thermal or electrical means. Since the cell walls of both axons and nerve cell bodies contain protein, this approach is certainly to be avoided.

339-803 O - 69 - 2

2. Any physical object such as an electrode or a cannula placed in the neural organization will cause some destruction of axons and neurons; thus, any object placed in the area must have as small an outside diameter as possible.

3. The pressure and volume of any liquid physically injected through a cannula will destroy axons and nerve cells, so if possible the volume of injected material should be kept minimal.

4. Any injected substance must not destroy the cells of the capillary walls or else blood will escape from these vessels into the area and act the same as an injected volume of fluid.

5. Sterility must be preserved.

LIGHTS ON

Neurons are vulnerable to anoxia; within minutes of oxygen depletion a neuron will die. Most of the metabolic processes utilizing oxygen for neuron viability occur in the cell body of the neuron in structures called mitochondria. Some mitochondria are found in axons, but relatively few compared to the number in the cell body. Consequently, if a chemical which would block the oxidative enzymes and which would be absorbed rather selectively by neurons could be introduced into the area, the nerve cell body with its relatively large surface area should absorb most of the chemical as it diffused through the tissue. Although a sufficient oxygen gradient for life would still exist, with the oxidative enzymes blocked the oxygen could not be utilized and the nerve cell would die. Arsenic is an element which will block the oxidative enzymes. We have synthesized arsenical compounds which will be absorbed by the neurons but which will not destroy the capillaries. The compounds are salts or complexes with bromide or chloride ions, each of the latter carrying a negative charge. Thus, the arsenical compound has a positive charge. When the arsenical salt is dissolved in water, it dissociates into its positive and negative radicals.

LIGHTS OFF - SLIDE 4

The solution is then placed in a syringe which carries an electrode. A special thin wall glass cannula is attached to the syringe and filled to its tip. The syringe and cannula are stereotaxically introduced into the central nervous system so the tip of the cannula only barely enters the site to be destroyed. The electrode inside the syringe is connected to the positive pole of a variable direct current source; a ground electrode from the animal is attached to an ammeter which is attached to the

negative pole of the current source. Thus, the animal has a negative potential in respect to the solution inside the cannula and simple electrophoresis will deposit the ions of the arsenical compound into the central nervous system without injecting any appreciable volume of fluid and without causing any protein coagulation of the needle tip. Varying the strength of direct current will vary the flow rate of the chemical ions; by monitoring the time and amperage the exact amount of chemical injected can be calculated.

A number of procedures have been undertaken to determine the effectiveness of the drug.

1. On an anatomical basis, I have injected the drug into the brain, waited 5-7 days for the dead cells to be cleared away, sacrificed the animal, and taken sections through the destroyed area.

SLIDE 5

Here you see the small lesion produced by the electrode tip (arrow); beneath the lesion is a clear area, whereas cells are stained in the surrounding area.

SLIDE 6

Upon enlargement you now see the clear area devoid of nerve cells but with an intact axonal background. On the edge of the clear area you see stained nerve cells which were not affected by the chemical.

SLIDE 7

2. On a physiological basis, I have stimulated neurons which send their axons through the destroyed area and recorded from cells distal to the lesion; thus, the axons traversing the area are physiologically intact. As you can see, stimulation of cell A excites cell B; cell B sends its axon through the lesion area and excites cell C. Recording from the axon of cell C, I can detect the same impulse before and after the lesion. Thus, the axon of cell B is physiologically and anatomically intact. In the same preparation, stimulation of cell D excites cell E before the destruction; cell E then exictes cell F and I record from its axon. After injection the potentials recorded from cell F when cell D is stimulated are absent, thus indicating the actual destruction of cell E.

LIGHTS ON

Further testing is planned which will include in vitro testing of the drug and eventually the biochemical confirmation of the exact locus of drug activity in the cell.

The significance of this technique is considerable. Although it would be of great use to basic scientists for determination of the physiological anatomy of many areas of the central nervous system, as indicated in the introduction, it has practical use for the military command. Upon the exact identification of the cells in the reticular system which control the sleep-wakefulness cycle and the cells involved in emotional attitudes, logical and orderly testing could proceed to determine chemical compounds which affect these cells to the benefit of the military. For example: A man is transported to the opposite side of the earth in 24 hours and must start performing a delicate job within hours of his arrival. His biological rhythm is 180° out of phase with his new environment and peak efficiency cannot be expected from him for up to at least two weeks. It is possible that future researchers could study the effects of various chemicals on the neurons identified as controlling the sleep-wakefulness cycle and thus could lead to the development of a drug which would facilitate the transition or even reverse his biological rhythm. By like means temporary control of the emotional attitudes of the manpower could certainly be of advantage to the military strategist or tactician. Further, if this technique could lead to the development of drugs which correct military-incurred mental disorders, the financial savings to the USAF could be considerable within itself.

The animals used in this study were handled in accordance with the "Guide for Laboratory Animal Facilities and Care" as promulgated by the National Academy of Sciences - National Research Council.

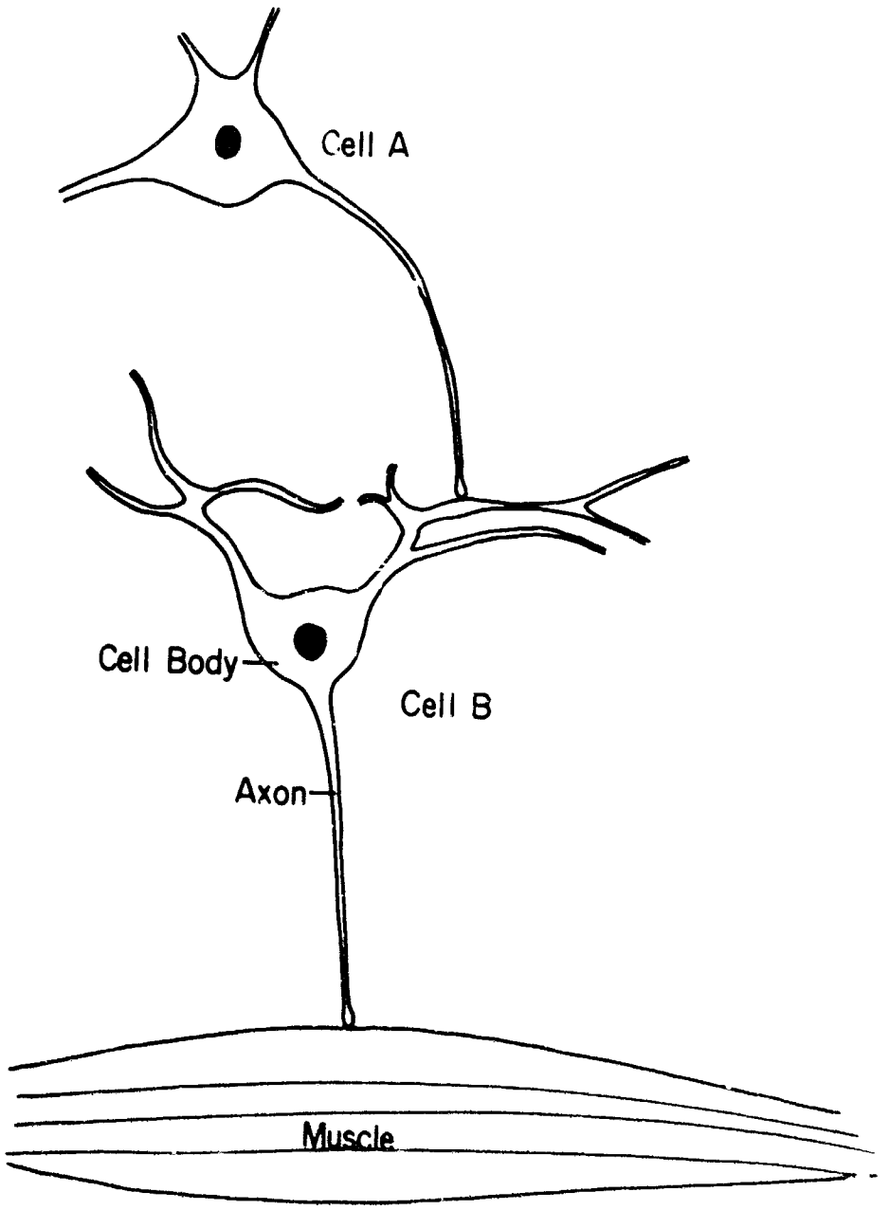

Slide 1

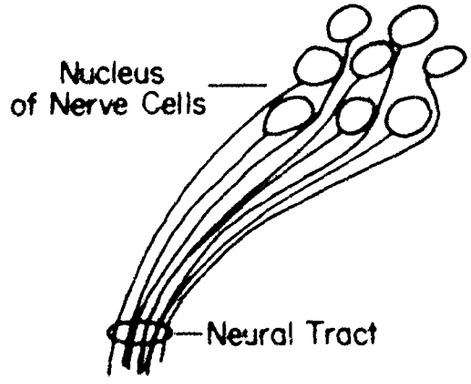

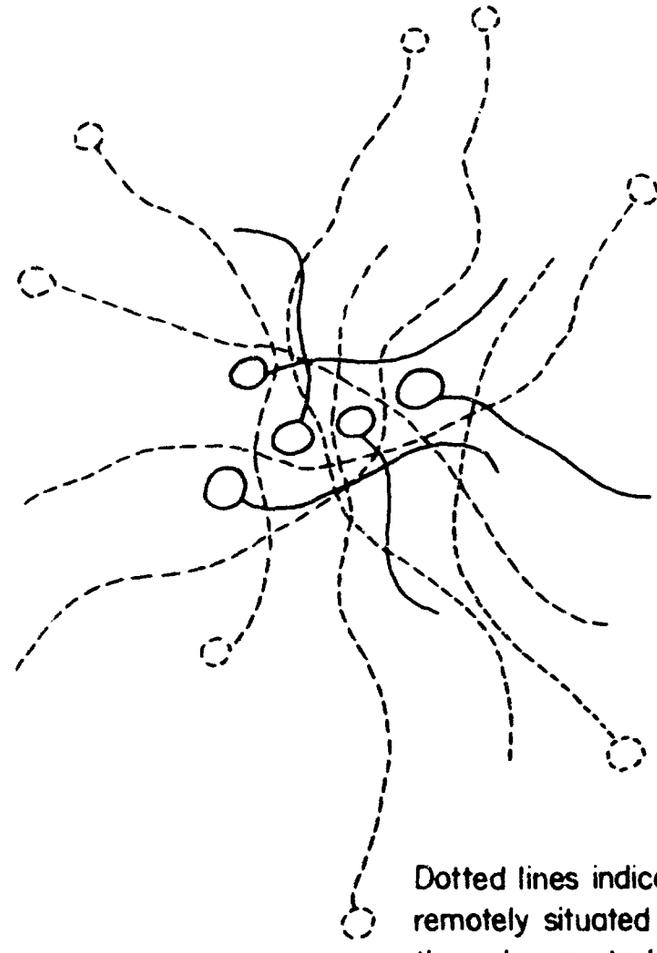

Dotted lines indicate axons from remotely situated neurons passing through area to be destroyed.

Slide 2

1. Avoid protein coagulation
2. Diameter of cannula small
3. Minimal pressure and volume of injected fluid
4. No destruction of capillary walls
5. Sterility maintainance

Slide 3

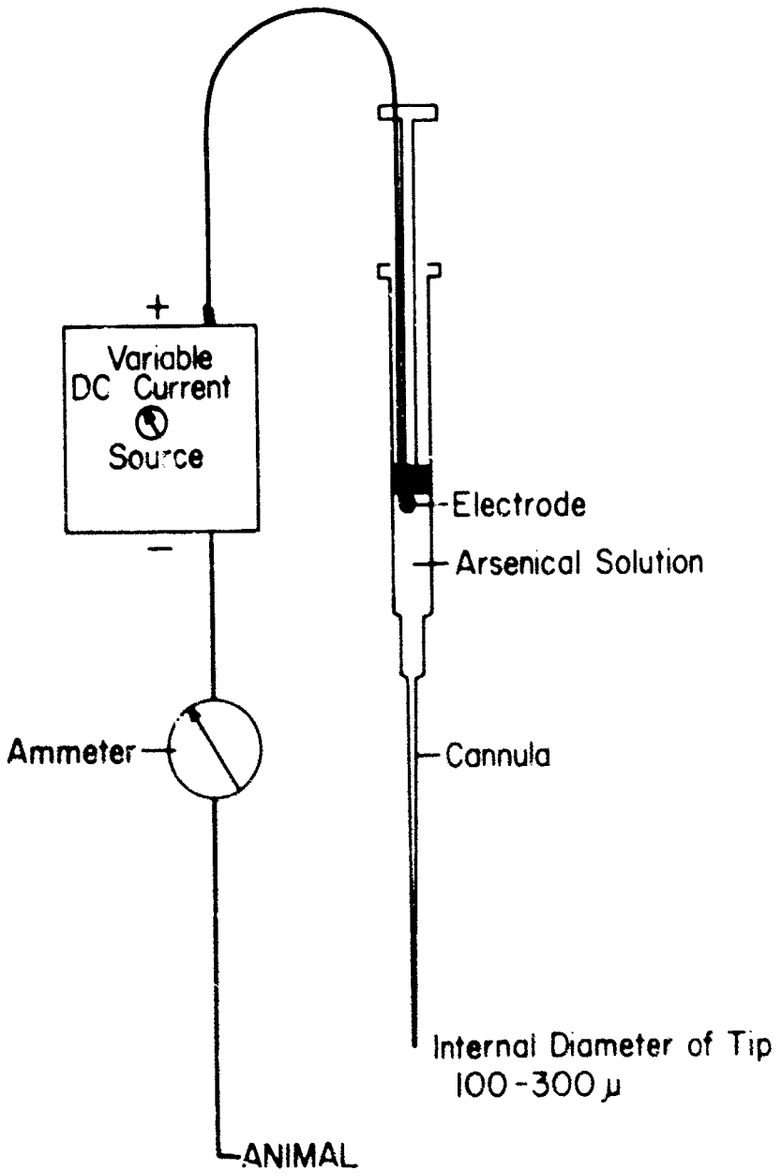

Slide 4

Slide 5

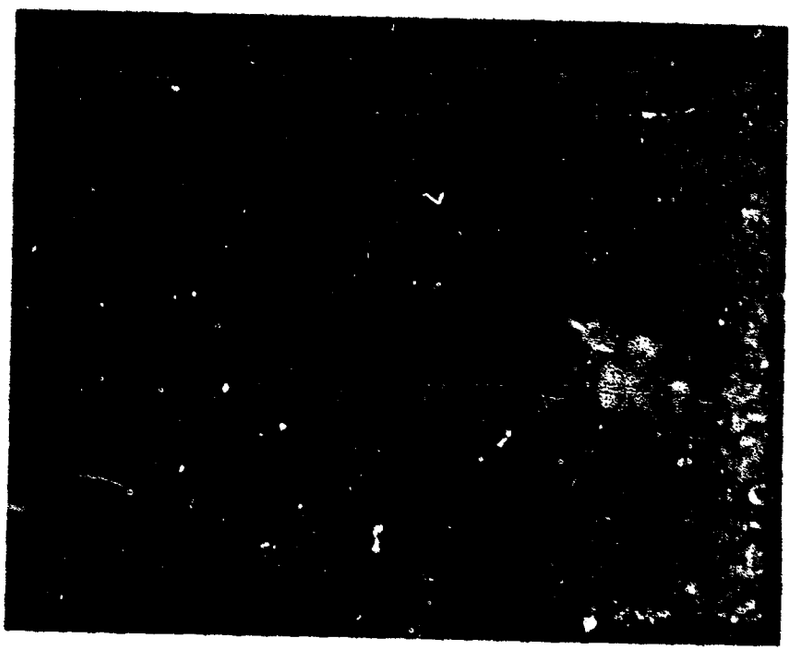

Slide 6

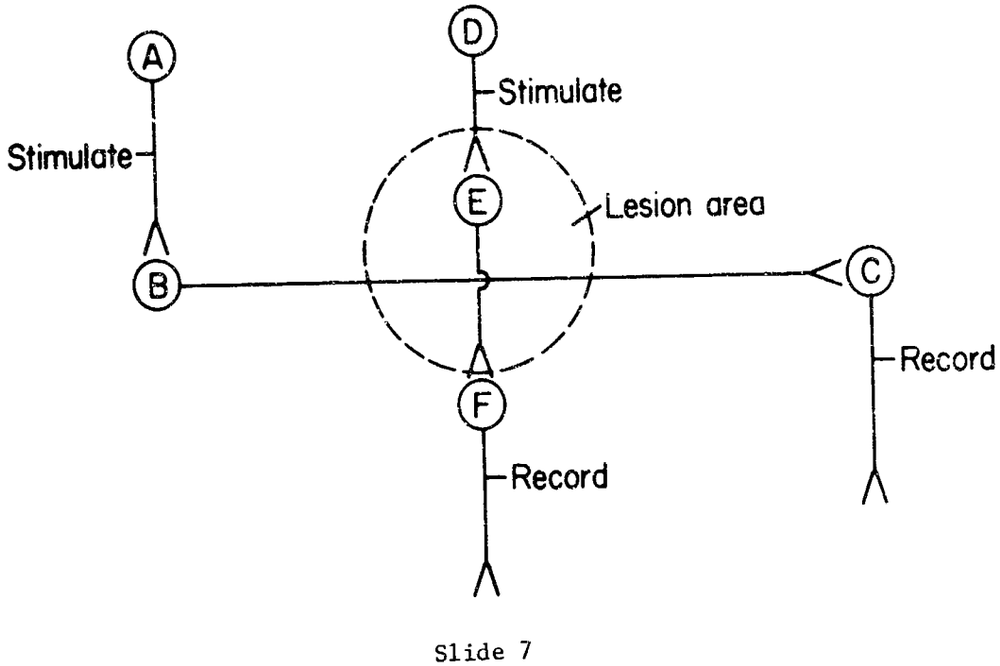

Slide 7

DEVELOPMENT OF HYPERBARIC OXYGEN THERAPY

FOR ALTITUDE DECOMPRESSION SICKNESS

By

Robert G. McIver
Lt Colonel, USAF, MC

Headquarters, Aerospace Medical Division
Air Force Systems Command
Brooks Air Force Base, Texas

ABSTRACT

In order to establish definitive treatment for altitude decompression sickness, experiments were conducted in anesthetized animals in search of an objective measurement of decompression sickness. Pulmonary hypertension and tachypnea in the face of bubble formation proved to be these objective measurements. Tests were conducted to show the treatment schedule of choice. After converting a research hyperbaric chamber to human use, the schedules were utilized successfully in 11 cases of refractory altitude decompression sickness. These schedules have become routine in the USAF and treatment capability has been extended to 5 USAF bases. This capability has also allowed extensive space flight decompression sickness experiments.

BIOGRAPHY

Lt Colonel Robert G. McIver is a native of Wichita Falls, Texas and attended North Texas State College where he received his B.S. degree in Biology in 1949. In 1953 he received his M.D. from the University of Texas Medical Branch after which he served his internship and residency at Henry Ford Hospital in Detroit, Michigan. In 1957 he entered on active duty serving as Chief of Anesthesiology from 1957 to 1959 at the USAF Hospital in Wimpole Park, England and from 1959 to 1961 at the USAF Hospital at Maxwell AFB, Alabama. In 1961 he was assigned to Brooks AFB serving as Chief of the Performance Physiology Section at the School of Aerospace Medicine and from 1967 as Chief of Aerospace Medicine, Research Directorate, Headquarters, Aerospace Medical Division. In July 1968 he assumed his present position as Commander of the 6571st Aeromedical Research Laboratory, Holloman Air Force Base, New Mexico. Colonel McIver is a graduate of the Primary Course in Aerospace Medicine, the Biomedical Research Methodology Course, and a course on Recognition and Treatment of Diving Accidents at the USN Deep Sea Diving School. His primary publications have been in the areas of anesthesiology and decompression sickness.

DEVELOPMENT OF HYPERBARIC OXYGEN THERAPY FOR ALTITUDE DECOMPRESSION SICKNESS

Robert G. McIver, Lt Colonel, USAF, MC *
Headquarters, Aerospace Medical Division
Brooks Air Force Base, Texas

The etiology, diagnosis, prognosis, and treatment of decompression sickness has been the subject of numerous research efforts since it was first described almost a hundred years ago. Until the late 1930's, decompression sickness was not a problem in flying since our aircraft were incapable of reaching altitudes at which decompression sickness occurs. During World War II, however, there were many reports of severe decompression sickness occurring at altitude in which the symptoms did not disappear upon recompression to ground level pressure. At least 400 of such severe cases were reported and many of these patients expired due to the fact that there was very little knowledge available which would guide the therapy of this disorder.

The United States Navy has been using for years recompression as therapy for caisson disease. This was a logical discovery since the disease was produced by decreasing the barometric pressure; therefore, the treatment should include increasing the barometric pressure. This same treatment was used for decompression sickness which developed at altitude merely by descending from altitude to ground level. In some instances, however, the symptoms which have occurred at high altitude do not disappear completely upon reaching the ground level pressure. In some instances the disease actually progressed so that circulatory collapse occurred, and in some instances, death. There was obviously a need to develop additional methods of therapy to be used in such cases of refractory altitude decompression sickness.

Decompression sickness for the most part is a subjective disease and there were no known objective measurements which could be used to diagnose decompression sickness in anesthetized animals. In order to develop proper therapy for altitude decompression sickness it was necessary to know diagnostic criteria and to utilize some objective measurements in the evaluation of new methods of therapy.

---

* The author is currently assigned as Commander, 6571st Aeromedical Research Laboratory, Holloman Air Force Base, New Mexico 88330.

Since decompression sickness was known to occur at a time when bubble formation took place within the body as a result of oversaturation of the body tissues with an inert gas, the mechanics of bubble formation and transmission were explored. Bubble formation takes place within the tissues and also within the blood stream. It is not known whether the bubble formation in the tissues is responsible for the symptoms of decompression sickness or whether some other factor is producing both the symptoms of decompression sickness and the bubbles. It would be difficult and thought unfeasible to devise an objective measurement of bubble formation in tissues; however, the bubble formation which occurs in the blood stream would lend itself to some type of objective measurement. The bubbles are formed peripherally and are carried by the blood stream into the chest, into the right atrium, from there into the right ventricle and thus, into the pulmonary artery which feeds the pulmonary vascular bed. As the bubbles arrive in the pulmonary vascular bed, they act as foreign bodies and therefore, produce constriction of the pulmonary vasculature. The mere presence of the bubbles also produces mechanical obstruction to the blood flow through the lung. The combination of mechanical obstruction to the blood flow and vasoconstriction will partially occlude the blood flow through the lung, and therefore, the pressure in the pulmonary artery should rise. There has been previously described an increase in pulmonary artery pressure and an increase in the respiratory frequency when multiple small foreign bodies such as starch granules are injected into the right heart.

In order to assess these changes in decompression sickness, large mongrel dogs were utilized in experiments simulating divers' decompression sickness and altitude decompression sickness. The anesthetized dogs were instrumented for the continuous recording of pulmonary artery pressure, systemic arterial pressure, respiratory frequency, heart rate, central venous pressure, and electrocardiogram. In order to visualize the presence of bubbles in the vascular system, viewing cuvettes were interposed in the circulation at the femoral artery and femoral vein levels. In the divers series, the animals were placed in an 800 cubic foot high-pressure chamber and compressed to a pressure of 6 atmospheres absolute (75 psi gauge) where they remained for a period of one hour before decompression at the rate of .5 atmosphere per minute to ground level. In the sixteen animals exposed there appeared after 26.1 minutes at ground level following the decompression, bubbles in the venous cuvette and simultaneously a rise in pulmonary artery pressure of 220 percent and a rise in respiratory frequency of 240 percent.

To explore the altitude response, anesthetized animals were instrumented in the same fashion as they were for the diving response. These five animals were decompressed to a 40,000 foot equivalent altitude breathing 100 percent oxygen administered via tracheostomy tubes from standard aviator's oxygen breathing regulators. In these animals, after

20.4 minutes at altitude, bubbles were observed to appear in the venous cuvette and simultaneously the pulmonary artery pressure rose by 142.7 percent and the respiratory frequency increased by 368.8 percent.

In another series of experiments it was shown that in the case of the pulmonary hypertension and tachypnea which were caused by bubbles produced from diving, these abnormalities were completely reversed by increasing the pressure to 3 atmospheres absolute. In the altitude exposures, the pulmonary hypertension and tachypnea were completely reversed in most animals by recompression to 20,000 foot equivalent altitude. There were some animals which had persistent pulmonary hypertension and tachypnea even after recompression to ground level. In order to assess the magnitude of overpressure necessary in order to completely reverse the pulmonary hypertension and tachypnea, the barometric pressure was progressively increased. There was suggestive evidence that small overpressures of the order of 5 to 7 psi could reverse these changes. This assumption, however, proved to be incorrect when actual patient treatments were commenced. The evidence was clear, however, that with persistent pulmonary hypertension and tachypnea, a further increase in barometric pressure would be of benefit as shown by these objective measurement.

With this point in mind, the hyperbaric research chamber at the USAF School of Aerospace Medicine was converted, with the assistance of the United States Navy, to a man-rated hyperbaric chamber and at the same time, an educational program was begun in the treatment of decompression sickness using hyperbaric therapy. Sufficient personnel were trained to maintain a 24-hour per day on-call coverage, since the nearest hyperbaric chamber to this facility was over 1,000 miles away and there were no other man-rated hyperbaric chambers in the United States Air Force inventory.

If one considers that bubbles which are formed at an altitude of approximately 40,000 feet would be compressed to one-sixth their original volume by repressurizing to ground level, then an increase of one additional atmosphere will decrease these bubbles to one-twelfth their original size. One must conclude that a great many patients should be relieved of their symptoms by the time one additional atmosphere of pressure has been applied. In treating patients with severe refractory altitude decompression sickness, however, it was found that relief was not obtained until pressures of 2 1/2 to 3 atmospheres absolute had been reached. These compressions were accomplished using 100 percent oxygen following the U.S. Navy Table 6, which was being developed at the same time by the United States Navy Experimental Diving Unit. I elected to use the three atmosphere, 100 percent oxygen treatment table as the primary method of treatment for decompression sickness developing near

35,000 feet, since a three atmosphere treatment pressure for altitude decompression sickness would be equivalent to a 400 foot treatment pressure in the case of divers' decompression sickness. The Navy Treatment Tables I thru IV for divers' decompression sickness may go to 6 atmospheres absolute pressure; therefore, it was thought that a twelvefold increase in pressure in the case of altitude decompression sickness should be sufficient to maximally contract the bubble size. It was thought very desirable to use 100 percent oxygen so that maximal oxygenation of the tissues could take place, since not infrequently neurocirculatory shock is a pronounced symptom. This original schedule has been maintained and incorporated as standard treatment procedure for altitude decompression sickness which is persistent after recompression to ground level. The Air Force currently has eight hyperbaric chambers located at strategic places throughout the United States and Europe. Four of these are functional and to date eleven cases of severe altitude decompression sickness have been treated, all successfully. This hyperbaric treatment capability has allowed at the School of Aerospace Medicine the exploration of many aspects of decompression sickness in space flight; many of these experiments would have been too hazardous without this treatment capability. Such experiments regarding MOL profiles have been reported in the literature and the following guidelines have been established for space flight based on the human experiments:

1. Denitrogenation periods required before lift-off.

2. Incidence of decompression sickness in space flight in which cabin pressures of 7, 5, and 3 1/2 psi are associated with oxygen-helium, oxygen-nitrogen, or 100 percent oxygen cabin atmospheres.

3. Anticipated incidence of decompression sickness using varying periods of denitrogenation and varying periods of partial gas equillibration.

4. Anticipated incidence of decompression sickness in the event of early extra-vehicular activity.

5. The ultimate fate of untreated decompression sickness occurring during space flight.

6. An estimate of the pressure altitude at which relief of symptoms will occur.

7. Suitable treatment schedule for decompression sickness if it occurs in space flight. This schedule will utilize maximum cabin pressure plus suit pressures for a period of five hours or more.

8. The time interval required for a second extra-vehicular activity if decompression sickness occurred on the first extra-vehicular activity.

Since this hyperbaric chamber is the only chamber in the near vicinity of this area of the country, it has also been used in life-saving instances in the treatment of gas gangrene in 10 cases, in the treatment of air embolus in 3 instances, and in the treatment of divers' decompression sickness in 1 instance.

ACCELERATED METHODS AND DEVICES FOR DIAGNOSIS AND TREATMENT OF INFECTIOUS DISEASES

By

Walter M. Sellers

USAF School of Aerospace Medicine
Aerospace Medical Division (AFSC)
Brooks Air Force Base, Texas

Accelerated Methods and Devices for Diagnosis and Treatment of Infectious Diseases

Walter Sellers

Abstract

A method has been developed for laboratory determinations of effective antibiotics for bacterial diseases which allows results to be secured 24 hours earlier than with the standard procedures. Laboratory determinations can now be routinely made available to the physician early enough to be of use in his decision as to choice of definitive treatment for the patient. The test makes use of the rapidity of the color change in red blood cells when oxygen is consumed by bacteria. In the presence of effective antibiotics oxygen is not consumed and the color of the red blood cells remains unchanged.

Three new culture media and one test for the identification of disease-causing bacteria will also be discussed.

BIOGRAPHICAL SKETCH

Walter M. Sellers, Microbiologist, was born in Seale, Alabama, September 18, 1917. He received B.S. (1938), B.A. (1939), and M.A. (1951) degrees from the University of Texas. Previous to joining the staff of the Microbiology Branch of the USAF School of Aerospace Medicine in 1953 he was associated with the Texas State Health Department. His main research interests are in the growth requirements of pathogenic micro-organisms and in the developme of diagnostic tests and culture media for their identification. Five of his culture media are commercially available. He is a consultant to the USAF Epidemiology Unit, Wilford Hall USAF Hospital, and the U.S. Public Health Service National Communicable Disease Center. He is the author of a chapter in a textbook in Microbiology and has published 29 articles in professional journals.

ACCELERATED METHODS AND DEVICES FOR DIAGNOSIS AND TREATMENT OF INFECTIOUS DISEASES

Walter M. Sellers

The antibiotic which is chosen for treatment of a patient is always decided upon empirically. At the time the antibiotic is administered, only a guess can be made as to what kind of bacterium is causing the disease. Different bacterial species, and even different strains of the same species, vary greatly as to the specific antibiotics to which they are susceptible. Because of this, different patients having the same clinically diagnosed disease often do not respond to the same treatment.

Due to the previous inability of obtaining from the laboratory the antibiotic sensitivity spectrum of a bacterium in less than 48 hours, the first evidence in deciding whether a given treatment was of use against an infection was the clinical response of the patient. The morning after antibiotic therapy had commenced, the patient was observed to determine whether his condition was unchanged, had improved, or had deteriorated. At that time a decision had to be made whether to continue the treatment or to change to another antibacterial agent. If it was decided to change antibiotics, the decision of which one to use again had to be made empirically. If it was decided not to change the treatment there was often uncertainty as to whether the decision was the correct one.

For information to be useful, it must be available at the time it is needed; not at a later date. A laboratory report of effective antibiotics for an infection is of little use, except for historical interest, 48 hours after treatment was started; it would have been of great value if it had been available 18 to 24 hours after treatment had begun.

The standard laboratory antibiotic sensitivity test requires 48 hours. The test was developed 21 years ago. It is the test used universally in hospital laboratories today. It depends upon a sequence of two periods of bacterial growth. An overnight incubation is required for bacteria to produce visible growth. Therefore the first 18 to 24 hours are spent growing the bacteria in pure culture from material such as spinal fluid, blood, or pus. At the end of this first growth period a small amount of the bacteria is spread over the surface of a nutritive gel in a small dish. (SLIDE 1) On this surface are placed several small paper discs, each containing an antibiotic. The dish then has to be incubated another 24 hours in order to "regrow" the bacteria. After this second 24-hour growth period, a visible film of bacteria has covered the surface of the gel everywhere except around those paper discs containing an effective antibiotic.

The two growth periods required for the standard test to us seemed analogous to the situation where a boy has an apple which he wants to eat very badly, so he plants it so he can have a tree which will produce an apple so he can eat it. (SLIDE OFF).

After the first growth period, bacteria are present in pure culture in enormous numbers. What was needed was an antibiotic test which would make use of the large quantity of bacteria already available. This would eliminate the need to "re-plant" a small amount of the organisms and then having to wait another day for the development of visible growth of a lawn of new bacteria. By eliminating the necessity for a second growth period, the antibiotic sensitivity spectrum of an organism would be available to the doctor early enough to institute rational rather than guess-work therapy for the patient. The end product, in addition to being useful in life-death situations, we believe, should result in a considerably more rapid hospital bed turnover.

Antibiotics are useful against infections because they interfere with or stop bacterial metabolism with little or no harm to the patient. If only some indicator system for the metabolic rate of an organism were available, bacteria from the first growth period could be used for direct sensitivity testing, thus eliminating the second growth period of the standard test.

Oxygen consumption, whether by man or bacterium, is one of the characteristic features of life. An indicator for disappearance of oxygen should faithfully reflect interference with bacterial metabolism.

Due to the rapidity with which red blood cells acquire or release oxygen along with a simultaneous and easily discernible change in color, and because of a complete lack of toxicity for bacteria, a 3 percent suspension of red blood cells in broth was chosen as the indicator system for oxygen consumption and therefore for the presence or absence of bacterial metabolism.

(SLIDE 2) The slide shows the new test. To each of the first 8 tubes was added a paper disc containing a different antibiotic. The first 6 tubes contain effective antibiotics for the particular bacterium being tested. In the first 6 tubes the metabolism of the bacterium was inhibited; therefore no oxygen was consumed and the color of the red blood cell suspension remained scarlet red.

The 7th and 8th tubes are marked P (for penicillin) and NB (for novobiocin). These two antibiotics were not effective for this particular bacterium. Therefore bacterial metabolism continued to function in these as it did in the positive control tubes. The metabolizing bacteria consumed the oxygen available from the hemoglobin in the red blood cells and this caused the color to darken. There

are two positive growth control tubes; the tube marked 2X had twice as many bacteria put into it as did the other tubes. It therefore turned dark faster than the other tubes. When the standard inoculum growth control (the tube marked +) became equally as dark as the double inoculum control, it was time to read the test. The last tube is uninoculated and shows the original color of all the tubes before bacterial metabolism occurred.

The number of bacteria used to inoculate the tubes governs the length of time required for tubes to darken. A heavy inoculum such as a drop of a very turbid suspension of bacteria will produce detectable darkening in 1 minute and maximum darkening in less than 3 minutes. The only factor which prevents this test from being a 5-minute antibiotic sensitivity test is that antibiotics need time to act on the bacteria. The test is therefore designed for an average reading time of 1 hour in order to provide necessary time for antibiotic interference with metabolism. This is accomplished by adjusting the bacterial suspension used for inoculating the test system to a standardized turbidity with the aid of a spectrophotometer. (SLIDE OFF)

One of the two principal advantages of this one-hour antibiotic sensitivity test is that it is based on interference with metabolism. Cessation or interference with metabolism is a better criterion of antibiotic injury to the bacterium than is failure to grow. Bacteria will not grow, for example, when placed in a refrigerator but they are not injured. This new test is not based on failure to grow but instead is based on actual injury to the normal physiology of the bacterium. The second advantage of the test is that it will usually give the antibiotic spectrum of the causative organism of a bacterial infection in 18 to 24 hours. It is at this time (not the following day) that this knowledge is of major importance to the well being and early cure of the patient.

The first part of this paper has been concerned with a contribution on the treatment of bacterial diseases. The remaining part of the paper is concerned with the diagnosis of these diseases.

For the diagnosis of bacterial diseases, use of bacterial culture media is indicated. A bacterial culture medium is any substance in which bacteria will grow. Bacteria differ considerably in the nature and extent of their nutritive requirements. The majority of culture media are made from empiric formulas of ingredients which experience has proved are adequate sources of energy and structural material for growth. Most of these media have been developed as tools for the study of certain phases of bacterial physiology as a means of identification. A bacteriologist can do better work with better tools; culture media are the essential tools used in bacteriology.

Citrate mannitol agar is a new commercially made culture medium which specifically identifies the organism most often confused with the bacterium causing bacillary dysentery. Previous to development of this medium, the identification of this organism required over a dozen tests. Several days were required for the identification. The organism is important for several reasons. First, it must be ruled out as the bacillary dysentery organism. Second, certain strains of this species are the cause of infant (summer) diarrhea. Third, it is the most common cause of infections of the urinary tract, including kidney infections. Fourth, it is frequently isolated from septicemias and wound infections. Fifth, it is the indicator organism for the detection of fecal pollution of water and food supplies.

(SLIDE 3, citrate mannitol). The organism which is specifically identified by the medium is the one with a yellow slope and butt and a small blue area at the junction of the slope and butt. The organism on the far right with a blue slope and yellow butt causes enteric fever. It is a relative of the typhoid fever organism. The organism on the far left has not grown. It is the bacillary dysentery bacterium. The butt and slope of the medium therefore have not changed color. The organism to the right of the bacillary dysentery organism, the one with the blue slope and green butt, is a non-disease-causing bacterium that also resembles the bacillary dysentery organism and requires work and expense to determine that it is not the causative agent of dysentery. The citrate mannitol agar specifically identifies one organism and is useful in differentiating and helping to identify several other bacteria.

(SLIDE 4, blood coagulation test). This test is to separate bacteria on the basis of citrate utilization. About half of the disease-causing bacteria use citrate and the rest do not. Citrate is used to prevent blood from clotting. This test is based on the fact that when bacteria can use citrate as a source of energy, it disappears from the blood containing culture medium which then solidifies to form a clot. This test is completed in between 1 and 3½ hours and replaces a test medium that was developed in 1926 and requires from 1 to 7 days to detect citrate utilization.

The previous part of this paper covered three items developed in 1967 in our laboratory and is the reason I am on this program. The letter from General Ferguson, however, said to describe any new developments since 1967.

A patent has been issued this year on a culture medium developed prior to 1967 in our laboratory. Bacteriologists have been making and using culture media since the days of Louis Pasteur. This is believed to be the first patented culture medium.

A new commercially made culture medium for detection of motility appeared this year. It was developed in our laboratory. Certain bacteria such as those causing anthrax, bubonic plague, and bacillary dysentery are nonmotile. Other organisms closely resembling these bacteria in other ways can be distinguished from them on the basis of motility.

To conclude, the Air Force School of Aerospace Medicine has been engaged in the development of rapid laboratory diagnostic procedures for the treatment of infectious diseases for several years. Why have resources been expended in this area? The reason may be succinctly stated: to assist in the reduction of noneffectiveness among Air Force personnel by returning them to duty as quickly as possible.

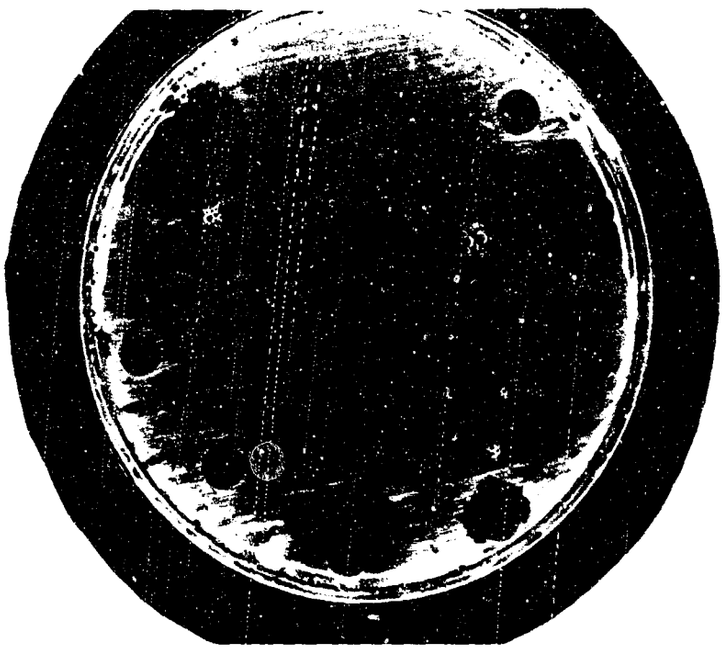

Figure 1

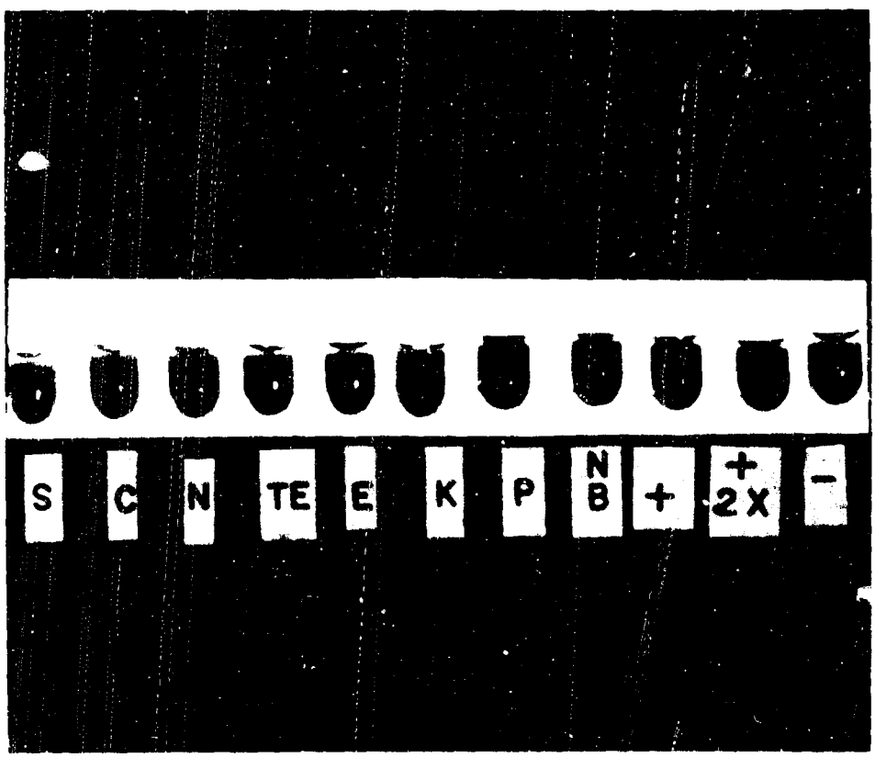

Figure 2

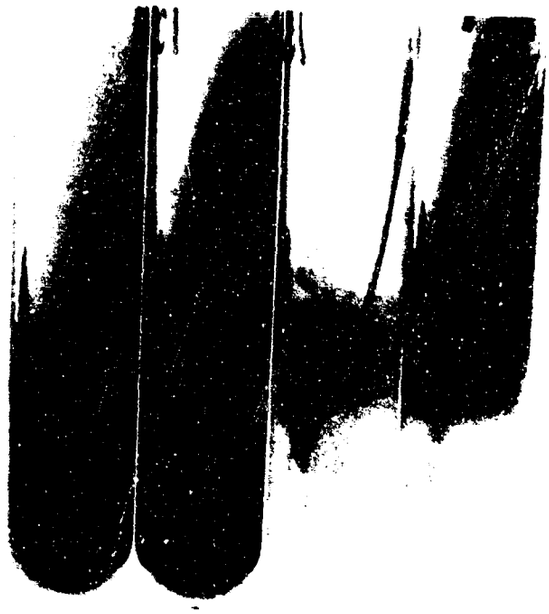

Figure 3

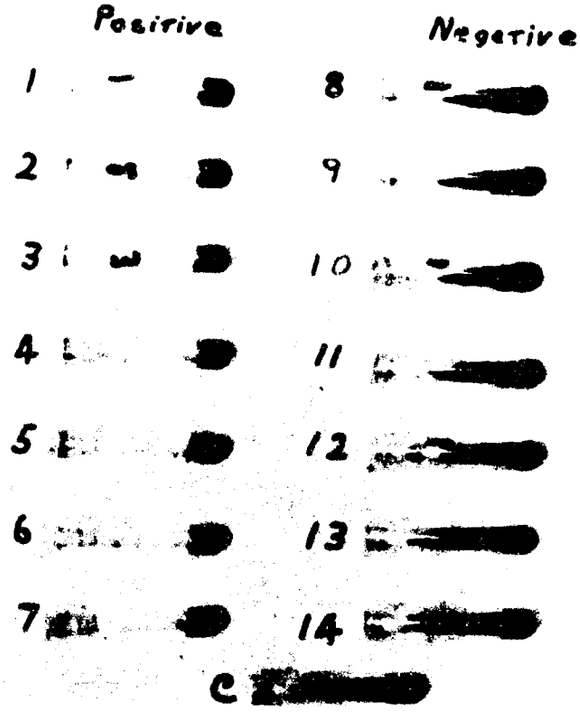

Figure 4

RARE EARTH-ZIRCONIA CERAMIC STORAGE HEATERS PROVIDING FLIGHT SIMULATION FOR AIR-BREATHING PROPULSION SYSTEMS

By

Larry L. Fehrenbacher, Capt, USAF

and

Gottfried Arnold, USAF

Metallurgy and Ceramics Research Laboratory
Aerospace Research Laboratories
Office of Aerospace Research
Wright-Patterson AFB, Ohio 45433

Arnold Engineering Development Center (AEET)
Air Force Systems Command
Arnold AFS, Tennessee 37389

RARE EARTH-ZIRCONIA CERAMIC STORAGE HEATERS PROVIDING FLIGHT SIMULATION FOR AIR BREATHING PROPULSION SYSTEMS

Capt. Larry L. Fehrenbacher
Gottfried Arnold

ABSTRACT

Heat transfer, aerodynamic heating, and propulsion problems associated with re-entry and hypersonic flight within the atmosphere have led to use of ceramic "pebble bed" storage heaters for the source of high temperature air in hypersonic "blow down" wind tunnels. The simulation of true supersonic flight conditions for the development of hypersonic air breathing propulsion systems is a current objective of the Air Force. Dust contamination, low mass flow rates, and maximum temperature instability of ceramic pebbles and insulation were problems that induced the TRIPLTEE Office at AEDC to initiate a testing and evaluation program of ceramic materials for storage heaters. This program led to the development of yttria-mixed rare earth stabilized zirconia and cored brick shapes for the heater storage bed which greatly improved heater operation, permitting high flow rates at 4400^{O}R with minimal dust contamination. These new material and design concepts are currently being exploited in the 14 inch diameter storage heaters at ARL and AEDC.

Further description includes: (1) the relevant property parameters of the ceramics and their application in the design of the heater vessel; (2) the results of the engineering evaluation tests on various commercial zirconia bed and insulation materials; and (3) the fundamental reasons for the superiority of rare earth stabilized zirconia refractories.

BIOGRAPHY

After completing the Ph. D. requirements (excluding thesis) in Ceramic Engineering at the University of Illinois under the AFIT-CID sponsorship, Captain Larry Fehrenbacher reported to the Metals and Ceramics Division, Aerospace Research Laboratories on July 14, 1967 to begin a four year directed duty assignment.

Captain Fehrenbacher was a 1961 Distinguished Military Graduate of the University of Illinois ROTC program and was assigned directly to AFIT to work on M.S. in Ceramic Engineering at the same school. Upon graduation in June 1962, he was assigned to the Air Force Materials Laboratory as a Materials Research Engineer in the Metals and Ceramics Division. During this tour from September 1962 to June 1966, he conducted in-house research involving high temperature applications of rare earth stabilized zirconium oxide compositions. His in-house programs also included flexure and tensile studies and fractography analyses of high density MgO and Al_2O_3 mechanistic sintering studies of single phase oxides, reactive hot pressing of mixed oxides, diffusionless phase transformation mechanisms in oxides, and co-precipitation of mixed oxides.

His research efforts not only resulted in six presentations at national scientific meetings and nine technical publications but they were climaxed with a Rare Earth Oxide-Zirconia Fabrication program at the

Oak Ridge Y-12 plant (AEC) Contract No. D.O. 33(615)66-5011 and by his intimate role in testing, evaluating, and consulting for the True Temperature Hypersonic Wind Tunnel Ceramic Storage Heater Program (TRIPLTEE) at Arnold Engineering Development Center (Contract AF No. 40(600)-1094).

Captain Fehrenbacher's analytical determinations and evaluations of commercial zirconias resulted in three separate reports on the tested heat exchanger samples that essentially dictated the property and compositional specifications for the pilot plant storage heater refractories. He received the Air Force Commendation Medal for this work.

During his doctoral study at University of Illinois (June 66 to June 67) he continued his cooperative efforts with the TTT Office by evaluating proposals for the pilot plant storage heater refractories and for an Uncooled Nozzle Throat Research Program for Tripltee Wind Tunnel (Contract AF No. 40(600_1186) in addition to consulting on numerous other technical problems.

His Ph.D. thesis work is being coordinated with TTT storage heater objectives in an investigation of the engineering and fundamental (atomistic) aspects of the creep (high temperature deformation) behavior of cubic stabilized zirconia.

Captain Fehrenbacher is married to the former Marsha June Smithson (B.S., University of Illinois, 62) of Bloomington, Illinois.

The report titled "Rare Earth-Zirconia Ceramic Storage Heaters Providing Flight Simulation for Air Breathing Propulsion Systems" to be presented at the 1968 Air Force Science and Engineering Symposium by Capt. Larry L. Fehrenbacher (ARZ) and Gottfried Arnold (AEDC) is unclassified.

AIR FORCE SCIENCE AND ENGINEERING SYMPOSIUM

Rare Earth-Zirconia Ceramic Storage Heaters Providing Flight Simulation for Development of Air-Breathing Propulsion Systems

INTRODUCTION AND BACKGROUND

Scientific-technical man recognized very early that testing and the availability of test laboratories are necessary for better understanding of phenomena in his environment and for technical progress in utilizing these environments for his benefit. Man's ancient desire to fly, therefore, made him aware of his lack of knowledge of aerodynamics which, in turn, made him start building devices to study and learn about the basic elements involved in flight. It is not per chance that the Wright Brothers were successful in their controlled, powered flight - they had studied in great details and with a scientific systematic approach the behavior of their craft in their own wind tunnel. It is perhaps significant that our knowledge of the aerodynamics of flight was far in advance of other categories involved in flight, for instance propulsion, only because wind tunnels had been available early enough to assemble a wealth of knowledge. It appears that the aerodynamicists and aircraft builders always managed to stay one or two steps ahead of their colleagues in the propulsion field. This is why many knowledgeable people believe that propulsion is a pacing technology area in the development of advanced aerospace vehicles. The increased activities, today, in new propulsion concepts seem to underline this situation.

During the next few years we are aiming at major advances in air-breathing propulsion, using supersonic combustion or a combination of several techniques, with the potential of reaching hypersonic flight velocities. The complexities of these advanced concepts present great challenges to the development engineer and emphasize the urgent need for test facilities which will simulate true flight environmental conditions. Some examples of problems which make tests in a ground facility necessary are concerned with supersonic combustion: inlet performance, fuel mixing, combustion delay times, exhaust configuration, base pressure and recirculation problems, interaction of fuel injection system, controls, inlet nozzle, combustors and exit nozzle. For a hypersonic flight vehicle the propulsion unit becomes an integral and vital part of the vehicle system. Its performance is greatly determined by the behavior of the vehicle's aerodynamic surfaces and, conversely, the propulsion system performance relates back to the aerodynamic characteristics of the system. These interrelated effects of the performance of the engine and the associated aerodynamic surfaces become extremely critical at hypersonic speeds and

have only recently been fully realized.

Resulting requirements for a ground test facility for investigating these problems are critical and border or exceed the capability of existing technologies. The test facility must be capable of full simulation of the flight environments, in terms of pressure, temperature and air velocity. True stagnation temperatures and pressures must be produced since factors affecting mechanical and thermal loading on structures must be mutually compatible with combustion and aerodynamic characteristics. These parameters cannot all be accounted for simultaneously by similitude considerations or by scaling. The facility, therefore, must be capable of delivering the high temperatures and pressures associated with the stagnation conditions of hypersonic flight.

A typical facility of this type would probably use the blowdown principle since a continuous operating capability would be much more costly. That means the hypersonic tunnel would use a ceramic storage heater for the source of high temperature, high pressure air. Ceramic regenerative heaters have been in use at several government and industrial operated facilities for many years.

A ceramic storage heater consists essentially of a steel pressure vessel containing the heat storage bed (Matrix) and several layers of insulation to minimize heat losses as well as protect the vessel shell. The designs have generally utilized composite beds of aluminum oxide, zirconium dioxide, and/or magnesium oxide spherical shaped balls (pebbles) surrounded with lighter weight insulation of similar compositions as shown in Figure 1. The matrix is heated by passing combustion gases of methane-propane, air and oxygen mixtures from the top of the bed to its bottom at a low flow rate. A "heat wave" is driven into the bed in the direction of hot gas flow resulting in a region of the matrix called the plateau (Figure 2). Below this uniform termperature region the bed temperature decreases linearly to about 1000^{o}F. at the bottom. After the plateau and temperature profile desired for specific operating conditions are reached, the reheat burners are shut off. For a wind tunnel run, cold air at the desired stagnation pressure is introduced at the bottom of the vessel and heated as it passes through the hot matrix in the counterflow direction. The heat energy which had been stored in the bed at low rates over long times during the reheat cycle is thus extracted by the cold air at a very high rate during the run. Stagnation conditions exist for a "useful run time" varying from seconds to a few minutes depending on the mass flow and pressure requirements. Useful run time is defined as that period of time during which stabilized conditions exist in the test stream at the desired Mach number, pressure, and temperature.

About ten years ago, the Arnold Engineering Development Center recognized the need for a large facility to accommodate trends in propulsion and aerodynamics, particularly in the high supersonic flight regime. This conceptual facility was called the True Temperature Tunnel or TRIPLTEE since duplication is accomplished over much of its operating range with respect to stagnation temperatures that a hypersonic vehicle actually experiences in free flight. The TRIPLTEE facility is being proposed in one of the future Military Construction Programs. Its complete operating envelope is shown in Figure 3. That portion, where tests could be performed at true temperature and pressure for the desired flight Mach number, is indicated in Figure 4 as superimposed over the well-known flight corridor for air breathing propulsion vehicles. As mentioned previously it is economically impractical to provide a continuously operating wind tunnel for testing of full-scale flight hardware; therefore, TRIPLTEE will operate intermittently using a ceramic regenerative heater for storing heat energy to raise the temperature of the high pressure air prior to entering the wind tunnel nozzle. This amount of stored air and heat will be sufficient to permit tunnel running times ranging from at least 30 seconds at the most demanding operating conditions of lowest altitude (Mach 7, 1500 psi, 4400°R) to several minutes at the higher altitudes.

During early engineering studies aimed at developing facility design criteria, it became evident that there existed numerous design development problems due to state-of-the-art limitations in several technology areas. One of the critical limitations was in the field of high temperature materials especially the refractories of the large storage heater.

The design parameters of TRIPLTEE imposed severe demands on the capability of existing storage heater refractories. Dust contamination, low mass flow rates and maximum temperature stability of the ceramic pebbles and insulation were problems that induced the TRIPLTEE Office at AEDC to initiate an extensive testing and evaluation program of ceramic materials for storage heaters.* The primary objectives of this study were to determine the optimum compositions and geometric configurations

---

* This work was primarily performed by the Fluidyne Engineering Corporation, Minneapolis, Minnesota, under AEDC Contracts AF 40(600)-1039, AF 40(600)-1094, and F40600-67-C-0004 with active participation by members of the ceramics industry, such as the Coors Porcelain Corporation, the Zirconium Corporation of America and others. Significant technical contributions were made by the Air Force Materials Laboratory and the Aerospace Research Laboratories.

of the matrix and insulation ceramics based on the inter-dependent criteria of fabricability, cost, and engineering performance. Since the use of other refractory oxides is precluded by significant drawbacks (ThO_2 and BeO by cost and health hazards and MgO by high expansion, high vapor pressure and low density), the product development and testing were concentrated primarily on zirconia refractories. The remainder of the paper will briefly describe the (1) relevant property parameters of the ceramics and their application in design of the heater vessel (2) the results of the engineering evaluation tests on various commercial zirconia matrix and insulation materials and (3) the fundamental reasons for the superiority of rare earth stabilized zirconia refractories. Engineering type studies and preliminary test results of this ceramic material development program have been reported in References 1, 2, and 3.

DESIGN CRITERIA

The tunnel operating conditions (mass flow rate, temperature, run time) serve to define the energy storage and energy extraction rate parameters for the storage heater design. An analysis of temperature changes during blowdown of a storage heater is given in Reference 4. The heater design and necessary quanities of ceramic matrix and insulation, in turn, require knowledge of the chemical, thermal, and mechanical properties of the zirconia refractories and how they vary as a function of density, chemical composition, size, shape, and atmospheric environment (pressure, temperature). Furthermore, these intrinsic properties (specific heat, thermal expansion, thermal conductivity, Poisson's ratio, strength etc.) can be used to estimate the maximum allowable thermal and mechanical (load bearing) stresses that the ceramics can tolerate. An excellent discussion of the application of these properties is given by DeCoursin. Hagford, Arnold, Male and will not be considered in detail here (3).

The most critical design consideration, especially for high flow rate tunnels such as TRIPLTEE, is bed floatation, i.e., lifting of the bed can occur if the force resulting from the pressure drop across the bed exceeds the bed weight. Bed floatation due to clumping (sintering of pebbles into large masses) and dust formation have been the two most serious problems encountered in the pebble bed heaters (5). These difficulties combined with the high mass flow rates required by the TRIPLTEE tunnel provided the impetus for considering new concepts in matrix design and zirconia compositions.

A hexagonal cored brick shape as shown in Figure 5 was proposed for the heater matrix. * Besides the obvious advantages of increased

---

* This cored brick shape was originally suggested by C. H. Weissinger, Norton Co., Worcester, Mass.

clumping and dusting resistance in comparison to ceramic pebbles, other attractive features of the cored brick design are the reduction of thermal stresses in the horizontal direction due to thin webs, lowering of pressure differential through the bed length minimizing bed floatation problems and significant improvement in mass flow rates and heat transfer properties. Advantages of a cored brick heater over one using pebbles have been analyzed in detail in Reference 2. The development of the cored brick element was an absolute necessity for TRIPLTEE heater design. The size of the large TTT pressure vessel (22 feet long - 12 feet diameter bed), which is considered the practical maximum, still necessitates cored brick dimensions (web thickness, hole diameter) that have almost exceeded the limit of current fabrication technology.

The testing and ceramic materials evaluation program of Fluidyne's was divided into two phases: subscale engineering tests designed to assess critical properties and in-service performance in operating heaters. Prior to discussing the test results, a brief review of the anamolous properties of stabilized zirconia refractories should help clarify the nature of the selected tests and provide a basis for understanding the behavior of the various specimens.

CHEMISTRY AND STABILIZATION PHENOMENA OF ZrO_2

The use of pure zirconium dioxide, ZrO_2, is precluded by severe volume changes associated with a reversible monoclinic-tetragonal phase transformation in the region of 1000°C to 1200°C as illustrated by the thermal expansion curve in Figure 6. Consequently, numerous studies have been directed towards the elimination of this deleterious phase change by modifying the crystal structure of zirconia with additions of other oxides (6, 7, 8). Thermal expansion curves of 5 mole percent Dy_2O_3 - ZrO_2 and 10 mole percent Dy_2O_3 - ZrO_2 compositions (Figures 7 and 8) represent examples of partially and fully stabilized zirconia, respectively. Commercial application of zirconia has resulted from the development of cubic ZrO_2 solid solutions partially and full stabilized by calcium and magnesium oxide additions. However, investigations by one of the authors and others have demonstrated that the Type "C" rare earth oxides are zirconia stabilizers of even greater potential (9, 10, 11). The fundamental reasons for improved stabilization of zirconia with rare earth oxides will be given later.

In the past, commercial suppliers have recommended the use of partially stabilized (85% cubic) zirconia for storage heaters in preference to fully stabilized zirconia (100% cubic) on the basis of the lower expansion and better thermal shock resistance of the partially stabilized composition. Recent studies have shown, however, that CaO and MgO additions form

cubic solid solutions of doubtful stability (12, 13). Decomposition of $MgO - ZrO_2$ cubic solid solutions occurs between 1850°-2500°F via expulsion of MgO from the zirconia lattice. The stability of calcia stabilized zirconia was found to be strongly influenced by the amount of retained monoclinic phase. The proposed mechanism of destabilization was that the stresses arising from the phase transformation of the small amount of monoclinic phase were sufficient to force CaO out of solid solution. This produced additional monoclinic zirconia and eventually destroyed the strength of the body. The complete elimination of the monoclinic phase resulted in a chemically stable material.

Since TTT design parameters represented new maxima in temperature (4200°F top of bed) and mass flow rates, the high temperature stability and thermal stress resistance of partially and fully magnesia and calcia stabilized ZrO_2 materials were highly questionable. Thus, Fluidyne's engineering tests were designed to measure permanence of stabilization-cycling between 500°F and 2000°F, high temperature stability from 3700°F to 4200°F, and thermal stress-cycling to failure.

DISCUSSION OF RESULTS

The results of an initial 262 hour - 3700°F thermal soak test suggested that magnesium and calcia stabilized zirconia compositions were unsatisfactory for top of bed maximum temperatures. Consequently, evaluations of the more expensive yttrium oxide (yttria) and yttria-mixed rare earth oxide* stabilized zirconia specimens were deemed necessary. Cored brick samples stabilized with various percentages of yttria, yttria-mixed rare earth, calcia, and magnesia were subjected to a flowing combustion gas-oxygen-propane atmosphere for 240 hours at 4200°F.

An extensive analysis of the before and after test specimens was made at Wright-Patterson. The analyses included X-ray diffraction for crystalline phase determination and lattice parameter measurements, optical microscopy and bulk density for microstructural comparison, and emission spectrography for purity analysis. The most significant conclusion obtained from the soak test and sample analyses was that the chemical and structural stability of yttria and yttria-mixed rare earth stabilized zirconia materials were vastly superior to the calcia and magnesia stabilized zirconia specimens. This superiority was not only

---

* The composition of the yttria rare earth oxide stabilizer is approximately 90% Y_2O_3, 8% Dy_2O_3, and 2% other Type "C" rare earth oxides. This stabilizer is being used in preference to pure 99.9% Y_2O_3 which is approximately twice as expensive.

reflected by visual observation, but was verified by the crystalline phase concentrations, the lattice parameters of the stabilized phases, the microstructural characteristics, and the bulk densities of the tested samples. The high temperature destabilization of partially and fully stabilized calcia and magnesia zirconia bricks was attributed predominantly to vapor loss of the stabilizing agent as confirmed by emission spectrographic results and decreasing lattice parameters for specific CaO or $MgO - ZrO_2$ compositions. The mechanism of this structural degradation is thus in contrast to the lower temperature phase destabilization that results from the stresses induced by the monoclinic-tetragonal phase inversion.

The yttria and mixed rare earth stabilized zirconia exhibited uniformily sized, equiaxed grain structures with small, spherical intragranular pores randomly distributed. These microstructures contrast sharply with the porous, exaggerated grain microstructures of magnesia and calcia stabilized zirconia. Typical before and after microstructures of calcia, magnesia and yttria stabilized zirconia are presented in the photomicrographs of Figures 9, 10, and 11. The dimensional and structural integrity of completely stabilized yttria zirconia cored bricks was further emphasized by the negligible change in bulk densities (90% theoretical) after 240 hours at 3200°F.

The rare earth stabilized zirconia specimens also performed satisfactorily in destabilization and thermal stress-cycling tests. Thus, yttria-mixed rare earth oxide stabilized zirconia cored brick and insulation refractories were recommended for the highest temperature regions of the TRIPLTEE storage heater. The compilation of property data permitted allowable limits to be specified for the composition (% Y_2O_3), density and purity of the cored brick and insulation components.

In terms of maximum structure stability and dusting resistance of the cored brick, the test results indicated that all the monoclinic zirconia phase should be eliminated to prevent destabilization. Since the large TTT storage heater will require approximately 20,000 pounds of the expensive yttria or yttria-mixed rare earth stabilizer, the compositional specifications represent the minimum contents that would produce a stable zirconia refractory. These concentrations (9.0 - 9.5 weight percent) are much lower than the amounts (10.5 - 17.0 weight percent) considered necessary by commercial and literature sources. The ability of the Type "C" rare earth oxides to form remarkable stable cubic (fluorite) zirconia solid solutions can be attributed to the peculiar properties of the rare earths.

STABILIZATION CONSIDERATIONS

The formation of fluorite-type ZrO_2 solid solutions can be explained in terms of the additive's atomic and electrochemical properties. Ionic size, valency, compressibility, and electronegativity are the parameters normally considered in crystal chemistry and solid solution characterization of a mixed crystal system.

Detailed studies of monoclinic ZrO_2 single crystals have revealed that the Zr ion is surrounded by seven nearest oxygen neighbors which is intermediate with respect to the rutile (6) and fluorite (8) coordination. Although the radius ratio of ZrO_2 is only 0.57, the fulfillment of a theoretical $r_c/r_a = 0.732$ requirement is not critical for the formation of an ionic fluorite-type structure. Stable fluorite MX_2 compounds require closest packing of cations with wide latitudes for filling of anion space. If the anion lattice is closely packed, MX_2 compounds usually experience a 3-6 coordination, assuming the rutile structure. Thus, the presence of anion vacancies in ZrO_2 encourages close packing of cations and subsequent fluorite lattice formation. Since the fluorite modification is also enhanced by ionic bonds, an increase in the electronegativity difference between Zr and oxygen ions would promote the development of stable fluorite ZrO_2 solid solutions. In essence, ZrO_2 stabilization is favored by creation of anion vacancies, improvement in ionic character of cation-anion bonds and an increase in anion-cation coordination. These criteria can be satisfied by cations with the following properties: (1) valence less than four, (2) greater electropositive character, and (3) larger, less compressible ions.

The rare earth oxides as a group satisfy all of the above parameters. Previous research has shown that the ability of rare earth oxides to produce stable cubic (fluorite-type) zirconia solid solutions increases with diminishing size (increasing atomic number) of the cation. Since only slight variations exist in the electronegativity, compressibility and valence factors, the type "C" oxides should readily substitute for Zr^{+4} on the cation sublattice due to the small cationic size difference.

The experimental superiority of rare earth stabilized zirconia in TRIPLTEE tests is reflected by an analysis of the crystal chemistry criteria as presented in the table below.

Oxide	Cation Valence	Cation Electronegitivity	Cation Radius
ZrO_2	+4	1.22	.79 Å
CaO	+2	1.04	.99 Å
MgO	+2	1.23	.67 Å
Y_2O_3	+3	1.11	.92 Å

Magnesia appears to be a very poor stabilizer because it does not satisfy the electronegativity and size criteria. Yttria and calcia would rate as cubic zirconia stabilizers of high potential even though stronger fluorite bonds might be expected with yttria due to its smaller cationic size. However, the distinguishing factor between these two types of stabilized zirconia for high temperature applications (4000°F) is the low vapor pressure of yttrium oxide.

The results of these zirconia material developments are being used presently in the TRIPLTEE pilot heater at AEDC. In addition, the storage heater at the Aerospace Research Laboratory has been converted from pebbles to cored bricks, and the two wind tunnel heaters at NASA-Ames Research Center are in the process of being converted.

The TTT heat exchanger has a 14-inch diameter, 16-foot length cored brick matrix consisting of yttria stabilized zirconia in the upper bed portion and alumina in the colder lower region. The brick dimensions are 2 7/8 inch across the hexagonal face with a 0.2 hole diameter - 0.085 web thickness and are keyed by tongue and groove to assure hole alignment along the stacked columns. These independent columns permit free thermal movement and greatly reduce the side loading of the insulation, thereby enabling lighter weight and more efficient insulation material to be used. A portion of the assembled cored brick matrix is shown in Figure 12 while Figure 13 presents a top view of the matrix and surrounding insulation as installed in pilot heater.

The TRIPLTEE heater is presently in its initial step-by-step shakedown and checkout operations. The bed is completely instrumented with Pt-6Rh/Pt-30Rh thermocouples throughout the matrix and insulation. The thermocouples in the upper bed region are sacrificial and after the 3000°F and higher temperature runs are reached, optical pyrometers will be used. These extensive temperature measurements will yield the data necessary to determine the heat transfer and mass flow characteristics of the bed as well as the overall heater efficiency.

CONCLUSIONS

The development of the cored brick shape for the matrix element and

the use of rare earth (ytt: a based) stabilized zirconia refractories have resulted in a regenerative ceramic storage heater that should be vastly superior in performance to the old pebble bed predecessors. The TRIPLTEE pilot and ARL storage heaters will continue to provide valuable information on present bed and insulation refractories in addition to serving as test beds for the exploitation of new design and material concepts in zirconia heat exchangers of the future. These improved rare earth stabilized zirconia (storage heater) compositions should also lead to a multitude of different applications in high temperature oxidizing environments.

REFERENCES

1. W. S. Hedrick, F. W. Larsen, B. C. Lindahl and D. G. DeCoursin, "Storage Heater Design Study for the Hypersonic True Temperature Tunnel", AEDC-TDR-64-48, Arnold Air Force Station, Tennessee, July 1964.

2. D. J. Harney, "Performance Analysis of Large Ceramic Storage Heaters", AEDC-TR-65-224, Arnold Air Force Station, Tennessee, December 1965.

3. D. G. DeCoursin, D. E. Hagford, G. M. Arnold and D. W. Male, "Recent Development of Storage Heaters to Provide Flight Simulation for Air Breathing Propulsion Systems", Paper presented at the AIAA Third Propulsion Joint Specialist Conference, July 17-21, 1967, Washington, D. C.

4. F. W. Larsen, "Rapid Calculation of Temperature in a Regenerative Heat Exchanger Having Arbitrary Initial Solid and Entering Fluid Temperatures," Int. J. Heat Mass Transfer, 10 (February 1967), 149-168.

5. C. H. Weissinger and G. W. Barnes, "Experience with Pebble Beds and Air Heaters," presented at Air Heater Conference, Worcester, Massachusetts, May 1963.

6. P. Duwez, F. Odell, and F. H. Brown, Jr., "Stabilization of Zirconia with Calcia and Magnesia," J. Am. Ceram. Soc., 35 (5) 107-13 (1952).

7. B. C. Weber, H. J. Garrett, F. A. Mauer, and M. A. Schwartz, "Observations on the Stabilization of Zirconia," J. Am. Ceram. Soc., 39 (6) 197-207 (1956).

8. B. C. Weber and M. A. Schwartz, "Zirconia: Its Crystallographic Polymorphy and High Temperature Potentials," WADC TR 58-646, Wright-Patterson Air Force Base, Ohio, July 1958, pp. 75.

9. L. L. Fehrenbacher, L. A. Jacobson, and C. T. Lynch, "The Role of Rare Earth Oxides in the Stabilization of Cubic Zirconia," Proceedings of the Fourth Conference on Rare Earth Research, pp. 687-705, Gordon and Breach, New York, 1965, pp. 749.

10. L. L. Fehrenbacher, L. A. Jacobson, and C. T. Lynch, "Sintering Behavior of Stabilized ZrO_2 Compositions," AFML-TR-65-394, Air Force Materials Laboratory, Wright-Patterson Air Force Base, Ohio, December 1965, pp. 20.

11. R. Collongues, M. Perez y Jorba, and J. Lefevre, "On the Equilibrium Diagrams of the Systems Zirconia - Rare Earths," Bull. Soc. Chim. France, 28, 70-74 (1961).

12. J. D. Buckley and H. H. Wilson, "Destabilization of Zirconia by Cycling Heating," J. Am. Ceram. Soc., 46 (10) 510 (1963).

13. R. B. Burdick and W. R. Hoskins, "Research on Thermal Properties of Zirconia," ARL 63-170, Aerospace Research Laboratories, Wright-Patterson Air Force Base, Ohio, September 1963, pp. 71.

FIGURE CAPTIONS

1. ARL Pebble Bed Storage Heater
2. Storage Heater Schematic
3. TRIPLTEE Performance Envelope Showing Region of True Temperature Testing
4. Typical Flight Corridor for Advanced Propulsion Systems
5. Cored Brick Configuration
6. Thermal Expansion Curve Showing the Monoclinic-Tetragonal Phase Transformation in Pure ZrO_2 in Air
7. Thermal Expansion Curve of a Partially Stabilized (50%) 5 Mole % Dy_2O_3 - ZrO_2 Body in Air
8. Thermal Expansion Curve of a Fully Stabilized (100% Cubic) 10 Mole % Dy_2O_3 - ZrO_2 Body in Air
9. Photomicrographs of Calcia Stabilized Zirconia Specimens Before and After 4200°F-240 Hour Heat Soak Test
10. Photomicrographs of Magnesia Stabilized Zirconia Specimens Before and After 4200°F 240 Hour Heat Soak Test
11. Photomicrographs of Yttria Stabilized Zirconia Specimens Before and After 4200°F-240 Hour Heat Soak Test
12. Portion of Yttria Stabilized Cored Brick Matrix for TRIPLTEE Pilot Heater
13. Installation of Matrix and Insulation in Pilot Storage Heater

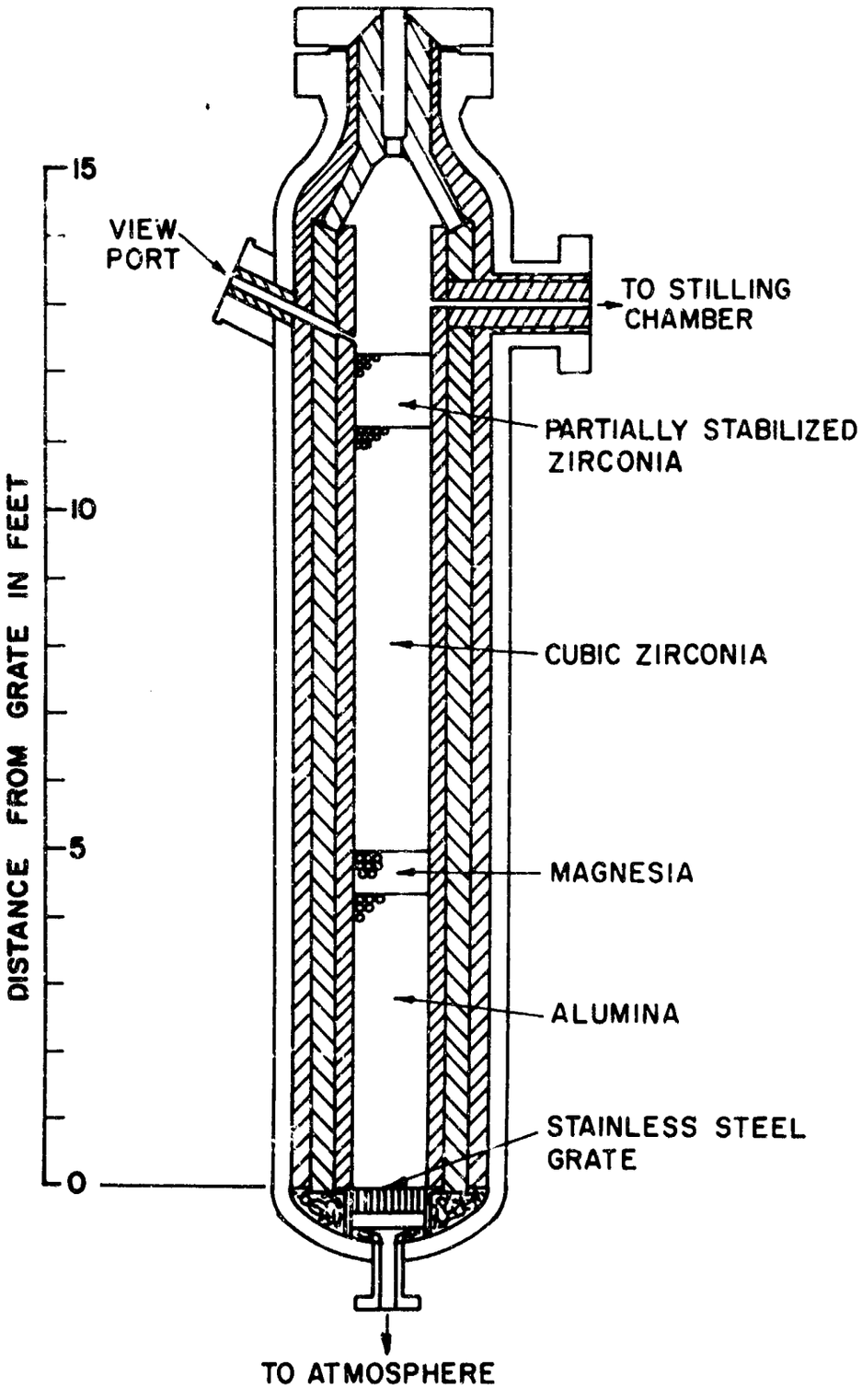
15
10
5
0
DISTANCE FROM GRATE IN FEET
VIEW PORT
TO STILLING CHAMBER
PARTIALLY STABILIZED ZIRCONIA
CUBIC ZIRCONIA
MAGNESIA
ALUMINA
STAINLESS STEEL GRATE
TO ATMOSPHERE

Figure 1

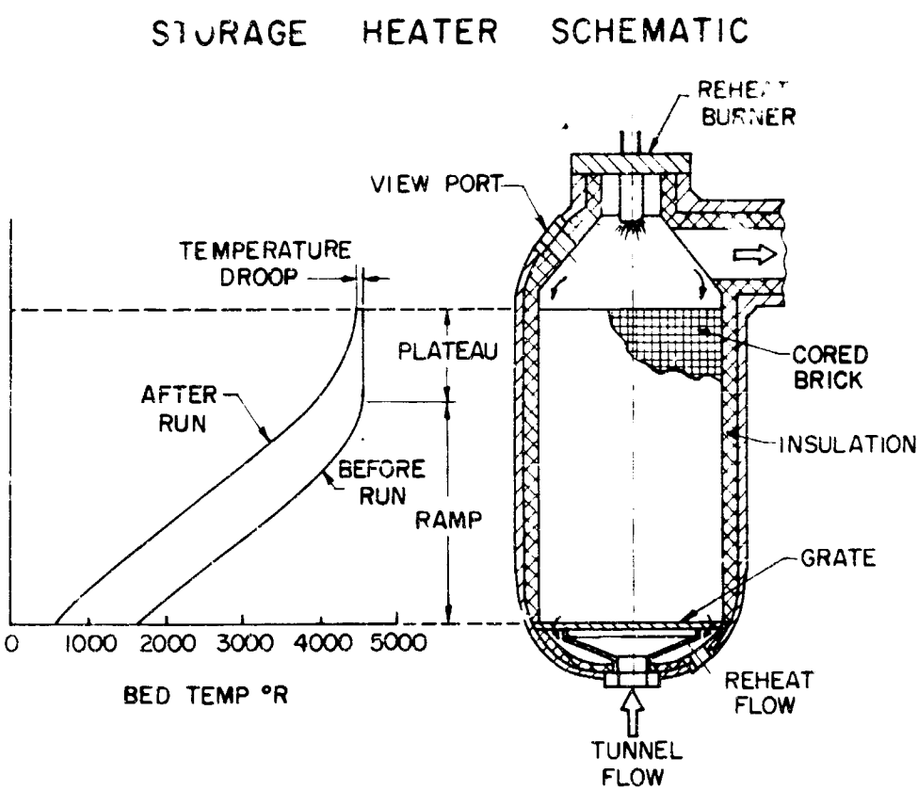

Figure 2

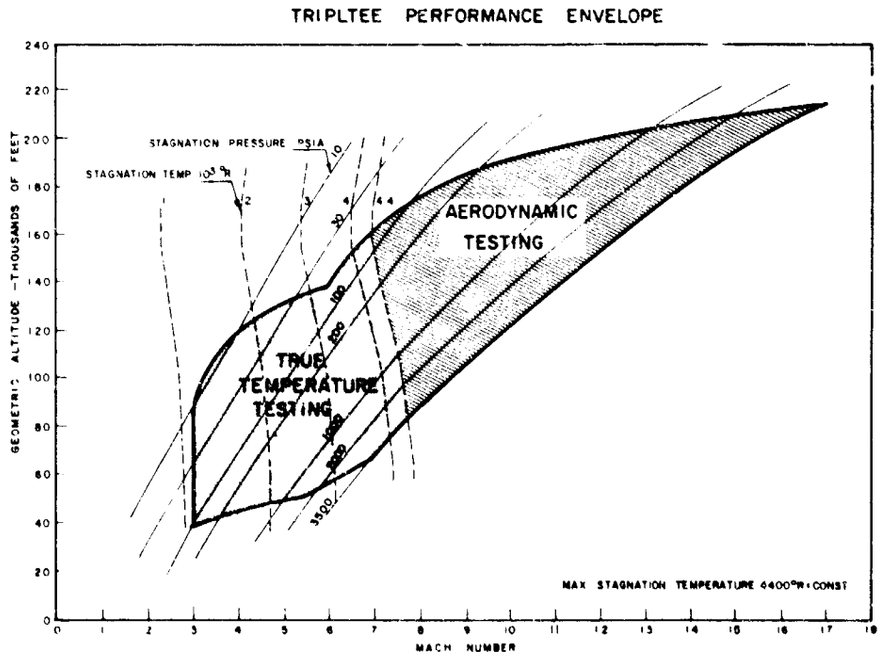

Figure 3

TYPICAL FLIGHT CORRIDOR FOR
ADVANCED PROPULSION SYSTEMS

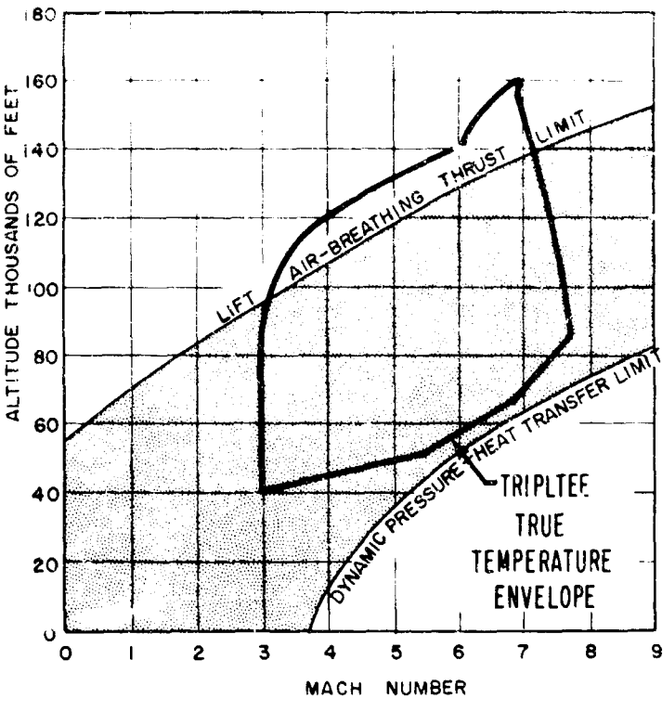

Figure 4

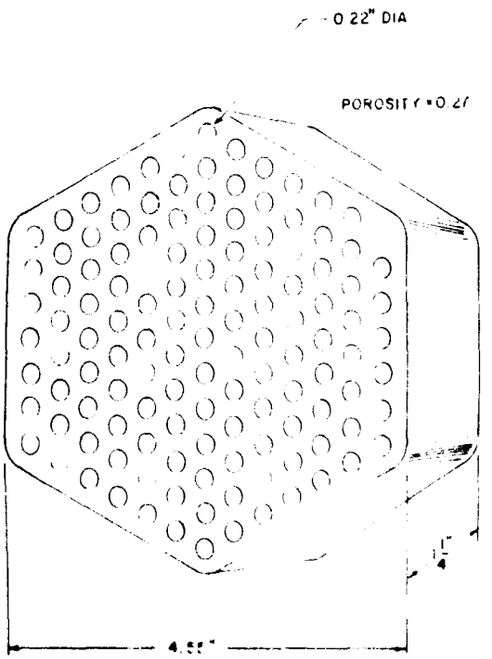

Figure 5

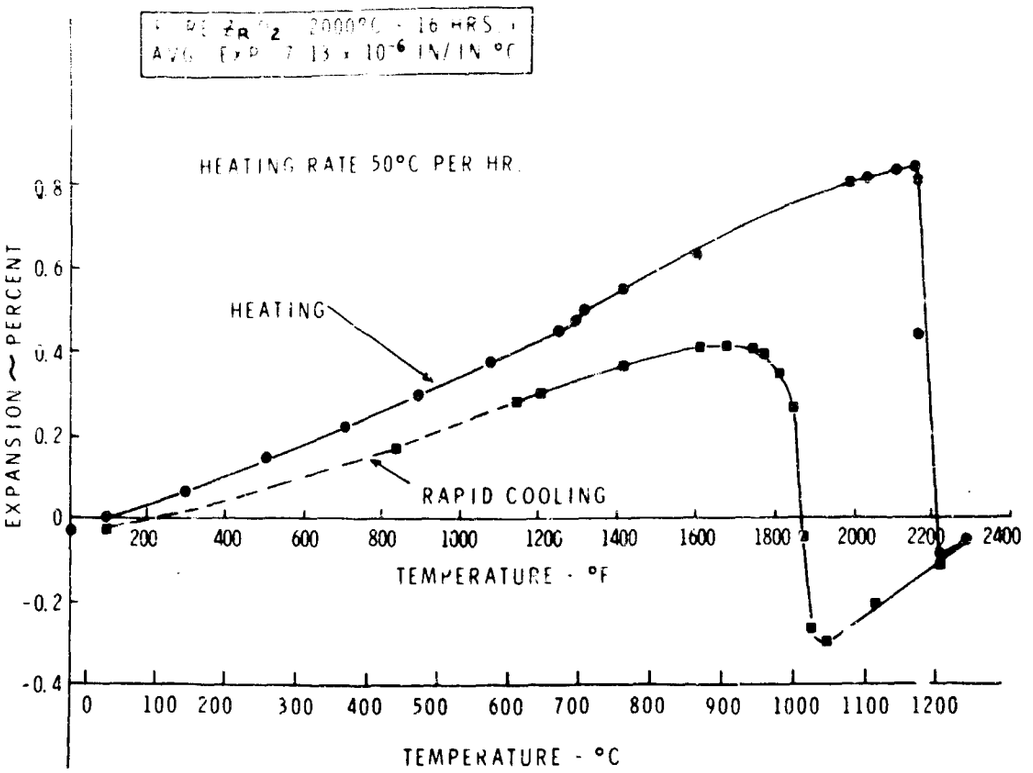

Figure 6

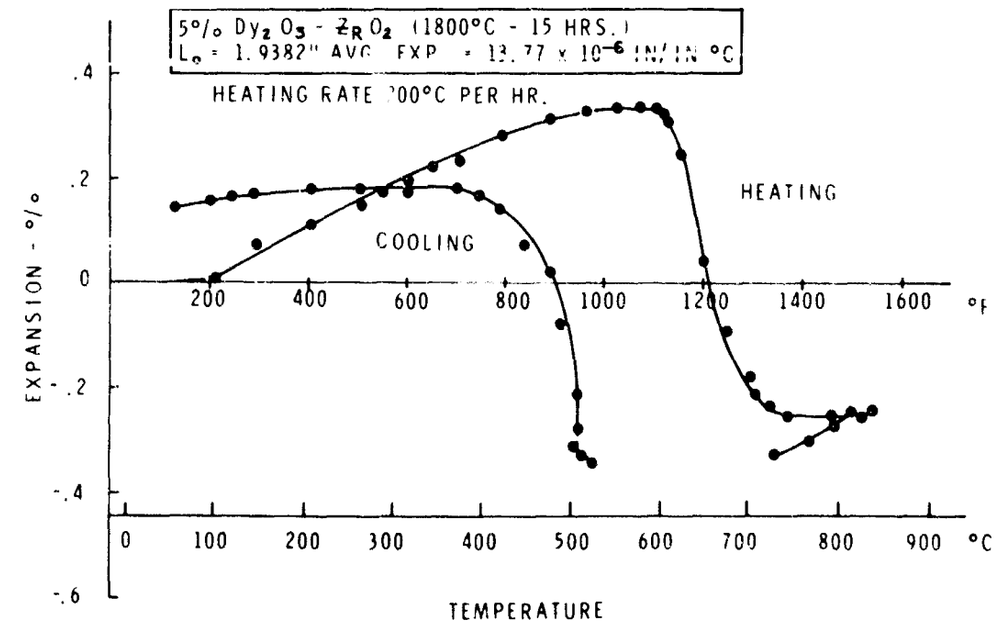

Figure 7

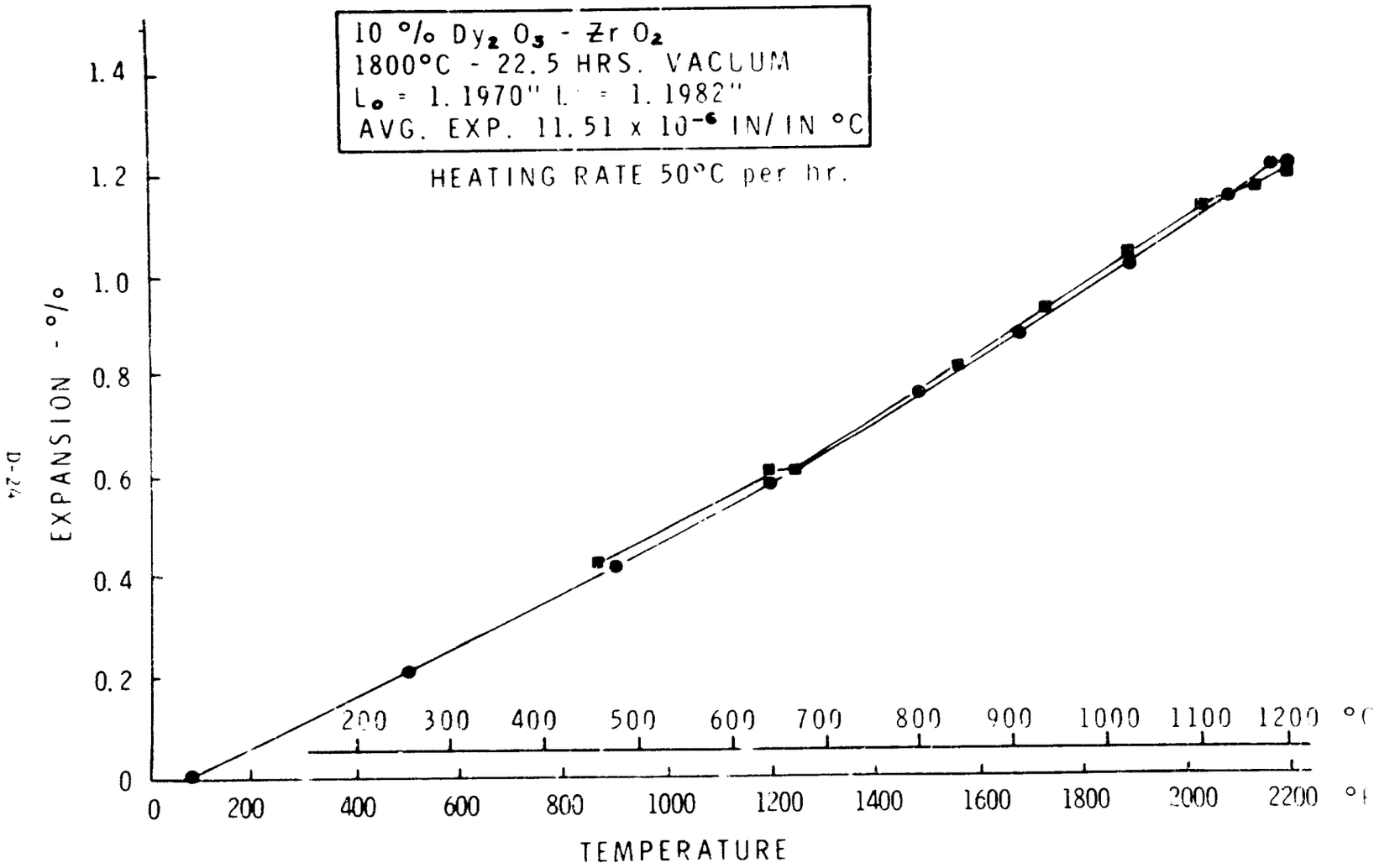
10 % Dy_2O_3 - ZrO_2
1800°C - 22.5 HRS. VACUUM
L_o = 1.1970" L_f = 1.1982"
AVG. EXP. 11.51 x 10^{-6} IN/IN °C
HEATING RATE 50°C per hr.
EXPANSION - %
1.4
1.2
1.0
0.8
0.6
0.4
0.2
0
200 300 400 500 600 700 800 900 1000 1100 1200 °C
0 200 400 600 800 1000 1200 1400 1600 1800 2000 2200 °F
TEMPERATURE

Figure 8

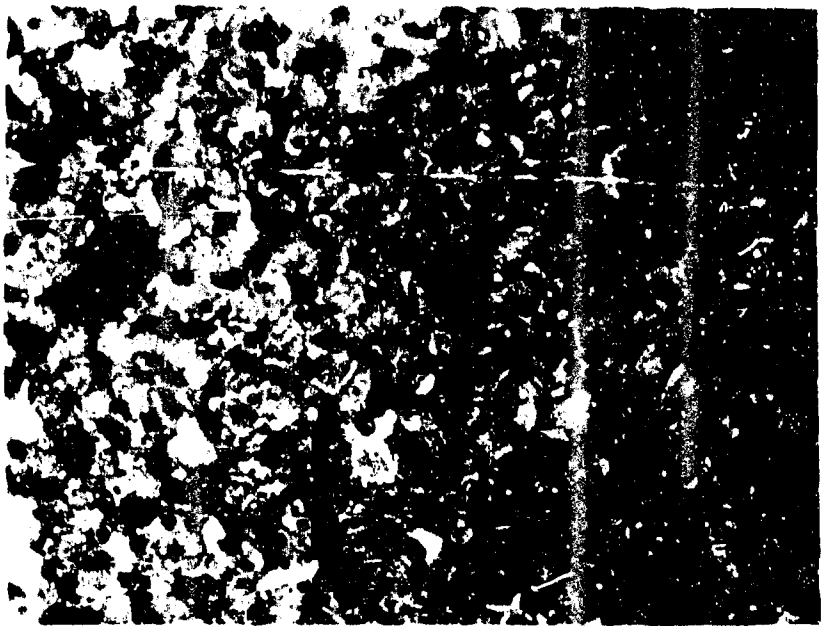

Figure 9 a. 3.85 w/o CaO
As Rec'd 12A 200X.

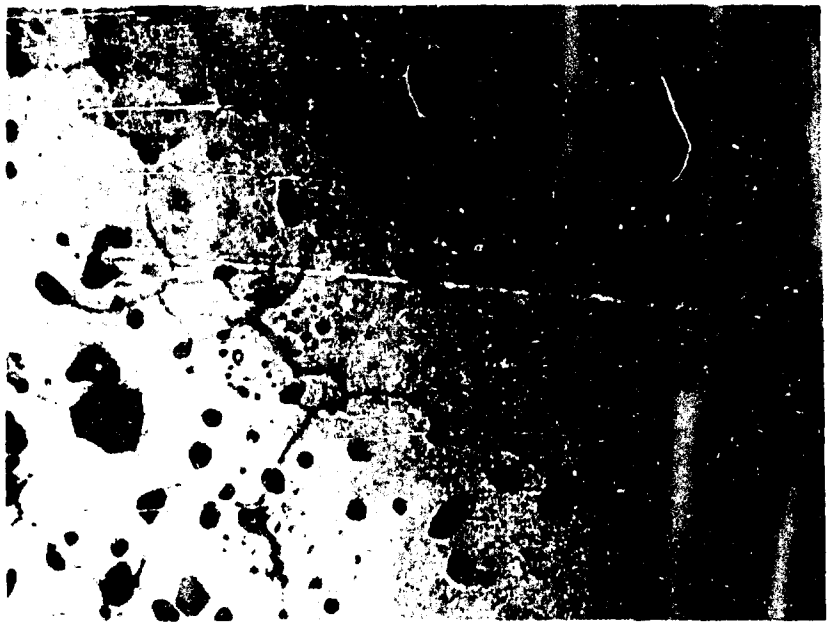

Figure 9 b. 3.85 w/o CaO
4200°F-144 Hrs-12A 200X.

Figure 9

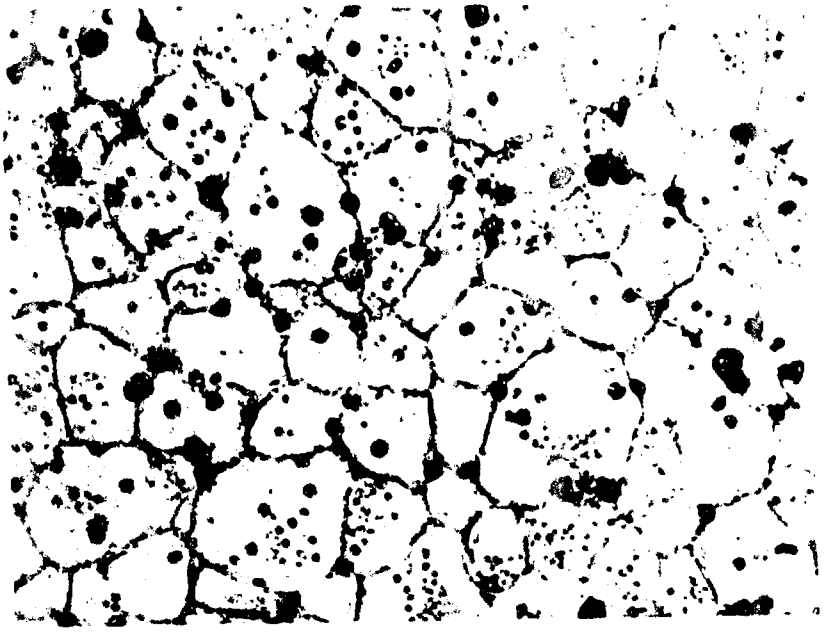

Figure 10a. Nr. 1027 Excess
As Rec'd 10A 200 X.

Figure 10b. Nr. 1027 Excess
4200°F-240 Hrs-10A 200 X.

Figure 10

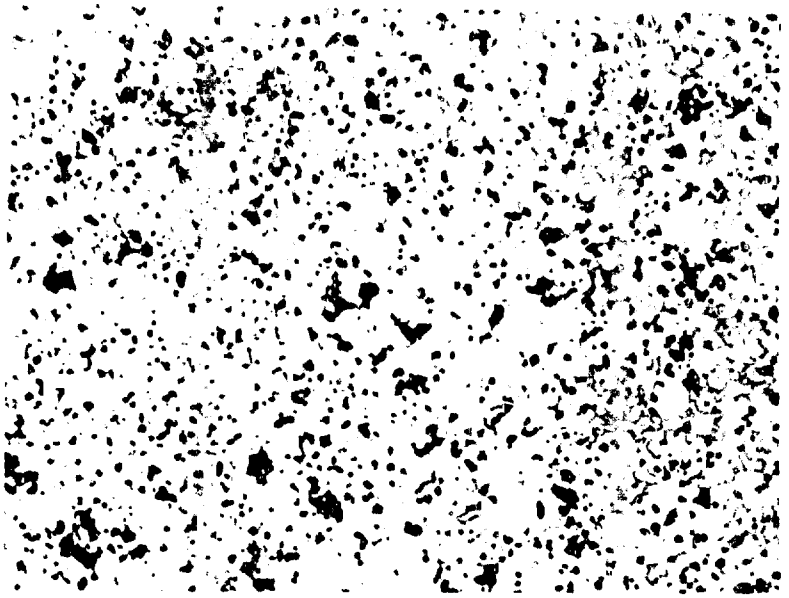

Figure 11 a. 8 w/o Y_2O_3
As Rec'd 6 A 400 X.

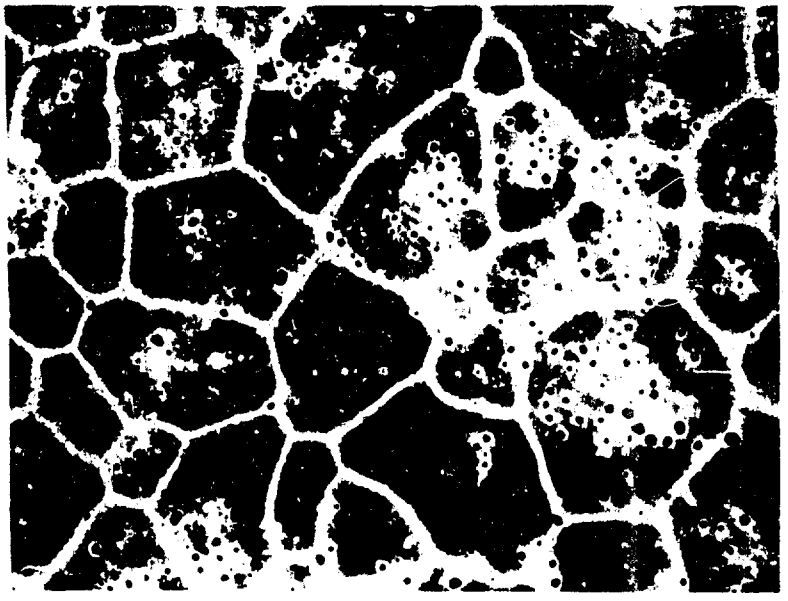

Figure 11 b. 8 w/o Y_2O_3
4200°F-240 Hrs-5A 100 X.

Figure 11

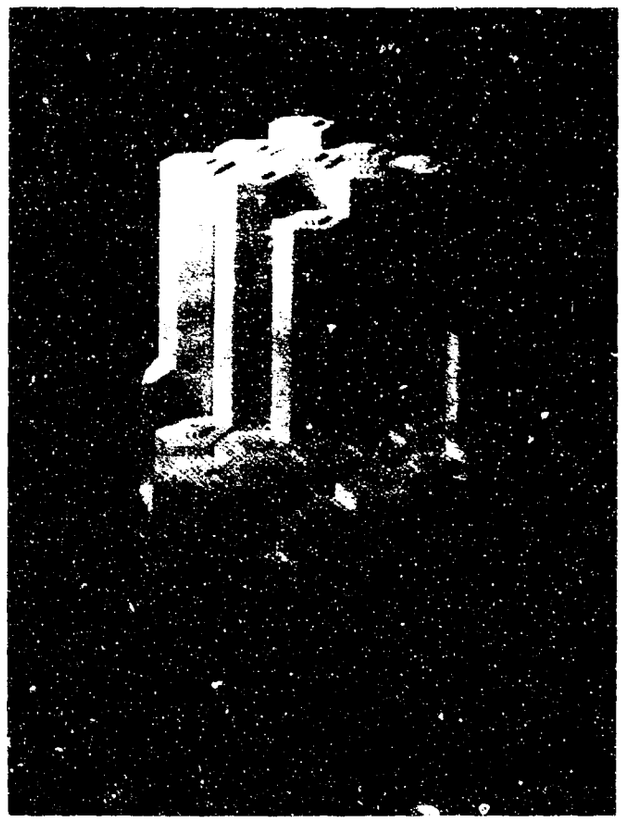

Figure 12

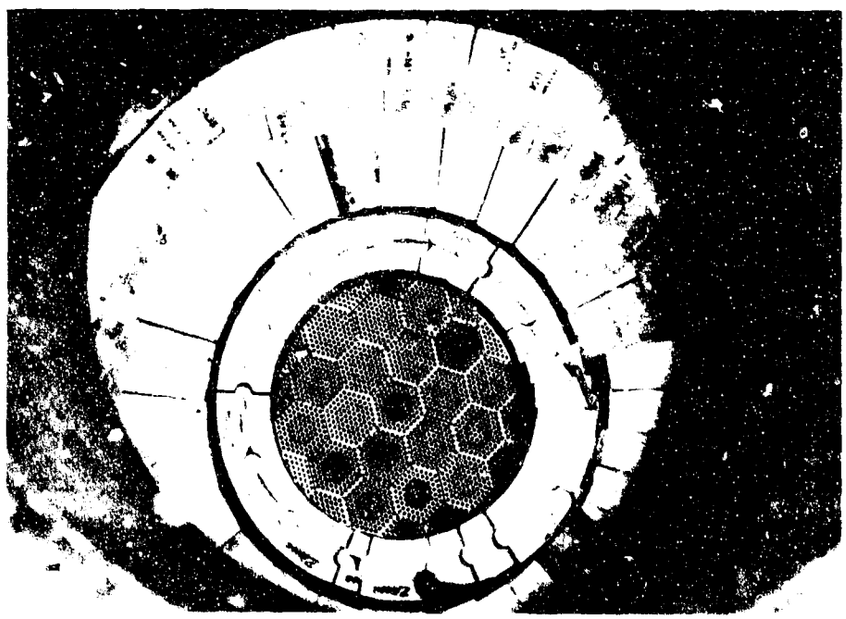

Figure 13

LABORATORY SIMULATION OF THE SERVICE NOISE ENVIRONMENT FOR SONIC-FATIGUE QUALIFICATION TESTING OF AIRCRAFT STRUCTURES

BY

Otto F. Maurer

Air Force Flight Dynamics Laboratory
Wright-Patterson AFB, Ohio

LABORATORY SIMULATION OF THE SERVICE NOISE ENVIRONMENT FOR SONIC FATIGUE QUALIFICATION TESTING OF AIRCRAFT STRUCTURES

Otto F. Maurer

ABSTRACT

A combined analytical, experimental approach is described by which it was shown that the noise fields of jet and rocket engines can be closely simulated in the laboratory. This is done for the purpose of qualifying the sonic fatigue endurance of full scale vehicular structures over the complete service life. The conditions for a test time reduction are discussed. The cost and time savings compared to previous approaches of testing in the true noise environment of the jet and rocket engines are pointed out. The described test method also can be employed for sonic fatigue design and development testing and thus may contribute to optimize structural designs from a strength to weight ratio standpoint.

BIOGRAPHY

Otto F. Maurer was born in Plochingen, Germany. He studied mechanical and aeronautical engineering at the University of Stuttgart, from where he received the degree Diplom-Ingenieur (equivalent M.S.). He became research assistant at the German Helicopter Society. There he worked primarily in the dynamics and aerodynamics of rotary wing aircraft. After spending a year in the aircraft industry he joined the Aircraft Laboratory, later Air Force Flight Dynamics Laboratory at Wright-Patterson Air Force Base. There he worked in the areas of dynamics, acoustics and sonic fatigue. Mr. Maurer is the author of several papers in the fields of rotary wing aircraft, aircraft vibration, and sonic fatigue.

INTRODUCTION

An environment which has plagued aircraft designers from various aspects is the high intensity noise field radiated from the jet efflux of turbojet and rocket engines. With the use of more and more powerful engines, structural fatigue caused by the noise started to become a serious structural problem and, consequently, the subject of extensive research efforts. Yet, because of the limitations inherent in the theoretical approaches, experimentation in small acoustic test facilities is still standard practice to select and obtain design information for structural components to withstand this environment. The fact that the laboratory fields are different from those acting on the structure in service, and the fact that changes in conditions are encountered by disconnecting the components from their surrounding structure leave some doubts as to the adequacy of the designs thus selected. Therefore, qualification of a full scale structural section to the service noise environment, becomes a necessity for most aerospace structures. It was generally accepted as a fact that the service noise field could not be approximated well enough in the laboratory; thus sound induced fatigue qualification of the endurance of full scale aerospace structural sections was performed in the true service noise environment. Frequently a complete prototype aircraft was used for this purpose, or an open engine test stand was constructed in which the engine together with the structure to be tested was mounted. Figure 1 shows a typical arrangement for an engine stand sonic fatigue test. High cost of operating the engines limited such tests to a few hours. The information obtained from the resulting data was sufficient to point out necessary design modifications, and a qualification of the structure to the time of the first major maintenance inspection could be obtained. However, no information resulted as to any sonic fatigue failures which might appear later over the total service life of the structure.

With the availability of the large chamber of the AFFDL Sonic Test Facility, which is also a research tool, the question arose as to the possibility of replacing costly full scale sonic fatigue tests in the service environment by less expensive laboratory tests, which in addition would be representative of the complete design service life of the structure. The opportunity to investigate several aspects of this problem presented itself, in particular the possibility of test time compression. It was possible to reduce the test time from 900 hours to 58 hours, or by a time compression factor of approximately 16, with the resulting obvious savings in time and savings of many thousands of dollars.

GENERAL APPROACH

Sound induced structural fatigue may be briefly described as a consequence of an accumulation of stress cycles caused by dynamic structural responses, which are excited by a randomly fluctuating

pressure field. For this reason a sonic fatigue qualification test is primarily concerned with simulating the structural responses over a sufficient length of time.

Depending on the information which is available about the noise environment and its effects on the structure, a sonic fatigue test conceivably could be approached from several viewpoints. If, for instance, the structural responses resulting in the service environment were known in detail, the simulation of such responses regardless of the type of excitation would be sufficient to perform a valid test. On the other hand, if the service sound field over the area where the structure is located can be described and simulated in all its parameters, the resulting responses of the test article, which is inserted into this dynamic pressure field, would be identical to those generated by the true environment. Unfortunately in very few instances is sufficient information available so that the design of a test cannot be based on either of these approaches.

As was the case in the test which prompted this investigation, the information that is frequently accessible consists of fragmentary data about several local responses and local parameters of the sound field. Thus the designer of a qualification test is essentially faced with reproducing and matching such known quantities.

For the wing flap section which was tested in the AFFDL Sonic Test Facility, strain and acceleration response spectra at the 62 locations of Figure 2 together with the noise spectra at 13 points as shown in Figure 3 were available in the form given in Figure 4. Also, the instantaneous value probability densities of several responses and local excitations were given. These response and excitation probabilities taken from the true service field exhibit close to normal distribution characteristics (Figure 5). From these data it can be deduced that the structure responds in the service environment over large portions in a linear fashion. Because of the dynamic coupling of the various structural elements it is concluded that, if the given response and excitation spectra could be simulated in the facility at this limited number of points, sufficient assurance would be provided that the sound field over the structure is in close agreement with the true environment. Thus, lack of knowledge of the space-time correlation or cross-spectra of the service noise field and their neglect of direct simulation would be compensated.

GENERATION OF RANDOM NOISE

This general approach required that several intermediate problems be solved, the first of which was the requirement for generating random noise with the thirty-five sound sources of the test facility. These sound generators may be described as discrete tone sirens, twenty-five

of which are located in a fixed position. Ten sirens can be moved as one unit. The control and drive system of these sound sources permit a certain latitude in control functions. Thus, it is possible by rapidly sweeping the siren frequency to generate a frequency modulation of the form shown in Figure 6. If the siren is frequency modulated in a random fashion the resulting continuous narrow band spectrum is proportional to the probability density of the modulating function.

In addition to the frequency modulation capability, a type of air valve in the siren permits the adjustment of the amplitude of the siren output. If this valve is rapidly oscillated in a random fashion, a random amplitude modulation can be superimposed on the already frequency modulated siren sound signal; thus an additional randomization and broadening of the individual siren bandwidth can be introduced.

Under the assumption that the siren generates a constant sound amplitude over its complete frequency operating range, it should be possible to generate any type of broadband spectrum desired. This requires that several sirens be operated as described above with different center frequencies that are so spaced that their individual modulated bands are adjacent to each other as shown in Figure 7. To actually control the sirens for this purpose, random noise signals recorded from an electronic noise generator were introduced into the siren controls in the manner shown in Figure 8. To these random noise signals, with zero means, constant voltages had to be superimposed, which determined the center frequencies of the sirens. These combined control signals resulted in the random variations of the siren frequencies around the mean or center frequencies of Figure 9.

Experiments indicated that in the horn mouth of an individual siren the narrow band sound output approached the theoretically calculated values; however a certain distance from the siren the spectrum was distorted. As was expected, the broadband noise obtained with the simultaneous operation of several sirens was nowhere close to the calculated values. The experiments proved, however, that a noise field could be established in the chamber which would be controllable, if various other factors were taken into account.

SIMULATION OF THE NOISE FIELD

The main factors which determine the sound field are the radiation directivities of the sirens and their individual locations. In addition, reflection from the chamber floor and from other objects in the test chamber, the multiple reflection and scattering from the test article and high intensity sound propagation effects strongly determine the properties of the sound field.

For instance, the fixed location of the sirens in the room is considered the only influencing factor for generating a desired noise field. By programming the thirty-five sirens and assigning each to contribute a certain part of the broadband spectrum, approximately 10^{40} possibilities are open of selecting a particular arrangement. It can be seen that inclusion of the other influences mentioned above raises the number of parameters which need to be considered to an even more untractable amount. However, a combined experimental treatment of these variables proved helpful in reducing them to a practical number.

In order to determine the general area in the chamber where the sound pressure levels, which were required for the test, could be reached, a brief acoustic survey was made. Several of the sirens were operated in sequence in a slow, pure-tone sweep such that the total required spectrum was covered. With the measured sound data thus obtained at various locations in the room, it was possible to interpolate the influence of the sound generators which were not operated. A general location of the test article was determined by this method which also resulted in some qualitative information as to the possible future center frequency and bandwidth assignment for the individual sirens. In the chamber area thus determined the same number of microphones was positioned as the number of local spectra known from the jet noise environment. The microphones were placed at the same heights with respect to the floor, and the same distances to each other, as they were mounted when the service noise data were obtained. The service noise spectra were then reduced by about 5 dB in order to compensate approximately for the reflections from the test structure. Based on the results from the previous experiment the sirens were programmed for their individual operating range and progressively adjusted to generate the reduced spectra at the 13 microphones.

After this first step to approximate the given noise data, the test article was installed with all transducers mounted. The discrete frequency survey was repeated with various sirens in order to determine any change in the shape of the local spectra which might have occurred due to the presence of the test structure. This was done at sound pressure levels below those which are usually thought of as contributing appreciably to the accumulation of fatigue damage. The effects of one siren on the sound field at one point on the surface of the test article is shown in Figure 11. One notices the marked difference between the discrete tone sweep spectrum at the structural location and in the siren horn mouth. The marked drop of sound pressure at many frequencies can be explained by the multiple reflections between the chamber floor and test article and the resulting wave interferences.

This type of information was obtained for all sirens at all sound monitoring points on the structure. Comparing these results with the

available service noise spectra at the same location on the structure gave a very good indication into which range of its complete operational spectrum each siren could be placed. This procedure was repeated with slightly different locations of the test article in order to obtain additional information for later application.

Then the sirens were programmed and operated at low sound pressure levels. It was expected that now the general shape of the spectra near most of the surface measuring points would be close to those desired yet reduced by an equal amount. The analyzed measurements confirmed that the shape of the spectra at 10 points was within the expectations. However, the microphones on the leading edge indicated sound levels in excess of those which were required. This was already suspected from the results of the preceding experiments. Therefore an acoustic baffle was placed under the leading edge in order to reduce the sound field over this part of the structure (Figure 12). The measured strain gage and accelerometer data generally exhibited slightly different spectral characteristics. The experiment had to be repeated several times at different locations. Various modifications in the siren program had to be made until all sound spectra and most of the strain and acceleration spectra were well within plus or minus 2 decibels of the desired shapes (Figure 13).

After raising the sound pressure levels of the individual sirens such that the service environment would be simulated, only a few minor adjustments in the siren program were required to obtain the desired objective. Figure 14 shows the test specimen in the large test chamber of the Sonic Fatigue Facility in its final position.

REDUCTION OF TEST TIME

To qualify the structure for the total exposure to the maximum noise levels it experiences over the complete design service life would have required 900 hours of testing. Therefore an investigation was made into the possibility of accelerating the test by exciting the structure with higher than the actual service noise spectrum levels.

A rational basis for such a test time reduction was found. If applied to the complete structure, the following two assumptions would have to be made: that the structure is composed essentially of one type of material and all structural components respond proportionally to the excitation; and that the Palmgren-Miner fatigue accumulation hypothesis is valid. Then the relationship between test time reduction and increase in sound pressure can be expressed by the formula shown in Figure 15a. This says that the logarithm of the ratio of the reduced test time T_A to the test time T_S in the service environment is proportional to the difference in sound pressure levels (in decibels) times a

material constant. This constant is generally a negative number and is the exponent of the S-N fatigue curve.

If this approach is applied to the present problem and if, for instance, the sound spectra over the test article can be raised by 4 decibels, then with $\alpha = -6$, a reduction in test time by a factor of 16 could be obtained. That is, the 900 hours of exposure to maximum sound pressure levels during the complete design service life can be replaced by 58 hours of testing time in the higher level simulated environment. The equivalent time of exposure would have to be evaluated separately for components that consist of different materials and have a different α. Also, any nonlinearities in local structural responses would have to be treated on a different basis.

For the experimental verification of this approach the air pressure of the sirens was raised to produce an increase of 4 dB in the spectra at the structural measuring points. After a slight correction of the siren program the resulting structural responses were evaluated for linearity by comparing their instantaneous value probabilities which resulted from the simulated service environment and from the increased excitation levels. Slightly nonlinear responses were observed at only four of the 62 transducer locations. This exhibited itself in deviations between the two probability density curves as shown in Figure 15. Most response signals, however, were close and similar to the expected values as shown in Figure 16. It was decided to continue the test on this reduced time basis. The assumption that the total structure is composed of aluminum then required that the equivalent service time to failure for the titanium and reinforced fiberglass components be calculated using the actual material S-N curves and corresponding values of α. This of course would only be necessary if actual failures occurred in such components.

QUALIFICATION TEST AND RESULTS

After completion of these preparations the actual qualification test was performed. The wing flap section was exposed for 63 hours to the previously established high intensity noise field. The acoustic noise environment was monitored continuously over the complete test duration. Recordings of all transducer signals were made once every hour. Frequent inspections of the test article were performed in order to detect any failures which might occur. Partial disassembly of the test structure was necessary for each inspection such that failures of interior components could be exposed. Frequently dye penetrants were used to make small cracks visible or to check whether an actual crack existed.

Over the total test duration, 56 structural fatigue failures were discovered. Most of the failures occurred in the interior structure. An individual evaluation of these failures showed that most damage in

load carrying components appeared in the last third of the complete design service life of the aircraft. Figure 17 shows the first visible state of a sonic fatigue failure in a spar shear web. Another more progressed state is depicted in Figure 18. The final damage is shown in Figure 19. The damage shown in these pictures is typical of the majority of the failures which occurred during the test.

If any of the failures progressed to a state as shown in Figure 19 before the last fourth of the complete test time, the damaged component was repaired or replaced. Figure 20 shows the damage of a flap rib which occurred after repair of an identical first failure.

Final analysis of these typical failures, taking into account the measured stress responses, permitted the proposal of changes in the design [illegible]. Changes were specified in such a way that they could be incorporated during normal maintenance of the aircraft. In some cases retrofit by attrition was recommended.

CONCLUSIONS

The results of the test and their detailed evaluation allowed recommendations to be made as to modifications of inspection procedures and inspection schedules for the last third of the design service life.

The significance of the results obtained from this test and the preceding investigations is not limited to the particular structure that was tested. Moreover, the essence of these results lies in the fact that they show that sonic fatigue tests can be performed in the laboratory and that the actual service conditions can be closely approximated, even for a large structural section. The resulting implications are that by conducting such laboratory tests on a prototype structure or in the early construction stages of an aircraft, information can be obtained that can fundamentally influence the final structural design as well as eliminate subsequent retrofits and their additional costs.

The present practice of testing only small individual components, which are taken out of the compound of the surrounding structure, in a noise environment which bears no resemblance to the service field, frequently results in poorly designed components. The strength to weight ratio usually further decreases during the so-called development cycle. Added modifications and fixes raise the structural weight without presenting any assurance of increased reliability with respect to the total service life. The laboratory test approach for sonic fatigue which has been proven feasible and can be performed with relatively inexpensive means will not only increase structural reliability and therefore reduce inspection and maintenance costs, but will also result in structural designs with optimum strength to weight ratios. In addition, reliable information about the sonic fatigue endurance over the total service life can be obtained.

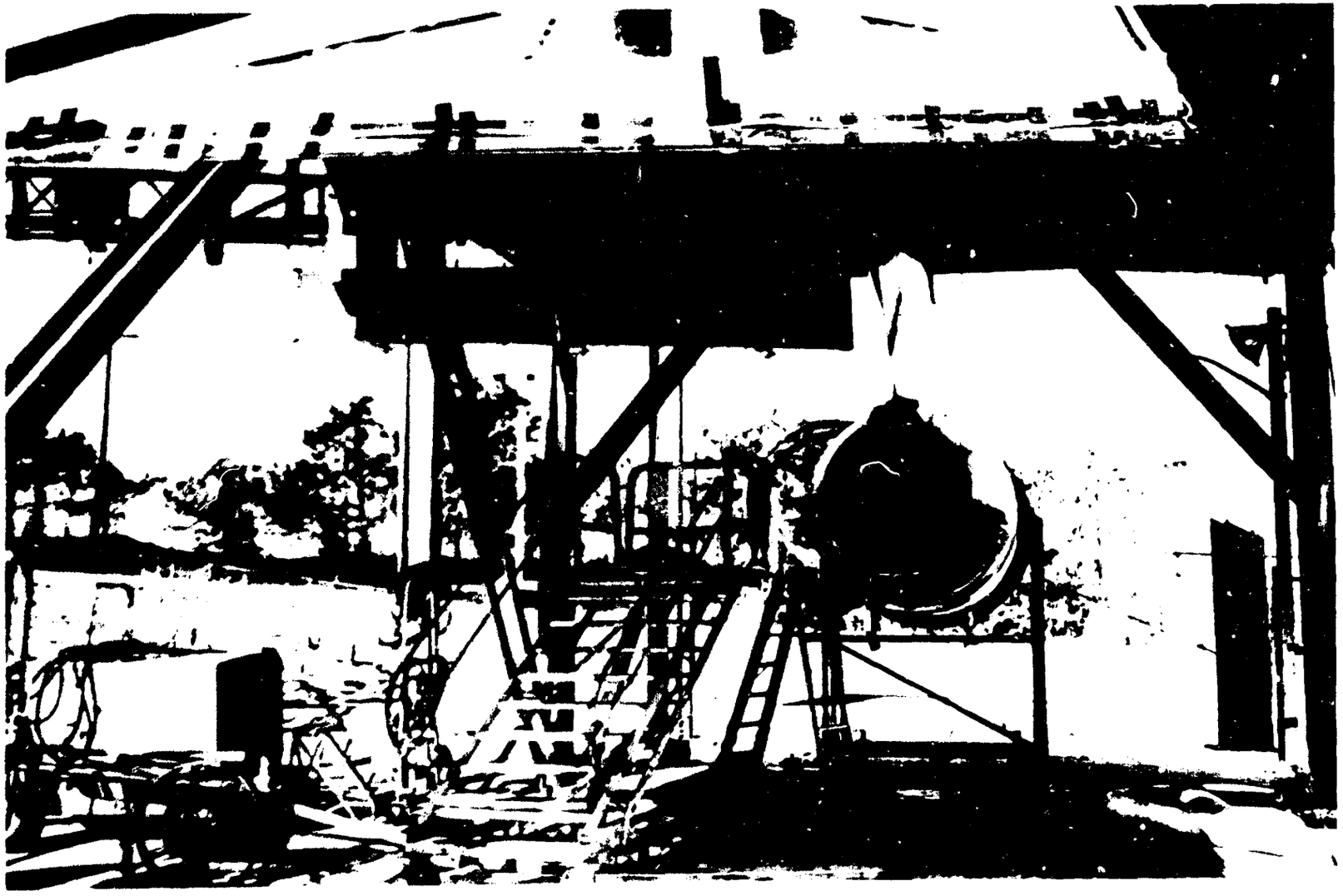

Figure 1. Engine test stand sonic fatigue setup.

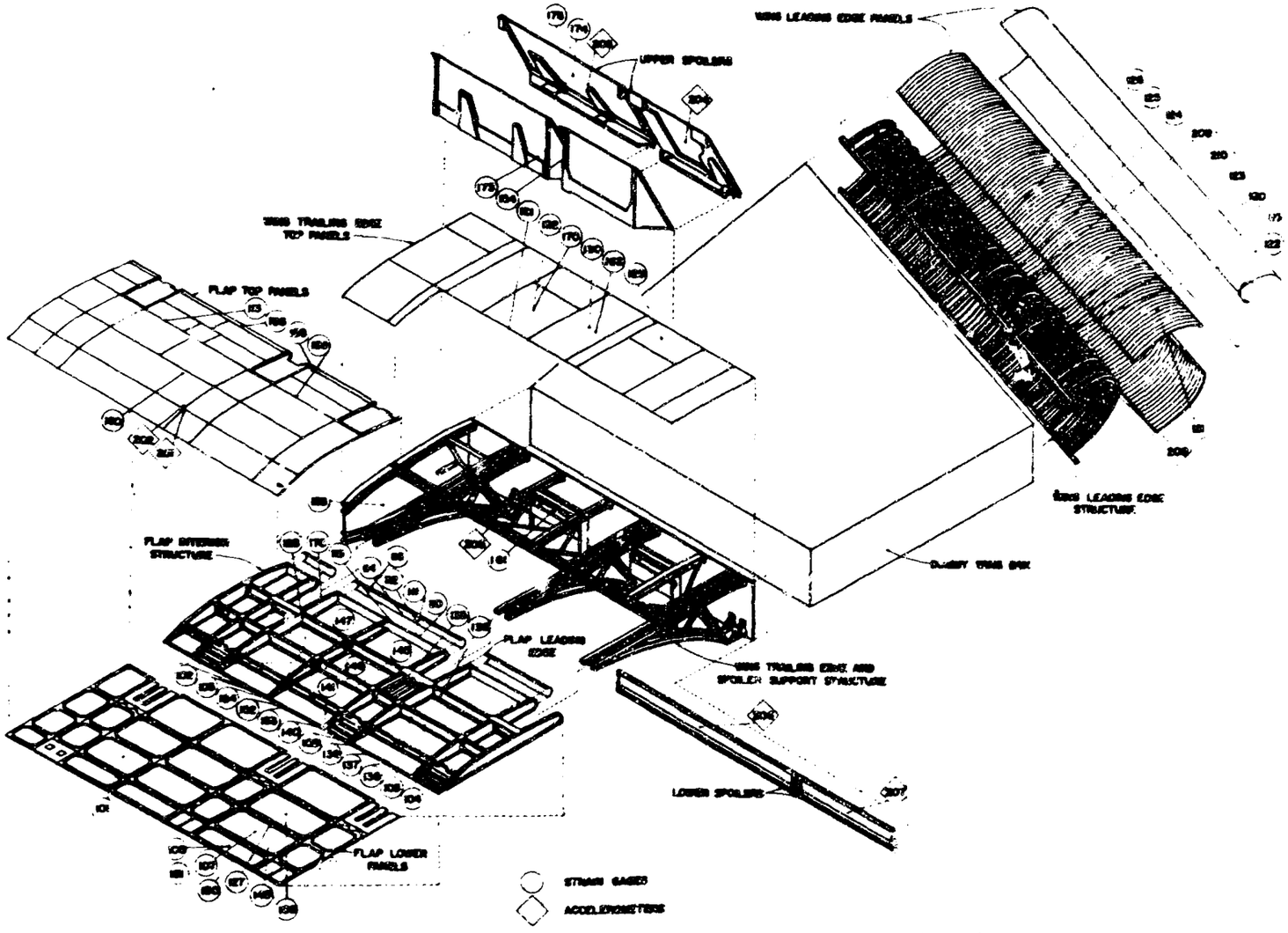

Figure 2. Transducer Locations on Test Structure

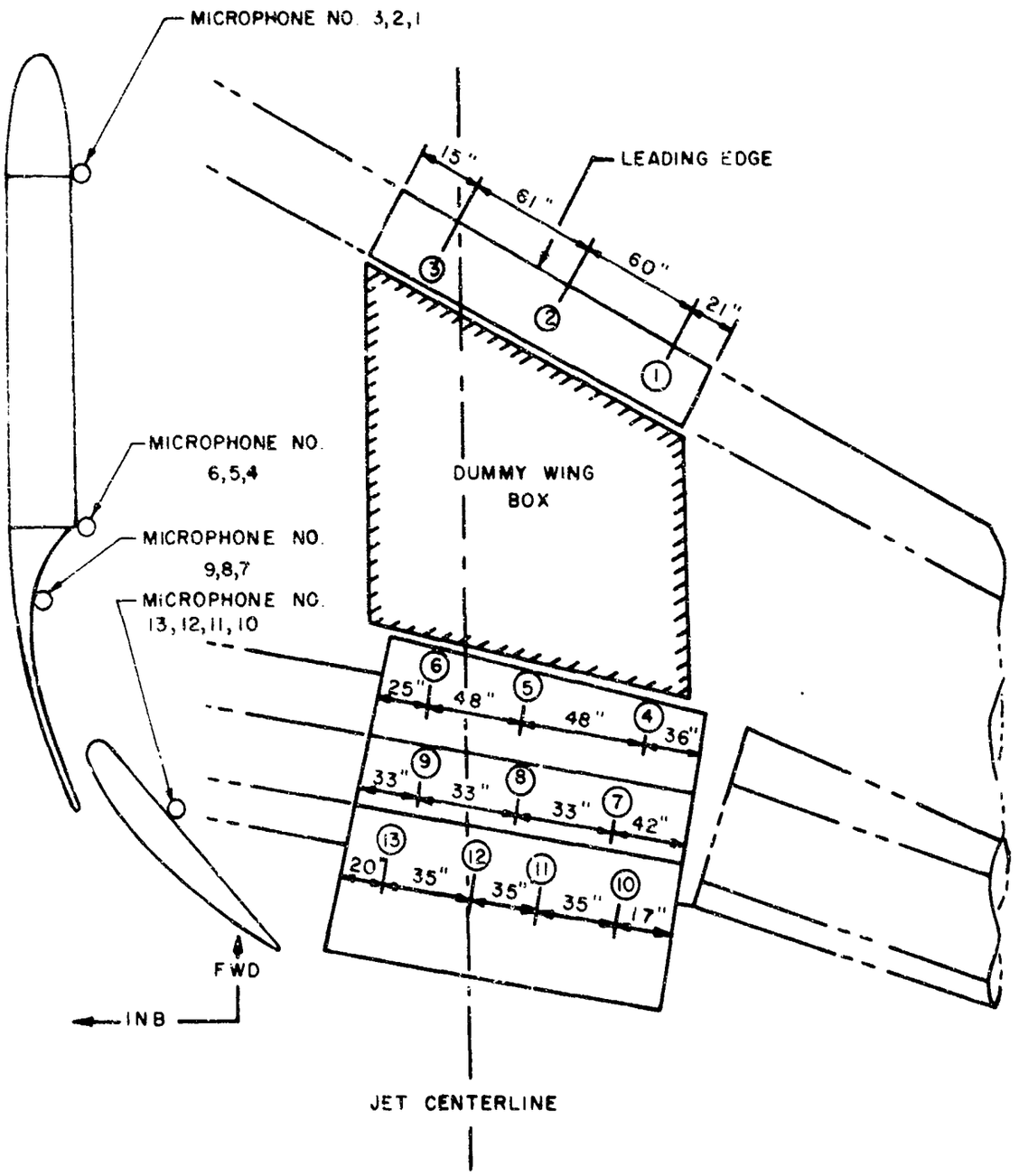

Figure 3. Microphone Positions on Structural Surface.

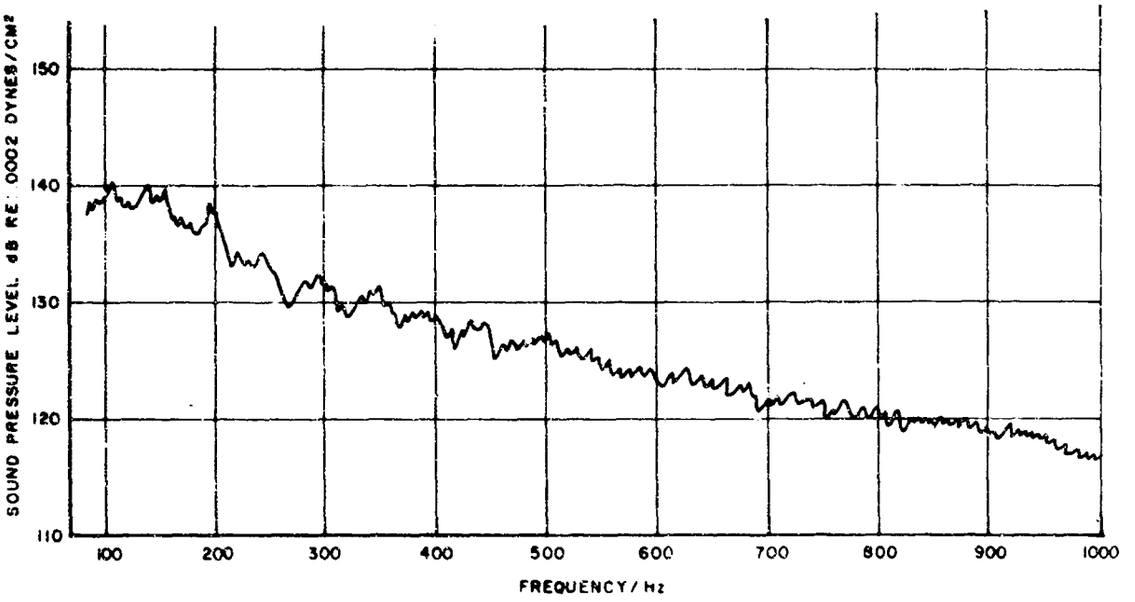

Figure 4a. Service Noise Spectrum at Microphone 13

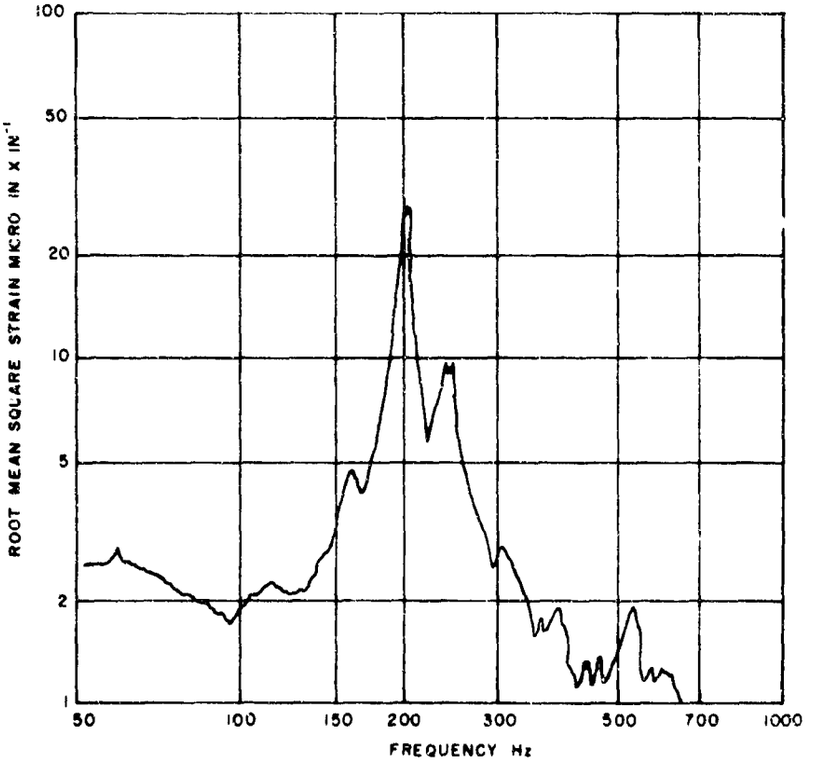

Figure 4b. Typical Strain Response Spectrum Resulting from Service Noise Environment.

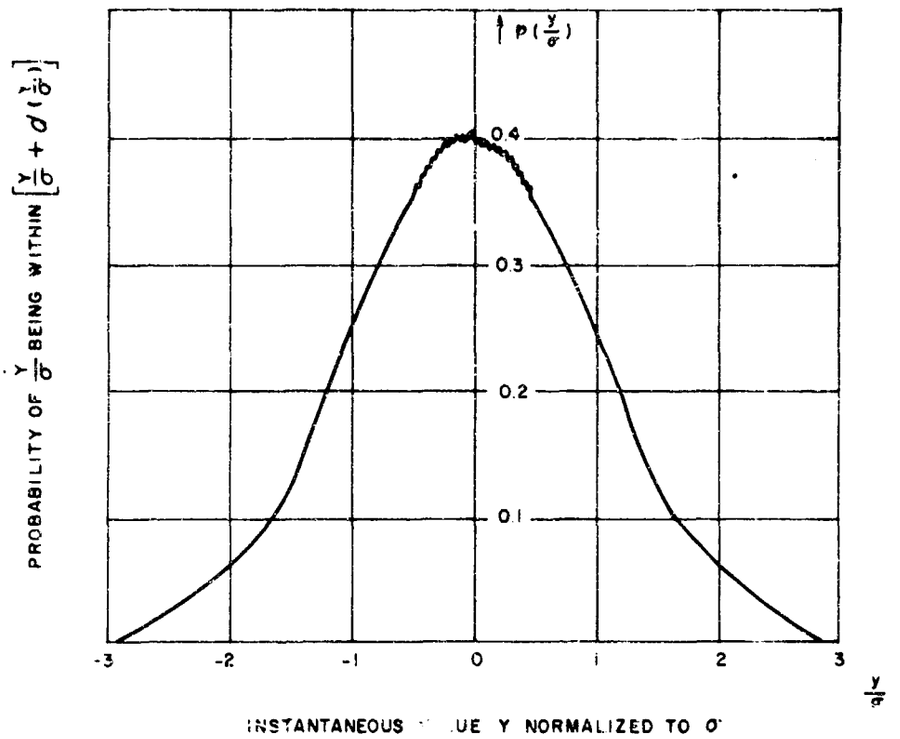

Figure 5. Instantaneous Value Probability of Strains and Service Noise Field.

$$C(t) = V \cos(2\pi f_c t + \psi(t))$$

$\psi(t)$ = RANDOM MODULATING FUNCTION

$$f_i = f_c + \frac{1}{2\pi}\frac{d\psi(t)}{dt}$$ INSTANTANEOUS FREQUENCY

$$\frac{1}{2\pi}\frac{d^2\psi(t)}{dt^2} \leq 270\ \frac{Hz}{sec}$$ ACCELERATION LIMIT OF SIREN

$$C(t) = V(t)\cos(2\pi f_c t + \psi(t))$$

$V(t)$ = AMPLITUDE MODULATION, BANDWIDTH-

LIMIT 0 – 30 Hz

Figure 6. Random Frequency and Amplitude Modulation.

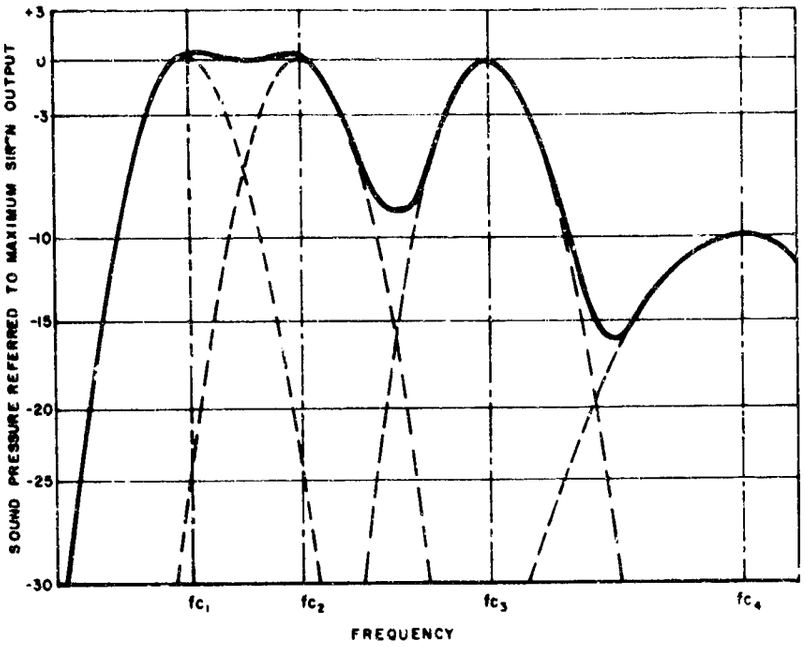

Figure 7. Calculated Broadband Spectrum Composed of the Narrow Bands of Four Frequency-Modulated Sirens.

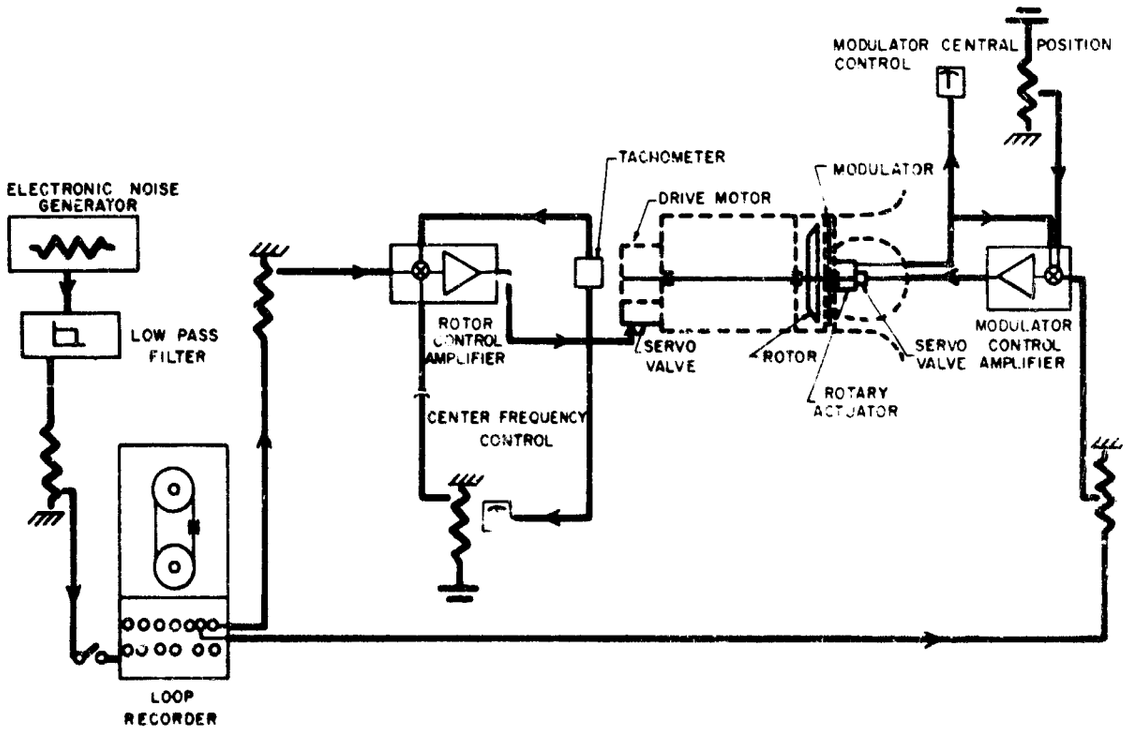

Figure 8. Block Diagram of Siren Control Arrangement for Random Frequency and Amplitude Modulation.

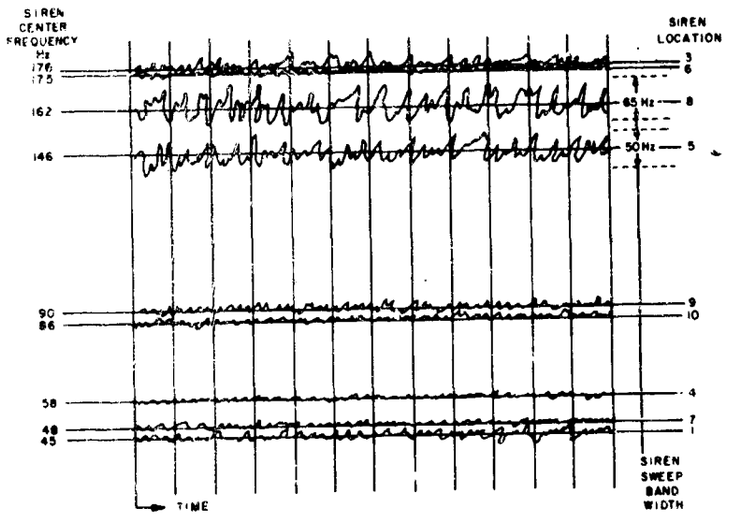

Figure 9. Typical Siren Control Signals.

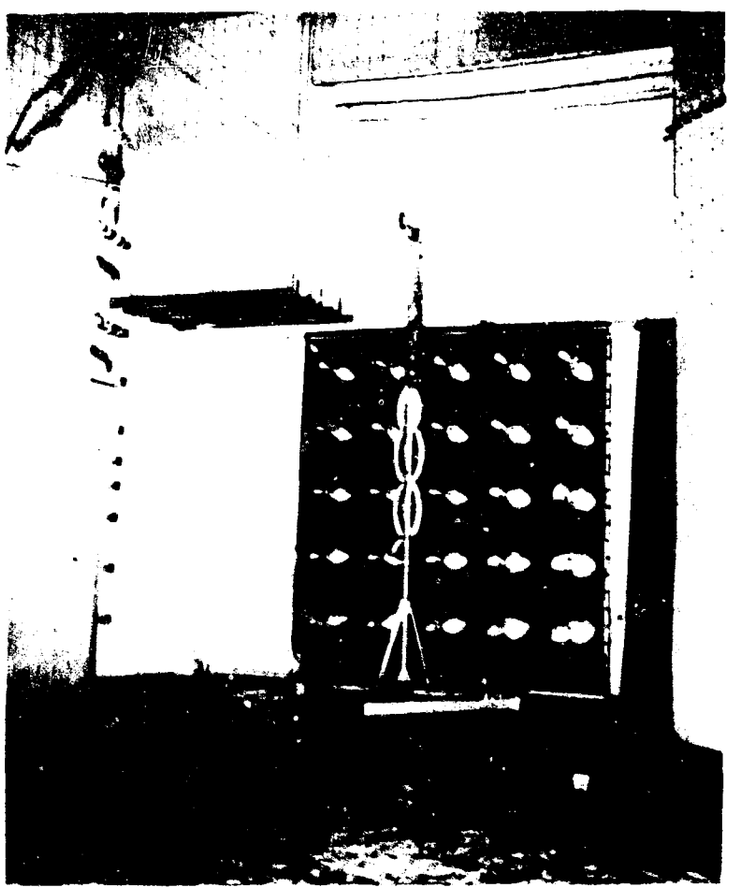

Figure 10. 25 Sirens with Fixed Location.

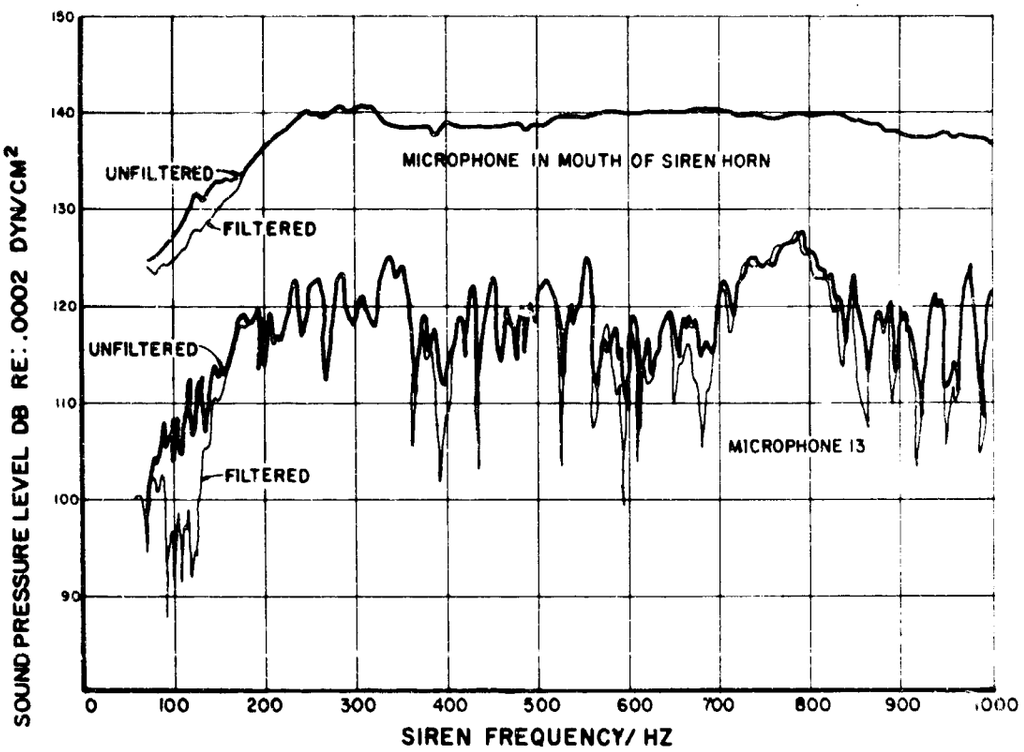

Figure 11. Discrete Frequency Sound Survey for One Siren and One Surface Point.

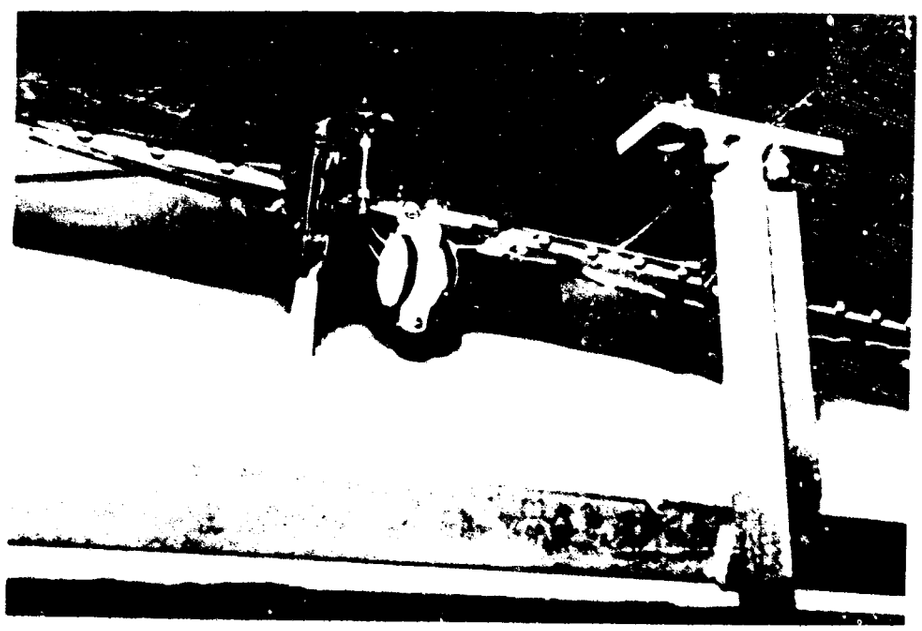

Figure 12. Acoustic Baffle under Leading Edge.

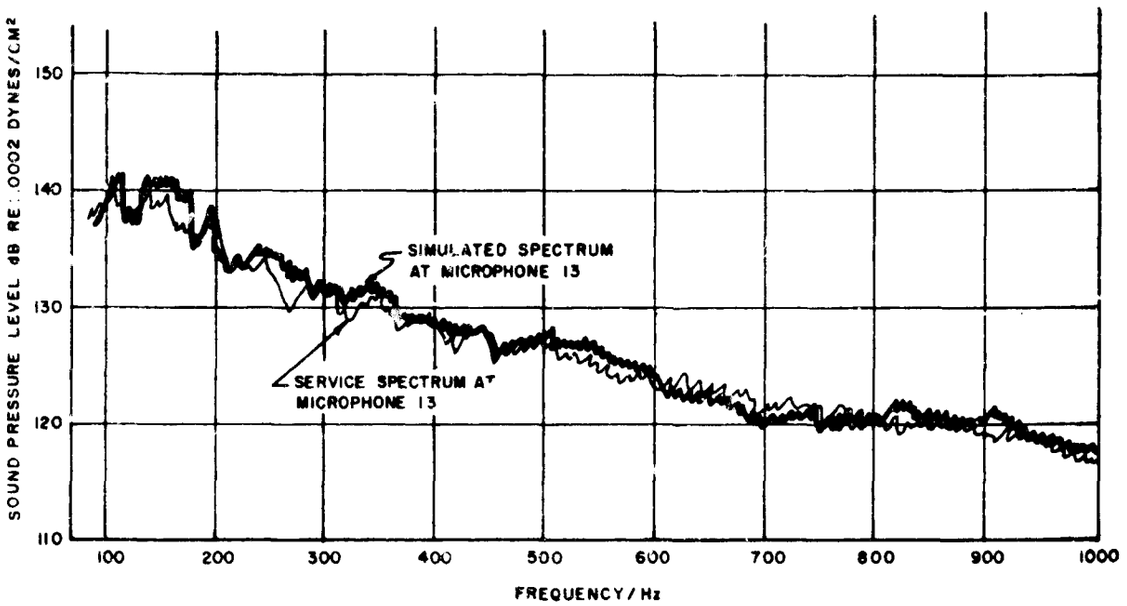

Figure 13. Typical Simulated Noise Spectrum Compared to Service Noise Spectrum at Identical Location.

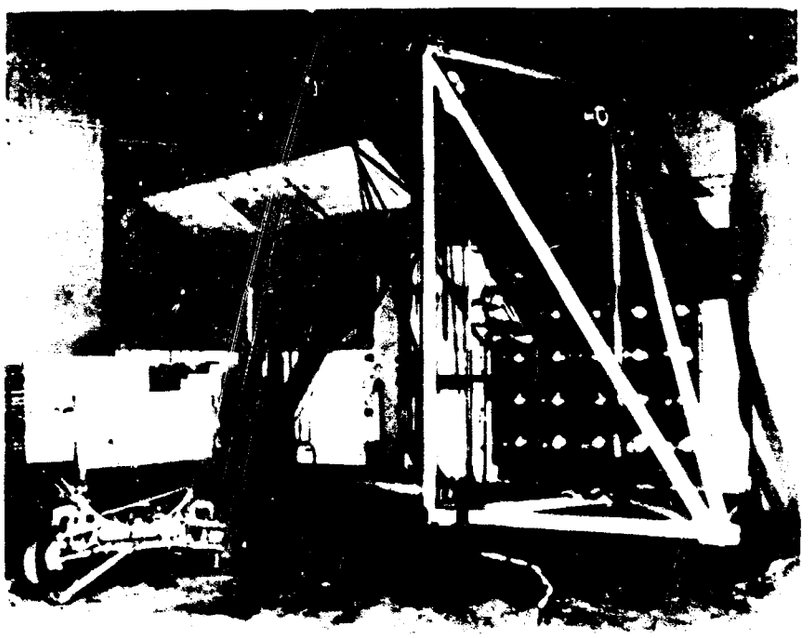

Figure 14. Final Location of Test Structure.

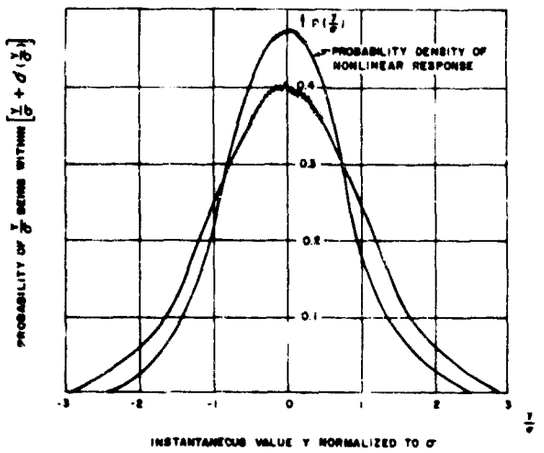

Figure 15. Comparison of Probability Densities for Linear and Non-Linear Response.

$$10 \log \frac{T_A}{T_S} = \frac{\alpha}{2}(SPL_S - SPL_A)$$

WHERE:

T_A = REDUCED TEST TIME

T_S = EQUIVALENT TIME OF SERVICE EXPOSURE

α = EXPONENT OF ANALYTICAL EXPRESSION FOR S-N CURVE ($|\alpha|<0$)

SPL_S = NARROW BAND SERVICE NOISE LEVEL IN dB RE. 0.0002 DYNES/CM^2

SPL_A = REQUIRED NOISE LEVEL FOR TEST TIME REDUCTION IN dB

Figure 15a. Test Time Reduction.

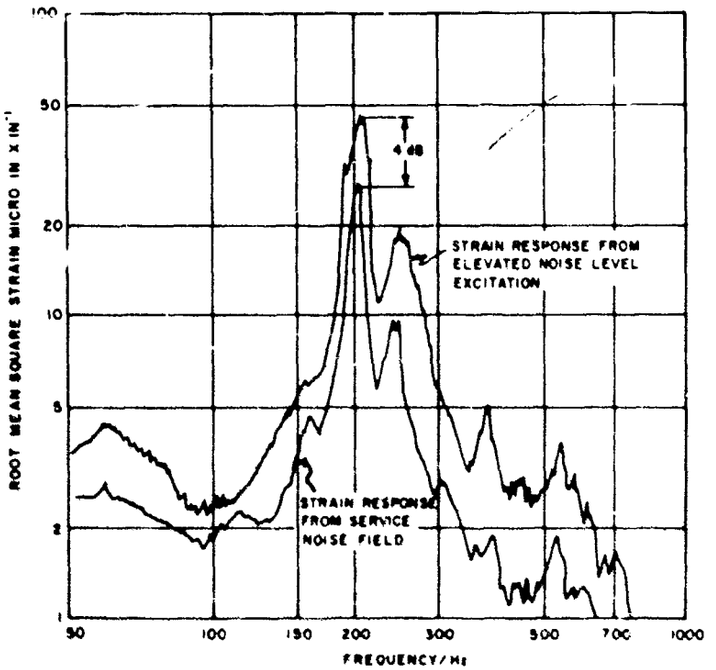

Figure 16. Comparison of Typical Strain Responses Resulting from the Service and Elevated Noise Field.

Figure 17. Initial Sonic Fatigue Cracks in Spar Web.

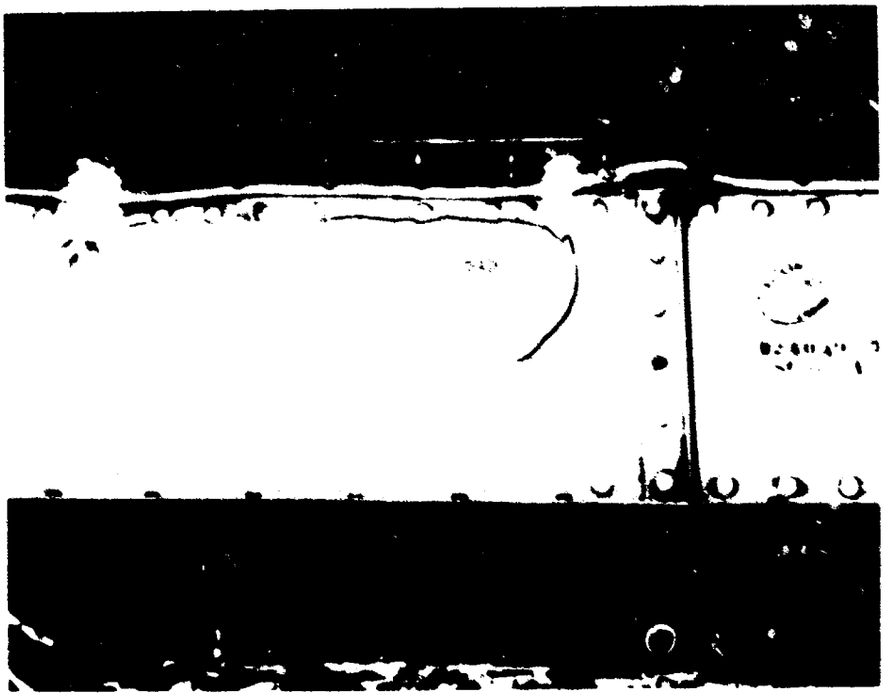

Figure 18. Progressed State of Crack in Spar Web.

Figure 19. Complete Damage of Spar Web.

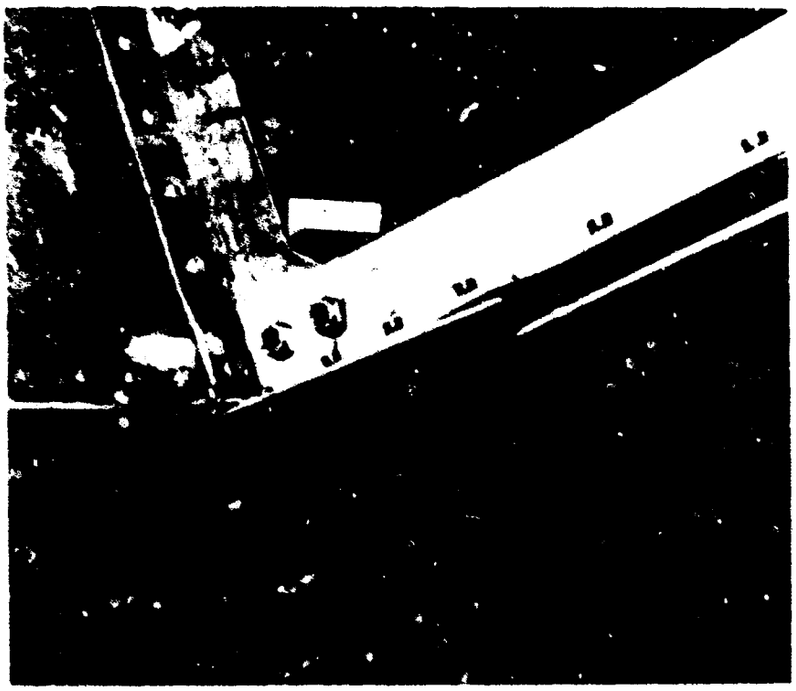

Figure 20. Failure of Rib after Repair.

STUDIES IN ORGANOMETALLIC CHEMISTRY

A NOVEL SYNTHESIS OF RUTHENOCENE(S)

By

George J. Gauthier, 1Lt, USAF

The Frank J. Seiler Research Laboratory
US Air Force Academy
Colorado Springs, Colorado 80840

STUDIES IN ORGANOMETALLIC CHEMISTRY
A NOVEL SYNTHESIS OF RUTHENOCENE(S)

1st Lt George J. Gauthier

ABSTRACT

In the last fifteen years, numerous substituted "sandwich-type" compounds called metallocenes have been synthesized, characterized, and polymerized yielding new types of metal containing polymers. Some of these metallocenes, particularly those of the ferrocene series, have been shown to possess desirable properties for use as catalysts or inhibitors in the polymerization of olefins, catalysts for the combustion of hydrocarbons, and for use as ablative materials. Their chemical properties as well as their thermal, oxidative, and hydrolytic stability also suggest that they might be useful as heat and light stable protective coatings, as reducing agents, as lubricants, and as free radical scavengers.

Except for exploratory studies, however, the cost and difficulties involved in the preparation and purification of many metallocenes have limited most work to the ferrocene series. Consequently, many potentially useful materials have not been prepared or studied. In particular, the interesting series of ruthenocenes has received too little attention.

This report describes the successful application of a novel ligand exchange reaction discovered at FJSRL to the synthesis of ruthenocene(s). A description of the parameters influencing the reaction and its application to the synthesis of several substituted ruthenocenes is also included.

BIOGRAPHY

1st Lt George J. Gauthier is assigned to the Frank J. Seiler Research Laboratory, Office of Aerospace Research, United States Air Force Academy, Colorado, as a research chemist.

Lt Gauthier reported to the Seiler Research Laboratory for his initial active duty assignment, following completion of his graduate studies as a Category C, United States Air Force Reserve Officer.

Lt Gauthier was born in Franklin, Merrimack County, New Hampshire, on 22 July 1940. He attended parochial and public schools in Franklin, graduating from Franklin High School in 1958. In the fall of 1958 he entered the University of Notre Dame, Notre Dame, Indiana. He was graduated in June 1962, with a B.S. degree in chemistry, and commissioned a Second Lieutenant, USAF Reserve. Lt Gauthier was then given a Category C delay to attend graduate school. He entered the graduate school of the University of New Hampshire in the fall of 1962. While a graduate student, he was a research fellow supported by grants from the National Cancer Institute and National Institutes of Health. His Ph. D. in Organic Chemistry was awarded in June 1966. Lt Gauthier's research concerned the reactions of nucleophiles with pyridinium ions.

Lt Gauthier was married to the former Frances Joy Steenbergen on 27 June 1964. They have a daughter, Pamela Lee, born 19 November 1965, and a son, Mark Gerald, born 14 June 1967.

Lt Gauthier is a member of the American Chemical Society and the Division of Organic Chemistry, American Chemical Society. He is also a member of Sigma Xi.

Studies in Organometallic Chemistry

A Novel Synthesis of Ruthenocene(s)

I. Introduction

One of the most important classes of organometallic compounds being studied by Air Force materials research is the group of sandwich-type compounds called metallocenes (I) because of their chemical similarity to benzene. The sandwich-type metallocenes (I) often exhibit higher thermal and hydrolytic stability compared with other cyclopentadienide containing organometallic compounds (II, III) and other materials.

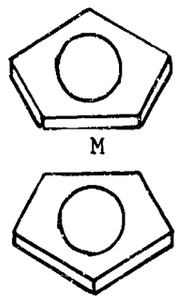

I

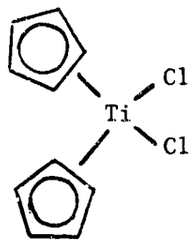

II

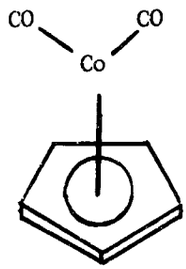

III

Many different metals (M) have been incorporated into the basic metallocene structure e.g. ferrocene (M = iron), ruthenocene (M = ruthenium), osmocene (M = osmium), cobaltocene (M = cobalt), and many others have been synthesized. The substitution of the ring protons of metallocenes by conventional organic reactions has produced many hundreds of metallocenes in the past 15 years.

Of all the sandwich-type metallocenes, the [illegible] ferrocenes has been the most widely studied. Ferrocene is inexpensive, stable, and converted easily[1,2] to a wide variety of substituted ferrocenes. Ferrocene and its derivatives have already found uses as ultraviolet absorbers for protective coatings, polymerization catalysts, additives for high temperature lubricants, reducing agents, catalysts for combustion of fuels, and antianemia drugs.[2,3]

Substituted ferrocenes have been converted to thermally stable polymers with a great diversity of physical, chemical, and mechanical properties.

While development of ferrocenes has been rapid, studies of other ever more promising metallocenes has been limited to exploratory work because of their inaccessability and expense. In particular, the interesting series of ruthenocenes has received too little attention. Substituted ruthenocenes would be expected to show even greater thermal and oxidative stability than ferrocenes but only a few have been synthesized.[4]

Presently, sandwich-type metallocenes are prepared by one of three basic methods.[2,4] The most important and widely used method involves a reaction of the cyclopentadienide anion with a metal salt.

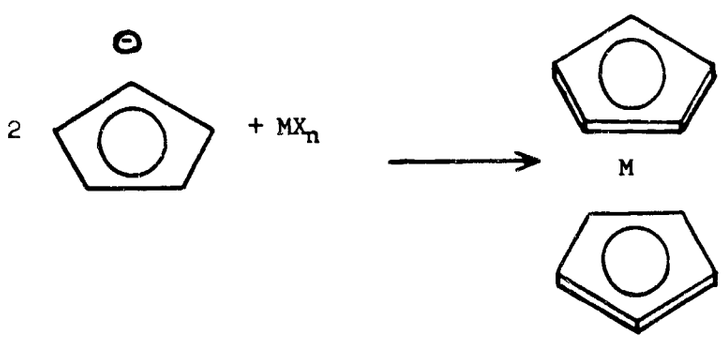

With few exceptions[4], syntheses of substituted metallocenes begin with the unsubstituted parent metallocene and proceed via conventional reactions to the desired product.

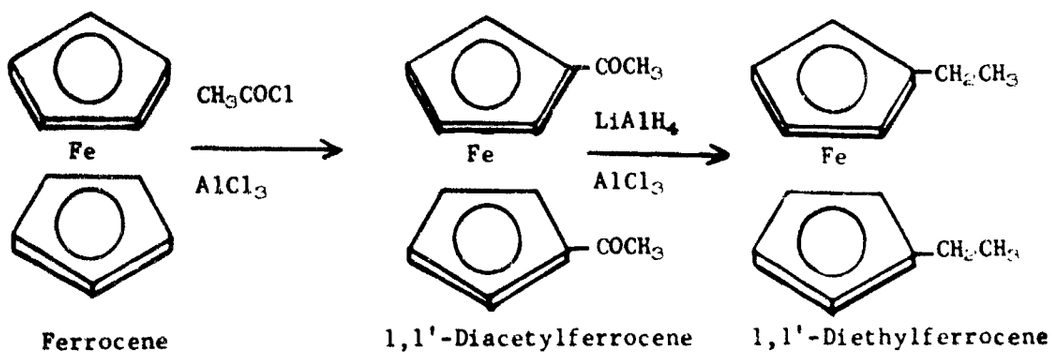

Ferrocene 1,1'-Diacetylferrocene 1,1'-Diethylferrocene

While such reactions are easily and inexpensively accomplished for ferrocene, the same reactions are accomplished with more difficulty and at considerably greater expense for ruthenocenes. Commercial ruthenocene is, for example, approximately 500 times more expensive than ferrocene. We have initiated a program at FJSRL to study new means for synthesizing substituted ruthenocenes and have discovered a novel ligand exchange reaction between ferrocene(s) and $RuCl_3$ which leads directly to the ruthenocene(s).

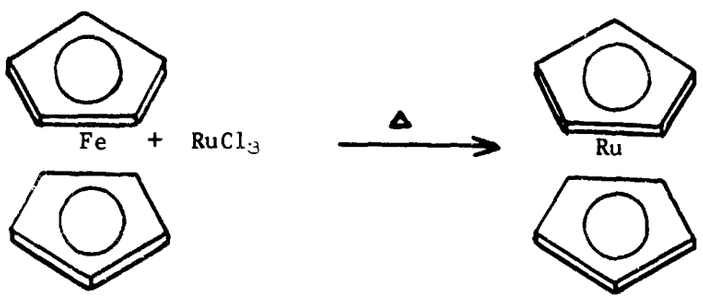

The scheme we wish to exploit involves the synthesis of a complex substituted ruthenocene by synthesis of the corresponding ferrocene followed by final reaction with $RuCl_3$.

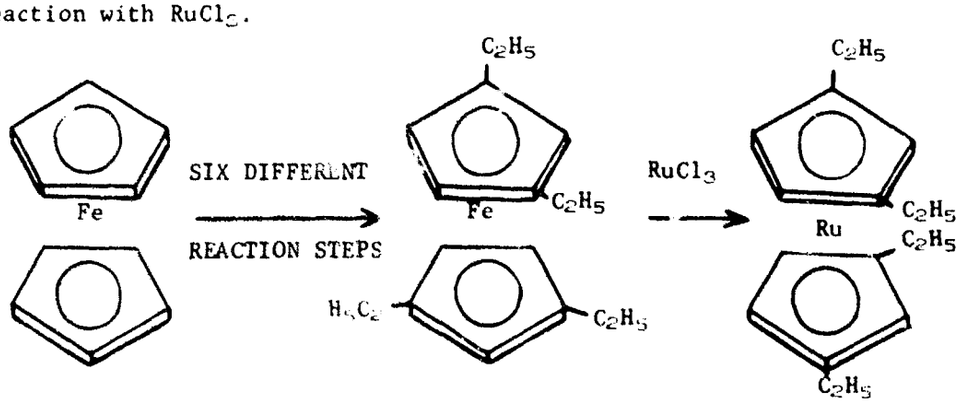

Such a scheme would eliminate the need for running several consecutive reactions on progressively more expensive ruthenocenes and only the last reaction in the sequence would involve ruthenium. We have synthesized

ruthenocene and several simple disubstituted ruthenocenes by this method and we wish to re, ort our findings of those parameters which influence this novel reaction.

II. Discussion

Two other studies supported our belief that such a ligand exchange reaction might be successful. Nesmeyanov[5] reported reactions of ferrocenes with aluminum chloride in aromatic solvents which resulted in ligand exchange of one of the cyclopentadienide rings for an aromatic solvent. Importantly, he found that electron withdrawing substituents (acetyl) hinder the reaction while electron releasing substituents (ethyl) facilitate the reaction.

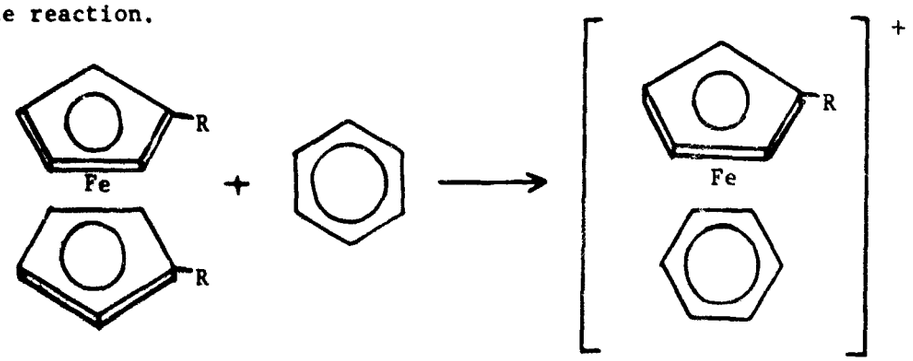

<u>% exchange of R</u> $(C_2H_5C_5H_4)_2Fe > (C_5H_5)_2Fe > (CH_3COC_5H_4)_2Fe$

Bublitz[6] reported the disproportionation of alkylferrocenes in the presence of aluminum chloride in methyl chloride solution.

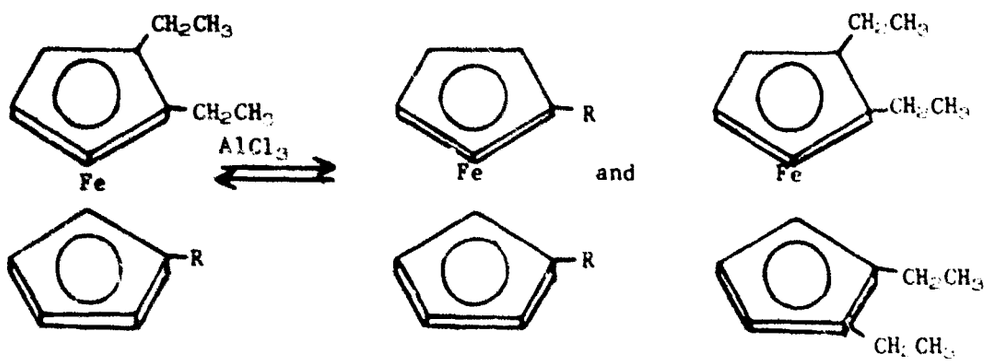

He demonstrated that the rearrangements proceeded via metal-ring cleavage rather than by ring-substituent cleavage. Unfortunately, only a few percent of the disproportionated materials were realized from his reactions.

For reasons of simplicity, most of our studies have involved the reaction of ferrocene and $RuCl_3$. The ligand exchange reaction was accomplished in the following manner.

Dry samples of ferrocene and $RuCl_3$ were mixed in a 6:1 molar ratio, and sealed in a Carius Tube under vacuum (see Figure 1). The tube was heated in an oil bath at 230-250° for 1-2 days, opened, and the metallocene mixture of ferrocene and ruthenocene separated by sublimation from inorganic contaminants and decomposition by-products. The metallocene mixture was studied by proton magnetic resonance (pmr) and gas liquid chromatography (glc) to determine the ferrocene/ruthenocene ratio. From this ratio and the total weight of the metallocene mixture, the amount of ruthenocene present was determined. The % conversion of $RuCl_3$ to ruthenocene averaged 50 ± 5 % by both pmr and glc analysis.

Ruthenocene was separated by:

a. glc and collection of the exhaust gases in tubes containing chloroform. The separation of standard mixtures of ferrocene and ruthenocene by this method resulted in an 8[illegible]-9[illegible] % recovery of available ruthenocene.

b. Preparative thin layer chromatography which resulted in a 75% recovery of available ruthenocene.

In all cases the identity and purity of collected products were established by comparison of melting points, and pmr and infrared spectra with those of authentic samples of the metallocenes.

We found that a number of factors can adversely influence the outcome of the reaction.

a. The presence of water or oxygen in the reaction tube led to complete decomposition of the metallocene.

b. Ruthenium trichloride with graphite-like properties did not react with ferrocene. Crystalline $RuCl_3$ had to be prepared by refluxing a mixture of hydrated $RuCl_3$ and thionyl chloride for several hours.

c. Because the reaction is heterogeneous (solid and liquid phase), the reaction tube had to be vigorously shaken in order to insure good mixing of the solid and liquid phases.

d. The temperature had to be carefully regulated. Temperatures above 280° C resulted in the decomposition of the metallocene while low temperatures caused the reaction to proceed sluggishly or not at all.

III. Conclusions and Future Work

The success of the exchange reaction in the synthesis of ruthenocene has caused the reaction to be applied to the direct syntheses of several symmetrically disubstituted ruthenocenes from symmetrically disubstituted ferrocenes. We have isolated a compound tentatively identified as the previously unreported 1,1'-diethylruthenocene (IV) on the basis of its proton magnetic resonance spectrum and its glc retention time. We also have evidence for the successful synthesis of the previously unreported 1,1'-dimethylruthenocene (V) and 1,1'-di-n-butylruthenocene (VI) by the ligand exchange reaction.

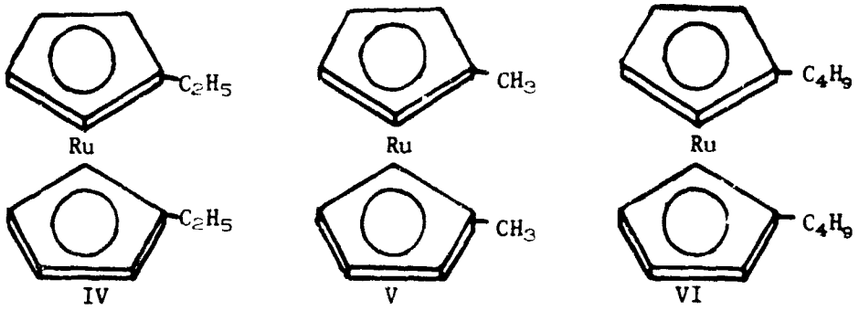

We anticipate that further studies of this novel reaction will lead to:

a. Simple reaction conditions for affecting the exchange reaction.

b. Better means for separating large quantities of the metallocene mixtures, and studies are being directed toward these ends.

Figure 1.

APPARATUS FOR LIGAND EXCHANGE REACTION

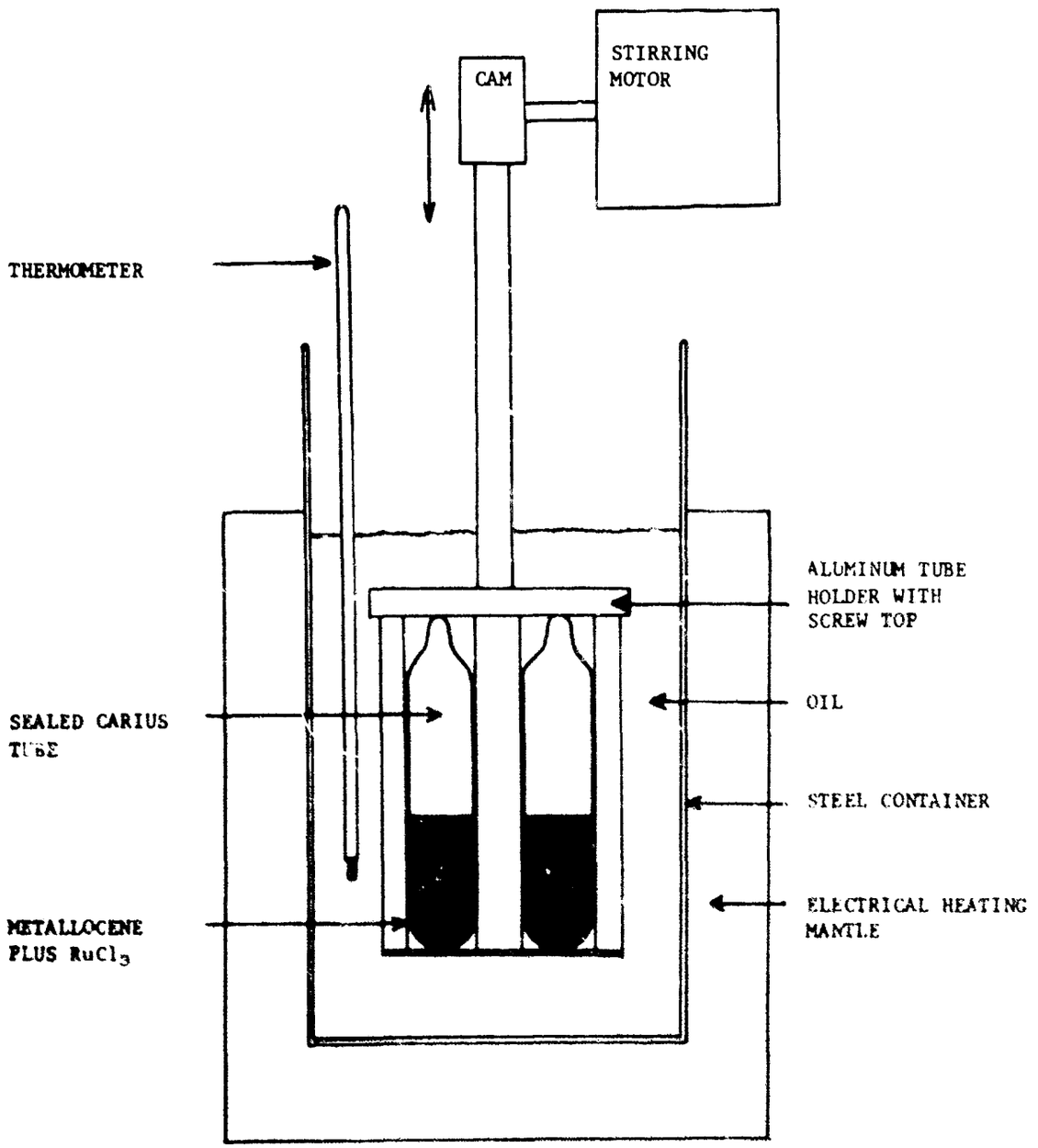

BIBLIOGRAPHY

1. M. Rausch, Can. J. Chem., 41, 1289 (1963).

2. J. Birmingham, Chem. Engr. Progress, 58, 74 (1962).

3. Metallocenes, No. 2, Arapahoe Chemicals, Boulder, Colo.

4. Chemistry of the Iron Group Metallocenes: Ferrocene, Ruthenocene, Osmocene, Part I, M. Rosenblum, J. Wiley and Sons, N. Y., N. Y., 1965.

5. A. Nesmeyanov, et al, Doklady Akad. Nauk S.S.S.R., 160, 203 (1964).

6. D. Bublitz, Can. J. Chem., 42, 2381 (1964).

FIBER TECHNOLOGY - SPINNING AND DRAWING OF A FUSED-RING POLYMER

by

Walter H. Gloor

Directorate of Laboratories
Air Force Materials Laboratory
Nonmetallic Materials Division
Wright-Patterson Air Force Base, Ohio

FIBER TECHNOLOGY - SPINNING AND DRAWING OF A FUSED-RING POLYMER

Walter H. Gloor

ABSTRACT

Fiber spinning and drawing techniques have been developed for poly(bisbenzimidazobenzophenanthroline), a semi-intractable polymer exhibiting extremely good thermal stability. Wet spinning from solution in concentrated sulfuric acid into a water/acid bath, followed by hot-stretching at temperatures up to 600°C resulted in fibers potentially useful in advanced Air Force systems.

Single-fiber property levels of nearly 4 grams per denier were achieved in this in-house effort, with indications of retention of useful properties to at least 200°C higher other known polymeric textile fibers. Resistance to direct flame is also outstanding.

Recent effort, under Air Force contract, by a major fiber producer, has resulted in an overall improvement in mechanical properties through intensive studies of all aspects of polymer synthesis, fiber formation and after-treatment.

BIOGRAPHY

Walter H. Gloor

Education: Cornell University, B. Ch. E., 1951

Employment:

1951-1954, B. F. Goodrich Research, synthetic fiber formation and after-treatment, properties of polymer solution

1954-1960, B. F. Goodrich Tire Co., research and development on tire yarns, cords, and fabrics, tire fabric adhesives

1960-1961, Dayton Tire and Rubber Co., Manager, Tire Fiber Research and Development

1961-present, Air Force Materials Laboratory, Task Engineer, exploratory development on organic and inorganic fibers

Miscellaneous publications and presentations on fiber formation, fiber properties and evaluation techniques.

LIST OF FIGURES

LIST OF TABLES

INTRODUCTION

Performance characteristics of advanced aerospace systems have resulted in requirements for fibrous materials possessing improved resistance to the effects of high temperatures and the ability to withstand short-duration direct flame exposure. In general, polymeric fibers exhibit the best overall balance of textile-like properties for these, and other applications. A limitation on the polymeric candidates for thermally-stable fibers is often imposed by the polymers themselves. Synthesized to provide resistance to environmental extremes, these materials are often sufficiently intractable to be non-fiberizable by conventional techniques. For a relatively intractable polymer with outstanding properties, use of unconventional techniques is clearly indicated. Such is the case with polymers of the benzimidazobenzophenanthroline type, synthesized by R. L. Van Deusen of the Air Force Materials Laboratory. Poly(bisbenzimidazobenzophenanthroline) is a linear polymer of high molecular weight, resulting from the polyphosphoric acid condensation of diaminobenzidine and 1, 4, 5, 8-naphthalene tetracarboxylic acid (Fig. 1). Because of the excellent thermal stability exhibited by BBB in thermal gravimetric analysis (Fig. 2) it was decided to investigate the material as a fiber-former, in spite of its lack of solubility in any common spinning solvent.

EXPERIMENTAL

Fiber Formation

All the experimental results to be discussed are based on research conducted with 10 g. or smaller quantities of polymer. Since Van Deusen reported solubility without degradation in concentrated sulfuric acid, this was selected as the solvent for fiberization trials. Initially, approximately 5 g. of a 10% solution by weight was prepared, with polymer of intrinsic viscosity (I. V.) 1.15 (H_2SO_4, 30°C). Solution was effected by stirring with mild warming (to 50°C. or so). This represented the first time a solution of this high concentration had been prepared. The solution was deep red or purple in color and appeared to be of sufficient viscosity for fiber formation. It was transferred to a 5-ml. hypodermic syringe fitted with a No. 20 needle, which had been cut off to provide about a 1/8 in. total capillary length. This was hand-held under water at 50°C while the solution was extruded. A filament formed readily and could be drawn the length of the bath (about 18 in.) slowly without breakage. Attempts to draw rapidly resulted in the fiber stream's breaking at the orifice.

Although not providing fiber of a quality suitable for mechanical characterization or for drawing studies, this simple experiment did indicate that BBB was a potential fiber-forming material. For the next spinning attempt, therefore, a larger quantity of solution was utilized, as was a ten-hole platinum spinneret of 0.008-in. hole diameter. The general fiberization scheme is shown in Figure 3. The solution is placed in a 50-ml. glass syringe, the plunger of which is positively driven by a variable-speed motor-screw drive system. Very close control of extrusion rate is achievable with this device. Figure 4 shows the syringe and type of spinneret assembly employed. About 40 g. of 10% polymer solution in conc. H_2SO_4 was placed in the syringe. Extrusion was at 0.3 cm.^{3}/min. into a water bath at 45°C. The ten-filament yarn formed readily and could be wound on a spool at low rates. About 100 ft. of lustrous dark-green yarn was collected at 3-3/4 ft./min. Higher wind-up rates were attempted but resulted in rupture of one or more filaments at the spinneret face. It seemed apparent that the pure water bath resulted in an excessive rate of coagulation, thereby limiting take-up speed. For a first try, however, it was felt that the run had gone quite well.

The spool of yarn obtained was given an overnight water soaking at room temperature and then was vacuum-dried 2 hr. at 60°C. The tensile properties were measured with a table-model Instron. The gage length

was 1 in. and the strain rate was 20%/min. The yarn exhibited 0.5 g./den. and 20% extension at break. X-ray diffraction analysis of the as-spun yarn gave no hint of orientation or crystallinity.

The next spinning run was with BBB polymer of 2.45 I.V. This was made up to 8% solids by weight in concentrated sulfuric acid and spun into a water bath under conditions similar to those used in the first run. Although not all spinneret holes delivered properly, three spools of yarn were collected at take-up rates of from 6 to 8 ft./min. and with extrusion rates ranging from 0.21 to 0.35 cm.^{3}/min. The yarns resembled that of the previous run in general appearance. Tensile tests conducted after water-soaking and vacuum-drying yielded as-spun tenacity and elongation of 1.10 g./den. and 31%, respectively. A portion of this yarn was left unextracted, so that the effect of residual acid could be determined in subsequent hot-stretch studies.

The next spinning run also utilized the polymer of 2.45 I.V., but the solution concentration was reduced to 6% in an attempt to obtain a higher degree of bath stretch. The bath composition used was 20 wt.-% H_2SO_4 at 65°C. Under these conditions it was possible to collect ten-filament yarn at 10 ft./min. for approximately 30 min. The extrusion rate was 0.44 cm.^{3}/min. These conditions represent approximately 100% bath stretch. The spool of yarn was vacuum-dried at 60°C. prior to stretching experiments. A length of the yarn was hot-water-extracted, to remove residual acid, and used for as-spun tensile property measurements. The weight loss on extraction indicated approximately acid 57% by weight in the dried, unextracted yarn. The as-spun tenacity was found to be 1.40 g./den. with 48% extension at rupture.

Another spinning run utilized a 7% solution of 2.0 I.V. material. Since it was decided to use a bath composition of 50 wt.-% sulfuric acid, certain changes in the apparatus were required. These consisted of substitution of a glass tank for the stainless-steel previously used and a protective enclosure for the stainless-steel spinneret assembly and tubing. Figure 5 shows the overall layout, and Figure 6 shows a close-up of the Nalgene spinneret assembly housing and platinum spinneret protruding.

With the bath temperature at 30°C. three spools of yarn were collected at take-up rates between 5 and 7 ft./min. The solution extrusion rate was 0.44 cm.^{3}/min. at the slower take-up and 0.51 cm.^{3}/min. at the higher. Attempts to wind the yarn faster resulted in breaks at the spinneret. For this run a water wash-bath was employed in-line with the acid coagulating bath. It provided an 8 in. immersion length for the yarn and was held at 47-50°C. The three spools of yarn collected were dried overnight in an air oven at 60°C.

Samples of yarn from each spool were boiling-water-extracted and dried prior to mechanical property determinations. The weight losses on extraction indicated an acid content in the dried as-spun yarns of about 3[illegible]-35%. As-spun tenacities on single fibers removed from these yarns ranged from 0.95 to 1.13 g./den.; rupture elongations varied from 28 to 38%. Figure 7 shows a typical stress-strain curve for a single filament of about 34 den.

Hot-Stretching Studies

The initial drawing studies conducted on BBB fiber and yarn all involved hand drawing. No suitable continuous drawing equipment was available to us at that time. Later in the effort a small drawing frame was designed and built; all subsequent effort utilized this device.

The majority of the hand-drawing studies involved a brass block 4 in. in diameter, heated electrically. A thermocouple was inserted in a well parallel to the top surface and 1/16 in. beneath it. With the block at the desired temperature a length of yarn was held against it, under tension, and drawn across the block from one to three times. Draw ratios were estimated from length and denier change. A few experiments were conducted in which the block was replaced by a small, electrically heated furnace with a hinged cover. This provided approximately 1-1/2 in. of heated length.

These hand-drawing experiments were designed to define broadly the drawing characteristics of BBB yarns and lay the groundwork for future continuous stretching work.

Yarn from the original multifilament spinning run, with polymer of 1.15 I.V., was hand-drawn over the brass block in a range of temperatures. In each case the draw ratio was held to that just short of filament breakage. Table I summarizes the results. Modest increases in tenacity are evident for low draw ratios. Rupture elongation is low; attempts at relaxation to increase elongation were unsuccessful. Initial modulus was measured on several of the tensile samples. It ranged from 28 to 36 g./den., the higher modulus values being associated with higher tenacity samples.

Yarn obtained from the second spinning run was evaluated for hot-stretching characteristics in both extracted and unextracted form. Table II summarizes the results of these hand-drawing experiments. Drawing of the unextracted yarn was accomplished at lower tensions and with less filament breakage than was encountered with extracted yarn. The data

show superior mechanical properties for the material drawn with residual acid present. For drawn, unextracted samples a hot-water wash and drying preceded the denier and tensile determinations. All succeeding hot-stretching studies utilized as-spun yarn containing 30-60% acid.

A few hand-drawing experiments were conducted with the unextracted yarn from the third spinning run (2.45 I.V. polymer, 20% acid in bath) prior to receipt of the small drawing frame subsequently employed. The highest property level was obtained with a draw temperature of 680°C., which resulted in a tenacity of 1.9 g./den., 7% elongation, and initial modulus of 74 g./den. The draw ratio was approximately 1.3:1.

Continuous drawing of 2.45 I.V. yarn was conducted over a range of temperatures and draw ratios, both in air and argon, using the drawing unit shown in Figure 8. The drawing unit consists of input and output godets, with idlers, infinitely variable in speed up to about 18 ft./min. Between these godets is a small furnace, electrically heated, capable of operation up to 870°C. The furnace contains an input manifold for inert atmosphere. A traversing take-up mechanism is provided for winding on tubes; let-off is provided to the left of the unit and is dependent on the type of yarn package. Drawing of single filaments is normally accomplished by using the input godets as the let-off and the output godets as the take-up. Table III summarizes the results of drawing experiments with the 2.45 I.V. yarn. For all runs the input yarn speed was 26 in./min. The residence time of the yarn in the hot zone is about 20 sec.

A single filament removed from the yarn drawn four passes tested 2.63 g./den., 9.0% elongation, and initial modulus 65 g./den.

In multifilament yarn-drawing the maximum draw ratio is limited to just short of the point at which individual filaments start to break. Therefore, in order to operate closer to maximum draw conditions, it was decided to conduct all future hot-stretching with single filaments separated from the yarns. An added advantage of this technique is the conservation of material.

Up to this point the best combination of mechanical properties obtained were a little over 2 g./den. with about 19% extension at break. This is not exactly a high-performance material. Additionally, the low initial modulus indicated a rather poorly drawn fiber. The emphasis of the single-fiber continuous-drawing experiments conducted subsequently on both 2.45 and 2.0 I.V. material was to increase tenacity and modulus while maintaining as much elongation as possible. Table IV summarizes the results of this effort. All runs were made with argon atmosphere.

Inspection of these data reveals that tenacities approaching 4 g./den. are associated with such drawn fibers. However, the rupture elongation for fibers drawn to these levels is about 4-5%. For one sample drawn at 650°C. the elongation dropped to under 3%. Attempts at relaxation have been unsuccessful, as shown by the second pass at zero tension and 610°C. on fiber originally drawn at 590°C. The low rupture elongation appeared as the outstanding problem associated with preliminary evaluation of BBB as a potential fiber for Air Force use.

Figure 9 presents typical stress-strain curves for moderately drawn and highly drawn BBB fiber. No yield point is evident on either of these curves.

The data presented in Table IV are shown graphically in Figure 10. Tenacity is plotted as a function of draw temperature, with draw ratio as a secondary variable. Thus plotted, a little order is obtained from the apparent chaos of Table IV. Tenacity is seen to increase with draw ratio for a given temperature and to increase with temperature at constant draw ratio. The data shown represent both 2.00 and 2.45 I.V. material with no noticeable difference. The stated relationships appear to be valid to at least 600°C. At the upper right are shown five data points for fibers drawn at ratios 1.58:1 or higher and at temperatures of from 565 to 650°C. These data are not as consistent as the others, but they indicate that degradation may be occurring at the extreme temperatures. This is consistent with the thermal gravimetric analysis curve in nitrogen, presented earlier, which showed a break at about 600°C.

Figure 11 is the same type of plot, but for elongation rather than tenacity. A single curve appears to be the best fit, irrespective of draw ratio, the elongation decreasing with rising temperature.

Conclusion

The preliminary spinning and drawing effort described clearly demonstrated that poly(bisbenzimidazobenzophenanthroline) can be fiberized, that the fibers can be drawn to provide a usable level of mechanical properties, and that thermal resistance is excellent.

Since this work was completed, a larger scale program has been initiated under Air Force Materials Laboratory contract. This work has fully justified our confidence in BBB as a fiber of exceptional thermal stability. Through intensive studies of polymerization, spinning, and after-treatment, high-quality yarn of nearly 5 grams per denier and

with 8-10% elongation at break has been achieved. Strength retention after a one-minute air exposure at 800°C has been measured as 43% of original. No degradation of fiber properties results from brief exposures to direct flame at 1200°C.

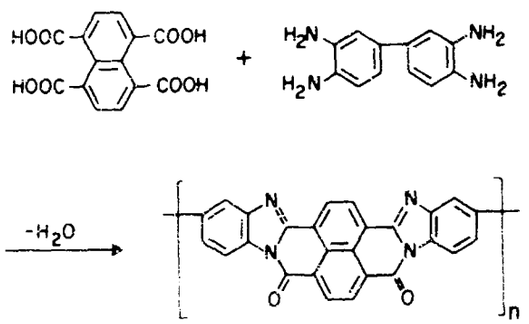

FIG. I BBB SYNTHESIS AND STRUCTURE

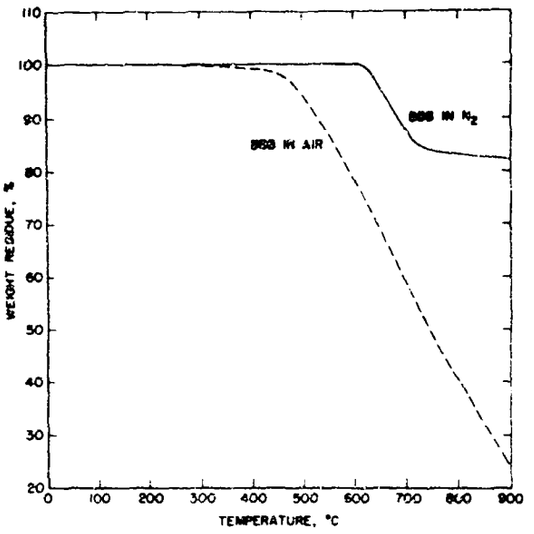

FIG. II TGA IN AIR AND IN N_2

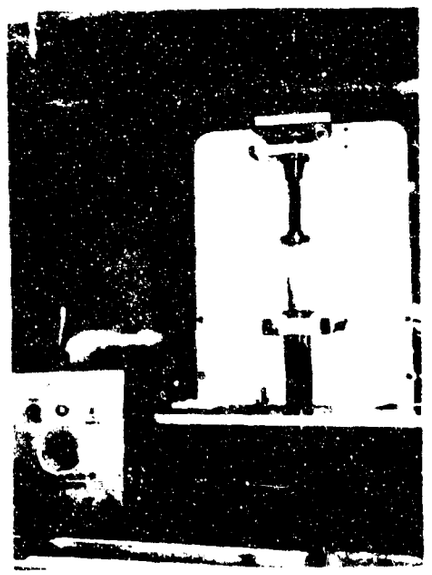

FIG. III SYRINGE DRIVE, WITH SPINNERET ATTACHED, IN POSITION OVER BATH

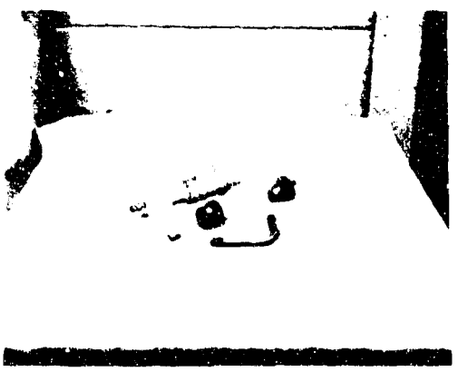

FIG. IV 50-ML SYRINGE AND SPINNERET ASSEMBLY

FIG. V FIBER FORMING SYSTEM WITH GLASS TANK

FIG. VI CLOSEUP SHOWING NALGENE HOUSING FOR SPINNERET ASSEMBLY.

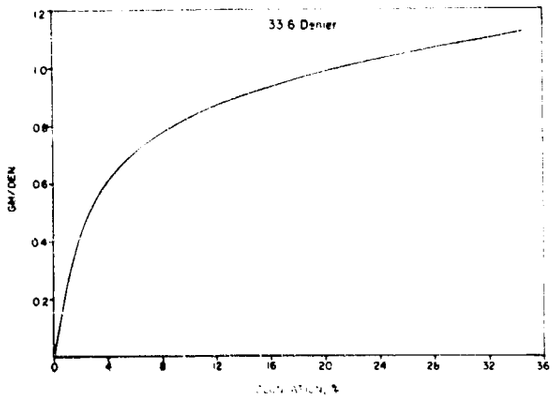

FIG VII STRESS-STRAIN CURVE AS-SPUN BBB FIBER

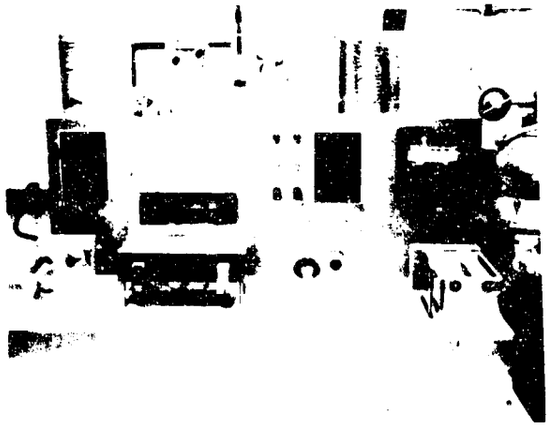

FIG. VIII DRAWING DEVICE WITH FURNACE OPEN

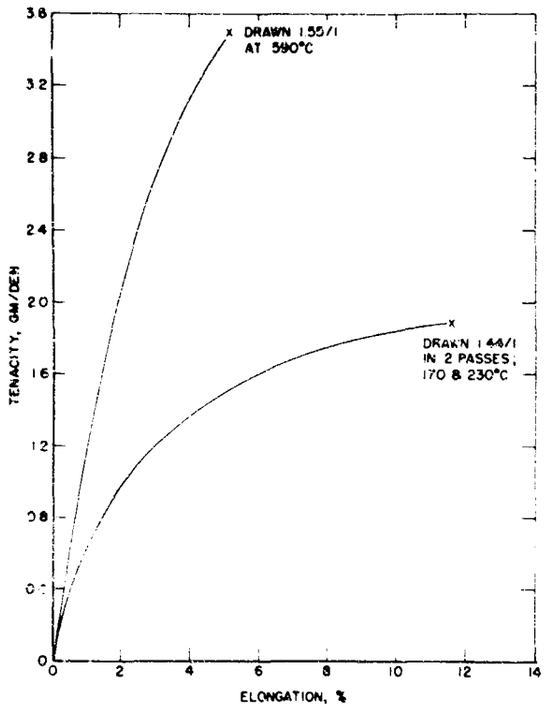

FIG. IX BBB SINGLE FIBER STRESS-STRAIN

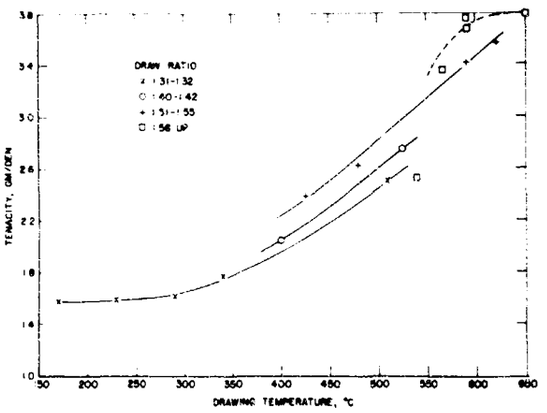

FIG X SINGLE FIBER TENACITY vs TEMPERATURE OF DRAW

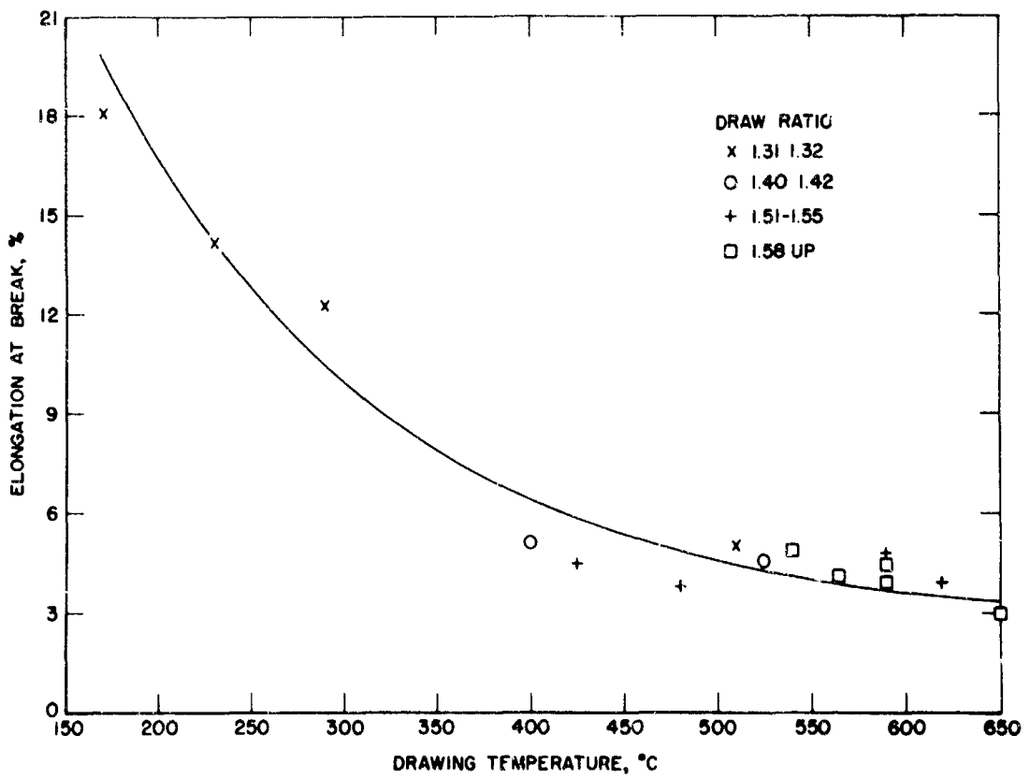

FIG. XI FIBER RUPTURE ELONGATION vs TEMPERATURE OF DRAW

TABLE I

Polymer I. V. 1.15

Block Temp., °C	No. of Passes	Draw Ratio	Tenacity, Gm/Den	Elong. at Brk., %
360	2	1.10	0.85	7.2
505	1	1.24	1.26	10.0
535	3	1.25	1.26	6.8
465	2	----	----	----
515	2	----	----	----
540	1	1.29*	1.33	7.1

*Total draw for 5 passes; final pass at zero tension.

TABLE II

Polymer I. V. 2.45

Drawing Temp., °C	Extracted or Unextracted	Draw Ratio	Tenacity, Gm/Den	Elong. at Break, %
380	U	1.15	1.53	19
330	E	----	----	--
380		~1.1 total	1.35	12.5
505	E	1.15	1.55	7.4*
700	U	~1.25	2.06	7.4**

*Initial Modulus 39 gm/den

**Initial Modulus 60 gm/den

TABLE III

Polymer I. V. 2.45

Continuous Drawing

Temp. of Draw, °C	Draw Ratio*	Atmosphere	Tenacity Gm/Den	Elong. At Break, %	Initial Modulus, Gm/Den
425	1.23	Air	1.92	14.5	56
525	1.31	Air	2.46	5.9	68
425	1.25	Argon	1.77	10.0	62
505	1.33	Argon	2.22	4.7	75
260	1.06	Argon	0.76	34	31
345	1.06	Argon	1.36	27	33
425	1.07	Argon	1.64	13	46
540	1.08	Argon	2.07	6.8	64

*Calculated from input and take-up speeds.

TABLE IV

Single Fiber Drawing

Polymer I. V.	Temperature of Draw, °C	Draw Ratio	Drawn Fiber Denier	Tenacity, Gm/Den	Elong. at Break, %	Initial Modulus Gm/Den
2.45	510	1.32	22.9	2.51	[illegible].0	87
"	525	1.42	19.7	2.75	4.6	111
"	480	1.51	21.3	2.63	3.8	119
"	565	1.59	18.0	3.36	4.1	126
2.00	540	1.66	25.8	2.51	4.9	129
"	170	1.31	30.2	1.58	18.1	60
"	230	1.31	30.6	1.59	14.2	61
"	290	1.31	27.1	1.61	12.3	74
"	340	1.31	26.9	1.76	10.0	58
"	425	1.53	23.6	2.39	4.5	126
"	150	1.20	26.8	1.56	17.2	51
"	230	1.20	26.6	1.84	10.3	64
"	620	1.55	24.5	3.57	3.9	144
"	590	1.55	24.7	3.42	4.8	147
"	610	0.95+	24.3	3.43	4.1	145
"	400	1.40	27.8	2.05	5.1	85
"	590	1.65	19.7	3.67	3.9	143
"	650	1.76	17.3	3.79	2.9	190
"	590	1.58	20.0	3.76	4.4	154

ELECTRON REDUCTION IN THE REENTRY PLASMA SHEATH

By

D. Jacavanco

Microwave Physics Laboratory
Air Force Cambridge Research Laboratories
Office of Aerospace Research
L. G. Hanscom Field, Bedford, Massachusetts 01730

BIOGRAPHY

Daniel J. Jacavanco received his B.S. and M.S. in Electronic Engineering from Lowell Technological Institute in 1960 and 1961. Since then he has been a member of the microwave Physics Laboratory of AFCRL where he has conducted experiments in plasma-electromagnetic interactions. He has published work on plasma covered antennas, and nonlinear interactions of microwaves and plasmas. He is presently conducting experiments in the diagnostics of a high temperature plasma jet.

Electron Reduction in the Reentry Plasma Sheath

ABSTRACT

This paper describes a new technique for the reduction of electron density in the reentry plasma sheath. A brief history of the problem and a description of various alleviation schemes are presented. A description of the room temperature experiment which first demonstrated enhanced attachment is given, followed by a description of the plasma arc-jet experiment used to demonstrate the effect at high gas temperature. It is seen that oxygen is added via a nozzle to a nitrogen arc jet. The resulting flow passes through an r-f coil and an S-band microwave diagnostic test section. The r-f coil is used to heat the electron gas. Curves are presented which show the measured reduction in electron density both when oxygen is present in the flow and when r-f heating is applied.

1. INTRODUCTION

The plasma sheath is that layer of shock-heated ionized gas which forms around any material body entering the dense portion of the earth's atmosphere at hypersonic velocities. Temperatures in excess of 5000° C are attained in the nose region of the vehicle which produce, by thermal ionization, electron densities that exceed 10^{12} electrons per

cc in certain areas of the sheath. The superheated air decomposes its main constituents nitrogen and oxygen to an atomic and/or ionized state and, along with the free electrons generated, is swept over the body constrained to a boundary layer in a manner which is determined by the vehicle's velocity, shape, angle of attack, and any roll, pitch, or yaw components of its movement. Any antennas mounted on the vehicle are enveloped by the sheath and their performance as transmitters or receivers is seriously affected. The degree to which they are affected is a function of the local electron density, the local collision frequency, and the operating frequency of the antenna.

From a communications viewpoint, the most important component of the plasma sheath is the free electron density. Due to their very light mass, compared to the ionic components of the sheath, they alone respond to the rapid variations of the electromagnetic signal. Propagation through the sheath is degraded when the electrons absorb the electromagnetic radiation and lose it through collisions with the other particles. Propagation through the sheath is impossible when the electron density is so high that the resulting media cannot support an electromagnetic wave. Therefore, it is already shown, that the electron density is the most important component of the sheath.

Early theoretical analyses showed that the effects of the plasma sheath could be circumvented by the use of higher microwave frequencies. This appeared to be a practical solution until it was found that at higher frequencies atmospheric absorption did as much damage to the communications link as did the plasma sheath. This solution would have generated its own problem, that is, —revamping the entire worldwide communications-tracking network to operate at higher microwave frequencies.

Some recent experimental work by Chen (Chen and Len, 1968) has shown the possibility of using very low frequencies for penetration of the reentry sheath. This new work is not simply the well-known low-frequency phenomenon of penetration of a plasma to its skin depth. This experiment uses the inductive nature of a plasma to tune out a short, mismatched monopole antenna. Delivering power more efficiently to the antenna caused the transmitted power level to be enhanced over the level in the absence of the plasma sheath.

Another early solution which has yet to materialize is the use of the so-called magnetic window. It was found that if a magnetic field of proper orientation and strength was applied to the plasma, electromagnetic waves of certain frequencies would pass through the plasma sheath which would otherwise be opaque to them.

Conventional magnets and their associated power supplies are impossible to apply to a vehicle due to size and weight limitations. The advent of commercially available, superconducting magnets hints at a possible breakthrough. However, the cryogenic problems of maintaining a magnet in a superconducting state in a reentry vehicle environment are still to be surmounted and prevent this device from being successfully flown.

Lasers have opened the possibility of an optical frequency communications system. Again, earth's atmosphere would hamper a vehicle-to-earth link. This difficulty could be circumvented by using conventional radar in an earth-to-satellite link with an optical frequency, vehicle-to-satellite link.

Present emphasis in research concerned with reentry physics is on the control and modification of the electrical properties of the sheath by external means. A number of different substances have been proposed and used under a variety of conditions. A measure of success was obtained by seeding water into the sheath on the Gemini III flights. Solids, liquids, and gases are presently being studied to find the most effective substance. Weight and ease of packaging are prime criteria to be met.

All of this work is being performed under strict laboratory conditions, which at best duplicate only a few of the parameters used to describe the reentry sheath. It is important to realize that under all of the controlled experimental conditions that exist, a variety of substances will appear superior. In other words, for each experiment there exists an optimum additive. This should not be surprising, since exact reentry conditions are only achieved during reentry for a specific vehicle, and will vary from vehicle to vehicle. The spatial distribution of electron density, electron temperature, the various ionic species, and their temperatures vary from vehicle to vehicle. Predicting these quantities is a formidable theoretical problem which has yet to be solved for all geometries. The various reaction rates which govern the production and destruction of the constituents of shock heated air are unknown and, in most theoretical analysis, the rate coefficients are extrapolated from room temperature experiments. For these reasons, all additive work should be evaluated for effectiveness based on the experiment involved. Furthermore, because reentry conditions vary widely as the vehicle descends, it is very probable that a combination of additives and techniques will, of necessity, have to be used in different regions of the trajectory, and may overlap. The apparent variety of solutions to the additive problem is testimony to the complexity of the problem.

2. NEW TECHNIQUE

This paper describes a new technique for the control and elimination of the free electron density in the reentry plasma sheath. Basically, the technique consists of causing the light, highly-mobile electron to attach to a heavy atom or molecule and hence lose its effectiveness upon electromagnetic waves in this manner. Once it is attached to a heavy

particle, it cannot respond to the very rapid variations of the electromagnetic field. The electron is made to attach to the heavier species by heating the electron gas by absorption of radio-frequency energy. At these higher energy levels the electron attachment rate coefficients to molecular species often reach a maximum which results in a lower ambient electron density.

This effect was first demonstrated by Rao and Taylor (Rao and Taylor, 1966) of AFCRL in a room-temperature oxygen plasma. In Figure 1 we see the plot of the measured electron density decay rate obtained from microwave diagnostics of the oxygen plasma. The plasma is turned on at t = 0 by a short duration, high voltage pulse, is allowed to decay to zero, and is repetitively ignited sixty times a second. The purpose of the experiment was to study loss processes in molecular oxygen plasmas using the Luxembourg effect. This technique consists of perturbing an otherwise normally decaying plasma with a high power signal that changes the decay rates. The high-power heating signal is absorbed only by the electrons, therefore, the new decay rates are due to elevated electron temperatures only.

Figure 2 shows a typical result by Rao and Taylor. When the high power heating pulse is positioned in the decaying portion of the plasma, the electron density was markedly reduced while the heating pulse was on. Normal density reduction is noted before and after the heating pulse, indicating the normal decay rates of recombination and diffusion.

The mechanism that has been proposed to explain this result is enhanced attachment. Oxygen, like all electrophillic substances on the right hand side of the periodic table, has an affinity for electrons. Depending on the energy level of the electron and the oxygen atom, a negative ion will form when attachment occurs. The resulting decrease in electron density was limited by the production of electrons by detachment collisions.

Based on the results of this experiment, Walter Rotman of AFCRL suggested the possibility of using this technique as a means of reducing the effect of the electron density in the reentry-plasma sheath. The proposal to investigate the possibilities of observing this technique using a d.c. plasma arc jet as the source of high temperature air was made by Lennon and Rao (Lennon and Rao, 1966). In their proposal they speculate that, since the dominant electronegative component of the sheath is the atomic oxygen concentration, attachment of the electrons to this specie will be the likely process to use to reduce the electron density.

The experiment used as a source of high temperature gas a commercially available 40 kW d.c. (forty kilowatt direct current) plasma torch manufactured by Thermal Dynamics of Lebanon, New Hampshire.

This device is a popular means of producing clean high-temperature, high-enthalpy flow in a variety of gasses. Its principal, but least utilized asset, is its ability to produce high-temperature, laminar flow free of any turbulence. This allows diagnostic probing of the resulting plume

with pulses of microwave energy and the subsequent analyses of them on a pulse-to-pulse basis. This feature permits the utilization of the Luxembourg effect —a very powerful plasma— diagnostic tool. It also means increased sensitivity in continuous wave diagnostic experiments because smoothing or the averaging out of the effects of the turbulent flow upon the detected microwave power is unnecessary.

For this experiment the arc jet was teamed up with a DeLaval expansion nozzle and was mounted in an evacuated chamber which would be maintained at one torr pressure. The DeLaval nozzle was operated in the subsonic regime, and provided a convenient means of injecting additives into the flow. The jet-nozzle combination could be moved inside the chamber to take advantage of the temperature and velocity gradient in the plume. This experiment approximates the reentry conditions in temperature, ambient pressure, electron density, and neutral species. This is accomplished by operating the jet with nitrogen gas at a mass-flow rate of about one gram per second. Oxygen is added to the hot nitrogen, via the nozzle in a ratio that will produce hot synthetic air.

Microwave diagnostics of the high-temperature synthetic air were performed downstream of the DeLaval nozzle. The flow was allowed to impinge upon a small hole in the broad wall of a section of water-cooled S-band (1.500 × 3.000") waveguide and is pictured in action in Figure 3. This techniques results in a small uncontained column of hot gas, 0.375" in diameter by 1.500 long whose properties are relatively uniform because it has been sliced from the center of a much larger plume.

The electron density and collision frequency is obtained by measuring the microwave impedance using standard slotted-line techniques. Use is then made of the well-known Marcuvitz equations for the impedance of a dielectric rod positioned across a waveguide, as a function of its dielectric constant. In the case of a plasma, the dielectric constant is complex, and a computer is employed to obtain the curves relating the real and imaginary components of the dielectric constant to the real and imaginary components of the microwave impedance. Figure 4 shows the physical relationship between the jet, nozzle, and water-cooled waveguide test section.

The inherent beauty of this technique is that it allows measurement of an overdense plasma. Normal cut off density in a typical propagation experiment for S-band frequencies (~3GHz) is 10^{11} electrons per cubic centimeter. Since measurement of impedance does not demand the media to support any particular mode of propagation of an electromagnetic wave, higher densities than cut off can be measured. The lower limit of the density measurement depends upon the accuracy to which one can measure the shift of the microwave voltage minimum. The particular slotted-line used in this experiment could measure shifts in the standing wave pattern as small as 0.01 centimeter. This corresponds to a minimum detectable electron density of 1×10^9 electrons per cubic centimeter. In practice, consistently reproducible densities of 5×10^9 electrons per cubic centimeter are measured which correspond to a shift of 0.05 centimeter. These accuracies were only possible when an ultra stable microwave oscillator was used as the source of power.

For ease of data reduction, an approximate equation is used for the relationship between the shift of the voltage minimum and the electron density. Leiby (Leiby, C. C. and Golden, P. D., 1962) gives this equation as,

$$Ne = \frac{7.102 \lambda \Delta x}{d^2 \lambda_g^2} \times 10^{12} \text{ electron per cc}$$

where λ and λ_g are the free space and guide wavelength, d is the diameter of the column and, Δx is the shift of the voltage minimum. It is only a valid approximation for small shifts in the voltage standing wave ratio, which corresponds to low electron densities in the range 10^9 to 10^{10} electrons per cubic centimeter.

In order to demonstrate the reduction of the free electron density by the enhancement of attachment, it was necessary to apply radio-frequency energy to the exhaust of the jet before the flowing high-temperature gas entered the waveguide diagnostic-test section. Previous attempts to demonstrate this effect had shown that heating the gas in a Luxembourg geometry using high power pulses of S-band microwaves were unsuccessful in reducing electron density. It is felt that this was due to the flowing nature of the gas or to insufficient absorption of the heating power due to either the high electron density or the very small (1 microsecond) heating pulse width.

These shortcomings were overcome by the physical arrangement shown in Figure 5. The heating of the electron gas was accomplished at a low frequency (7 MHz) where the large skin depth insured penetration and absorption of the heating energy by the plasma. The cylindrical symmetry of the geometry lent itself very well to the use of a water-cooled radio-frequency coil as the coupling mechanism. This could be energized on a continuous basis by a one kilowatt transmitter which insured an ample amount of heating power.

Figure [illegible] shows a schematic of the entire heating experiment. The plot of electron density as a function of position in the lower half of the figure shows the measured values along the axis of the plume of the jet in the upper half of the picture. This is the range of electron densities in which the radio frequency heating was performed. In practice, the heating process and the resulting density reduction was limited by the nonlinear, radio-frequency breakdown which engulfed the coil at high-power levels. Due to the electric-field gradient produced by the current in the coil, the discharge is driven outward from the center to the coil itself. This process shields the center of the coil and reduces the heating there.

Figure [illegible] shows the results of the heating experiment. The curve labeled $N_2 + O_2$ is the result of adding oxygen to the nitrogen jet. The

[illegible] increasing oxygen addition [illegible] attachment. The curve labeled $N_2 + O_2 + RF$ is generated by applying radio-frequency power to the coil. It is seen that when oxygen is added and the coil energized, a reduction in density over the case of no heating is obtained. The density reduction plotted is the maximum obtained for the amount of radio-frequency power available.

3. DISCUSSION AND CONCLUSIONS

The experiment has shown that modification of the electron density at the high gas temperature (~3000°C) available in the exhaust of an arc jet is possible. The mechanism is seen to be affected by several competing processes all of which have not been fully investigated. The following discussion will explore the nature of the competing processes and give the reader an idea of the direction in which future research could go.

For reentry flow-field temperatures and pressures such that an appreciable amount of oxygen remains undissociated, the r-f heating technique would tend to enhance electron attachment to molecular oxygen.

Molecular oxygen was the additive selected for this experiment based upon the results of Rao and Taylor, and the desire to synthesize high-temperature air. The results of research now in progress indicate that more efficient additives than oxygen exist. In particular, the attachment resonance phenomena of such complex molecules as sulfur hexafluoride are particularly promising. The combination of a more efficient attaching additive with a radio-frequency heating scheme should yield results superior to either technique alone.

It was observed that the efficiency of electron density reduction increased as the heating and diagnostic-test section (which were fastened together for convenience) were moved downstream; that is, as the jet moved away from the waveguide and coil. This indicates a dependence on two fundamental characteristics of the flow —its velocity and its temperature. This is an important result and underscores the necessity of knowing the relationship between the position of injection (if there are additives to inject) and the position of the heating of the electron gas relative to the antenna that is blacked out. The particular species available, to which the heated electrons may attach, will be a function of the temperature of the ambient boundary layer into which the additive is injected, the physical state of the additives (solid, liquid, gaseous), and the speed with which it is swept over the body. These factors are in turn related to the time required for actual attachment to occur. At the

elevated gas temperatures involved, these rate coefficients have not been measured.

In an attempt to increase the maximum attainable electron-density reduction, variations in the radio-frequency heating scheme were employed. The use of water-cooled capacitor plates of various sizes and spacing did not yield any significant improvement over the inductive heating scheme, nor was the movement of the region of heating upstream (relative to the waveguide) of any help. Use of capacitor coupling insured a better-defined, heating-electric field and allowed a rate measurement of the r-f power. Measurement of the incident and reflected power indicated that as much as twenty watts were required in the density reduction experiment.

As was mentioned earlier, the original heating was performed at S-band frequencies in a Luxembourg geometry unsuccessfully. Arguments, that centered upon the alleged supersonic flow, dictated that the heating take place upstream. Upstream heating did produce density reduction, but recent impact pressure measurements indicate that supersonic flow does not prevail in the region of interest.

Finally, a word concerning temperature. Measurements made by inserting a tungsten-rhenium thermocouple into the nitrogen jet indicated temperatures in excess of 2800°C, the upper limit of the device. The manufacturer cautions against the use of the device in an oxidizing atmosphere. However, it was felt that the low oxygen flow rates at the low ambient pressures would not affect the thermocouple. When the thermocouple was inserted into a synthetic air mixture, although it did not decompose, thermochemical reactions in the surface of the exposed junction caused the output voltage to fluctuate in polarity in a random manner. Operation in a plain nitrogen jet for short periods of time at high temperatures corrected this situation. Spectroscopic temperature measurements will be attempted.

REFERENCES

Chen, K. M., and Len, C. C. (1968) Enhanced Radiation From a Plasma-Imbedded Antenna. Paper presented at 1968 G-AP Intern'l Symp., Boston, Massachusetts

Leiby, C. C., and Golden, P. D. (1962) Microwave Diagnostic Techniques for Plasma Transmission and Plasma Post in Waveguide Configuration, Scientific Report No. 3, Contract No. AF19(604)-7473

Rao, K. V. N., and Lennon, J. (1966) A Proposal for the Use of Low Power R. F. Heating to Reduce the Electron Density in a Plasma Through Enhanced Negative Ion Production. Unpublished Communication

Schroder, L. C., Sims, T. E., and Cuddehy, W. F. (1965) Experimental T-1 Reentry Communications on Gemini III, NASA Langley Research Center, NASA Document N65-36107

Taylor, R. L., and Rao, K. V. N. (1966) Alteration of Electron Loss Processes in Oxygen Magnetoplasma by Microwave Absorption, Proc. of VII International Conference in Phenomena in Ionized Gases, Vol. 1, Belgrade, Yugoslavia

Figure 1. Electron Density Decay in an Unperturbed Oxygen Plasma

Figure 2. Electron Density Decay in an Oxygen Plasma which has been Pulse-Heated

Figure 3. Artist's Conception of Waveguide Test Section Intercepting the Core of the Arc-Jet's Plume

Figure 4. Physical Relationship Between Arc-Jet, Nozzle, and Water-Cooled Waveguide Test Section

Figure 5. Waveguide Diagnostic-Test Section with RF Heating Coil Attached

Figure 6. Schematic of Experiment Showing Axial Variation of Electron Density Before RF Heating

Figure 7. Measured Electron Density Reduction as a Function of Oxygen Addition and RF Heating

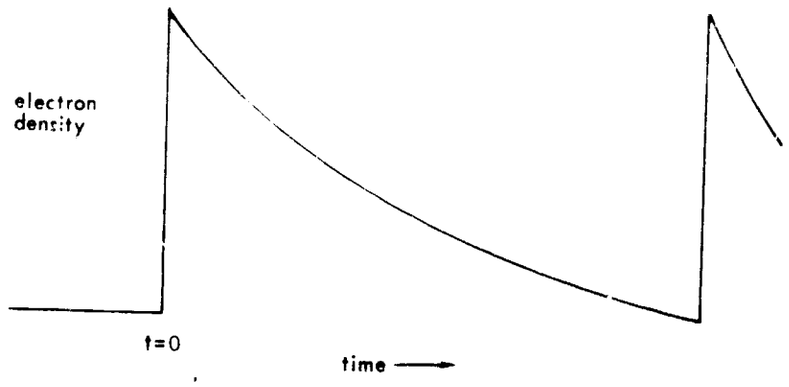

Figure 1

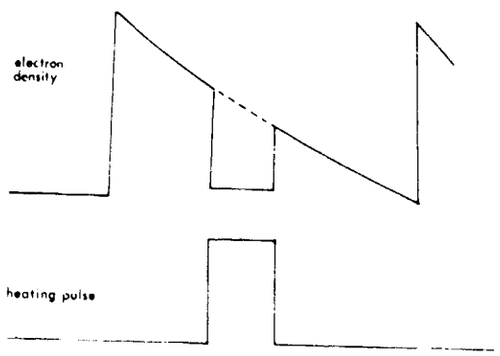

Figure 2

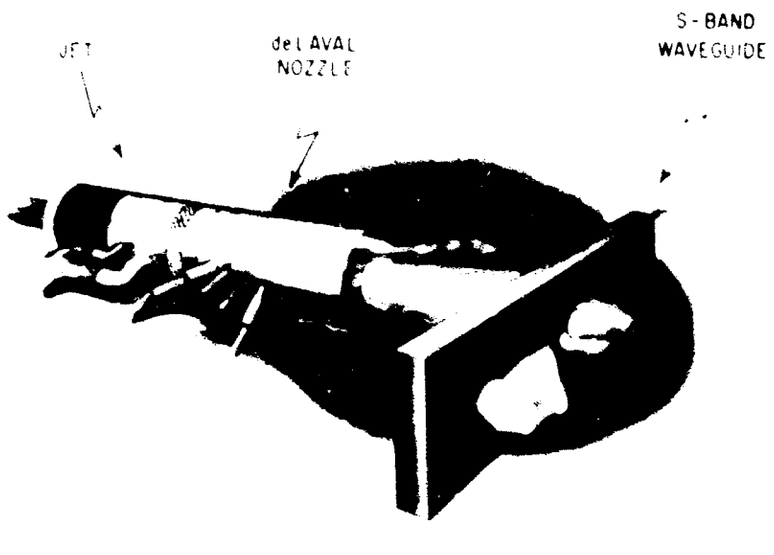

Figure 3

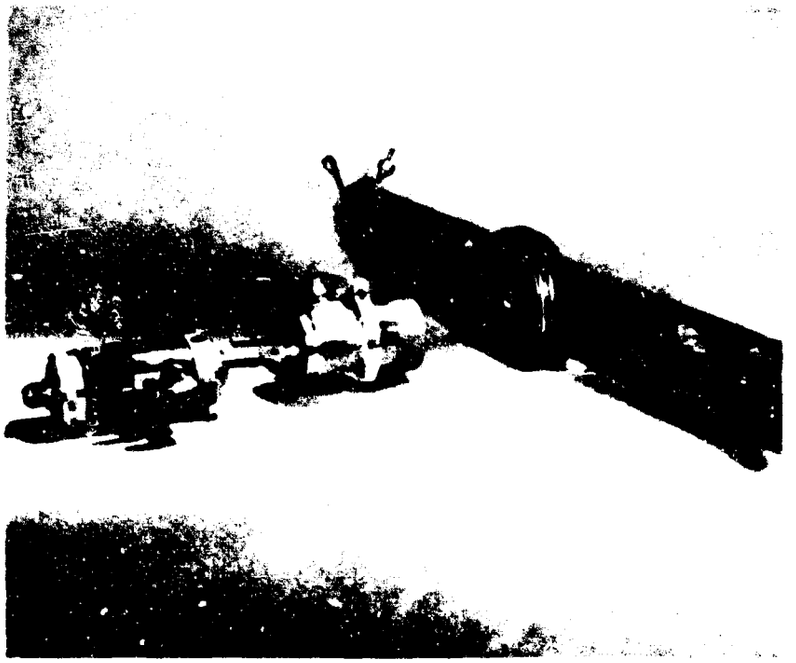

Figure 4

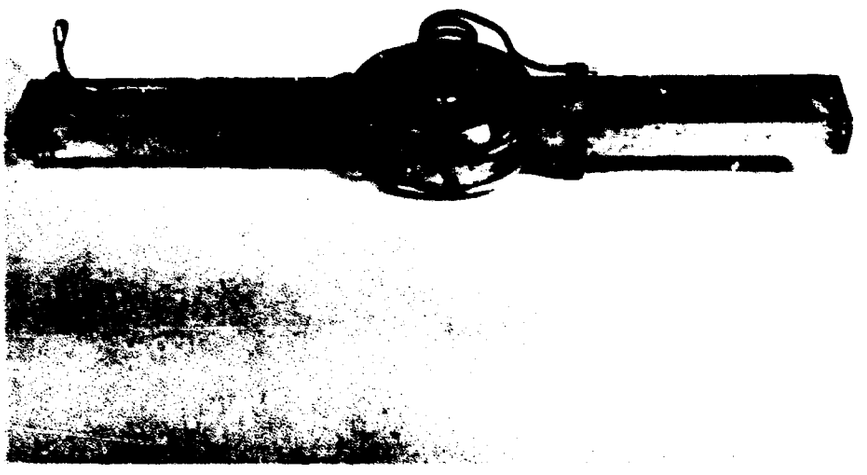

Figure 5

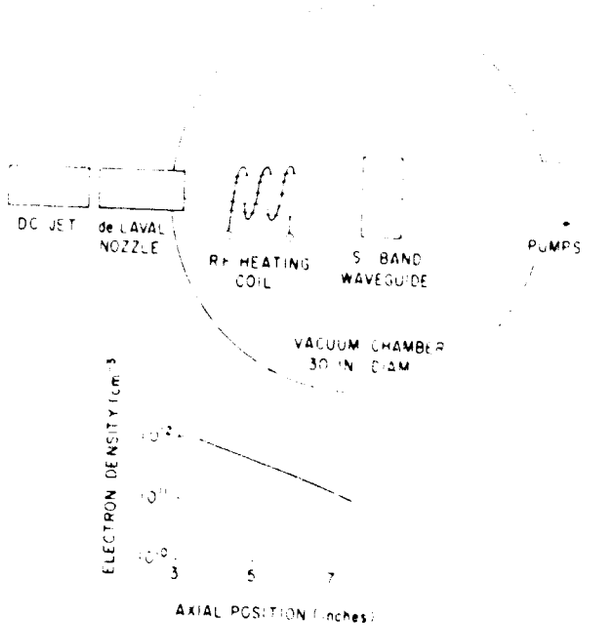

Figure 6

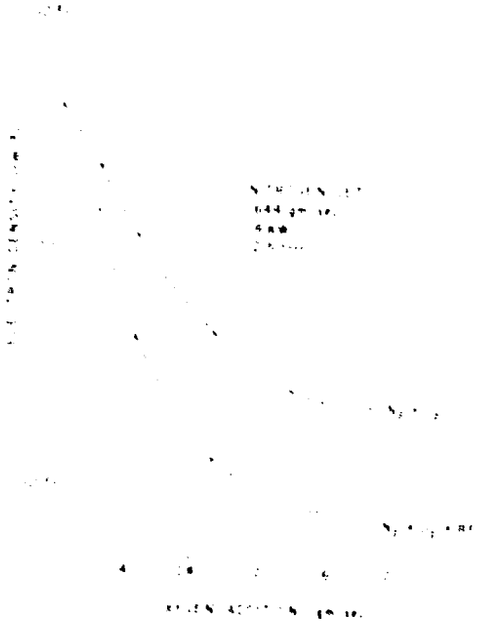

Figure

VELA IV "LID" EXPERIMENT

SPACE EVALUATION OF LITHIUM DIFFUSED SOLAR CELLS

By

A. HOWARD HAYDEN, JR., Capt, USAF

VELA SATELLITE PROGRAM
SPACE AND MISSILE SYSTEMS ORGANIZATION
AIR FORCE SYSTEMS COMMAND
LOS ANGELES AFS, LOS ANGELES, CALIFORNIA

VELA IV "LID" EXPERIMENT

SPACE EVALUATION OF LITHIUM DIFFUSED SOLAR CELLS

ABSTRACT

The purpose of the Vela IV LID experiment is to provide on-orbit evaluation of the self-annealing lithium doped silicon solar cells. Early evaluation of the on-orbit cell performance was desired since they potentially can extend the lifetime of satellites exposed to short term or low level radiation. The experiment was flown at no additional cost to the government through the cooperation of several government agencies and by having USAF personnel in the Vela Satellite Program Office at Hq SAMSO design and fabricate the electronics, perform the prelaunch testing, and evaluate the on-orbit data. The experimental cells have successfully survived the launch environment and several on-orbit maneuvers. In addition, the cells have not exhibited any apparent degradation while operating in the normal orbital solar radiation environment. The lack of a significant solar proton event has prevented on-orbit evaluation of the annealing characteristics of the lithium cells. However, solar proton events of sufficient intensity to permit such evaluation are expected during the lifetime of the satellite.

BIOGRAPHY

Captain A. Howard Hayden, Jr., has been a Detection Systems Engineer for the Vela Satellite Program, Hq SAMSO, since October 1965. He received a Bachelor of Electrical Engineering degree from the University of Virginia in June 1960 and received his commission through the AFROTC. In August 1960, he began working on solid state energy conversion as a civilian electronics engineer for the Electronics Technology Laboratory, Wright Air Development Division, Wright-Patterson AFB. In January 1961, he was ordered to active duty with the 6595th Aerospace Test Wing, Vandenberg AFB, and worked on the development and flight testing of the Atlas "F" weapon system. In July 1963, he was augmented into the Regular Air Force. Captain Hayden subsequently studied nuclear and mechanical engineering at the Air Force Institute of Technology and graduated from the Graduate Nuclear Engineering Program in March 1966. He is a member of the Institute of Electrical and Electronic Engineers, and the American Institute of Aeronautics and Astronautics. He received the Air Force Commendation Medal for his work with the Atlas "F" and an Oak Leaf Cluster to the Commendation Medal for his work on the fourth Vela Satellite Launch.

VELA IV "LID" EXPERIMENT

SPACE EVALUATION OF LITHIUM DIFFUSED SOLAR CELLS

1.0 INTRODUCTION

The purpose of this paper is to discuss the Vela IV "LID" experiment (Figure 1) which was flown aboard one of the two Vela satellites launched in April 1967 to provide space evaluation of lithium solar cells. The paper has three sections (Figure 2). The events which led to the experiment and the purpose of the experiment will be discussed first. Secondly, the constraints placed on the experiment to allow it to be flown on Vela IV and the resulting experiment design will be covered. The results from the experiment, to date, will then be discussed.

2.0 BACKGROUND AND PURPOSE OF EXPERIMENT

The Vela Satellites (Figure 3) fly in circular 60,000 nautical mile orbits. In this orbit, the satellites have minimal protection from the earth's magnetic field and, in fact, spend a significant portion of their time outside of the magnetosphere. Therefore, solar array degradation is expected primarily from solar protons. The satellites have not seen a significant amount of solar proton degradation, since most of the time spent in orbit has been during the minimum of the 11 year solar cycle. However, 6 to 8 percent degradation has occurred, primarily as the result of the solar proton flare on 2 September 1966. The peak of the solar cycle is expected during the later part of 1968 and typically is preceded and followed by significant solar proton events. The fifth Vela launch was anticipated to be on orbit during these solar proton events, and we were interested in the possibility of obtaining a radiation hardened solar cell for use on Vela V.

There are basically two methods (Figure 4) that can be used in countering a radiation environment. The method normally used is to design the array, using a high bulk resistivity N/P solar cell with thick cover glass and, if necessary, provide sufficient power margin to allow some degradation to be acceptable. However, the higher resistivity solar cells have lower efficiency and thick cover glass even further lowers the overall efficiency of the solar arrays. Therefore, a greater array area is required to meet a given power requirement. To provide a power margin would require an additional increase in the solar array area. Since the shape of the Vela satellite was specifically designed to provide a maximum field of view for its payload sensors, it is not possible to increas the surface area of the satellite without extensive redesign. As a result, the use of a radiation hardened solar cell was investigated. The possibility of annealing radiation damage on orbit with normal spacecraft

temperatures appeared particularly attractive. The normal silicon solar cell can exhibit radiation annealing properties if heated to very high temperatures. However, these temperatures are generally excessive for normal satellite application.

Another possibility, doping a silicon solar cell with lithium to allow annealing at lower temperatures, was being investigated and discussed in the solar cell literature during mid-1966. The lithium doped cells which were being tested at that time had exhibited annealing characteristics at the normal temperatures which would be expected by the Vela solar arrays on orbit.

The solid line in Figure 5 shows the normal power degradation which would be expected for the Vela solar arrays as a function of radiation exposure. The dotted line depicts the annealing curve which apparently may typically be expected using lithium doped cells. The lithium cells appear to have a degradation characteristic similar to the normal cells during irradiation, but recover to the lithium power curve after the exposure has ceased. The rate of recovery depends on the annealing temperature. This theoretically would have been an ideal cell to use on the Vela satellite, since the Vela satellites are normally subjected only to a low radiation background except for high level radiation during solar proton events. Therefore, the use of this type cell should result in a short term power drop, which could be supplemented by the spacecraft batteries or by partial shutdown of the payload until the solar array recovers to a more normal power level.

The Directorate of Technology at Hq SAMSO was contacted to determine the availability (Figure 6) of new cells for Vela V. Based on the information they had and the information they obtained from the Air Force Aero Propulsion Laboratory at Wright-Patterson AFB, it was determined that the cells were under laboratory evaluation and had shown annealing characteristics which would make them promising for the intended use. However, the cells were not in production at that time, and it was unlikely that the cells would be put into production until additional testing was performed. In particular, the need for on-orbit testing prior to the use of the cells as the primary power source for a satellite was emphasized. In our discussions with the Directorate of Technology and the Aero Propulsion Laboratory, we were asked if there was any way in which the Vela Program could assist in obtaining early on-orbit testing of the new lithium cell.

The possibility of performing on-orbital test associated with the next Vela launch was investigated, and the prime requirement was the delivery of hardware within approximately six months (Figure 7). Two possibilities were considered. The possibility of using the excess booster capability to fly small experimental satellites was considered.

However, because of the flight plan used to put Vela in orbit, a small experimental satellite would be left in a transfer ellipse rather than in the 60,000 nautical mile circular orbit. In addition, an experimental satellite would require greater development time, and most of the existing payload capability had already been promised to other users. The possibility of flying the experiment on a Vela IV spacecraft was also considered. This had the advantage of placing the experiment in a 60,000 nautical mile circular orbit and having the extensive background radiation instrumentation already included in the Vela satellite payload readily available for determining the radiation environment. In addition, in discussion with Sandia Laboratory, it became apparent that there were four analog to digital telemetry channels available for instrumentation. However, to fly the experiment physically on the satellite required the permission of the Vela Joint Technical Group (JTG).

The advantages of the lithium cell and the rationale for flying the experiment on Vela IV were presented to the JTG in December 1966. At that time, the JTG stated that we could only proceed with the experiment under a specific set of ground rules (Figure 8). The first ground rule, and the one which was the basis for the experiment design, was that the interface with the satellite could in no way decrease the satellite reliability. This meant that no mode of experiment failure could be permitted which could in any manner result in a change in satellite reliability. The second was that there could be no impact on the present Vela schedule. The third was that the experiment could not have any funding impact on the Vela Program. Last, but not least, the normal operation of the experiment could not interfere in any way with satellite performance. This was especially critical in the area of electromagnetic interference since the payload carried sensitive receivers for use in the EMP subsystem.

3.0 EXPERIMENT DESIGN

The information which was desired from the experiment (Figure 9) included both information on the possible degradation of the solar cells and the environment to which the cells had been subjected. There is particular interest in any solar cell degradation due to solar radiation, or from any possible cell degeneration, such as loss of the lithium. Information concerning the accoustical and vibration levels experienced during launch, as well as any forces experienced by the cells during orbital maneuvers, was of special importance since fabrication of contacts which would survive substantial mechanical forces was one of the primary fabrication problems at that time. In addition, information on both the normal radiation background and any solar proton events would be needed. Information concerning the temperature of the array was also needed to evaluate cell performance, since solar cell output varies with cell temperature.

The thermal-mechanical environment (Figure 10) had already been predicted for the satellite environmental specification based on previous

Vela and Titan III launches. In addition, existing flight measurements would be available to verify the environment during both the launch and orbital phases of the mission.

One of the greatest advantages of using the Vela Satellite for the experiment was the extensive background radiation instrumentation (Figure 11) built by the Los Alamos Scientific Laboratory as part of the Vela payload. This instrumentation is designed to measure both solar X-ray and particle radiation and is more than sufficient for evaluation of the normal background radiation. In addition, the LASL instrumentation provided sophisticated solar proton fluence measurements in two ways. First, as the fluence of protons greater than approximately 25 MeV and, secondly, in terms of the proton spectrum with 13 spectral channels between 0.55 to 100 MeV. The data on background measurements would be available both in 'quick look' form and from LASL as reduced data for use in solar cell evaluation.

The measurement of solar cell performance is normally made by plotting the current versus the voltage as shown in Figure 12. The maximum power occurs at the knee of the curve and defines the voltage at which solar arrays are normally operated. However, within the weight, space, power, and data restrictions for the experiment, it was not feasible to measure such a curve. As a result, we chose to measure the short circuit current and the open circuit voltage which are indicative of cell performance. In addition, a set of standard cells was to be flown to provide a comparative measurement.

Figure 13 is a simplified circuit diagram of the experiment which is divided into three sections: the solar array, the LID experimental electronics, and the payload logics.

The three strings of solar cells were fabricated and installed by Hoffman Electronics Corporation. The cells were fabricated under a NASA Goddard Space Flight Center solar cell research contract, and were made available for this experiment through the efforts of the Aero Propulsion Laboratory. The largest string consists of ten 1X2 cm 10 ohm-centimeter n/p silicon solar cells with 6 mill cover glass. This string provides the power for the experiment and has sufficient excess power to allow the experiment to operate under relatively small illumination. This was necessary since the satellite is spinning for thermal control and is earth oriented, causing a varying illumination angle except during small portions of orbits during eclipse season. A Zener diode is used to limit the bus voltage to 4.2 volts to provide a constant bus voltage as much of the time as possible. Use of the payload analog to digital converters required use of a positive ground system to match the payload power system which operates between 0 and -6 volts. The lithium experiment's array consists of four 1X1 cm p/n solar cells using 6 mill cover glass. The standard array consists of four 1X1 cm n/p 1 ohm-centimeter

silicon solar cells using 6 mill cover glass. The negative side of both the lithium and standard arrays is routed directly to the payload analog to digital converters and the positive side to ground.

The electronics for the experiment were designed, built, and tested by personnel in the Vela Satellite Program Office at Hq SAMSO, and provided to the spacecraft contractor (TRW Systems) as payload equipment (GFE). The final thermal, vibration, and EMI testing was performed by TRW Systems as part of the normal GFE integration effort. The analog measurements made by the experiment electronics are fed into the payload through the AEC payload harness which had been modified by Sandia Laboratories to accept LID experimental data.

The selection of an open circuit voltage or short circuit current measurement is achieved by use of a data switching network within the LID electronics. When the transistor switch is nonconducting, it presents a high resistance to ground and the voltage on the data line is essentially the open circuit voltage. When the bistable flip-flop draws sufficient base current to turn the transistors on, the transistor switch provides a known resistance path to ground for the current from the array. Since the A/D converter input impedence is much higher than the data switch in the conducting mode, the voltage across the data switch is directly correlatable to the short circuit current of the solar array. The bistable flip-flop is driven by a uni-junction transistor clock and alternates the measurements made on the two arrays. One of the remaining data lines monitors the state of the bistable flip-flop to determine which data is being measured at a given time. The remaining data line is a tap on the silicon power array and indicates when the experiment is powered.

The advantage of this design is that it provides the capability of measuring both open circuit voltage and short circuit current for both arrays during normal operation and provides one or the other data points if the switching circuitry ceases to function because of low bus power or circuit failure. Since the analog to digital converters can satisfactorily operate with the input being short circuited, totally open, or with the maximum array voltage, and since the experiment is independently powered, there is no failure mode of the experiment which can in any way inhibit the function of the payload or spacecraft.

The analog to digital converts the input voltage which varies between 0 and -3 volts into a 5 bit sample. The four data lines are sequentially sampled at 9 second intervals and transmitted by the spacecraft telemetry system whenever the satellite is operating payload real-time readout.

4.0 RESULTS

Figure 14 is a summary of the results at this time. To date, there has been no apparent degradation for either the lithium or the silicon standard solar arrays. This includes post boost and orbital maneuvers

which have resulted in an accoustical level of approximately 129 db overall and vibration level in excess of 3.5g. This indicates that lithium cells can be satisfactorily fabricated to withstand normal launch operations. The present operation of the experiment has also indicated that the lithium cells will operate in the hard vacuum of space over the nominal operating range of -80 to 140 degrees F. So far, the cells have been subjected to a $\geq$ 25 MeV proton fluence of approximately $5X10^8$ protons/cm^2 by the ambient background. The only objective of the experiment which has not been achieved is the result of not having had a significant solar proton event while the experiment has been on orbit. However, this information would primarily be used for correlation with laboratory data and since the lack of proton events has meant a longer solar array life for those satellites on orbit, no one truly objects to not having this data. In addition, based on the typical lifetime of Vela satellites, we expect to observe significant proton events in the future and, at that time, information concerning the relative radiation hardness of the lithium array and silicon standard array should be available.

5.0 ACKNOWLEDGEMENTS

The success of this experiment has been due in large part to the excellent cooperation among several organizations. In particular, I would like to thank Mr. Jim Ewing, who was in the Air Force and a member of the Vela Program Office at the time, for his contribution to the overall effort. Also, I would like to thank Major Jim Kapitzke of the Directorate of Technology at Hq SAMSO and Mr. Joe Wise of the Aero Propulsion Laboratory for their efforts in obtaining the solar cells. Last, but not least, I would like to express our appreciation to Sandia Laboratory, Hoffman Electronics Corporation, and TRW Systems for their assistance in the effort.

VELA IV "LID" EXPERIMENT

I-10

Space Evaluation of Lithium Diffused Solar Cells

Figure 1.

OUTLINE

- Background and Purpose of Experiment
- Experiment Design
- Results

Figure 2

INTEREST IN HARDENED CELLS

- Vela Satellites in 60,000 NM Circular Orbit
  - Minimal magnetospheric protection
- Solar Array Degradation
  - Primarily from solar protons
  - Noticeable degradation from Sep 66 flare
- Solar Cycle Peak in 1968
  - Vela V to be launched in peak
  - Expect significant proton events

Figure 3

SOLAR ARRAY HAPDENING

- Array Design
  - High resistivity N/P cells
  - Thick cover glass
  - Power margin
- On-Orbit Annealing
  - Normally requires high temperature
  - Lithium lowered annealing temperature

Figure 4.

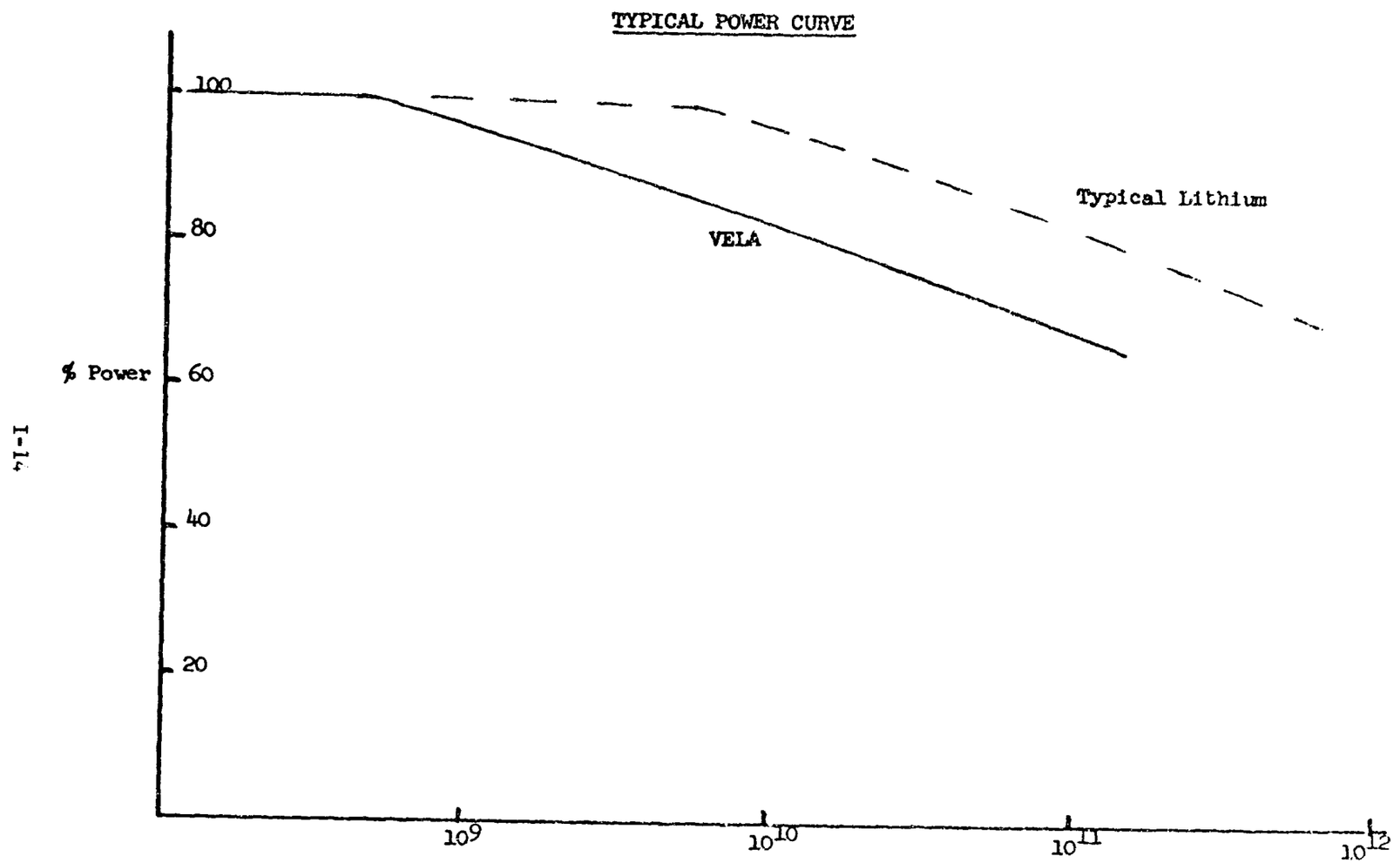
TYPICAL POWER CURVE
100
80
60
40
20
% Power
Typical Lithium
VELA
10^9
10^{10}
10^{11}
10^{12}
protons ≥ 25 MeV/cm^2

Figure 5.

1966 LITHIUM CELL AVAILABILITY

- Cells Under Laboratory Evaluation
  - Have shown healing characteristics
- Not Available for Vela V
  - Not in production
  - Need orbital testing

Figure 6

VELA TESTING POSSIBILITIES

- o Requires Delivered Hardware within 6 Months
- o Experimental Satellite
  - Not in 60,000 NM circular orbit
  - Required development time
- o Vela IV
  - 60,000 NM circular orbit
  - Extensive radiation instrumentation
  - Four A/D telemetry channels available
- o Requires Vela Joint Technical Group Permission

Figure 7

VELA GROUND RULES

1. No decrease in satellite reliability
   - No experiment failure can change satellite performance
2. No impact on Vela Satellite Schedule
3. No cost to Vela Program
4. No interference with satellite performance
   - No electromagnetic interference

Figure 8

INFORMATION DESIRED

- o Solar Cell Degradation
  - Radiation damage
  - Degeneration
- o Environment
  - Lau..ch
  - On-Orbit maneuvers
  - Solar radiation
  - Thermal

Figure 9

THERMAL-MECHANICAL ENVIRONMENT

- o Predicted for Satellite Specification
  - Based on previous flights
- o Flight Measurements Available

Figure 10

RADIATION ENVIRONMENT

- o Instrumentation Built by Los Alamos Scientific Laboratory, AEC
- o Analyzes Solar X-ray and Charged Particle Radiation
- o Solar Proton Measurements
  - Protons 25 MeV
  - 13 spectral channels between 0.55 to 100 MeV
- o Reduced Data Available from LASL

Figure 11

SOLAR CELL PERFORMANCE MEASUREMENTS

- o Cell Performances
  - Short Circuit Current
  - Open Circuit Voltage
- o Standard Cell Comparison

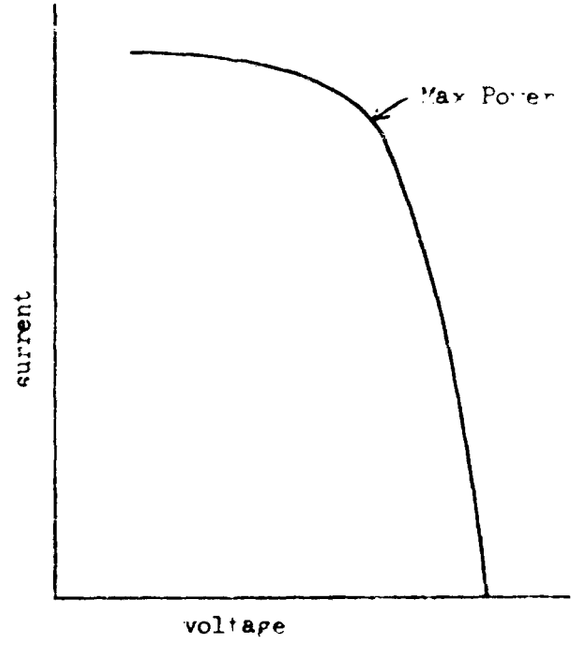

Figure 12

RADIATION ENVIRONMENT

- Instrumentation Built by Los Alamos Scientific Laboratory, AEC
- Analyzes Solar X-ray and Charged Particle Radiation
- Solar Proton Measurements
  - Protons 25 MeV
  - 13 spectral channels between 0.55 to 100 MeV
- Reduced Data Available from LASL

Figure 11

SOLAR CELL PERFORMANCE MEASUREMENTS

- Cell Performances
  - Short Circuit Current
  - Open Circuit Voltage
- Standard Cell Comparison

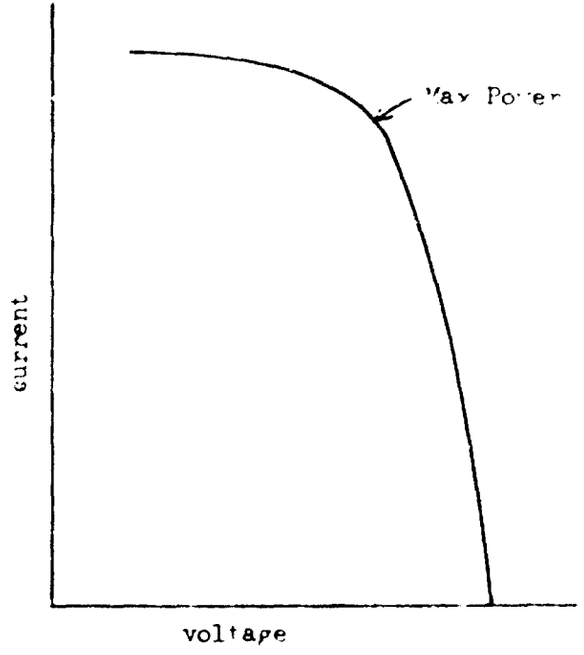

Figure 12

CIRCUIT DIAGRAM

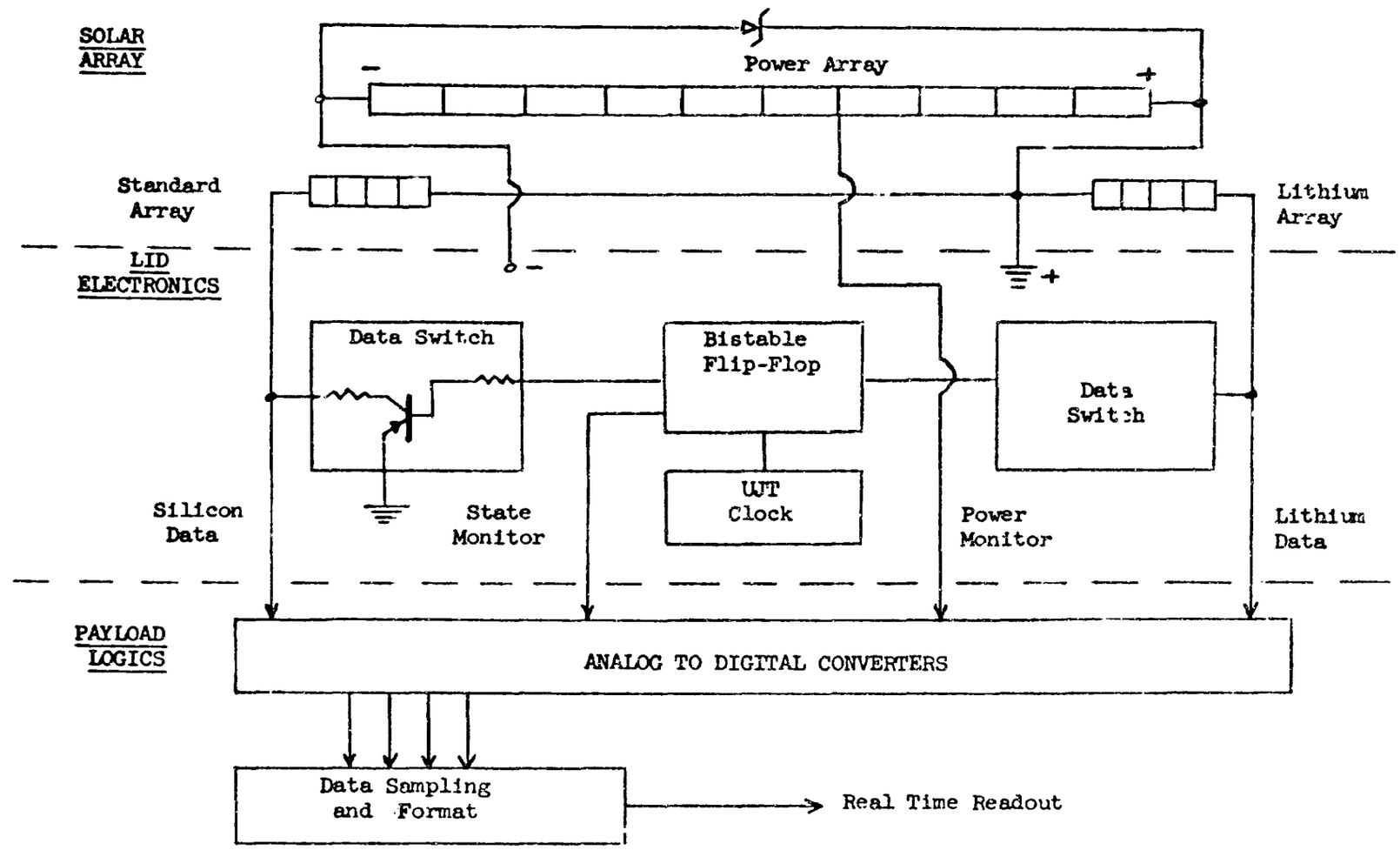

Figure 13.

RESULTS

- o No Apparent Degradation
- o Thermal-Mechanical Environment
  - Accoustic: 129 db overall
  - Vibration: 3.5g
  - Thermal: -80°F to 140°F
- o Normal Orbital Environment
  - Hard vacuum
  - Approximately $5X10^8$ protons > 25 MeV
- o Solar Proton Environment
  - No significant events

Figure 14

PHOTOELECTRIC MEASUREMENTS OF OPTICAL GLINTS FROM ORBITING SPACECRAFT

By

Richard C. Vanderburgh

General Physics Laboratory
Aerospace Research Laboratories
Wright-Patterson AFB, Ohio 45433

PHOTOELECTRIC MEASUREMENTS OF OPTICAL GLINTS FROM ORBITING SPACECRAFT

Richard C. Vanderburgh

Abstract

Even for pencil-beam radar sensors, the power limitations and pulse rate limit the inference of dynamical motions of distant spacecraft to that derivable from short-duration specular returns. Since even these returns are lost to the inverse-fourth power law at somewhat greater slant ranges and since specular transients contain useful information relating both to spacecraft identification and dynamics, it is desirable to have a means of recording them at slant ranges in excess of 5000 kilometers. This can be readily accomplished if one observes space targets in the optical wavelength region. If the sun is used as the illuminator and photomultiplier as a detector, one gains the advantage of a powerful, remote, and continuous source radiating at very short wavelengths compared to the dimensions of the spacecraft.

In this paper, the author demonstrates the effectiveness of a relatively simple and inexpensive method for rapid time-response measurement of the intensity of sunlight scattered from orbiting spacecraft. The equipment, consisting of a four-axis mounted, 61-cm Cassegrain telescope, a logarithmic-feedback photoelectric photometer capable of millesecond time response recording equipment and other ancillary devices, is described, as well as prediction and tracking techniques. Lightcurves from three diverse orbiting spacecraft are presented and analyzed, with emphasis upon the detection and utilization of short-duration specular flashes.

The first of these, the British Ariel III, was designed with mirrors strategically placed on the spacecraft structure to enable determination of the angular momentum vector of the spin-stabilized spacecraft by observation of sun reflection patterns on the ground. ARL photoelectric measurements of this satellite, because of their large useful dynamic range in brightness and excellent time resolution, enabled project scientists to determine not only the angular momentum vector with greater accuracy than could be achieved by on-board sensors, but also the precession or coning angle, even though it could not be detected by the on-board solar aspect cell. Individual mirrors could be identified, glint by glint, by comparison with pre-launch measurements of the mirror dispersion patterns.

The second spacecraft considered here is a spun-up U. S. payload with at least sixteen flat reflecting surfaces evenly distributed about the spin axis. The recorded data show the recurrence of dispersion patterns identifying each flat (even at distances exceeding 4000 km), and an overall pattern leading to the inference of a spin-axis vector.

The third object is the active GEOS 2 geodetic satellite which is equipped with four directional xenon flash lamps to be discharged in various combinations for photography by ground stations. Photoelectric measurements have been made by ARL of many flash sequences to determine performance of individual lamps, to compare the intensities of the various lamp combinations, and to verify spacecraft attitude.

BIOGRAPHY

Mr. Richard Cartwright Vanderburgh, Research Space Scientist (Satellite Tracking) at the General Physics Laboratory, Aerospace Research Laboratories, began his employment in ARL under an Ohio State Research Foundation contract in October 1964. He joined the ARL scientific staff under a U.S. Civil Service appointment in May 1966.

Born in Shanghai, China, Mr. Vanderburgh moved to Hawaii with his parents and brother in 1936, where he attended local schools through two years at the University of Hawaii. He continued studies at Springfield College (Massachusetts) and returned to Hawaii to take a B. A. degree in economics in 1950.

In January 1951 Mr. Vanderburgh entered active USAF military service, with basic training at Lackland AFB, primary aviation cadet training at Goodfellow AFB, and advanced pilot training at Reese AFB. As a pilot-rated second lieutenant, Mr. Vanderburgh completed jet transition training at Moody AFB and was assigned to Shaw AFB for jet photo reconnaissance training. During the winter 1962-1963 he flew 100 combat missions from Kimpo airfield in Korea, and returned to Shaw AFB completing his tour of active service as an instructor-pilot.

During the spring and summer of 1955, Mr. Vanderburgh served as a member of the Hawaii Air National Guard, with full-time duties as assistant operations officer. In December 1955, he joined Pan

American World Airways as a pilot-navigator, and from a San Francisco base, flew scheduled routes throughout Pacific and Orient areas.

Mr. Vanderburgh entered the satellite tracking field as a Smithsonian Baker-Nunn observer at the Hawaii station atop Mt. Haleakala in 1959, and became a Rotarian, serving as Secretary to the Maui Club. In 1960 he became manager of the Baker-Nunn station at Shiraz, Iran, where he was active in the local community as director of the Shiraz Philharmonic Society, and a board member of the Iran America Society.

From 1961 to 1964 Mr. Vanderburgh served as Smithsonian's director of project MOONWATCH, coordinating the efforts of several hundred amateur satellite trackers located throughout the world. Upon his initiation, experienced observers in Milwaukee were alerted to observe the atmospheric reentry of the Russian Sputnik IV satellite, resulting in the successful recovery of a 20-lb. piece of metal found to yield valuable radiological measurements.

In the fall of 1964, Mr. Vanderburgh left Smithsonian to collaborate with K. E. Kissell, ARL physicist, conducting research on the optical properties of orbiting satellites. He began under contract with the Ohio State University Research Foundation, and continues now as a research space scientist in satellite tracking, with ARL's General Physics Laboratory. His current work includes the collection of optical data with the ARL 24" four-axis mounted telescope at Sulphur Grove, Ohio, the

refinement of prediction and reduction techniques, the initiation of technical reports, and liaison with individuals and groups engaged in cooperative efforts.

Mr. Vanderburgh is married to the former Mary Helen Schell, who prior to their marriage had been a stewardess and purserette with Pan American World Airways. They have six children, Richard Schell, David Francis, Paul Montgomery, Mark Peter, Elizabeth Ann, and Mary Margaret.

INTRODUCTION

The Optical Group of the General Physics Laboratory has been conducting research on the optical properties of orbiting satellites for some six years. In the course of recording optical signatures of a thousand transits of two hundred satellites during the last four years the author has become aware of using passive detection in the optical region of the spectrum for measuring specular glints from spacecraft as compared to returns at radar wavelenghts. Ground-reception of radar back-scatter at an orbiting spacecraft is handicapped by an inverse-fourth-power signal loss, a finite pulse repetition rate, and confusion due to resonant interference effects since the wavelengths are comparable to spacecraft structural dimensions. In contrast, ground-reception of scattered sunlight or of light from vehicle-bourne discharge lamps suffers only from inverse square signal reduction, is continuous in character, and is at wavelengths very small compared to structural dimensions. These advantages of optical sensing are particularly applicable to targets at large distances, targets of small cross-section, and/or with surface characteristics which produce specular glints. In some cases, optical and radar sensing can complement each other as data sources leading to the inference of spacecraft physical characteristics and dynamical motions (Ref. 1); in other cases, optical sensing is the only available means. A recent and excellent example of the use of specular glints from spacecraft was the photograph of Lunar Orbiter V by the 1.5 meter telescope of the University of Arizona Lunar & Planetary Observatory (Ref. 2) while in lunar orbit.

After briefly describing the ARL photoelectric system, I will present light-curves of three spacecraft, reduction and utilization of these data, and conclusions encompassing system limitations and future recommendations.

EQUIPMENT

Figure 1 shows the 61-cm satellite tracker consisting of a conventional Cassegrain telescope supported by a four-axis mount. A photoelectric detector is mounted at the Cassegrain focus; the output of the photomultiplier tube is used in several ways. It is recorded directly by a galvanometer recorder and by an FM tape recorder, it is used to modulate an audio tone for the observer to confirm telescope aiming, and it is fed back through circuitry to maintain a constant anode current. This latter operation reduces photomultiplier tube fatigue and provides a large dynamic range (logarithmic through six decades) of brightness sensitivity. A serious limitation of this feedback system is a slower time-response than would obtain from linear signal processing, as will be discussed later. Tracking within a two arc-minute field aperture has been accomplished by manual adjustment of a rate control and an orthogonal centering control as the observer monitors the target image through either a 5-inch finder scope with a wide-view field or a more recent 8-inch guiding telescope not shown

in the figure. More precise tracking is now possible with a new velocity-computer servo system which has recently been installed. Visualizing the 4-axis arrangement may be enchanced by a look at Figure 2, which demonstrates the system as a conventional astronomical (equatorial) mount carried by an azimuth-elevation base. Since the apparent path of a satellite across the sky is closely approximated by a small circle of a particular spherical coordinate system, the azimuth, elevation, and declination are all set to those positions for which motion about the polar axis aims the telescope along the required small circle (Ref. 3, 4). Thus most of the satellite's apparent motion is matched by telescope drive (motor-gear or servo) about the polar axis. Mis-matching is easily corrected for by the manual cross track control.

Quantitative calibration of the detector is accomplished by photometry of solar-type stars whose intensities have been measured by astronomers. The procedures used for calibration are, in fact, borrowed directly from astronomy where reference brightness standards of accuracies of one percent or better exist over dynamic ranges of 10^5. The assumption that steady state calibration techniques are valid for glint measurements appears to be justified by the ARIEL III measurements discussed later.

THE TARGETS

Figure 3 is a pre-launch view of the British ARIEL III environmental-measurement satellite whose design incorporated the placement of optically reflecting flats at strategic angles and intervals to aid in the determination of vehicle attitude in orbit. Since the spacecraft was to be spin-stabilized, sun-glints from a particular group of flats (all at the same angle to the spacecraft axis) would define a locus of possible spin-axis vectors if these glints could be detected from the ground. The British plan was to combine glint-timing data with on-board solar aspect telemetered measurements to produce an unambiguous spin-axis vector. The three groups of flats: body solar cell panels, echelon mirrors, and boom solar cell panels are distinguishable from each other by their number. Thus there are twelve body panels, six mirrors, and four boom panels. Normals to the body panels are perpendicular to the vehicle axis; normals to the echelon mirror surfaces are at an angle of 30°; and those of the booms at angles of 25° and 155°.

Figure 4 shows possible vehicle aspects to produce glints from the several panel groups as viewed by a single ground-based observer. If the spacecraft were spinning at each depicted aspect, the observer would in one case see twelve glints per turn, in another six, and for either of the boom panel conditions four.

In planning the panel-glint scheme, the ARIEL III project scientists had considered only photographic and visual sensing as being readily available. But after examining the first ARL photoelectric record, they realized that photoelectric photometry was not only superior for glint timing, but that the quantitative brightness measurements that it made

possible allowed determination of a slight "coning" angle. If the spacecraft spun about an axis slightly off the geometrical body axis, the individual panels of a group producing glints would not present their respective normals at the position for maximum glint at the same time, as Figure 5 shows for body solar cells. From the simple case illustrated, it is apparent from the geometry that the angle formed at the observer by the line-of-sight vectors to the spacecraft when it is at positions where opposite body panels respectively produce maximum glints, is four times the coning angle. Thus a measure of the time difference of opposing-panel glint maxima may be converted into a position displacement with orbital ephemerides.

Figure 6 shows condensed slight-curves for two transits of ARIEL III. The 10 May record gives six glints per rotation, and hence identifies these as echelon mirror glints. The 17 July record gives twelve glints, identifying these as from body solar cells. By mapping separately the intensity time-dependence of each mirror or panel, one arrives at groups of curves represented orthographically in Figures 7 and 8. Time differences between maxima are related to the coning angle; areas under each curve are related to the optical dispersion of the reflecting surfaces. As expected, the more precisely figured echelon mirrors show less dispersion than the many-faceted and more irregular solar cell panels. From the ARL photoelectric records, the ARIEL III project scientists (Ref. 5) were able to measure the spin axis (angular momentum vector) to better than ± 1°, and the coning angle to ± 0.1°.

While ARIEL III proved to be an excellent target to show the potential of photoelectric glint measurement, the geometry of its orbit produces two significant limitations: the relatively rapid local transits (due to the low orbital altitude) significantly limit the time duration of elevated transits for continuous photometry; and the orbital inclination severely limits the percentage of favorable optical transits during each visibility cycle. A search of available targets of opportunity turned up a US spacecraft (Space Object 2403, International Designation 1966-77A) which at times produces long sequences of specular glints, and has a sufficiently high orbital altitude to allow relatively long continuous photoelectric monitoring of favorable transits, up to 25 minutes in some cases. This target serves well to illustrate some additional aspects of the use of optical glints in the diagnosis of spacecraft motions and geometry, in part because its actual configuration is not known to the author.

Figure 9A shows two sections of a single transit of this object. The sun-satellite-observer geometry of this particular transit produced a continuous burst of bright glints during a two-minute interval followed by about seven minutes of widely spaced weak glints (not shown), and then another two minute burst of continuous bright glints. Even from this condensed record, a periodicity is evidenced by the one missing glint in every sixteen (except at the very end); one can sort out the individual glint-producing sources (most probably solar cell panels) and plot their time-dependent intensities (as was done with ARIEL III). In this case, however, the resulting curves are not single peaks, but undulate in a a rather complicated manner.

Figure 9B shows a time expansion of four rotation cycles selected from Figure 9A. It is clearly seen that identifying characteristics are associated with each glint surface, characteristics which remain recognizable throughout the transit, and indeed on transits weeks apart. Had a pre-launch measurement been made identifying the dispersion pattern of each surface, as was done by the experimenter on ARIEL III (Ref. 5), the photometric record would allow each surface to be identified absolutely, and the rotation roll angle specified to an accuracy of a few arc minutes.... in this case at a distance of over 4000 km. . . . without the need for telemetry of any sort. Observations every few days would allow a continuous time history to be interpolated between the observation intervals.

Attempts to infer structural details of unknown spinning targets (other than smooth spheres) requires knowledge of the spin-axis direction (angular momentum vector). In the case of ARIEL III specular bursts from two groups of glint surfaces (inclined at different but known angles to the spin axis) sufficed for an ambiguous spin axis determination. In the case of object #2403, the solution is not so apparent, although the nature of the entire light curve suggests a probable spin axis. In seeking such a solution, it is convenient to construct a satellite-centered reference system with vectors directed toward the sun and the observer, with a third vector bisecting the angle formed by the other two, the phase angle. Figure 10 shows, in a celestial reference frame, the motion of the phase-angle bisector during the observations. Near the times of Figure 9A, the mirror-like flat surfaces on the spacecraft must have coincided with this trace of the phase angle bisector, producing the direct reflections of a portion of the sun's surface. Assuming that the glint-surface normals are perpendicular to the spin axis one can tentatively place the spin-axis 90 degrees away from the two locations of maximum specular brightness. The glint-surface normals would then have moved along the trace represented by the dashed curve as the spacecraft rotated. This great circle is observed to cross the trace of the phase angle bisector at the two times of maximum glints and to lie near it during the intervening period. Support for the assumptions leading to this choice of spin axis is provided by the persistence of the panel #9 glint during the seven minute "quiet" interval. As noted in Figure 9B, the ninth panel has the largest apparent dispersion of all the panels..... probably enough to direct observable glints to the telescope between the most favorable times, since the maximum separation between the normals and bisectors curves was about 2.5 degrees.

Another useful parameter easily measured from most light curves of spinning or tumbling targets is the rotation rate. Such measurements throughout the 29 March 1968 record of object #2403 produced a range from 9.90 seconds to 9.93 seconds per revolution.

The GEOS B geodetic satellite is the third target considered here, and although its Xenon lamp flashes are technically not specular glints, the observed effect is practically the same. Figure 11 shows the spacecraft pointing earthward as governed by its gravity-gradient stabilization boom (Ref. 6). Continuous alignment with the local vertical (with a residual small-angle libration) produces a simple and easily predictable lamp-angle computation, an important parameter for determining received intensity,

since the lamp reflectors were designed to make received intensity dependent upon direction (lamp angle). The spiral antenna hemisphere on the underside of the spacecraft is a diffuse white and serves to provide a steady but faint amount of sunlight to the observer, giving him a continuous target for guiding

Figure 12 shows photometry of three five-flash sequences of a single lamp, a time expansion of one of the flashes, and a comparison of its waveform with that of a pre-launch laboratory measurement by The Johns Hopkins Applied Physics Laboratory. On the condensed record, note that the flashes rise from a slight plateau above the sky brightness level. This plateau is the faint steady return from the antenna hemisphere. The flash at $00^h\ 16^s$ U. T. was only partially recorded, since the target was not entirely in the sensing aperture. The expansion of the $00^h\ 46^m\ 16^s$ flash was made by slow play-back of the FM tape into the recording oscillograph to obtain best advantage of the galvanometer response. At this scale, one sees that the flash rise point is measurable against the WWV time tick to a few tenths of a millisecond. Conversion of this curve to linear units and comparision with the APL measurement shows a difference between the two curves which is probably due to the response time limitations of the ARL logarithmic-feedback photoelectric mode. Since tests have shown that the ARL system (as arranged for optimum response in the logarithmic mode) has approximately a one millisecond rise-time, a noticeable difference between the two compared curves is expected. One might also expect the ARL curve to peak at a lower absolute intensity than it would have with a faster response time, but this effect is likely to be similar in the case of all light pulses of similar rise times and similar widths.

For this reason, despite the response time limitations, I felt that a plot of measured peak intensities of all four lamps in various combinations over a five month period might reveal information on the performance of the flash lamp system. Figure 13 shows the distribution of the peak intensities (given in an arbitrarily but absolute visual stellar magnitude, i. e., all observed intensities have been adjusted to a 1000-km slant range) of 96 flashes of various combinations of the four lamps as a function of lamp angle calculated on the basis of true verticality of the spacecraft. I should note here there should have been no measurable degradation of the lamp intensity during the period covered. Laboratory tests (Ref. 7) indicate only a 10% intensity loss should occur after 100, 000 flashes; by 5 July 1968 each lamp had been fired less than 18, 000 times. The dashed curve represents laboratory measurements of the distribution of energy (integral of the intensity over the flash) to be received from the flash as a function lamp angle.

Five groups of 3-lamp flashes are in reasonable accord with this predicted distribution although there are two 3-lamp groups significantly above the curve. Although confirming telemetry has not yet become available, it appears that the two plotted 4-flash groups represent the actual firing of only three lamps, and that one of the 2-lamp groups may represent the actual firing of only one lamp. Not infrequent difficulties have been encountered with the GEOS B spacecraft command injection system and other types of lamp malfunctions, including spurious triggering

in mid-sequence have occurred. All such events which we observe are reported to the GEOS Project Office at NASA.

IMPLICATIONS OF RESULTS

The basic ARL 24-inch photoelectric system, which could be duplicated for less than $100,000, is capable of recording specular glints from small mirrors or mirror-like surfaces on spacecraft in rapid dynamic motion producing data that are of sufficient quality to make possible determinations of these dynamical motions more precisely than can presently be done with current on-board sensors and telemetry channels, at least with spin-stabilized spacecraft. Modifications of the photoelectric circuitry could reduce signal rise times from a millisecond to a few microseconds for targets of predictable brightness ranges; this would allow accurate quantitative measurements of such very brief light pulses as are produced by the geodetic satellite lamps. The great penetration range of the present system may be illustrated by noting that sunlight from a 3-inch mirror over 100,000 km distant could be detected.

Thus from the standpoints of cost, response time, and penetration the use of optical techniques is quite attractive in the study of space objects. The photoelectric tracking system as developed at ARL can be considered a prototype for an operational device applied to Air Force problems where diagnosis of dynamical motion, in-orbit configuration, or in-orbit system performance are required and where judicious use of optical signatures will allow these diagnoses.

REFERENCES

1. Mohlke, B. H., Vanderburgh, R. C., Kissell, K. E. "Initial Results of Simultaneous Radar-Optical Signature Measurements (S) Proceedings of Second GISAT Symposium at The MITRE Corp., Bedford, Mass., 1967.

2. "First Photographs From Earth of a Lunar Satellite" Sky & Telescope Vol 35, No. 4, pp 220-221, April 1968.

3. Kissell, K. E., "Advantages of a 4-Axis Tracking Mount for the Photoelectric Photometry of Space Vehicles" ARL Technical Documentary Report #65-260, Dec 1965

4. Vanderburgh, R. C., "A Prediction and Tacking Method for Small-Aperture, Continuous Optical Tracking of Artificial Satellites" ARL Technical Documentary Report #66-0008, Jan 1966.

5. Bent, R. B., "Attitude Determination of the ARIEL III Satellite" Nature Vol 216, No. 5110, pp 45-47, 7 Oct 67 & Proceedings of the Symposium on The Optical Properties of Orbiting Satellites (OPOS) Univ of Miami, Dec 1967.

6. NASA - GSFC Operation Plan 20-67 Geodetic Satellite (GEOS-B) Nov 1967.

7. Private Communication with R. Willison (Johns-Hopkins Applied Physics Laboratory).

ACKNOWLEDGEMENTS

Grateful appreciation is due K. E. Kissell (ARL) for his early insight to the potential value of the photoelectric photometry of satellites, and for his many helpful ideas and suggestions on the interpretation of the photometric data on Space Object 2403 and GEOS B.

Credit is due R. B. Bent (RSRS, England) for designing the ARIEL III mirror system, and for recognition of the coning angle information contained in the ARL light curves.

Thanks are also due personnel of the NASA Goddard Space Flight Center's Geodetic Operations Control Center and the Johns-Hopkins Applied Physics Laboratory for their kind assistance in providing GEOS B information to the author.

Acknowledgement also must be given to the late Kenneth L. Mulvaney for his many useful contributions and improvements to the data collection system, which have greatly simplified technical aspects of data collection.

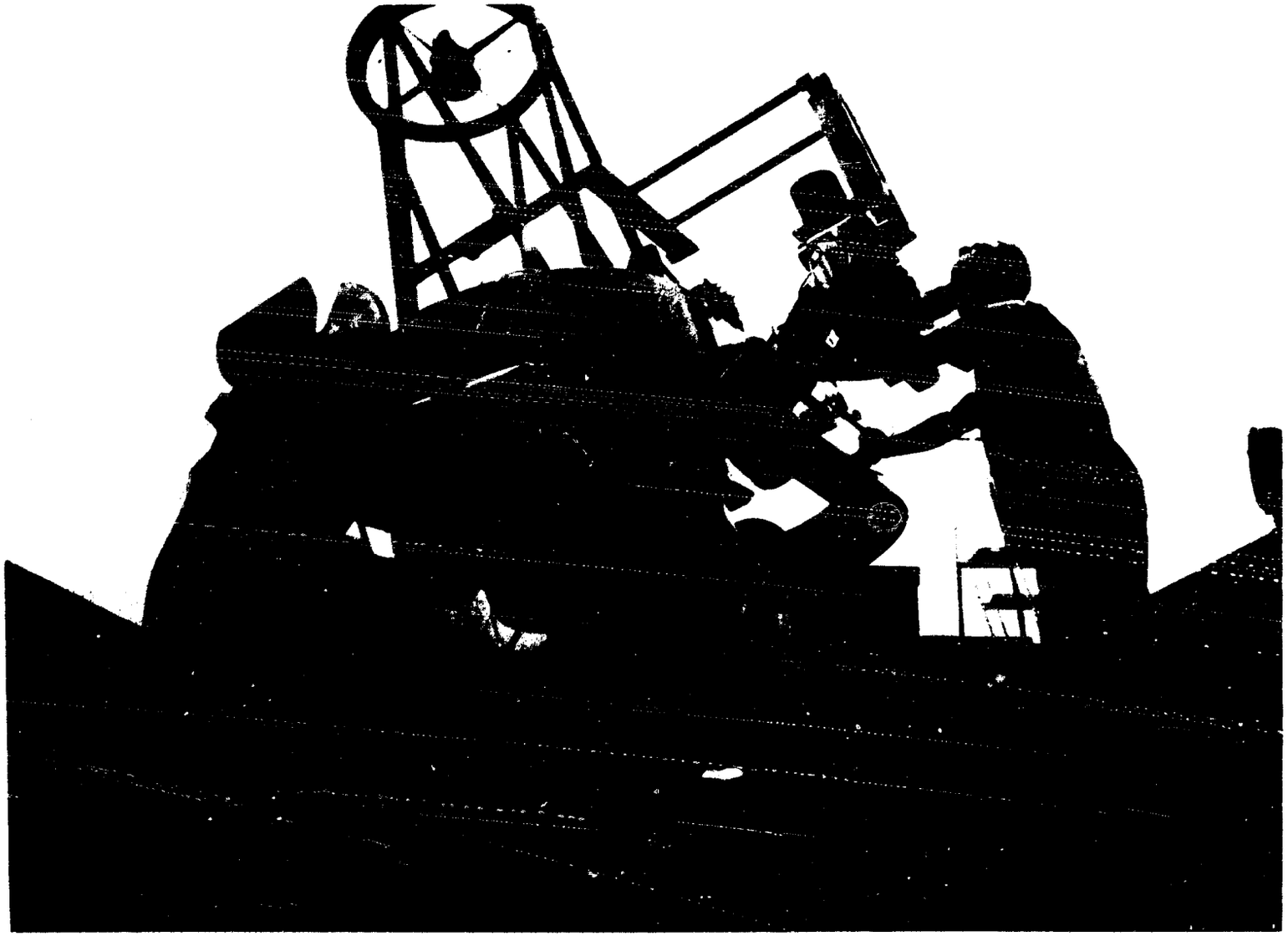

Figure 1 - The Author with the ARL 24-inch Photoelectric System

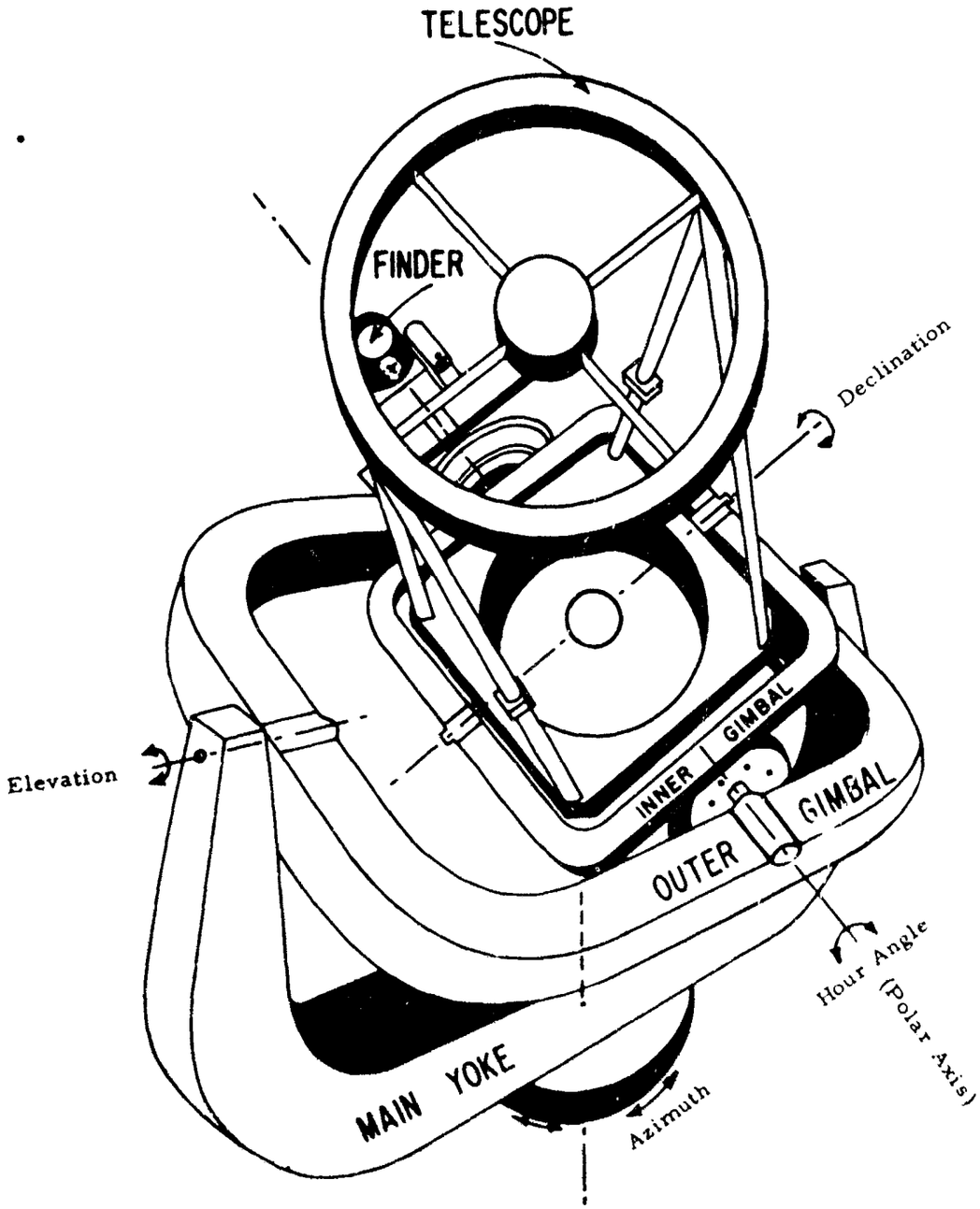

Figure 2 - The 4-Axis Telescope Support System Viewed as a Conventional Equatorial Mount Carried by an Alt-Az Base

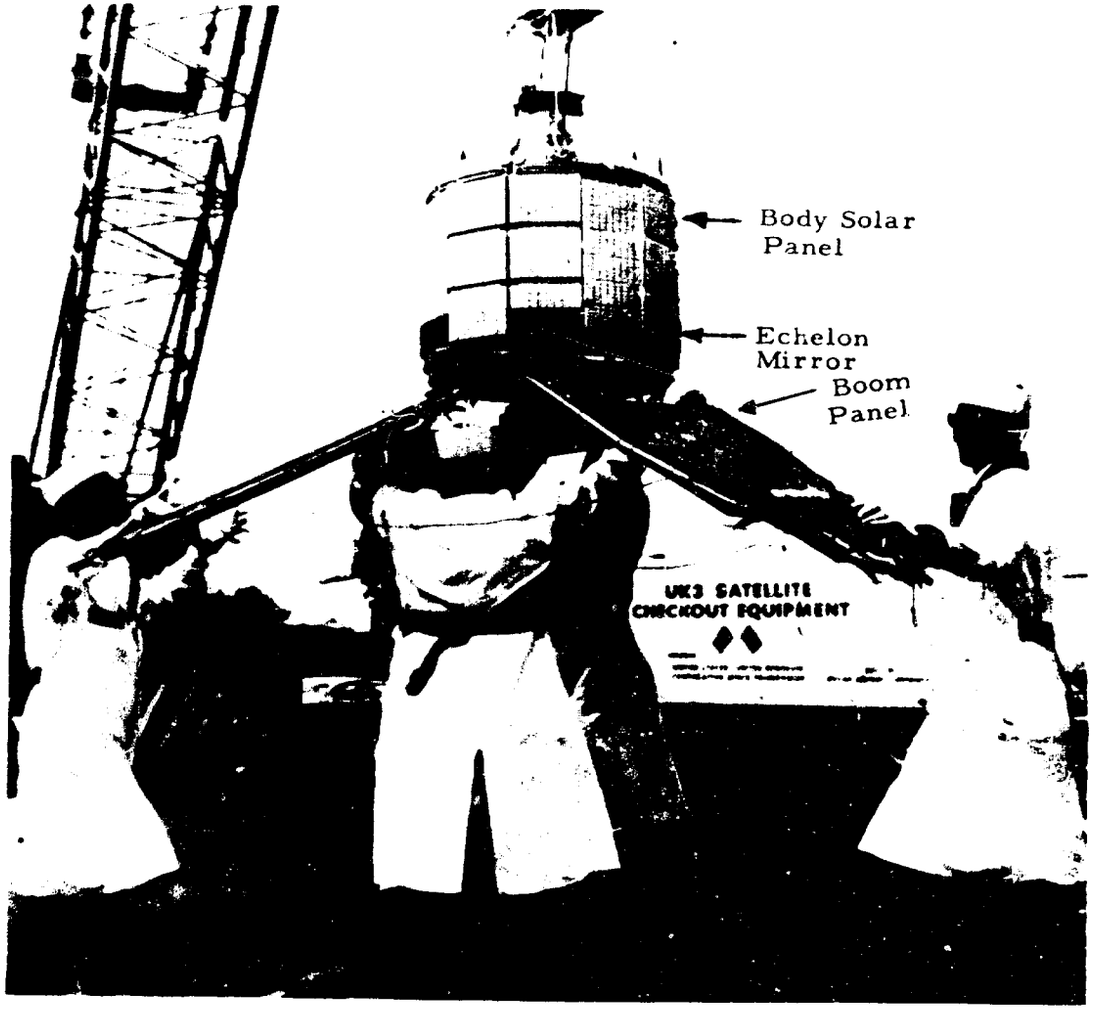

(Photo - Courtesy of R. B. Bent)

Figure 3 - Ground Check-out of ARIEL III (SDC #2773)

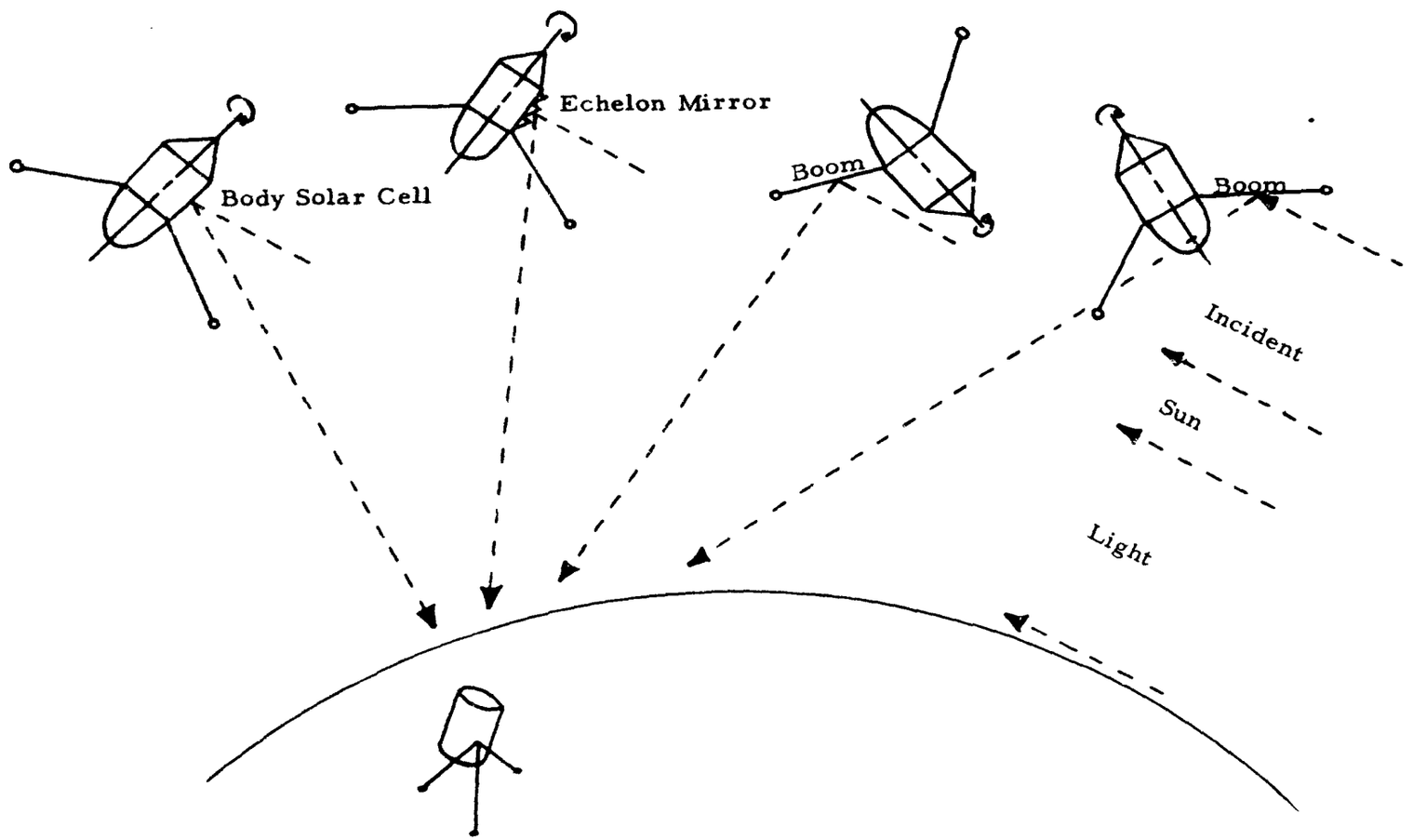

Figure 4 - Sun-Satellite-Observer Geometry to Produce Glints from ARIEL III Specular Surfaces

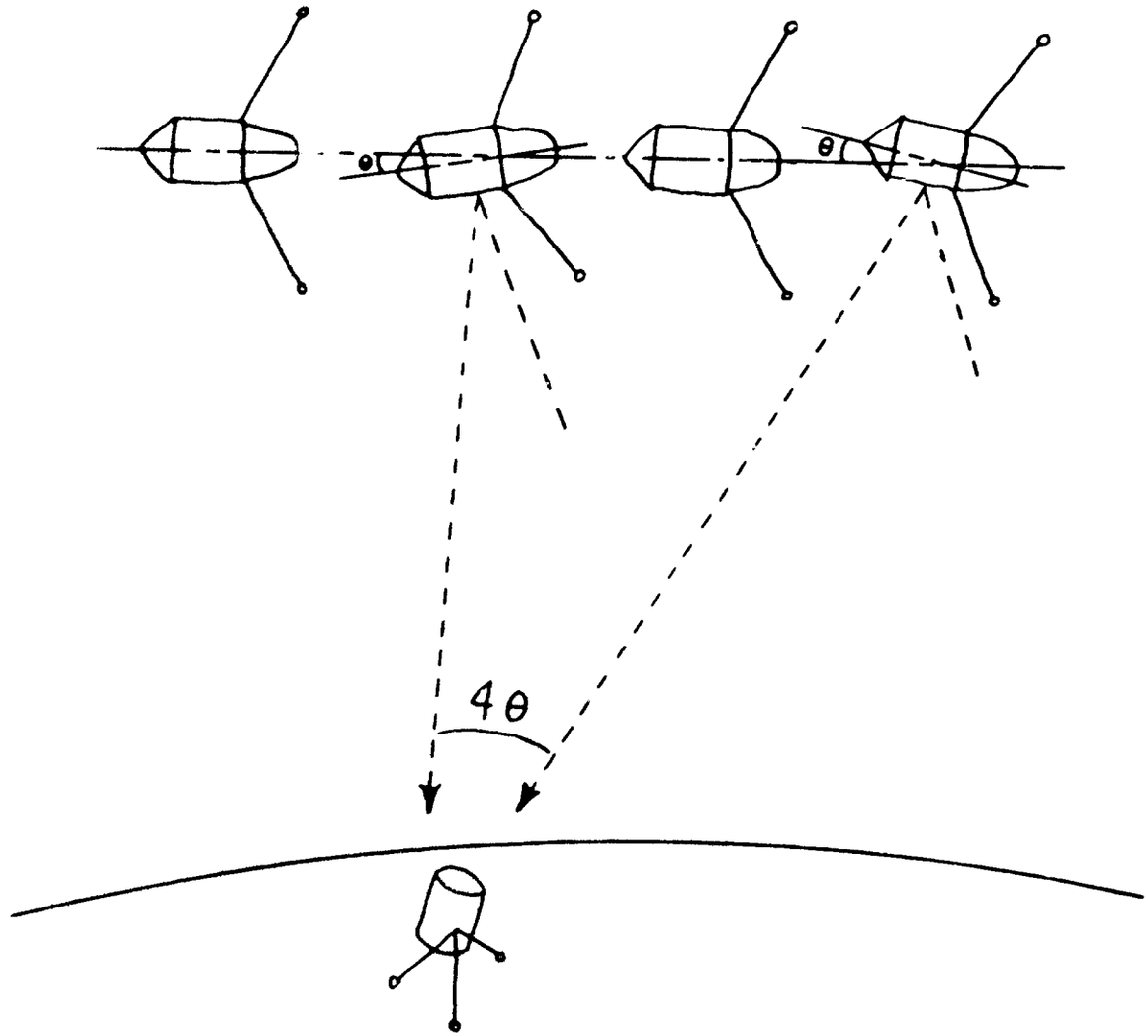

Figure 5 - ARIEL III Coning Geometry

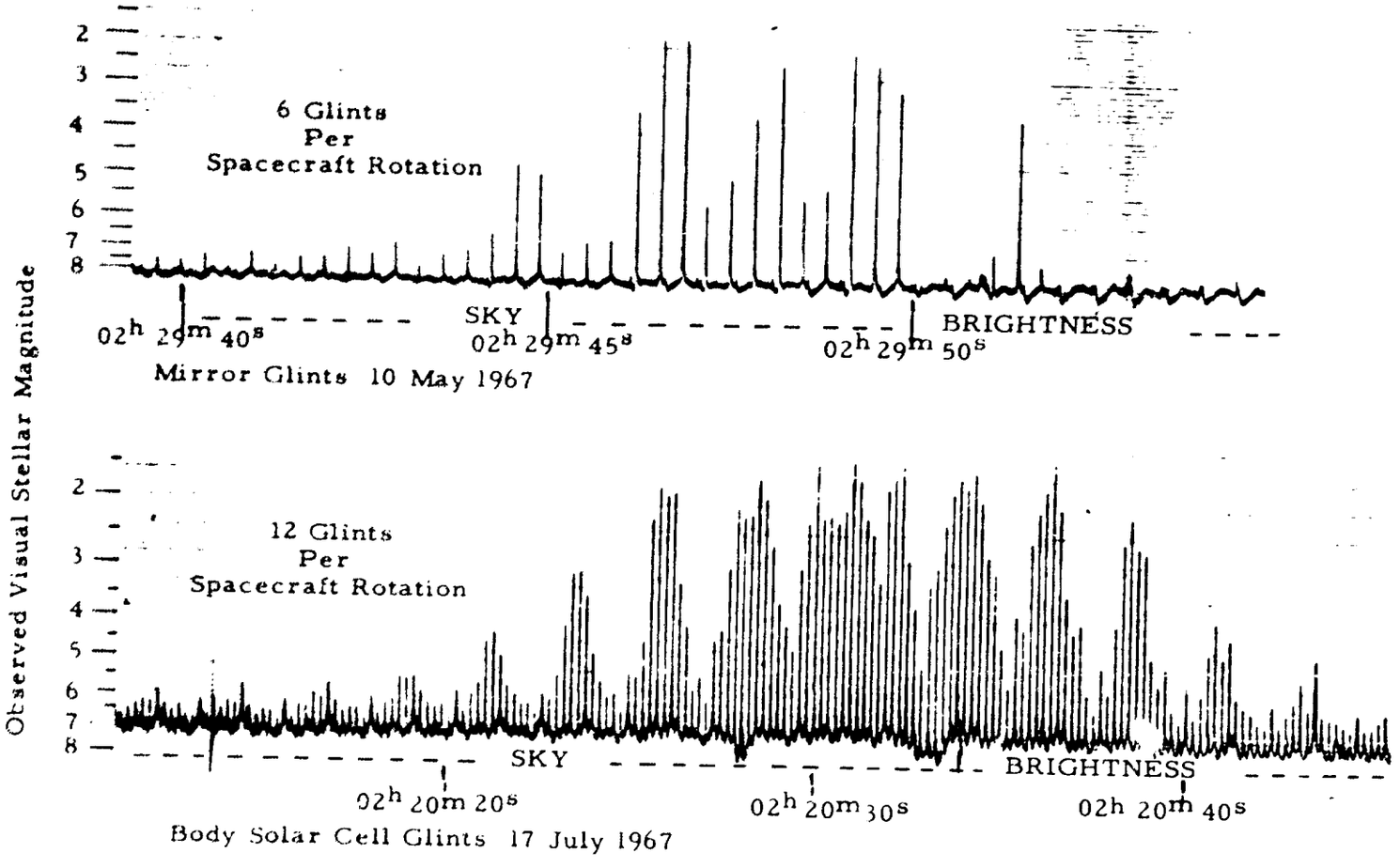

Figure 6 - Photoelectric Photometry of ARIEL III at Distances (Slant Ranges) of 900-1600 km

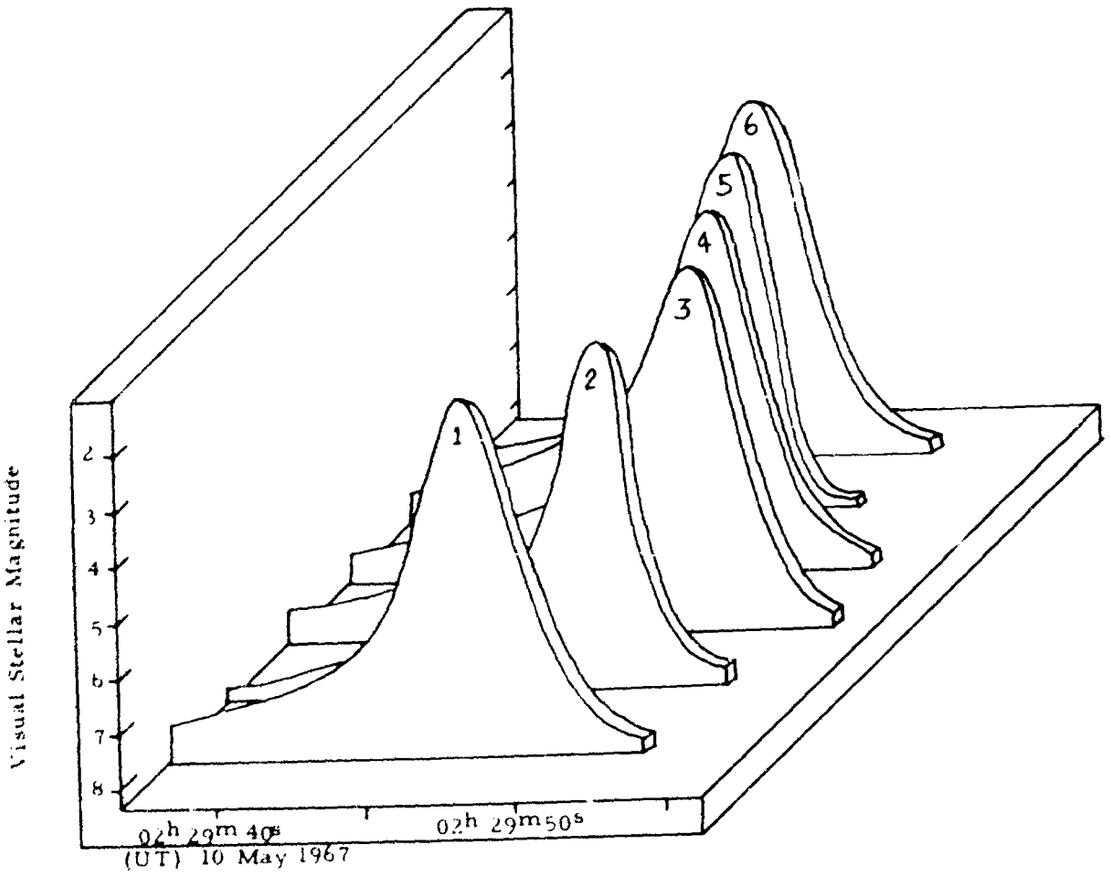

Figure 7 - Time Dependence of the 6 Echelon-Mirror Peak Intensities as Determined by Photoelectric Measurements

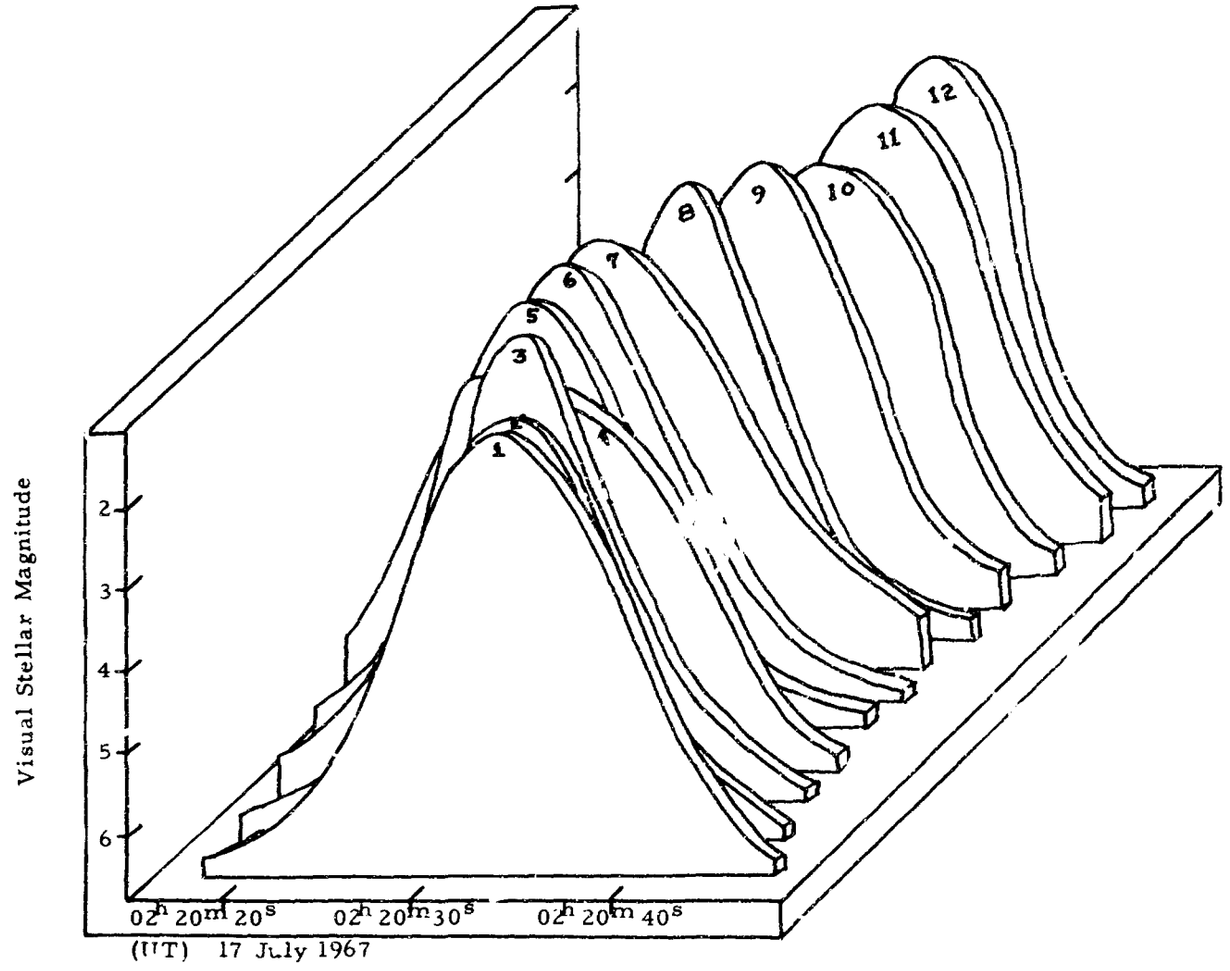

Figure 8 - Time Dependence of the 12 Body-Cell Peak Intensities as Determined by Photoelectric Measurements

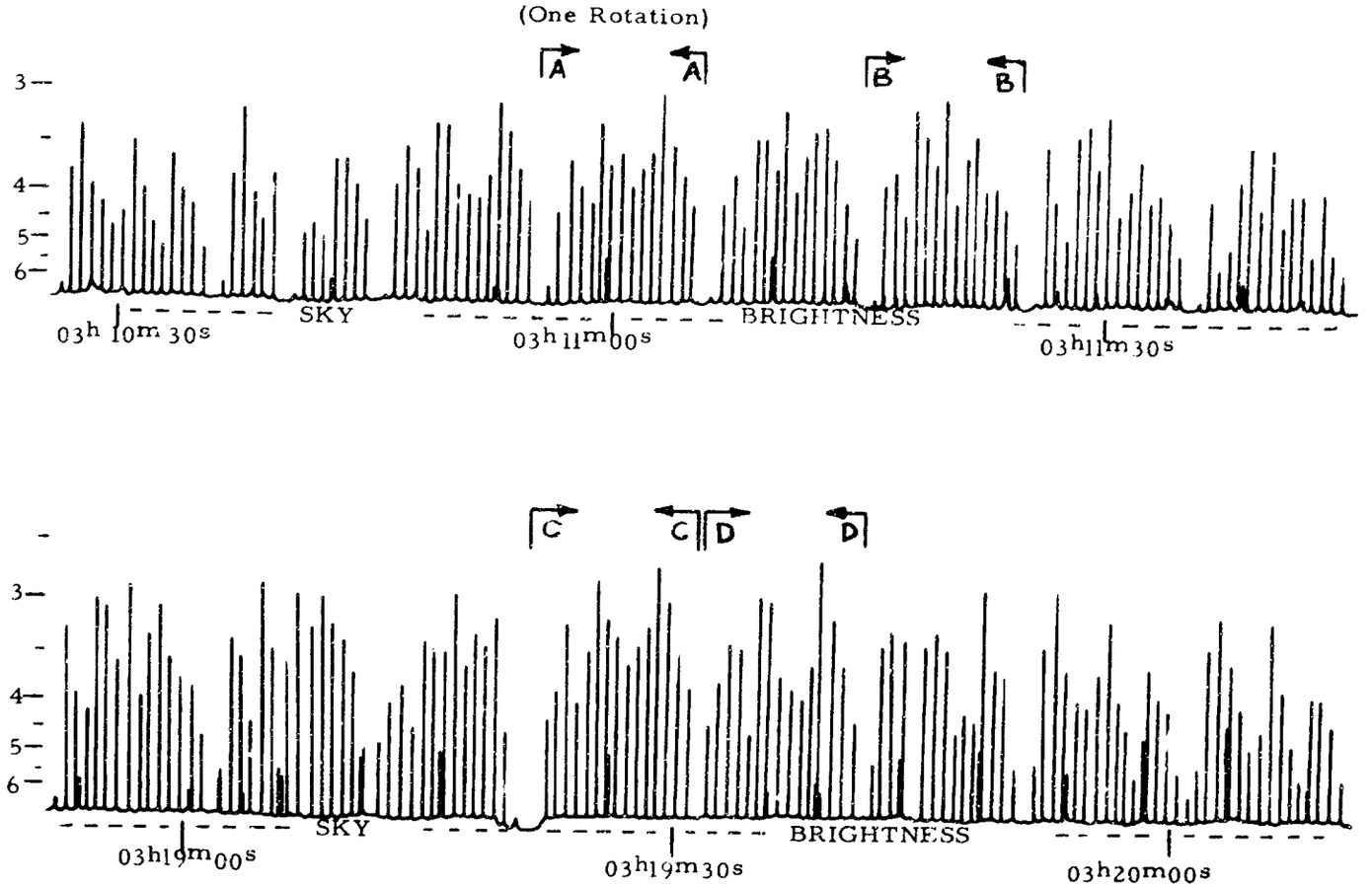

Figure 9A - Photoelectric Photometry of a USAF Spacecraft (SDC #2403) on 29 March 1968 at Distances (Slant Ranges) of 3900 - 4000 Km

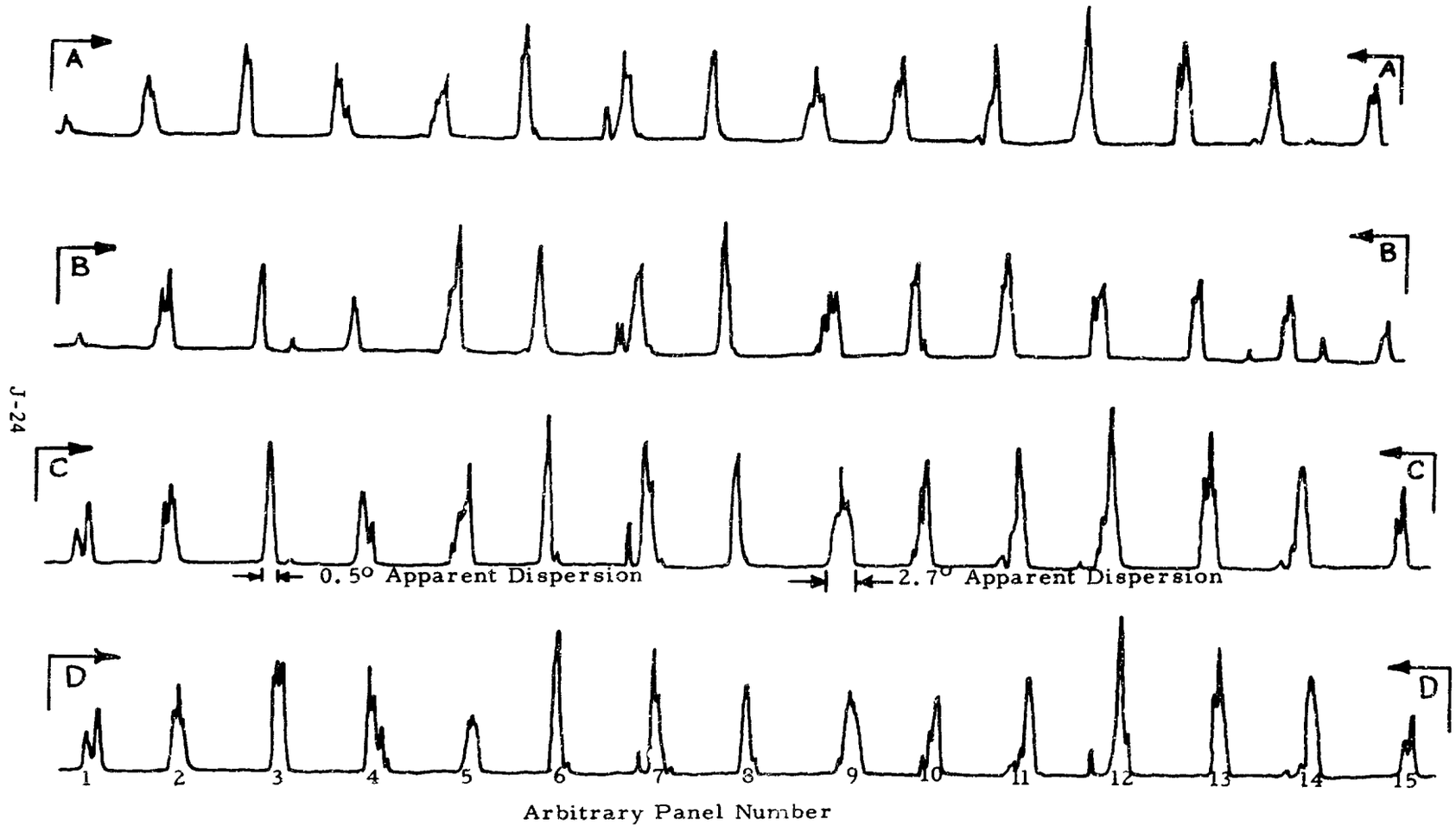

Figure 9B - Expansion of Figure 9A - Sections to Show Optical Signatures of Each Glint Surface

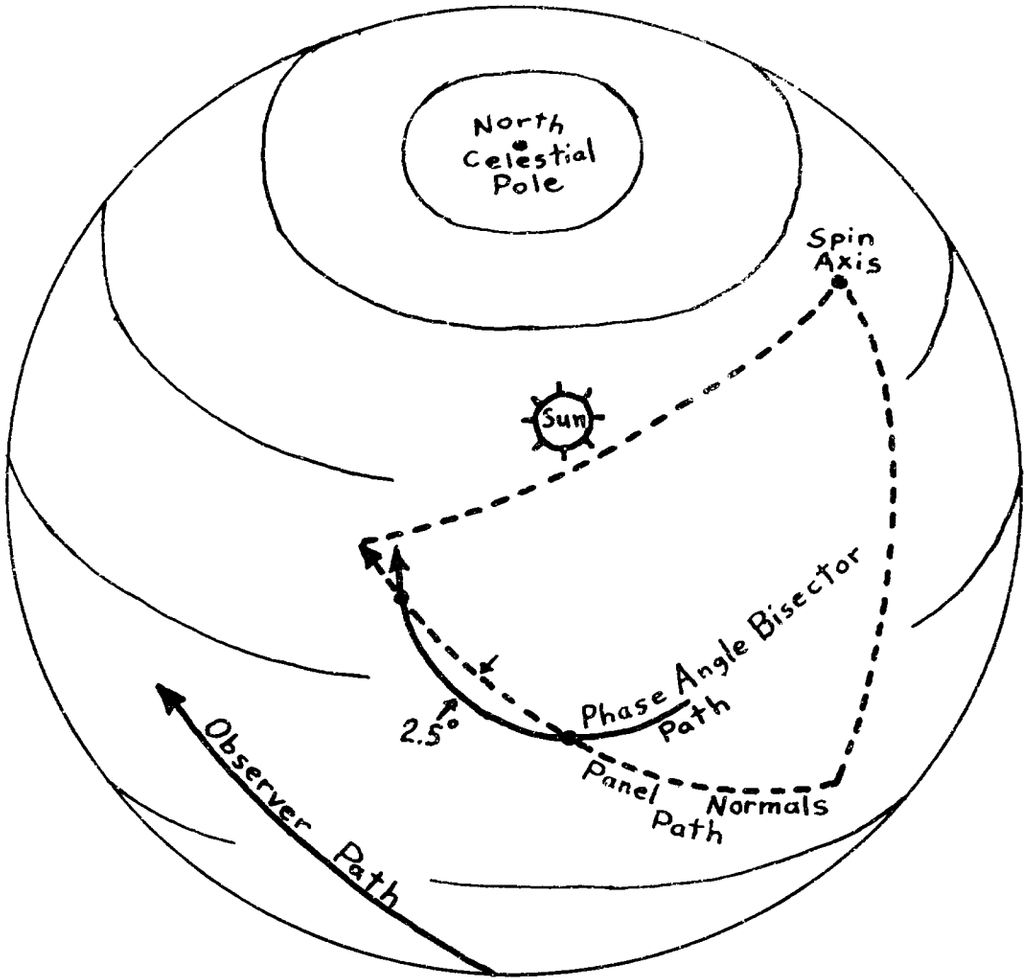

Figure 10 - Satellite-Centered Celestial Sphere Representing
Illumination Geometry Determining Object #2403 Spin Axis on 29 Mar 1968

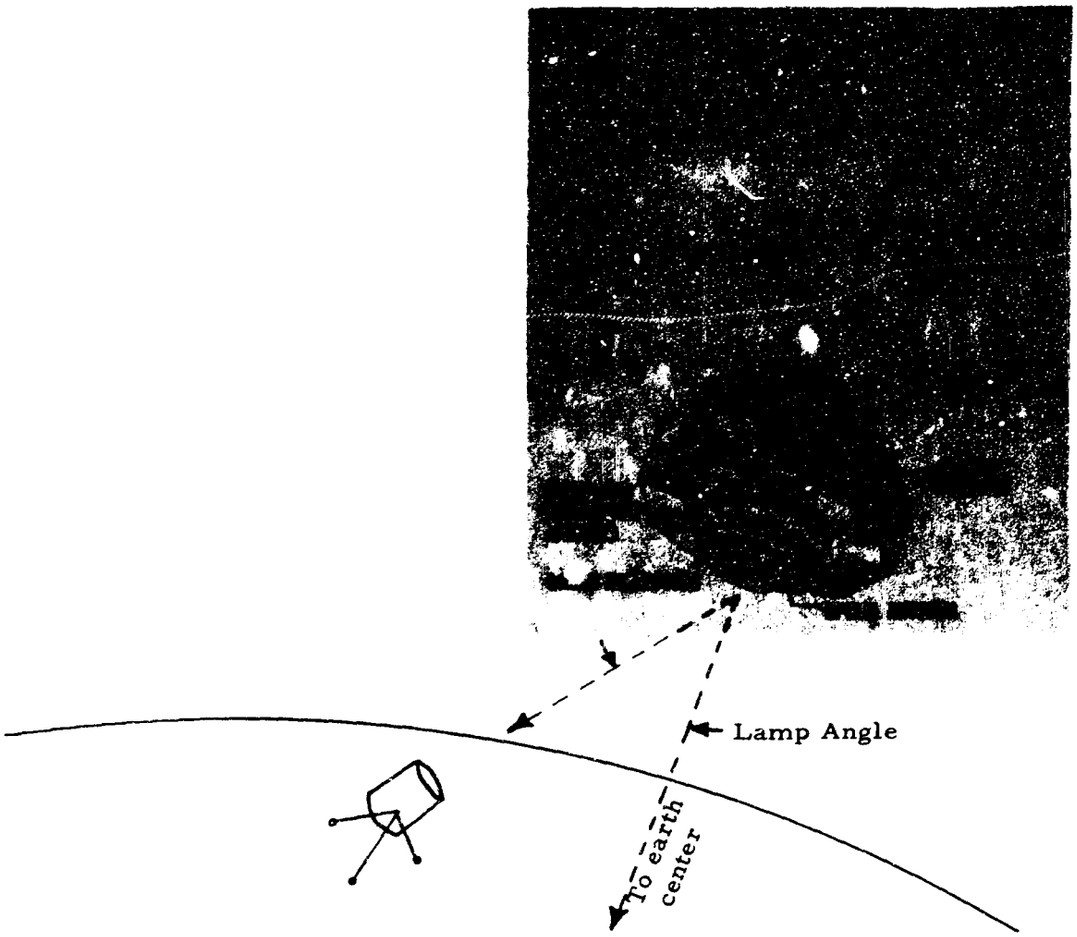

Figure 11 - The GEOS-B Spacecraft (SDC #3093)

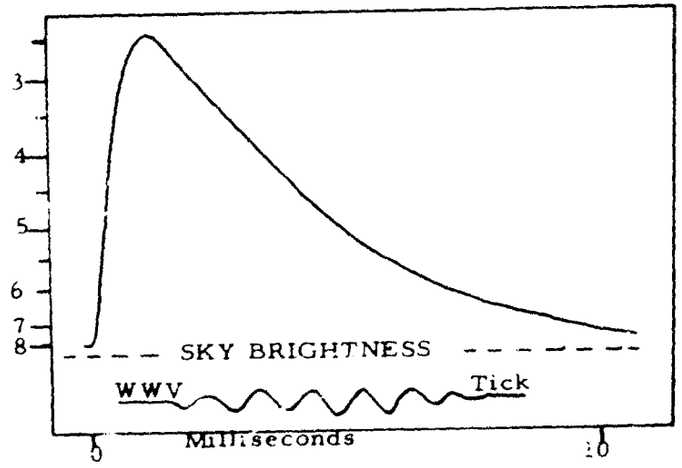

Expansion of $00^h46^m16^s$(UT) Flash

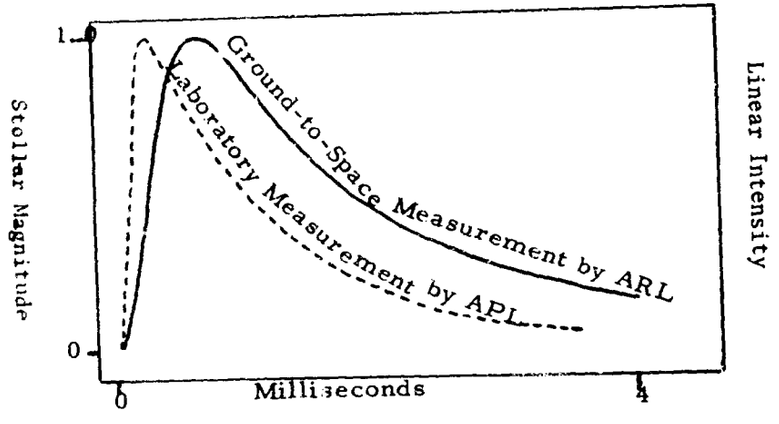

Con parison of Pre-Flight and In-Flight Intensity Measurements

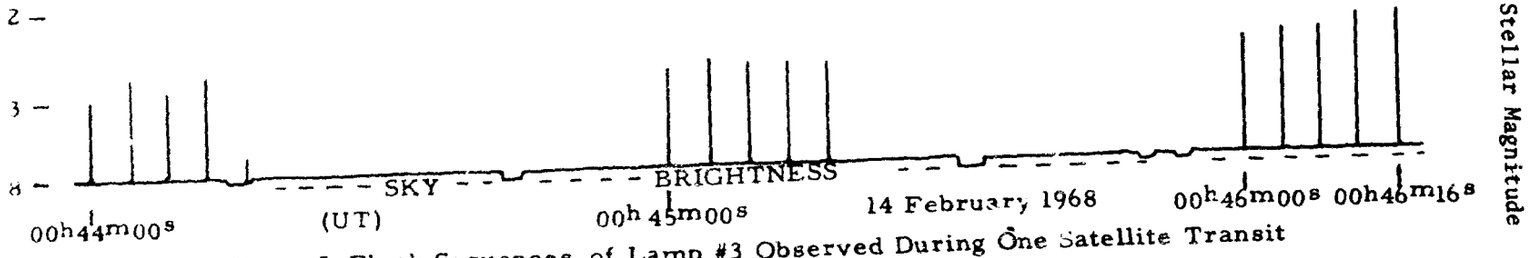

Three 5-Flash Sequences of Lamp #3 Observed During One Satellite Transit

Figure 12 - Photoelectric Photometry of GEOS B (SDC #3093)

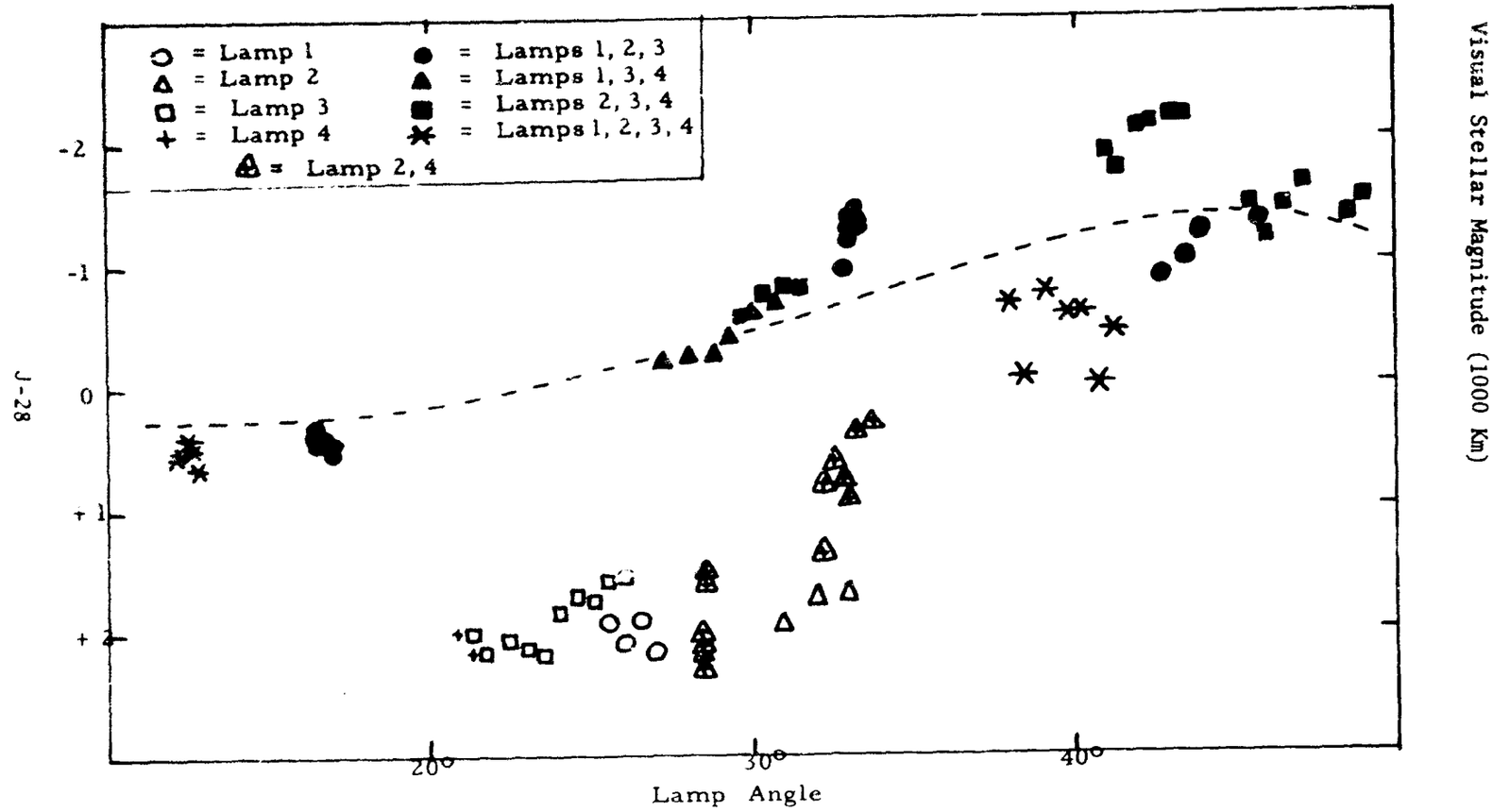

Figure 13 - Light Angle Dependence of GEOS B Flash Lamp Peak Intensities As Determined by Photoelectric Measurements from 4 Feb 1968 to 5 July 1968
(Dashed Curve Represents Pre-Launch Measurements)

MINUTEMAN ORDNANCE RELIABILITY AND SERVICE LIFE PROGRAM

By

L. Keith Norseth
Aerospace Engineer
Service Engineering Division
270th Airmunitions Wing

For the

19[illegible]
UNITED STATES AIR FORCE
SCIENCE AND ENGINEERING SYMPOSIUM

31 October 19[illegible]

MINUTEMAN ORDNANCE RELIABILITY AND SERVICE LIFE PROGRAM

L. K. Norseth

Abstract

A surveillance program for the explosive components on the Minuteman Weapon System was established jointly by AFSC (SAMSO) and AFLC (OOAMA). It included testing of both R&D and operational items. Tests on both full scale explosive components and special test samples of the various components have been conducted since 1960.

The objectives of the surveillance program are to determine the ultimate service life of the age sensitive items, to detect trends in the data that will provide information concerning when procurement of replacement items must be initiated to be available at ageout, and to determine accept/reject criteria.

Testing includes both destructive and nondestructive methods. Nondestructive test facilities include visual inspection, borescopic inspection, and radiographic inspection utilizing 24 MEV linear accelerators. Bench checks of electrical circuits in the electro expolsive devices are also conducted. Destructive tests are performed in the laboratory on components to determine physical and chemical properties. Static tests are conducted on Hill AF Range on full scale first, second, and third stage motors and small components are tested at Hill AFB, Arnold Engineering Development Center, and at contractor facilities at both ambient and altitude conditions. Operational missiles are flight tested at Vandenberg AFB.

Data is compared with model specification limits and with lot acceptance or quality assurance data to determine serviceability. A regression analysis is made on the data to determine trends and make predicitons of service life.

Formal reports which describe the test article and test conditions and includes test results, data analyses, and recommendations and conclusions are prepared on each of the destructive tests.

As a result of the surveillance program, the estimated service life of the explosive components of the Minuteman Weapon System has been extended from three years to as much as ten years on the various components with further extensions anticipated. This has resulted in saving a considerable amount of money through const avoidance. Also, a high reliability of the Weapon System explosive components has been demonstrated in the program.

BIOGRAPHY FOR MR L. K. NORSETH

Mr Norseth received his BS Degree in Mining Engineering from University of Utah in 1954. He also studied Chemical Engineering at the University of Colorado and a three month Chemical Warfare School at Edgewood, Maryland.

After receiving his degree, Mr Norseth worked for five years with FMC Corporation as a mining and development engineer. He advanced to a supervisor of engineers and technicians working in process development and research development in mining methods and crystal growth. While at FMC Corporation he discovered a new mineral $BaMg(CO_3)_2$ which was given the name Norsethite. His published paper, "New Mineral From Green River Formation", contains the details of this discovery. He has several patent applications pertaining to mineralogy and processing. He joined Hercules, Inc in 1961 as a solid propellant production and process engineer. He became superintendent over a technical coordination and material control group.

In 1965 Mr Norseth was employed as a Project Egnineer for the USAF at Hill AFB, Utah in the 2705th Airmunitions Wing, Service Engineering Division. Since then, he has been actively engaged in conducting tests on solid propellant rocket motors and explosive devices for the Minuteman Weapon System to determine serviceability, aging trends and predict component life.

MINUTEMAN ORDNANCE RELIABILITY AND SERVICE LIFE PROGRAM

1. INTRODUCTION

a. Gentlemen, I appreciate the opportunity to speak to you about my work with the Air Force. Although we who spend our time in operational weapons engineering have very interesting work, we do not often get to tell about it.

b. Some of you must wonder what my subject, "Ordnance Reliability and Service Life Program", is about and how it applies to an Air Force weapons system, such as the Minuteman. I should like to spend the next few minutes explaining what it is, economically justify its' existence and tell how an engineer expends his time in such a program.

c. Our primary objective is to ensure that Minuteman will function, as intended, if called upon. However, it should be remembered that we have limited resources available. Therefore, the payout by which we measure the results is a trade between cost and operational reliability of the system. As an example an item is designed and manufactured to meet a specification. This specification might state the product must be 99.9% reliable 90% of the time. If the mission requirement is 90% reliability with 90% confidence, it is obvious that some performance deterioration of the component can be allowed and the mission can still be successfully completed. This means you do not have to run out and buy replacement components when the reliability drops a little. Instead establish a surveillance program, test periodically and watch for trends. Only when it is reasonably certain performance will be unsatisfactory in the near future must you replace the item. This is what a service life program is all about.

2. ORGANIZATION

a. Before I go into the details of a surveillance program, I should like to describe the organization to which I belong. I am a member of the Engineering Division of the 2705th Airmunitions Wing. The Wing is headquartered at Hill Air Force Base as a part of OOAMA, which is a part of the Air Force Logistics Command.

b. The Wing has management responsibility for all operational ordnance, other than nuclear, in the Air Force. These include bombs, conventional airmunition, aircraft escape mechanism ordnance, missiles and rockets and containers for storage and shipment. The responsibilities for these ordnance items consist of logistic support, engineering, safety and disposal of defective munitions. The efforts directly related to Service Engineering include field support, procurement support and operational surveillance. As has been stated, I shall concentrate on the Ordnance Reliability and Service Life Program of the Minuteman Missile System.

3. FACILITIES

a. For OOAMA to have the capacity to test all the various Minuteman and other ordnance, extensive facilities have been assembled. These include:

(1) Hill Air Force Range: This Range is located at Lakeside, Utah, which is west across the Great Salt Lake from Hill Air Force Base. There are three test pads, storage facilities, personnel buildings, machine shops and a 25 MEV linear accelerator.

(2) Small Ordnance Range: These facilities are located at Hill Air Force Base. There are several test bays, vibrator, humidity and temperature cabinets, altitude chambers, block house with a drop tower and x-ray facilities. In addition there is a large capacity high altitude chamber being installed. We use this equipment to test small rocket motors, squibs, initiators, detonators, linear charges and bulk explosives.

(3) Laboratory: This laboratory contains all equipment necessary to test JANAF specimens and many other special physical tests on solid propellants. The laboratory can also perform chemical analysis, heat of explosion, erosion studies and many other kinds of tests.

(4) In addition to the facilities described above, many government and contractor facilities are available as needed. These are located throughout the United States.

4. HISTORY OF SURVEILLANCE

There have been observations and tests made on old ordnance for many years, both by the military services and private industry. However, it was not until sophisticated rocketry with very high reliability requirements came into being that Reliability and Service Life Programs, as we know them today, were formalized. Most of this activity has been within the past ten years.

5. SURVEILLANCE OBJECTIVES

Determining the effects of aging on ordnance within the environment of its' use is our objective. Early studies must be conducted to identify the failure modes and establish criteria to measure trends towards failure. Periodic testing against these criteria allow you to develop trends. These trends can then be used to determine the maximum useful life of the ordnance.

6. ESTABLISHING A PROGRAM

We, the 2705th Airmunition Wing, normally receive engineering responsibility for an item after it has become operational and units are

in the field. In this case it is after they have been emplaced in silos at one of the six Minuteman Wing locations. In some instances the Air Force R&D Agency, that developed the system, has established a surveillance program. If so, we modify the plans to suit our needs and continue. If not, we establish a program and look to the operational force to provide aged samples for testing. For Minuteman Missiles, Wings I-V, we at OOAMA have responsibility for three main propulsion motors, site ordnance, G&C package, penetration aids, interstage, batteries and some of the non nuclear ordnance in the reentry vehicle. There are approximately 100 pieces of ordnance per missile. With the various generation changes of some of these items, we have responsibility for more than 200 pieces of ordnance in Minuteman.

7. ORDNANCE ANALYSIS

a. To begin, we examine an ordnance component as an assembly and then break it down to the sub component or material level. The problem is to determine if the propellant, explosive, bending material, etc will be stable for an estended period of time in the environment of its use. It may be that an explosive material by itself is stable, but when placed next to an expoxy resin at a predetermined temperature and relative humidity, it may react. If we can decide the material is not sensitive, we exclude it from further detailed study and examine it further as a part of the whole component only. If we decide the ordnance or any part thereof is age sensitive we then:

(1) Look at similar ordnance previously used by the military industry for stability information.

(2) Examine the chemical history of the material and compare stability with time.

(3) Examine the environment the component will be exposed to during storage and flight.

(4) Look at the flight and static test data available.

(5) Make a regression analysis.

(6) From all the data collected and regression analysis, make conclusions concerning reliability.

(7) Make life predictions.

b. Regression analysis and life predictions are made after each periodic series of tests, until the ordnance is no longer useful.

8. TESTS

Our testing guidelines are:

(1) Measure as many useful parameters from each test sample as possible.

(2) Test the oldest samples available.

(3) Use the smallest sample size necessary for statistical analysis.

(4) Collect variables data if possible. Increase sample size and test attributes if necessary.

9. MOTOR TESTS

a. The three main propulsion motors for Minuteman are tested at the Lakeside facility. The test engineer is responsible to prepare the test directive, determine the data necessary from the test and oversee the firing.

b. Because of the high cost of motors the sample size is limited. We statically test about five motors of each type yearly and use the available flight test data to supplement the information necessary for proper statistical analysis. While flight test data is limited, both in quantity and quality, it has worked out successfully. The motor data available from most flight test include:

(1) Ignition delay.

(2) Internal pressure vs time (All stages).

(3) Thrust termination (Stage III).

c. The static test data are more accurate and in addition to those parameters listed for flight data the following parameters can also be measured:

(1) Thrust vs time.

(2) Nozzle movement data.

(3) Case temperature.

(4) Case strain.

Typical parameters measured are shown in an attached figure.

10. LABORATORY TESTS

a. The tests ran in the laboratory are generally sub component tests in support of the large motor program. The samples include standard JANAF solid propellant dog bones, mini-bones, dynamic shear and several bond strength types. The type data from these test include:

(1) Hardness.

(2) Tensile strength.

(3) Bond strength.

(4) Modulus of elasticity.

(5) Dynamic shear modulus.

(6) Heat of explosion.

(7) Burning rate.

(8) Composition.

(9) Ignitability.

(10) Volatiles.

b. The data which has been the most useful has been physical tests on propellants such as strain at max stress, strain at rupture, shear strength and other physical properties. A typical example would be when dynamic shear modulus test indicated the propellant representing a motor was changing as it becomes older. An investigation would ensue to see if the motors were being adversely affected by this change in physical properties of the propellant.

11. SMALL ORDNANCE TESTS

a. We test the many small Minuteman rocket motors, gas generators, linear charges, squibs, detonators and other small ordnance devices at the Small Ordnance Range. The parameters measured include:

(1) Electrical continuity.

(2) Electrical resistance.

(3) Electrical arming time.

(4) Pressure vs time.

(5) Ignition Delay.

(6) Brisance.

(7) Rate of detonation.

(8) Go/no-go

b. Typical test are those made on interstage ordnance (see figure). These ordnance include electric bridgewire detonators, RDX linear charges, time delay boosters, mechanical S&A devices, electrical A&D switch, H Boosters and instantaneous boosters. The attached schematic diagram can be used to illustrate the interstage ordnance functions as follows:

(1) The A&D switch is armed on the ground.

(2) Bridgewire detonators are fired by battery impulse.

(3) The RDX linear charge explodes cutting the interstage skirt and ignites the delay boosters. The delay boosters ignite the pellets in the mechanical S&A after it has been armed by the accelerating upstage motor.

(4) The H Booster explodes the RDX linear charge to cut the forward end of the skirt and ignite the instantaneous boosters to ignite the four longitudinal charges.

(5) The longitudinal charges cut the interstage into four pieces.

c. Variables data is very difficult to collect on several of these items. Therefore, a large sample is used. Usually 11 samples semi-annually. The inspection and tests include x-ray, g-load, vibration, temperature-humidity, altitude and function. We try to design these tests to include as many items and as many test parameters as possible in each set-up.

12. DATA ANALYSIS

a. The data from the above mentioned tests are analyzed for anomalies in ordnance performance and for trends. One of the most useful tools we have in helping to determine service life is the regression analysis as shown in the attached figure. Test data from the ordnance is collected over a period of time from several tests. The tests represent samples from zero age to several years old. From these data a regression analysis can be developed. A regression line with reliability-confidence bands can be constructed as shown in the attached figure. This analysis, in addition to the historical information and sub scale data collected,

is the basis for [illegible] life prediction. It must be emphasized, however, that life predictions, with resulting official service life extension, should be made with extreme caution. As a general rule we do not extend the life of the ordnance more than one year longer than the oldest test samples. In special cases we must go further, but we do not extend beyond replacement time plus the interval until the next test occurs.

b. An attached figure represents a test on the SE-13G Battery. There are two of these batteries per missile. They are used to provide electrical power to the missile during the propulsion portion of its flight. The entire missile would have to be removed and recycled back to the OOAMA Repair Depot if the batteries aged out. Therefore, we watch them with keen interest.

c. In this real life example the ordinate is voltage and the abscissa is age, in months of the samples. The points at the left of the chart are zero time points, (lot acceptance test of new batteries). They represent the first high current demand on the battery. As can be observed they average about twenty-five and three quarters volts. At 50 months and 60 months are additional points with lesser average values. Additional tests, which support the regression line, have been run but are not included for pictorial clarity. A regression line is constructed from these points which indicate voltage decrease with time. From the data a set of 90% reliability with 90% confidence lines are constructed. Observe the line, "Previous Specification Limit". By definition, voltage below that line is unacceptable. This means we must replace the batteries by the time they are 80 months old. Had the item been less costly and easier to replace, we might have let it drop there, instead we investigated the specification limit. Specifications are established before the hardware exists. Therefore, the tendency is to be conservative and make them too rigid. We found that 23 volts was ample to perform the task. The limit was consequently changed to 23 volts. The battery's performance is now predicted to be good for some time. We shall continue to test older samples to see if trends change. The savings by this study can be measured in millions of dollars.

13. ECONOMIC RESULTS OF PROGRAM

a. The United States has been saved more than a billion dollars by being able to extend the life of the Minuteman Motors from three to seven and a half years and the other ordnance from three years to as many as twelve years.

b. More benefits are yet to come if further testing indicates the ordnance will remains serviceable for longer periods. In addition, intangible benefits are gained because SAC receives periodic reliability assessments. They in turn can target their missiles more intelligently.

[redacted]

a. The Minuteman Surveillance Program has provided a useful and necessary service to the Air Force. By analyzing and testing ordnance as it gets older we make predictions concerning serviceability of the various devices. Life extensions are made from these predictions. Replacements buys are postponed until the last possible moment. This in turn has saved the country more than a billion dollars in the last four years. The possibility exists for large additional savings.

b. The work is extremely interesting and rewarding. As an engineer you are responsible to establish a program to study the chemical and physical properties of the ordnance, test periodically, analyze the data and predict serviceability with time. You save the Air Force money if you find the weapons remaining good. If you find unacceptable performance in some of the components and forward these data to the responsible people, they have the time to replace the defective items before the system reliability is compromised. In either event, if you have done your job well, the Air Force and the U. S. defense posture has been visibly enhanced.

[illegible] TRANSFERRED

AND ITS APPLICATION TO DEVICES

By

Fritz L. Schuermeyer, Ph.D.

John M. Blasingame

Directorate of Laboratories
Air Force Avionics Laboratory
Air Force Systems Command
Wright-Patterson Air Force Base, Ohio

RESEARCH ON THIN FILM SCHOTTKY BARRIERS AND ITS APPLICATION TO DEVICES

Dr. Fritz L. Schuermeyer

ABSTRACT

The rectifying contacts between metals and semiconductors or insulators which are often referred to as Schottky barriers are discussed. Quantum mechanical considerations are outlined and applied to the electronic behavior of these barriers. The experimental techniques employed at the Air Force Avionics Laboratory to characterize barrier parameters, such as barrier heights, electron injection, and hot electron scattering and its implications are discussed, with emphasis being placed on the role of surface states and surface charge with respect to barrier heights. Schottky barriers are of interest for technical applications due to their inherent high internal speed, ease of fabrication, high-temperature capability, relative radiation resistance, and high injection efficiency; for example, Schottky diodes are currently being used as microwave detectors up to almost 100 GH. Several proposed technical applications of these barriers are discussed. One such application, the cold cathode, is based upon a graded insulator concept. Possible applications of these concepts in modern electronic circuits include photocathodes, thin-film transistors, and injection luminescence devices. The feasibility of such devices for Air Force applications is outlined.

BIOGRAPHY

Dr. Fritz L. Schuermeyer was born in Munich, Germany, in 1935. He attended the Technische Hochschule there and received the Ph. D. degree in physics in 1961 with a dissertation on traps in luminescent materials. He was engaged in cryogenic equipment research for Linde Eismaschinen for two years before coming to the United States.

Since joining the Air Force Avionics Laboratory in 1963, Dr. Schuermeyer has made an intensive study of thin films and the mechanisms of electron injection across potential barriers in metal-insulator and metal-semiconductor structures. Since 1966 he has published five technical papers on his experimental work on internal photoemission measurements on thin film oxides. He has developed a theoretical model which permits detailed analysis and interpretation of these data in terms of scattering within the insulator. Dr. Schuermeyer recently discovered a new principle for electron injection devices based on graded bandgap insulators, to date six patent disclosures using this principle have been submitted, and exploratory development is under way.

Dr. Schuermeyer has become one of this country's foremost authorities on thin film micro-electronics. Through application of his concepts, significant advances can be expected in future micro-electronic equipments for Air Force use in computers, reconnaissance, navigation, guidance, fire control, communications, and electromagnetic warfare.

I. INTRODUCTION

In general, when any arbitrary metal comes into intimate atomic contact with any artibrary semiconductor or insulator, there is more than a 90% probability that the result will be a rectifying contact due to the potential barrier which forms at the interface (Ref. 1). Indeed, one of the most difficult problems still remaining in modern solid state electronic-device technology is how to avoid these rectifying contacts and achieve good ohmic contacts. These rectifying hetero-junctions are commonly known as Schottky barriers since Schottky developed the basic model used to explain their behavior. The study of the fundamental properties of these structures has recently become of great practical significance as more and more device applications are being found for charge-injecting barriers.

Metal-semiconductor Schottky barriers have been studied extensively on Si and GaAs, and a number of low-noise microwave mixer diodes and high-speed switching diodes are already commercially available. An Avionics Laboratory exploratory development program on Schottky-barrier field-effect transistors is now under way and appears to be extremely promising. Since metal-insulator Schottky barriers have not been so extensively investigated, recent in-house work in the Avionics Laboratory has been concentrated on this type of structure; the remainder of this paper will be devoted to a brief review of this work. The objective of this program is to study basic current carrier injection and transport mechanisms in metal-insulator-metal (M-I-M) structures and determine possible applications for these phenomena in advanced electronic devices.

II. EXPERIMENTAL MEASUREMENT TECHNIQUES

For samples with relatively thin insulator layers, less than 100 Å, the tunnel emission mechanism can be used to inject current carriers into the conduction band of the insulator. Hence, simple current-voltage measurements can be used to derive information about barrier heights. Data of this type has been taken by use of dc electrometers, a Tektronic 575 curve sweeper at 60 Hz, and by pulse techniques.

A far more accurate and powerful technique, however, is that of internal photoemission. In this technique monochromatic radiation of well-defined energy can be used to excite electrons over a Schottky barrier, and the photoemission yield can be studied on much thicker, more stable samples. Photovoltage as a function of wavelength has been measured by means of a chopped-light, phase-sensitive technique developed in this Laboratory (Ref. 2); this technique has eliminated distortions of the photovoltage by the dark current and the problems due to leakage currents encountered by some other investigators. Photocurrent response as a function of wavelength and applied bias voltage has been measured

by means of the apparatus shown in Fig. 1. This technique has been described recently, in a review article by Goodwin of RCA (Ref. 3), as one of the most effective tools available for studying the properties of insulators.

An additional technique used in this Laboratory is the photo-excited vacuum emission of electrons as measured by the apparatus shown in Fig. 2. This is essentially an external photoemission measurement and thus has the added advantage that the energy distribution of electrons emitted into vacuum can be measured by means of a modulated retarding-grid technique.

Other techniques used for film thickness measurements in this laboratory are: capacitance by means of simple bridge techniques, a quartz-crystal-oscillator microbalance, and a Fabry-Perot interferometer.

III. SAMPLE PREPARATION

Thin film samples for these experimental studies were prepared by electron-beam evaporation in an oil-pumped vacuum system which contained a liquid-nitrogen trap; 99.999%-pure metals were evaporated onto quartz substrates. These films were electrochemically anodized in a 3% solution of ammonium tartrate. Oxide layers of different thicknesses were obtained by controlling the voltage between the Al film and the cathode in the electrolyte. A semitransparent Au counter electrode was then deposited by electron-beam evaporation to form an Al-Al_2O_3-Au junction. The thickness of each electrode was approximately 200 Å; insulator thickness ranged from about 60 to 400 Å.

IV. THEORY

The theoretical quantum mechanical considerations governing the electrical behavior of thin film metal-insulator Schottky barriers can be understood most easily by reference to the energy band diagram shown in Fig. 3. An Al-Al_2O_3-Au sandwich is shown as a typical example of the type of structures investigated; extensive work has been done also on Ta-Ta_2O_5 barriers with various counter electrodes. F represents the Fermi level of the metal electrodes, Φ_1 is the barrier height at the Al-Al_2O_3 interface, Φ_2 is the barrier height at the Al_2O_3-Au interface, and Φ_{max} is the maximum of the barrier. The applied bias voltage is shown by V_{appl}. The model assumes a trapezoidal barrier with image force lowering of the barrier maximum as shown by the rounded corners. hν represents the energy of an incident photon absorbed in the Al-metal electrode.

In general, when an M-I-M structure is illuminated, conduction electrons in both metal electrodes will absorb photons and become excited. There is a probability that excited electrons from both electrodes will pass from one electrode through the insulating film and reach the opposite electrode. However, in this specific example, the Al_2O_3-Au barrier is so large that it effectively eliminates the electrons from the Au electrode when radiation of $h\nu < 4$ eV is used. The photoyield (collected photoelectrons/absorbed photons) can be determined theoretically from the energy distribution of the electrons which are injected from the electrode into the insulator together with the transmission probability through the insulating film. Quantum mechanical reflection of the electrons at the Al_2O_3-Au interface has been neglected since it is believed that this effect cannot be calculated adequately (Ref. 4).

If one assumes that electron-phonon scattering effects occur mainly in the image-force region (that is, the region between the Al-Al_2O_3 interface and the maximum of the barrier), then photoyield data can be analyzed to obtain information on the scattering in this region. The Fowler relation $Y = C(h\nu - \Phi)^2$ is assumed to describe the emission from the Al-Al_2O_3 interface; however, in order to calculate the absolute yield of collected photoelectrons, the Fowler relation must be modified to account for scattering losses in the insulator. Monte Carlo techniques (Ref. 5) have been used with the computer to calculate the theoretical yield curves to be expected with various λ_i's, the mean free path between scattering events. These results were normalized to actual values of experimentally determined photocurrents in order to determine the best fit of scattering parameters.

V. SUMMARY OF RESULTS

Extensive internal photoemission measurements have been made in this Laboratory in order to characterize the properties of Al-Al_2O_3-Au and a number of other thin film sandwich structures. Figure 4 shows a typical Fowler plot of the square root of the photoyield as a function of the energy of the incident photon $h\nu$ for a number of applied bias voltages V_{appl}. The experimental points are circled; the solid lines are theoretical curves calculated by Monte Carlo techniques. The intercept extrapolated from the linear portion of these curves yields the barrier height of the metal-insulator interface. The value of 4 eV discovered for the Au-Al_2O_3 barrier height is one of the highest ever reported and suggests important device applications described below. A mean free path λ_i of 10 Å was found and a dielectric constant of 2.3 for these particular samples; this latter value agrees with the value for the high-frequency dielectric constant in bulk material. This plot vividly demonstrates the influence of scattering; ideally, if no scattering occurred, the calculated curves would be parallel lines. Due to scattering, however, the straight portions of the curves are not parallel even at accelerating internal fields ($V_{appl} > \Phi_2 - \Phi_1$) where scattering influence should be small.

Figure 5 shows the electron energy distribution curves obtained from the vacuum-emitted photoelectron experiment; the number of electrons per unit energy is plotted as a function of electron retarding voltage for two different wavelengths and for three different sample voltages. These measurements reflect the following behavior of electron-phonon scattering within the insulating film: (1) the low-energy limit (that is, positive voltage in the retarding-voltage side) is the same for all curves, (2) the upper energy limit changes linearly with bias voltage and wavelength (that is, the measurements taken at $\lambda = 5460$ Å appear wider than those theoretically expected because a large grid-modulation voltage was used to increase sensitivity), and (3) the integral rate of emitted electrons decreases with sample bias voltage (that is, the emitted photocurrent is attenuated more than the internal photocurrent). Thus, it can be seen that electron-phonon scattering within the insulator film changes the energy distribution of the vacuum-emitted photoelectrons considerably; these results are in agreement with the model for internal photoemission (Ref. 6).

VI. DEVICE APPLICATIONS

That the above basic research results have application to practical Air Force problem areas will be shown by the following examples:

Example 1: One problem frequently encountered with integrated circuits in micro-electronic systems is due to the limited values of capacitance which can be achieved using ordinary Si p-n junction depletion capacitors. Due to the low value of the Si dielectric constant, a large and expensive amount of substrate area is required for very large coupling capacitances. One proposed solution is the use of an overlayer of SiO_2 or Ta_2O_5 thin film capacitors; however, these materials are somewhat lossy in thin film form. Figure 6 shows another proposed solution based on the concept of a graded-insulator thin film capacitor (Ref. 7). Recent studies (Ref. 8) have shown that many of the unusual properties of Ta_2O_5 capacitors can be explained more easily on the basis of Schottky barrier theory than on the previous conductivity profile theory of Smyth, et al. (Ref. 9). The device takes advantage of the relatively large Schottky barrier of the $Al\text{-}Al_2O_3$ interface ($\Phi = 1.8$ eV) to prevent electronic conductivity losses; in addition, the relatively high dielectric constant of Ta_2O_5 ($k \sim 27$) yields a high-capacitance, low-leakage device.

Example 2: A second problem area is that of charge carrier injection into wide bandgap semiconductors and insulators. The Air Force has urgent need for efficient electron and/or hole injection in many solid state devices used in micro-electronic equipment for computers, navigation, guidance, fire control, communications, and electro-magnetic warfare in various weapon systems. Charge carrier injection is a key factor which determines the high frequency

performance characteristics, gain, output power, and noise properties of almost all solid state devices such as transistors, microwave mixer diodes, switching diodes, photovoltaic infrared detectors, electroluminescent diodes, and others. As high-temperature applications and high-power requirements force the use of materials with wide energy bandgaps, this problem becomes even more acute since the use of conventional p-n junctions for injection is no longer feasible due to fundamental material properties, such as self-compensation, which make the fabrication of efficient injecting junctions difficult or impossible. Figure 7 shows a possible solution to this problem for transistor-like devices. This device is somewhat analogous to the metal base transistor except that in this case, advantage is taken of the injecting properties of M-I-M thin film Schottky barriers. The problem of epitaxial growth of a semiconductor on a metal film, which has presented great technological difficulties for conventional metal base transistors is therefore avoided. Very high barriers and low-leakage operation can be achieved. Barrier capacitance can be made quite low and very high frequency operation should be possible.

Figure 8 shows another proposed structure for an injection luminescent device based on the same principle using a wide bandgap semiconductor such as ZnTe as the luminescent material. Brightness levels as high as 10^5 fL have been reported possible if efficient means of injecting this much charge can be achieved (Refs. 10 and 11).

Example 3: Although the use of vacuum tubes in Air Force equipments has decreased considerably in recent years, it is generally conceded that these tubes will never be replaced entirely by solid state devices. The achievement of a reliable electron source which requires no heater or standby power represents a long-sought dream of every tube research man. It now appears that modern solid state technology may develop such a "cold cathode" in the near future. One proposed structure for such a device is shown in Fig. 9. Again, this device is based on the use of a graded bandgap insulator to achieve a thin film Schottky barrier capable of injecting electrons over the vacuum barrier. The recent discovery of a 4-eV barrier at Al_2O_3-Au interfaces makes such a structure appear theoretically possible since techniques are available to lower the vacuum work function of surfaces to as little as 1.5 eV. Emission currents at least as high as 1 A/cm^2 appear possible if good-quality, trap-free insulator layers can be made.

It should be pointed out that while the above devices are conceptually feasible, the performance characteristics which can be achieved by all of these devices, except the first, will depend very strongly on the quality of the materials available, crystalline perfection, trap density, purity, etc., as in all solid state devices. Transmission of appreciable electron currents through insulator films depends very strongly on having trap-free insulators and avoiding electron-phonon scattering (Ref. 12). It is recommended that future research and development on these advanced solid-state-device concepts be concentrated on these areas:

1) epitaxy of thin film single crystals, 2) studies of electron scattering mechanisms and measurements of this characteristic in various materials, 3) improved methods of removing or avoiding traps in oxide films, 4) detailed studies of Schottky barrier heights in various materials and methods to optimize these parameters to specific device requirements.

VII. CONCLUSIONS

In conclusion, thin film metal-insulator-metal Schottky barriers have been investigated extensively. The techniques of internal and external photoemission have been found to be powerful methods for studying the electrical properties of these barriers. A number of possible device applications for these basic research results have been proposed. Lastly, suggested directions for future research and development work on these devices have been presented.

REFERENCES

1. C. A. Mead, Solid State Elec. 9, 1023 (1966).
2. F. L. Schuermeyer, J. Appl. Phys. 37, 1998 (1966).
3. A. M. Goodman, J. Electrochem. Soc. 115, 276C (1968).
4. J. L. Moll, Presentation at the 131st Meeting of the Electrochemical Society. Dallas, May 1967.
5. F. L. Schuermeyer, C. R. Young, and J. M. Blasingame, J. Appl. Phys. 39, 1791 (1968).
6. F. L. Schuermeyer, C. R. Young, and J. M. Blasingame, Air Force Avionics Laboratory Technical Report 68-100, June 1968, Wright-Patterson Air Force Base, Ohio.
7. F. L. Schuermeyer, Patent Disclosure, "Graded Insulator Thin Film Capacitor", 9 May 1968.
8. F. L. Schuermeyer, "Barrier Studies from Capacitance Measurements", to be published.
9. Smyth, et al., Presentation at the 131st Meeting of the Electrochemical Society, Dallas, May 1967.
10. F. L. Schuermeyer, Patent Disclosure, "Injection Luminescence Device", 19 September 1968.
11. A. G. Fischer, Solid State Elec. 2, 232 (1961).
12. R. M. Handy, J. Appl. Phys. 37, 4613 (1966).

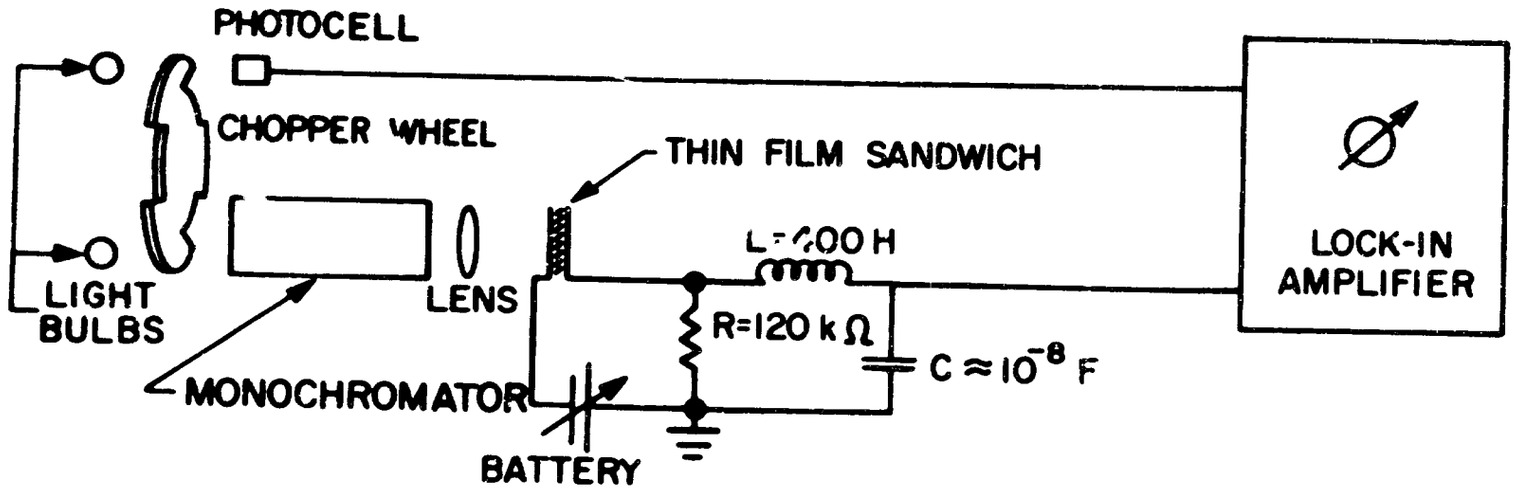

Fig. 1 Equipment for Internal Photoemission Measurements

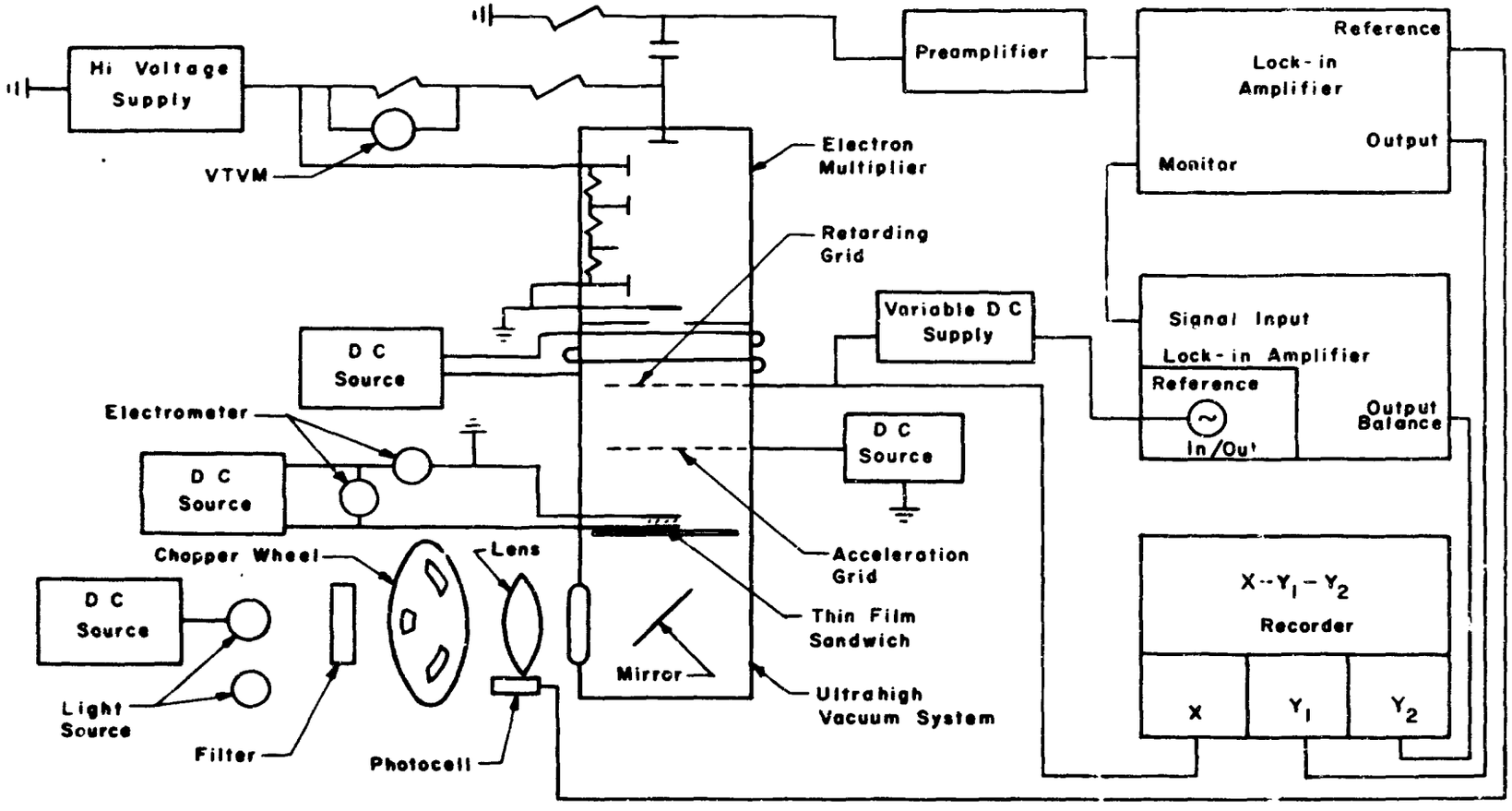

Fig. 2 Equipment for External Photoemission Measurements

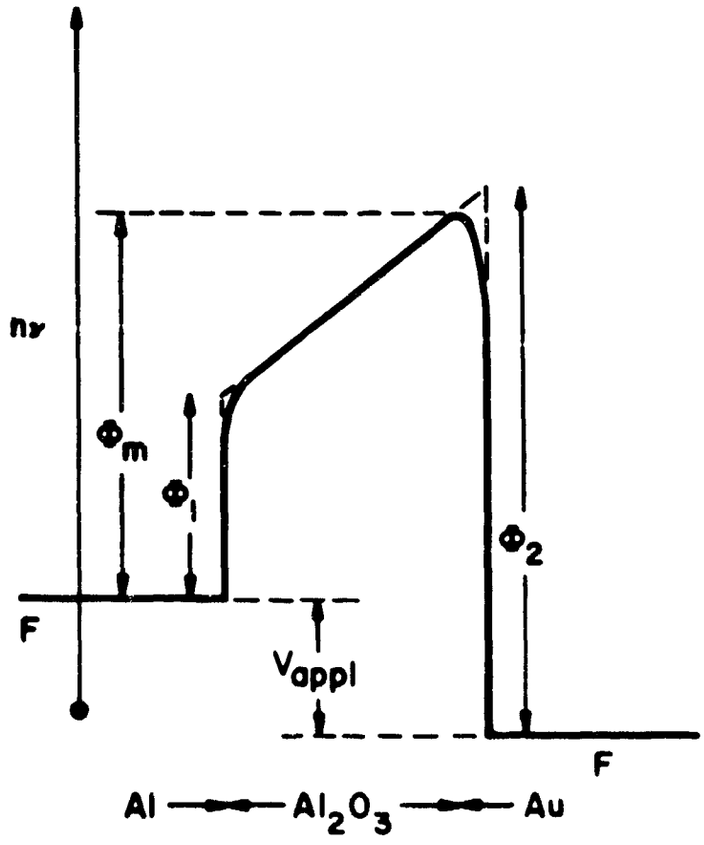

Fig. 3 Energy Band Diagram of an Al-Al_2O_3-Au Metal-Insulator-Metal Thin Film Schottky Barrier Structure

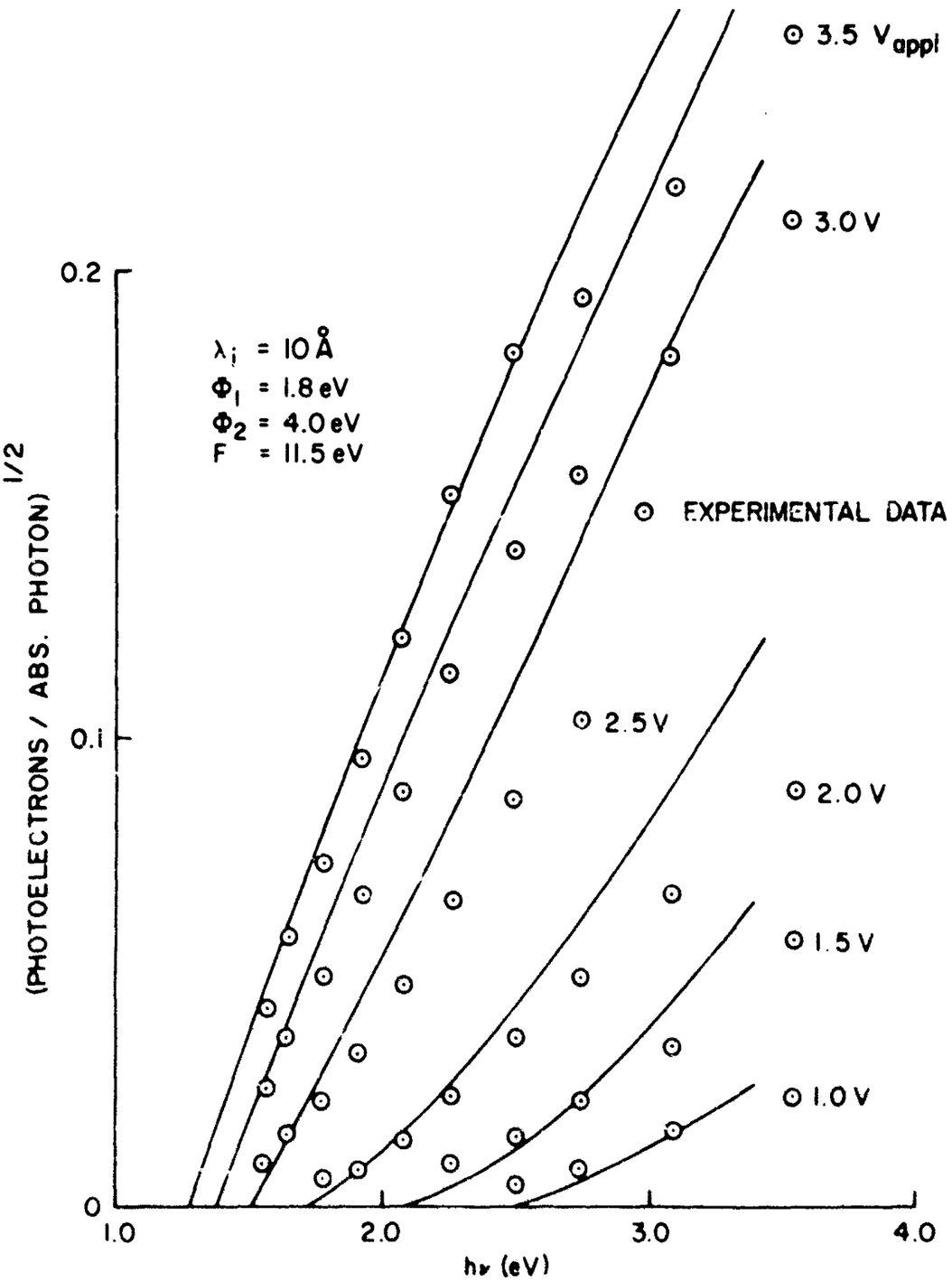

Fig. 4 Fowler Plot of Theoretical and Experimental Internal Photoemission Yield on Al-Al_2O_3-Au Thin Films. Theoretical Yields Normalized to Overlap with Experimental Data at hν = 2 eV, V_{appl} = 3.5 V

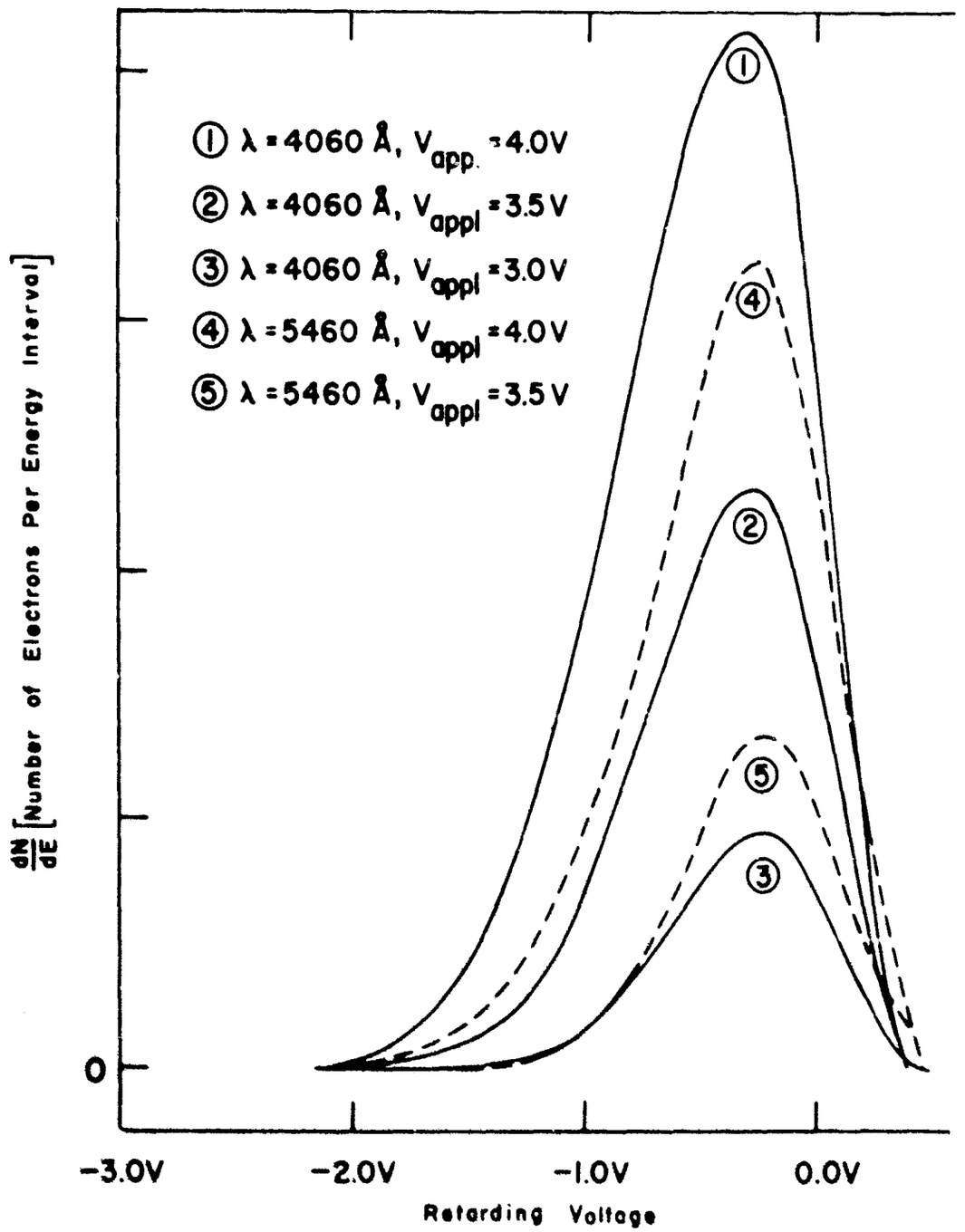

Fig. 5 Electron Energy Distributions for Photo-Excited Electrons Emitted into Vacuum at Various Wavelengths and Sample Bias Voltages

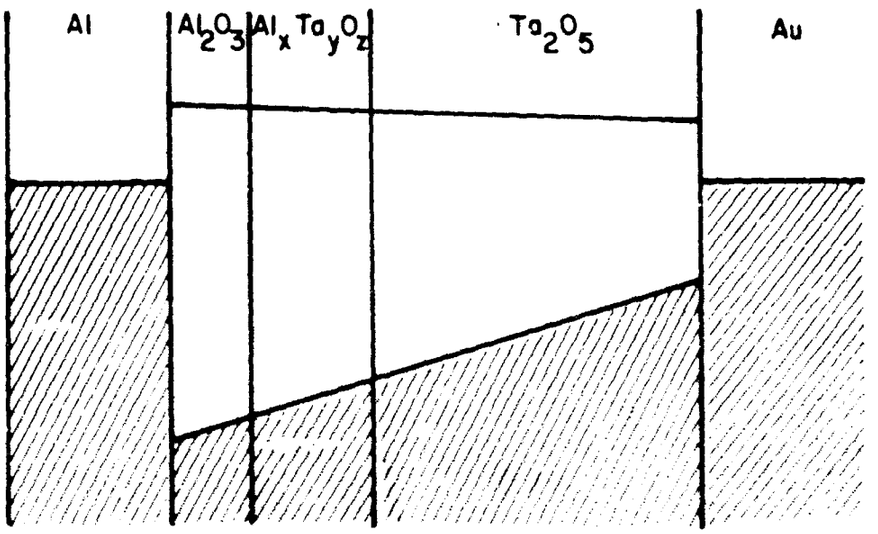

Fig. 6 Proposed Graded-Insulator, Low-Leakage, Thin Film Capacitor for Micro-Electronic Circuit Applications

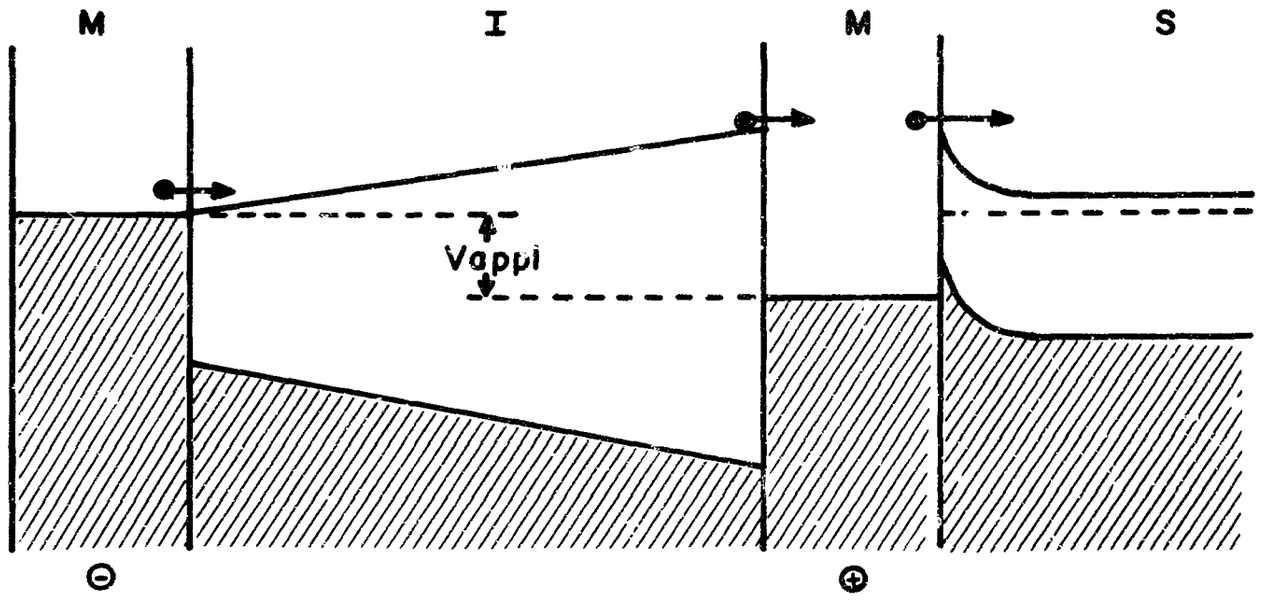

Fig. 7 Proposed Graded-Insulator, Hot-Electron Injection Transistor Structure

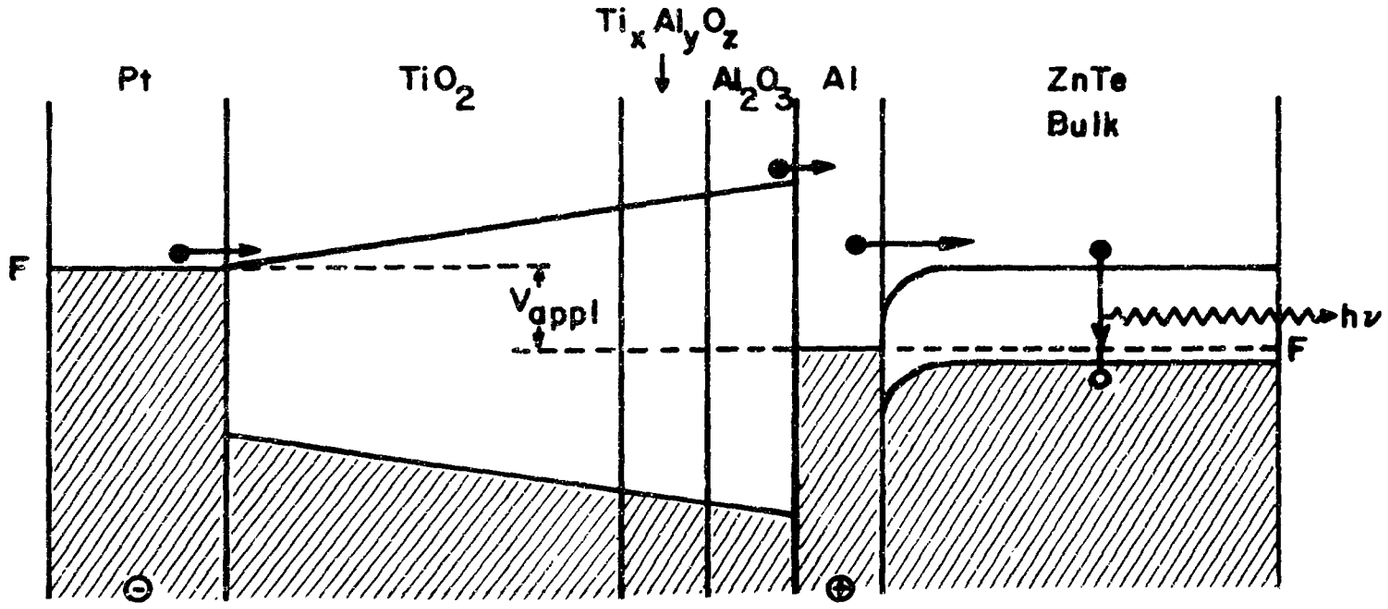

Fig. 8 Proposed Graded-Insulator, Hot-Electron Injection Luminescence De·ice

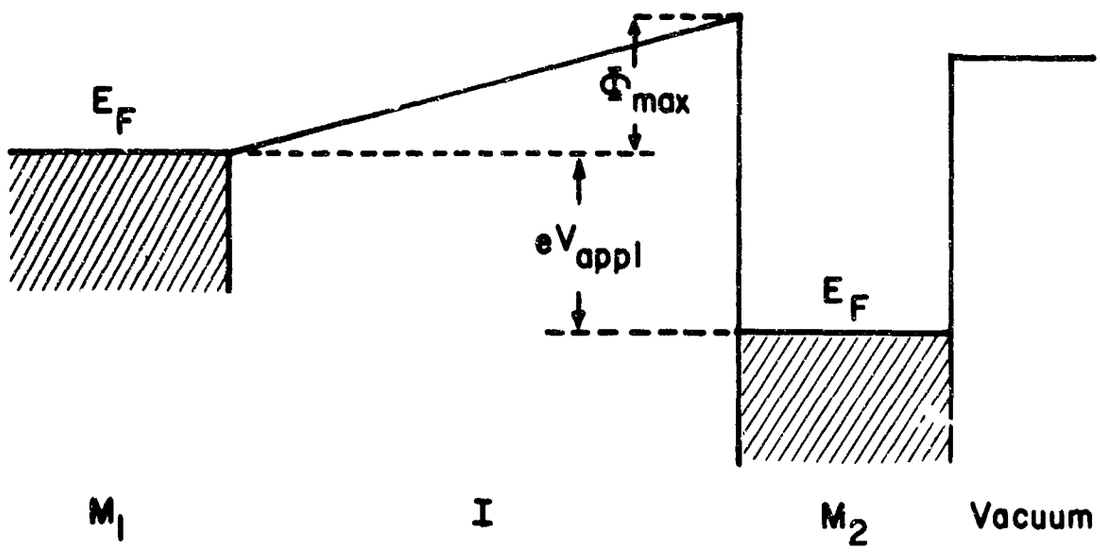

Fig. 9 Proposed Graded-Insulator Electron Emitter for Application as a Cold Cathode

STRESS EFFECTS AT THE Si-SiO_2 INTERFACE AND ITS RELATIONSHIP TO INTERFACE STATES AND METALLIZATION PROBLEMS IN SILICON DEVICES

By

Clyde H. Lane

Rome Air Development Center (EMERM)
Griffiss AFB NY 13440

339-893 O - 68 - 15

STRESS EFFECTS AT THE $Si-SiO_2$ INTERFACE AND ITS RELATIONSHIP TO INTERFACE STATES AND METALLIZATION PROBLEMS IN SILICON DEVICES

Clyde H. Lane

ABSTRACT

The existence and origin of interfacial stress between thermally grown silicon dioxide and single crystal silicon are demonstrated. An oxide grown at 1200°C will be under about 50,000 psi compressive stress. Interface state density is shown to be correlated to the magnitude of this compressive stress. An attempt is made to explain the correlation using a vacancy model for the interface states. The oxide stress is shown to be a potential problem when contacting the silicon by metallizing over cuts through the oxide.

The information and treatment are considered to apply to all solid-solid interfaces and are, therefore, of general interest, not restricted simply to the $Si-SiO_2$ system.

BIOGRAPHY

Clyde H. Lane was born in Rochester, NY in 1929. He began his college training as an evening student at Utica College of Syracuse University in 1953 and graduated cum laude, six and one half years later with a B.A. in Physics. In August 1960 he began his Civil Service career starting in a newly organized microelectronics group. This group developed an in-house facility for microcircuit fabrication which Mr. Lane now heads. He has personally conducted research in anodized and reactively sputtered valve metal oxides for thin film capacitors, diode sputtered thin film cermets of high resistivity, dielectric isolation techniques and, most recently, alloying for ohmic contact formation in integrated circuits.

STRESS AT THE Si-SiO_2 INTERFACE AND ITS RELATIONSHIP TO INTERFACE STATES AND METALLIZATION PROBLEMS

CLYDE H. LANE
Rome Air Development Center (EMERM)
Griffiss AFB NY 13440

INTRODUCTION: Surface, or interface, states in the silicon-silicon dioxide system are grudingly yielding information about their true nature under the intensive, concerted effort of many outstanding investigators.[1] The effects of protons and sodium ions within the oxide are now reasonably well understood[2-4] and can be controlled in laboratory or pilot line construction of MOS devices. This has allowed a closer look at that interface without the masking effects of oxide contamination. One of the peculiar effects seen when the oxide is grown in dry oxygen under very clean conditions was presented by investigators (5) at Fairchild Semiconductor. They saw an increase in interface state density as the oxide growth temperature was reduced. In this article an explanation for that effect will be set forth from which more insight may be gained about the nature of all solid-solid interfaces. Two problems in integrated circuit metallization will be treated also, one of vital interest to those concerned with the yield and reliability of these circuits and the other of more fundamental interest in the field of solid state, particularly interface processes.

DISCOVERY AND ANALYSIS OF THE INTERFACE STRESS

In order to develop a dielectric isolation process for incorporation into failure analysis and transient radiation effects studies on integrated circuits, an intensive study of the etching and lapback problems associated with dielectric isolation was undertaken. Very simply, dielectric isolation consists of etching a predetermined pattern into a single crystal silicon wafer. The etch depth must be about 0.0018 inches. An oxide is grown over the silicon containing the etched patterns, and a layer of polycrystalline silicon is grown over the oxide to a thickness of about 0.010 inches. The single crystal material is then lapped away until the polycrystalline silicon has been intercepted. One now has islands of single crystal silicon surrounded by silicon dioxide and supported by polycrystalline silicon.

During study of the etching process some peculiar optical effects were seen in the etched patterns after the moats had reached a depth of about 0.001 inches and before the oxide was removed. They are especially noticeable in photographs taken with oblique light in a dark field, as seen on Figure 1. The white lines were initially explained as the light reflecting back through the opening in the oxide; actually they are due to focusing by the moat itself. Figure 2 is a photograph of an actual moat. The black line is one micron of thermally grown oxide. The concave up portion is the polycrystalline silicon side. This pattern was traced and a simulation of the focusing effect constructed in Figure 3. It is interesting that what appears as a single line or focal point when vertical illumination is used

is a double line when illuminated with two lights from oblique angles as shown in Figure 4, confirming the effect.

The next feature, interference colors in the oxide, comes from the fact that the moat etch can attack the oxide from the under side only where the silicon has been removed. Therefore, oxide at the initial opening will be thinner than oxide over the unetched silicon and will taper from one to the other.

The scalloped appearance of light within the overhanging oxide perpendicular to the axis of symmetry is due to a waviness in the SiO_2. The waviness is seen in Figure 5 as the alternation of points of sharp focus at the oxide edge. From this photograph quantitative measurements were made. For simplicity one can construct an arc and chord to represent the observed wave. The measured chord length was 103.0 microns and the wave amplitude was 4.0 microns. The arc would be formed by the silicon dioxide whose length we could not measure. This approximation is satisfactory because of the small arc involved.

Waviness in the undercut oxide has been shown. The release of compressive stress was suggested as the explanation for its presence. The paramount question now concerns the origin and magnitude of the compressive stress. Normal practice is to grow the oxide in steam at about 1000°C. Since the measurements were made at room temperature, let's examine the difference in contraction of silicon dioxide and silicon. The coefficient of linear expansion of silicon and fused quartz for the temperature range of interest is approximately $4.5 \times 10^{-6}/°C$ [6] and (6) $0.6 \times 10^{-6}/°C$ respectively. (7) Using the chord length from Figure 5 as the length of the silicon beneath the oxide

at 25°C, the height to which the undercut oxide would rise if compression generated solely by the difference in linear coefficients of expansion were released was calculated

103.00 microns Si at 25°C will be

103.45 microns at 1000°C

103.45 microns SiO_2 at 1000°C will be

103.4 microns at 25°C

Fixing the ends of the silicon and silicon dioxide at 25°C, we have the situation shown in Figure 6, where S is the length of the oxide and C is the length of the silicon. To calculate h for comparison with the measured value, Huygens' approximation for small arcs is used to first find a value for c':

$$S = 1/3\ (8\ c' - c)$$

$$c' = \frac{3S+c}{8}$$

$$h = (c')^2 - \left(\frac{c}{2}\right)^2 = (3S+c)^2 - \left(\frac{c}{2}\right)^2$$

$$= 2667.72 - 2652.25 = 15.47$$

$$= 3.93 \text{ microns}$$

This is an excellent agreement with the measured value, 4.00 microns, indicating that stress due entirely to thermal expansion differences is sufficient to cause the observed waves. It is possible to calculate the height of the wave by a very simple approximation when the chord is at least 10 times the distance from the chord to the arc it subtends. Take the difference in the thermal coefficients of expansion α_1 and α_2, of the two

materials, in contact, multiply by the difference in temperature, Δt, between that at which the measurement was taken and that of the silicon when the oxide was grown, and multiply the product by 10 times the distance (c) between the successive minimums of the wave. That is:

$$(\alpha_2 - \alpha_1)\ (\Delta t)\ (10c) \approx h.$$

Other factors do influence the height of the wave. A significant one can be the fact that the oxide is only free at one end, extending a distance of one-half the difference between the moat width and the oxide opening over the moat. Another factor is the sag in the overhanging oxide due to its own weight.

It may be instructive to know how large the compressive stress is in pounds per square inch (psi). To calculate this, the formula $S = E\alpha(t_2 - t_1)$ is used. S is the unit stress of a bar of material which was cooled from t_2 to t_1 where E is Young's modulus and α is the coefficient of linear expansion. If one lets α be the difference between the linear expansion coefficients for fused quartz and silicon and multiples by the temperature difference, he will get a quantity corresponding to the deformation of the hypothetical interface material having the artificial α. Actually, the deformation represented by $\alpha\Delta t$ is almost entirely taken up in the oxide, placing it in compression, while tension will be seen in the silicon surface layer. To obtain the unit stress S in psi, $\alpha\Delta t$ is multiplied by the modulus of elasticity E for the oxide film. An average of values given for fused silica and fused quartz (8) was used.

$$S = .0039\ E = .0039 \times 110 \times 10^5 \text{ psi}$$

$$S = 43{,}000 \text{ psi}$$

Graphs can now be constructed for the stress at a given temperature as a function of oxide growth temperature, as shown in Figure 7.

APPLICATION TO INTERFACE STATE DENSITY

If a plot of the compressive stress at room temperature as a function of oxide growth temperature is put on the same graph as a plot of the room temperature interface state density, Qss as a function of the growth temperature for dry oxygen an interesting correlation is observed as illustrated by Figure 8. The Qss data points were calculated from the Snow Grove, Deal, Sklar paper (5) by averaging the data for both p and n type materials. Notice the good agreement between the two functions at the actual growth temperatures. The deviation becomes marked below 1200°K, but no oxide films were actually grown below 1200°K for the surface state measurements. These points were obtained by growing 1500°K, then cooling to the desired temperature and allowing time for equilibrium to be established. The plot of stress versus temperature was simply calculated from the equation $S = 43\ \Delta T$ for the $Si\text{-}SiO_2$ interface. Unfortunately, C-V measurements give us little information about the physical properties of an interface state and certainly none concerning its mechanical properties. But it is the mechanical properties that are important here. In looking for the real nature of these states we are looking for something which has a surface density of about $1 \times 10^{11}/cm^2$. The density of atoms on the <111> surface of silicon is 1.4×10^{15} atoms/cm^2. This assumes a volume density of 5×10^{22} atoms/cm^2 for pure single crystal silicon. Such a number comes from the assumption of a perfect lattice, but there are a certain number of vacancies in equilibrium with the material atoms

at all temperatures above absolute zero. At 1000°C, one would in fact expect a vacancy density of about 1×10^{-5} vac/atom based on information available on other materials (9). Therefore, that one might expect about 1×10^{10} vac/cm^2 at the oxide growth temperature. Quoting from A. S. Grove's book, Physics and Technology of Semiconductor Devices, "The theoretical estimates of the density of surface states yield values of the same order as the number of surface atoms 10^{15} cm^{-2}. Such densities have indeed been observed on very clean semiconductor surfaces obtained by cleaving samples under high vacuum. However, germanium and silicon samples after exposure to air for only a few minutes show surface state densities of the order of only 10^{11} cm^{-2}, and thermally oxidized silicon surfaces can show densities yet another order of magnitude smaller." He is of course referring to the number of dangling bonds as the theoretical number of surface states, and what is a vacancy but a collection of unsatisfied bonds.

It is known that the ratio of surface states, Qss, on the <111>, <110>, <100> faces is of the order of 3:1.5:1. If vacancies are responsible for these surface states the same ratio should apply to number of vacancies per cm^2 on the orientations in question. Since the vacancy density is just some factor times the number of surface atoms the ratios will be the same as the ratio of surface atoms for these orientations.

The ratio of vacancies for <111> <100> is then 3:1.5:1.2. This ratio looks similar to the empirical ratio. In fact data from Snow, Grove, Deal, Sklar paper(5) for oxidation in dry oxygen at 920°C gives a ratio of 3:1.3:1.1. This certainly suggests that a model for interface states tied to the vacancy concentration is reasonable.

Since a vacancy model is being proposed, the compressive stress is acting on the available number of vacancies causing a portion of them to disappear. Such interactions have been discussed in the literature (10) along with vacancy stabilization, annealing and precipitation following quenching (11). Assuming that vacancies are disappearing as a linear function of the compressive stress, and that equilibrium prevails, the model will be as follows:

The equilibrium number of vacancies at any temperature per atom has the form:

$$N_v = \exp(S_f/k - E_f/kT) \qquad (12)$$

where:

S_f/k = the entropy of formation for a vacancy other than that due to mixing

E_f = Formation energy of a vacancy

k = Boltzmann's constant

T = temperature in °K

The number of vacancies per centimeter squared V_s equals $N_v N_s$ where N_s is the number of atoms on a <111> single crystal silicon surface. The number of vacancies which disappear has the form:

$$V_D = 43\ K\ (\Delta T)$$

Where K is the number of vacancies which disappear per psi, 43 ΔT gives the stress in psi and ΔT is the difference between growth and measurement temperature. Putting these terms together we have S_D, the equilibrium surface density of vacancies equals:

$$S_D = N_s \exp\ (S_f/k - E_f/kT) - 43\ K\ (\ \Delta T)$$

This equation gives a curve which is concave down while the experimental data for the surface states gives a curve which is concave up. The trouble with this approach is that the data requires a vacancy density which is flat with temperature over the range from 800 to 1600°K. To obtain such a curve with this equation would require an E_f of about 1×10^{-5} ev and the vacancy density would be of the same order as the number of surface atoms.

Since that approach is unsatisfactory, let's work backwards. First, we'll assume that the interface state densities for oxides actually grown at the indicated temperatures are legitimate, but the other points may be nonequilibrium points or other effects must be considered. Through the four highest temperature points, a straight line is drawn, see Figure 8. Now, assume arbitrarily that 5×10^6 vac/psi disappear with the application of compressive stress. This will allow the construction of a curve for the equilibrium number of vacancies per centimeter squared as a function of temperature. The curve is shown in Figure 9. To account for the deviation of vacancy density for oxide films grown below 1200°K, simply realize that these films were actually grown at about 1500°K, cooled to the indicated growth temperature, and allowed to anneal until the surface state density no longer changed. Using Figure 9, one can see that for oxide grown at an indicated 800°K we actually have a reduction in vacancy density equal to $5X10^6X43\ (1500 - 800) = 1.5X10^{11}$ vac/cm^2, curve number 3. This stress is allowed to anneal out which should bring the density back essentially to the level at 1500°K. However, the density seems to have increased beyond the 1500°K level. Perhaps we're now forcing the solution, but it is conceivable that relaxation of the compression is a source of vacancies, so that one does not simply return to the original value. The literature

does support such a conclusion (13). If this idea is accepted, the shape of the curve for surface vacancy density below 1200°K can be explained. To explain the shape of the curve for the original number of vacancies as a function of growth temperature, is most difficult since this whole procedure of oxidation and quenching does not allow the assumption of equilibrium.

In a paper concerning vacancies and dislocations in quenched graphite (14) chemical interactions at the surface were suggested to account for the abnormally high vacancy and dislocation density at the surface following the quench. Oxidation of silicon also produces mechanical disruption since the oxide is less dense than the silicon. Both chemical and mechanical effects appear to be sources of vacancies independent of temperature. Oxidation is, therefore, a process which could deliver the required vacancy concentration in the temperature range of interest. Interface disorder generated by oxidation has been correlated with interface states (15). Disorder, however, is a very general term. To be more explicit interface states must be tied to specific defects. Since the phenomena of vacancy supersaturation and aggregation are quite well established (16) and fit into the pattern of known interface state properties this seems like a good place to start. Therefore, this paper is setting forth the hypothesis that (1) Oxidation ties up most of the unsaturated bonds thus reducing the number of surface states down to about 1×10^{12} to 1×10^{13} states/cm^2, (2) Oxidation creates a vacancy concentration far above the thermal equilibrium concentration at the silicon surface, (3) Quenching the interface by withdrawing from the oxidation furnace causes vacancy supersaturation and aggregations, (4) Under compression vacancy aggregates and vacancies vanish by creation of dislocations and interaction with them, (5) When the stress is annealed additional vacancies are created.

APPLICATION TO METALLIZATION PROBLEMS

For the sake of this paper, only aluminum metallization will be discussed, but the information is applicable to any metallization system. First, look closely at metallization over an oxide step. Assume that the aluminum is evaporated from a point source over a silicon dioxide to silicon step created by etching the oxide with a buffered HF solution through a photoresist mask. If the oxide is 8000 angstroms thick and the aluminum 2000 angstroms thick, you will see the cross sectional profile shown in Figure 10. This is already a bad situation, but now remember that the oxide is in compression. When the contact cut is made through the oxide there is an avenue for release of this compression. That release will take place as Figure 11 depicts. The expansion will be largest at or near the silicon dioxide surface and zero at the bottom of the cut. As the figure shows, the net effect is to increase the slope of the cut. If the angle is equal to or greater than 90°, the aluminum will be discontinuous. We have seen photographs which confirm this effect and show a tendency for a negative slope in the oxide.

A nonuniform etch rate would also explain the negative slope. This probably is a real effect also since the best oxide is at the top while the most disordered is at the bottom. It is known that over etching when making the contact cut can cause dips into the silicon at the edge of the cut. This effect has been related also to the interface stress, since an etch will proceed faster wherever a stress gradient exists. All three effects coupled with the naturally thinner aluminum on slope of the oxide opening point to a failure sensitive area. The negative slope is very significant because it indicates problems even with metallization as thick as the oxide. Two other

effects associated with alloying add to the problem. First, silicon alloying with aluminum causes a volume reduction (17); second, the silicon having a higher valence than aluminum will cause the resistance of the metallization to increase in the region of the contact area. Under these circumstances, burn out and conductor opens in this area are not surprising. These effects have been reported and we see this weakness on integrated circuits fabricated in our own laboratory.

A second interesting aspect of the influence of stress or metallization and contacting was provided by an investigation to establish a single-step process for metallization and ohmic contacts. Previous practice had been to deposit 2000 angstroms of aluminum, raise the temperature to above the eutectic point for two to three minutes, strip the remaining aluminum, and remetallize with 6000 to 8000 angstroms of aluminum. Attempts to simply metallize to the final thickness and then alloy for ohmic contacts, produced large equilateral triangles under the contact area. This effect was so intriguing that further investigations were conducted. The triangles follow orientation of the silicon substrate, have the appearance of aluminum and are sunder the oxide as expected. Time-temperature experiments were conducted and are summed up on the graph of Figure 12. As the graph shows the triangles formed only above the eutetic temperature. The curve of Figure 12 is approaching zero asymptotically. The warm-up time or time to come to temperature was not deducted from the time required to see the aluminum begin to grow outside the contact area beneath the oxide, which makes the approach to zero slower than it would be if only time at the temperature indicated was recorded. It was noted that after the triangles attained a certain size,

holding at temperature simply caused the triangles to round their corners and dissipate. Figure 13 shows a full grown triangle. This grew in two minutes at 620°C. To grow the same size triangle at 595°C required three minutes. Actually the growth time may be much faster. There seems to be considerable variance in the process and only an average time to see a full grown triangle is being reported. The induction time could be a considerable part of the reported growth time.

It is felt that these triangles are related to the oxide stress, the argument being that when the oxide is opened, stress will be relieved around the opening along the crystallographic planes. Where stress is relieved the surface vacancy density will be one to two orders of magnitude higher than elsewhere. This allows the Al-Si eutetic to move rapidly in a lateral direction, being confined only by planes still under stress. If so the size of the triangle associated with a cut in the oxide will be set solely by the size and geometry of the oxide opening. For a square opening, one will find that the largest triangle is the one which incloses the square touching at least three corners of the square with its sides. An inspection of Figure 13 confirms the thesis because it is representative of all pictures of oxide cuts and the associated triangles showing that the triangles' sides are always tied to the corners of the oxide cut, regardless of size or whether the cut is square, rectangular, or some other geometry.

CONCLUSIONS AND RECOMMENDATIONS

The case for interface stress at the silicon-silicon dioxide interface is reasonable and convincing. Application and generalization of its effects may not be quite as convincing. However, adequate demonstration of such applications have been made to warrant further investigations particularly of the relationship between interface stress and surface vacancy concentration. Greater appreciation for the role of stresses in bulk materials resulting from diffusion alloying, oxidation, etc., should be realized. The purity of the $Si-SiO_2$ system has offered insight into all surface and vacancy associated problems. For example, the initiation and propagation of a crack can be understood using the concepts advanced in this paper. Stress alternation has been suggested as a vacancy source for some time. If the concentration is high enough, vacancies will agglomerate and form voids. This weakens the material exactly where maximum stress exists. As the process continues the surface will come apart and the vertex of the crack will be the focal point for the stress, thus continuing the process causing the crack to propagate until the stress has been relieved. Chemical as well as mechanical initation of vacancies seems likely as stress corrosion indicates. The hypothesis suggests a few rules for selecting a dielectric film process which will show a minimum of surface states. (1) Grow the film at the temperature at which the device will be used, (2) The film should be epitaxial and (3) Film should have a good thermal coefficient match to silicon. This seems like a tough set of conditions but the gas anodized films reported by RCA (18) may well fill those requirements to a large extent. (1) The deposition of aluminum requires only a 200°C substrate temperature, (2) Evaporated aluminum films are highly

oriented even on amorphous substrates having the <111> plane parallel tc the substrate and (3) The thermal coefficient of expansion of the resulting Al_2O_3 film after gas anodization should be less then 7.4×10^{-6} since this is for pure Al_2O_3 (fused) but this film may be contaminated with SiO_2 especially at the boundary lowering the expansion coefficient. Gases like nitrogen and helium in affecting surface state annealing are perhaps simply satisfying dangling bonds associated with vacancies. More studies in this field are now required to provide quantitative data for the surface vacancy density of silicon under oxidation as a function of temperature, the number of vacancies created or destroyed per unit stress, and number of states annealed per millimeter of hydrogen or nitrogen introduced.

For metallization processes one can only say that knowledge of the problem will immediately suggest numerous solutions to it. A study of sputtering as a technique to provide a more conformal coating and one offering greater adherence for aluminum metallization is in order. Realizing that when silicon is added to aluminum the alloy shrinks, the use of a 1% Si doped cathode is suggested. Of course, one might suggest simply looking for a dielectric material having a better thermal coefficient match with silicon, but it must be obvious that there are certain advantages to having the surface in compression.

We hope this discussion has revealed a new dimension in interface studies, providing some answers to existing problems and suggesting areas of further study to correlate vacancies with chemical and mechanical stress.

ACKNOWLEDGEMENT

I wish to thank members of the Reliability Physics and Solid State Applications Sections of the Reliability Branch, RADC, for helpful discussions and suggestions. Particular thanks to Thomas Walsh and Janson Engler for the photolithographic work, and the alloying experiments.

LEGEND - For Figure 9

1. Theoretical curve for vacancy density, where oxide is grown at the indicated temperature and the measurement is made at 300°K.
2. Curve for measured number of surface states from Deal, Sklar, Grove and Snow paper (5) Data from p and n type wafers has been averaged.
3. Vacancy density if the oxide is grown at 1500°K and cooled to a lower temperature.
4. Vacancy density as a function of growth temperature.
5. Vacancy density if the oxide is grown at 1500°K, cooled to a lower temperature and then annealed, assuming no new vacancies are generated upon annealing.
6. Vacancy density when oxide is grown at 1500°K, cooled to a lower temperature and annealed, assuming vacancy generation upon annealing.

REFERENCES

1. E. H. Nicollian and A. Goetzberger, "The Si-SiO_2 Interface - Electrical Properties as Determined by Metal - Insulator - Silicon Conductance Technique", The Bell Technical Journal, Vol. XLXI, No. 6, pp 1055.
2. S. R. Hofstein, "An Investigation of Instability and Charge Motion in Metal - Silicon Oxide - Silicon Structures", IEEE Transactions on Electron Devices, Vol. ED-13, No. 2, pp 222-237, Feb 66.
3. E. Yon, W. H. Ko and A. B. Kuper, "Sodium Distribution in Thermal Oxide on Silicon by Radiochemical and MOS Analysis", IEEE Transactions on Electron Devices, Vol. ED-13, No. 2, pp 276-280, Feb 66.
4. S. R. Hofstein, "Stabilization of MOS Devices", Solid State Electronics, Vol. 10, No. 7, pp 657-67 , Jul 67.
5. B. E. Deal, M. Sklar, A. S. Grove and E. H. Snow, "Characteristics of the Surface-State Charge (Qss) of Thermally Oxidized Silicon", J. E. S., Vol. 114, No. 3, pp 266-273.
6. Integrated Silicon Device Technology, Vol. V, "Physical/Electrical Properties of Silicon", ASD-TDR-63-316, pp 20, Jul 1964.
7. Integrated Silicon Device Technology, Vol VII, "Oxidation", ASD-TDR-63-316, pp 4, June 1965.
8. Chemical Engineers Handbook, Perry, McGraw-Hill, pp 1548, Third Edition.
9. Physical Metallurgy, Cahn, pp 691, 1965.
10. L. A. Girifalco and D. Kuhlmann-Wilsdorf, "Theory of the Interaction of Vacancies with Stress Fields in Metals", J. A. P., Vol. 35, No. 2, pp 438-443, Feb 64.

11. F. J. Fraikor and J. P. Hirth, "Vacancy Concentration and Precipation in Quenched Pure Gold and Gold Silver Alloys", J.AP.P., Vol. 38, No. 5, pp 2312-2318, Apr 67.

12. Physical Metallurgy, Cahn, pp 687, 1965.

13. Physical Metallurgy, Cahn, pp 709, 713, 721-724, 1965.

14. G. Hennig, "Vacancies and Dislocation Loops in Quenched Crystals of Graphite". J. AP. P., Vol. 36, No. 4, Apr 65.

15. A. G. Revesz, K. H. Zaininger and R. J. Evans, "Interface States and Interface Disorder in the Si-SiO_2 System", J. Phys. Chem. Solids, Vol. 28, No. 2, pp 197-204, Feb 67.

16. Physical Metallurgy, Cahn, pp 420-422, 1965.

17. Physical Metallurgy, Cahn, pp 186, 1965.

18. A. Waxman, "Thin-Film Transistors Don't Have to be Drifters", Electronics, pp 88-93, 18 Mar 68.

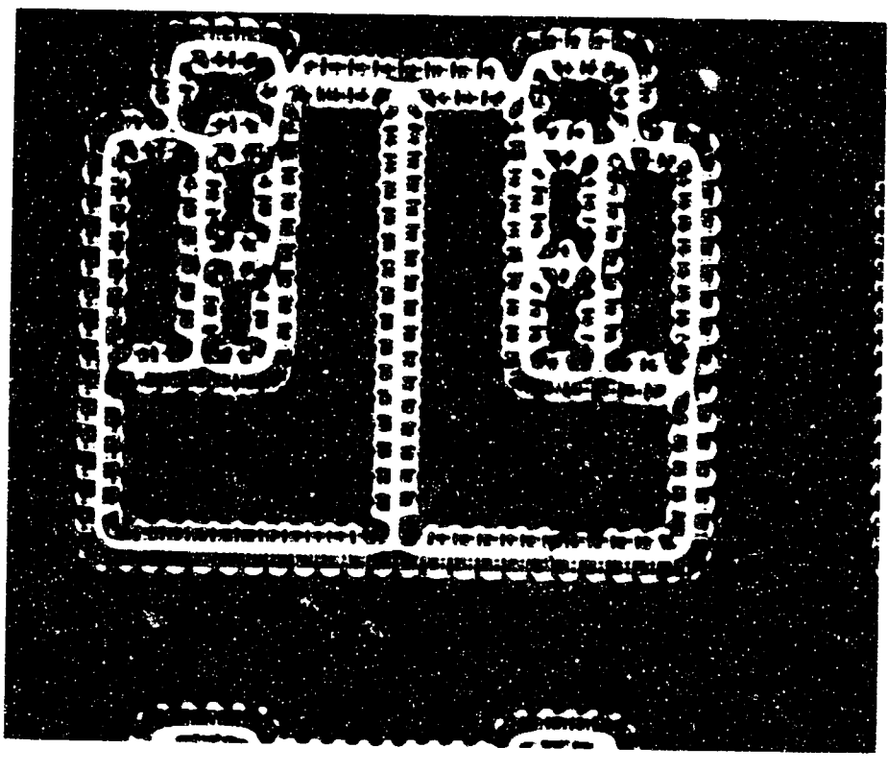

Figure 1. Optical Effects in an Oxide Covered Etched Isolation Pattern.

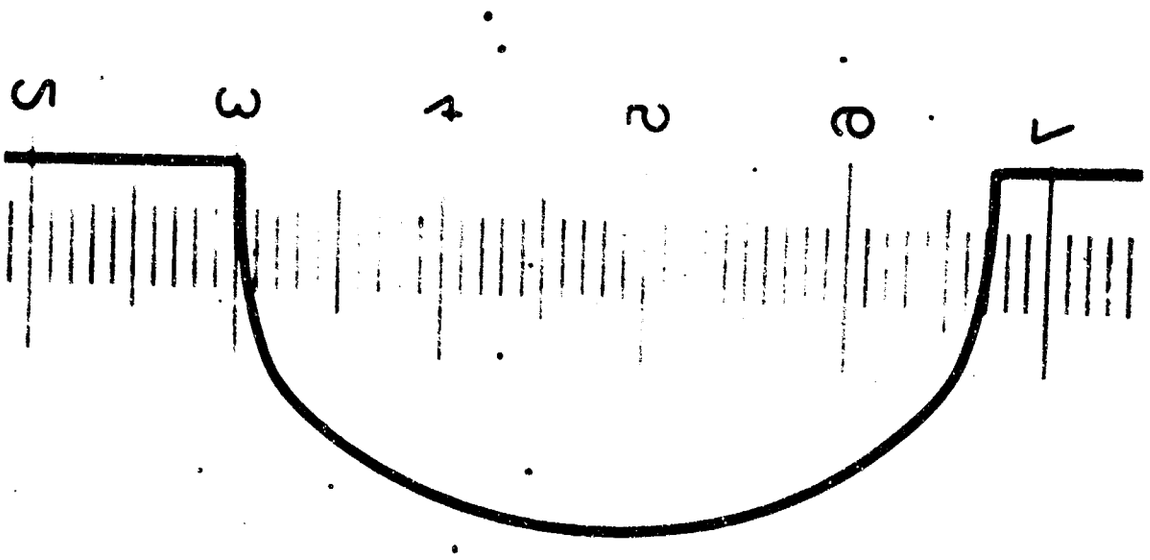

Figure 2. Profile of a Moat Cross Section 2.5 Microns per Small Division.

FOCUSING EFFECT OF MOAT

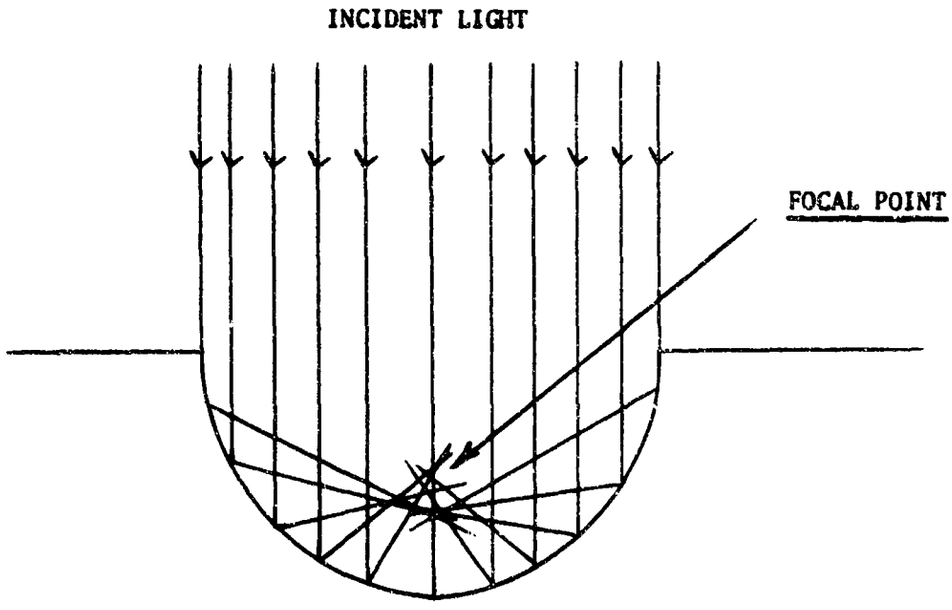

Figure 3

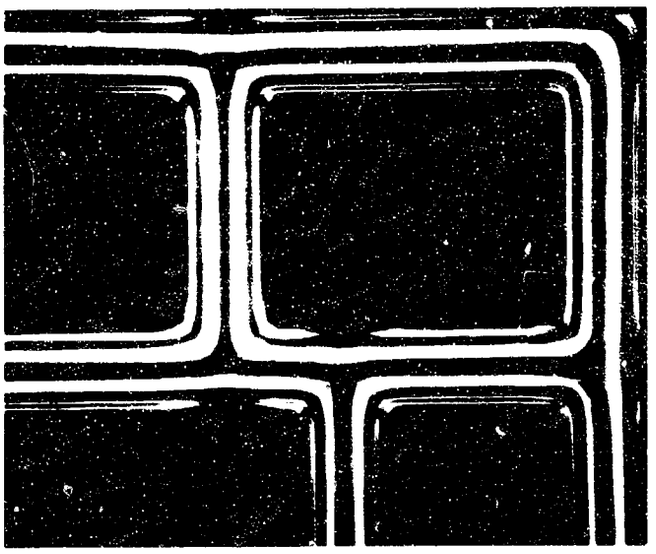

Figure 4. Moat Pattern Reflection Using Two Oblique Lights.

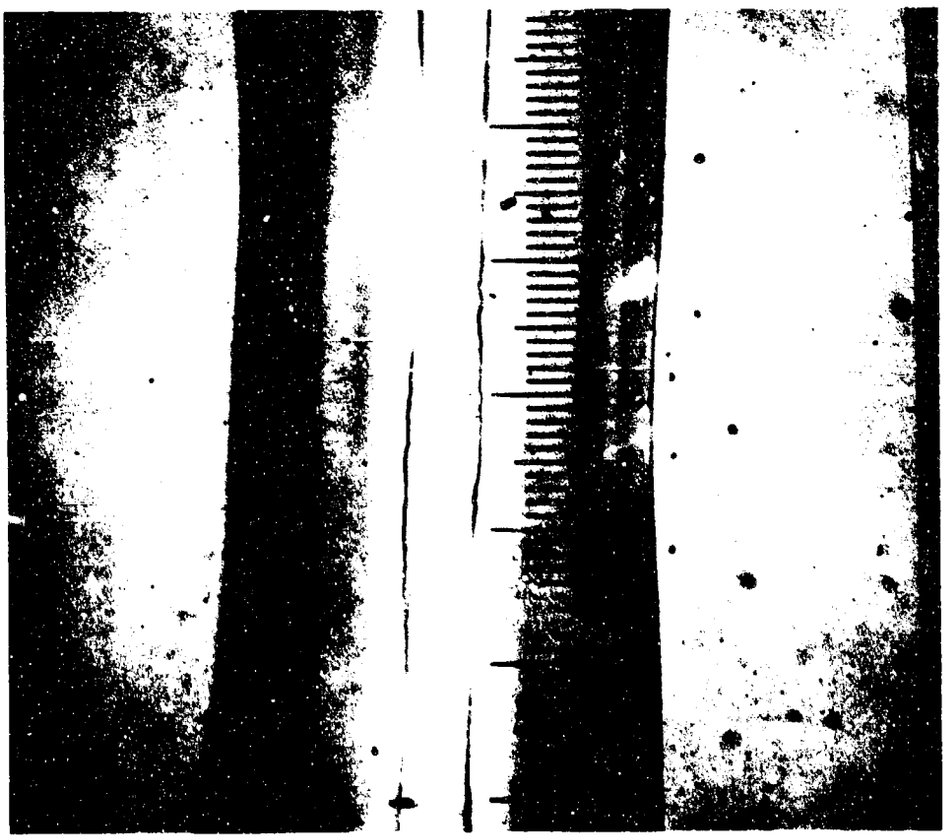

Figure 5. Wavy Nature of the Undercut Oxide 2.5 Microns per Small Division.

GEOMETRY FOR CALCULATING THE MAXIMUM SEPARATION OF TWO MATERIALS AFTER DIFFERENTIAL CONTRACTION

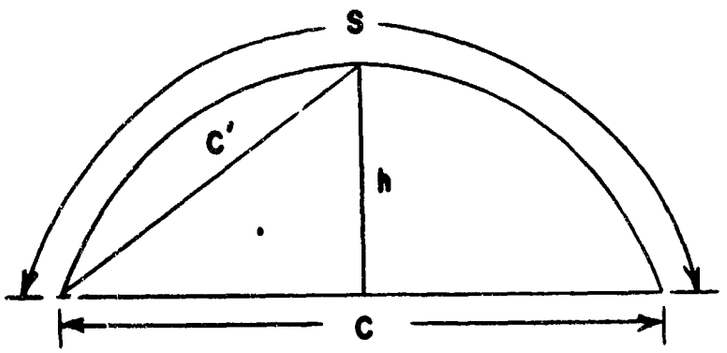

Figure 6

Compressive Stress in SiO_2 at

Various Temperatures for Different

Growth Temperatures

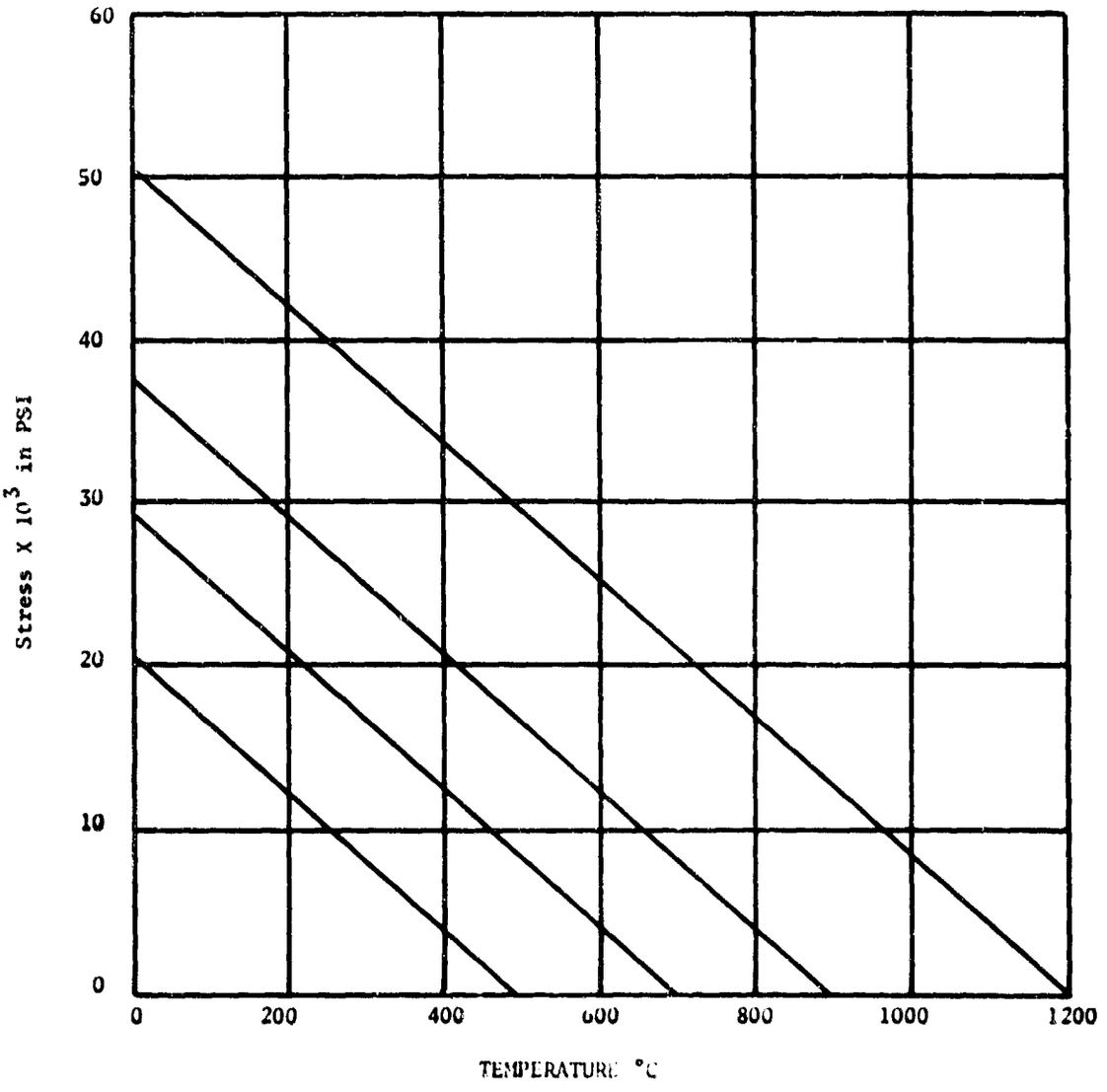

Figure 7

Surface State Density and Oxide Stress

as Functions of Oxide Growth Temperature

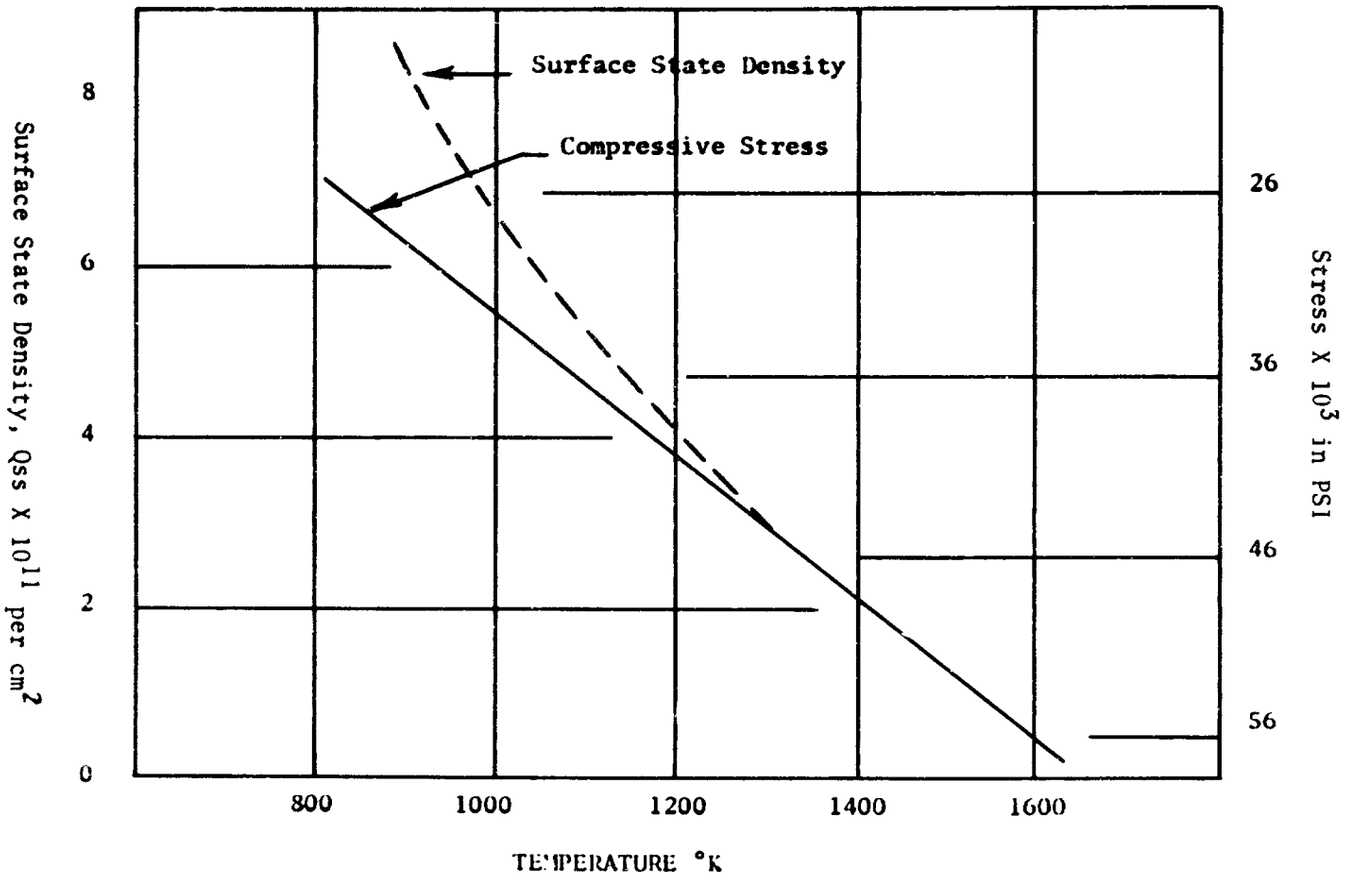

Figure 8

INTERFACE VACANCY DENSITIES UNDER VARIOUS CONDITIONS

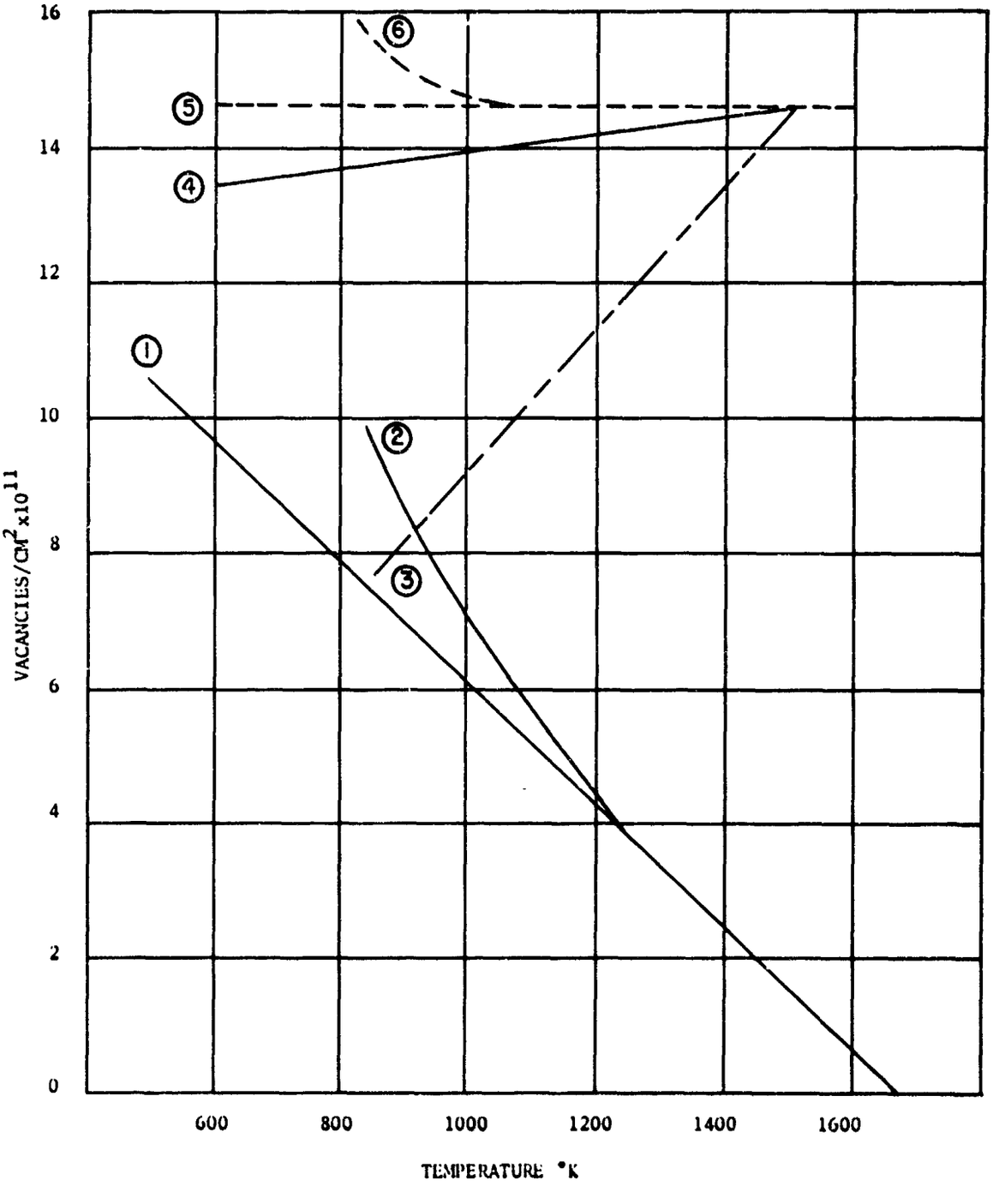

Figure 9

PROFILE OF METALLIZATION OVER A CONTACT CUT

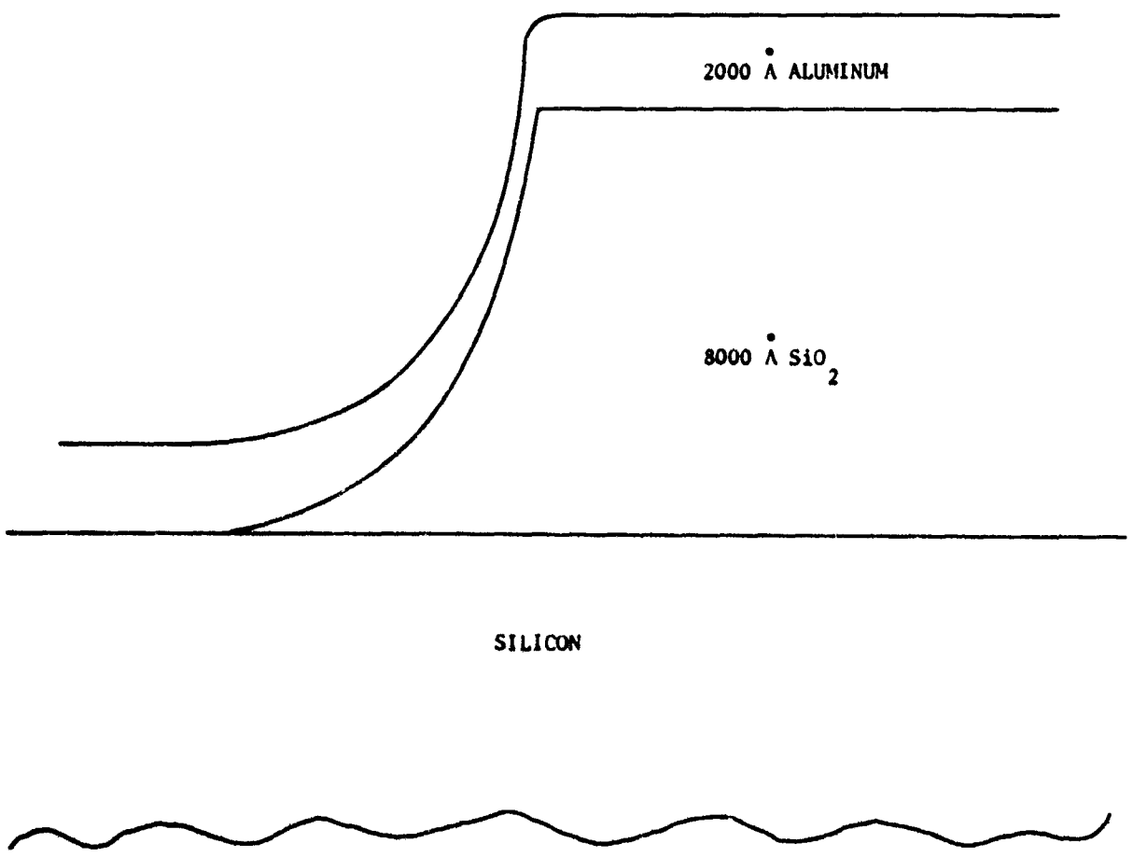

Figure 10

THE EFFECT OF OXIDE EXPANSION ON

ALUMINUM THICKNESS AT A CONTACT

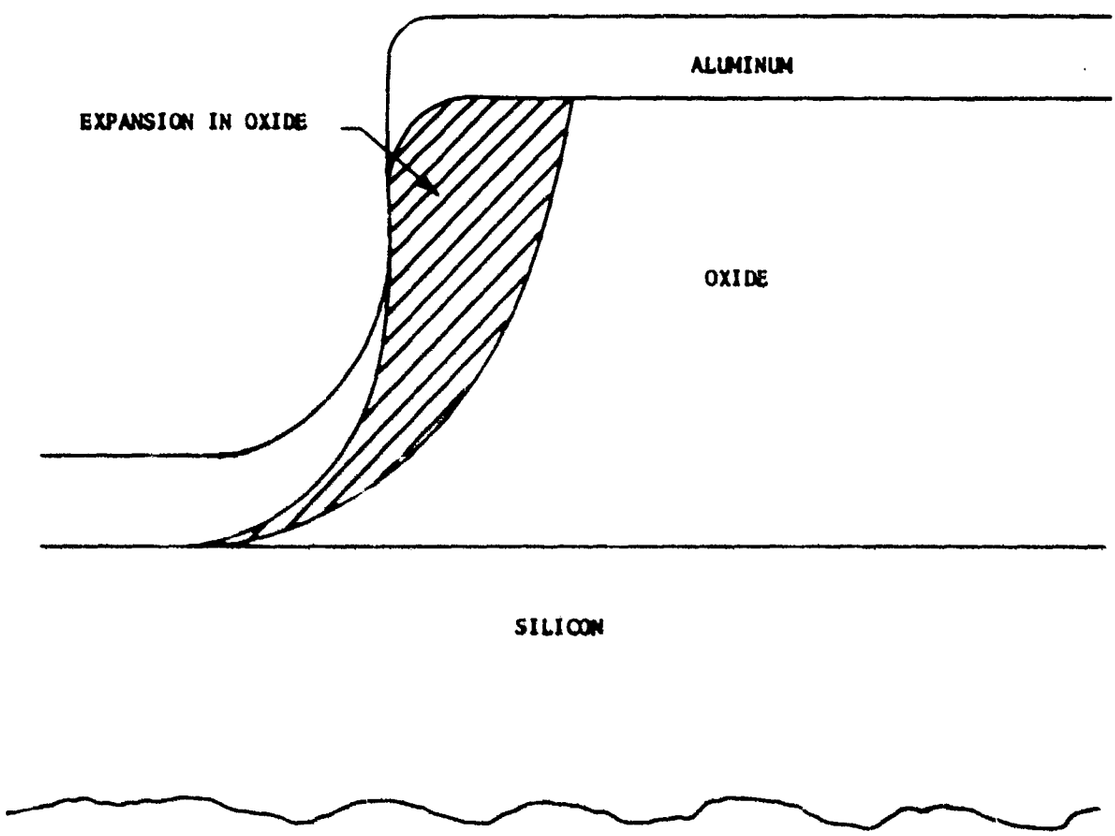

Figure 11

TIME TO SEE TRIANGLE FORMATION AS A FUNCTION OF TEMPERATURE

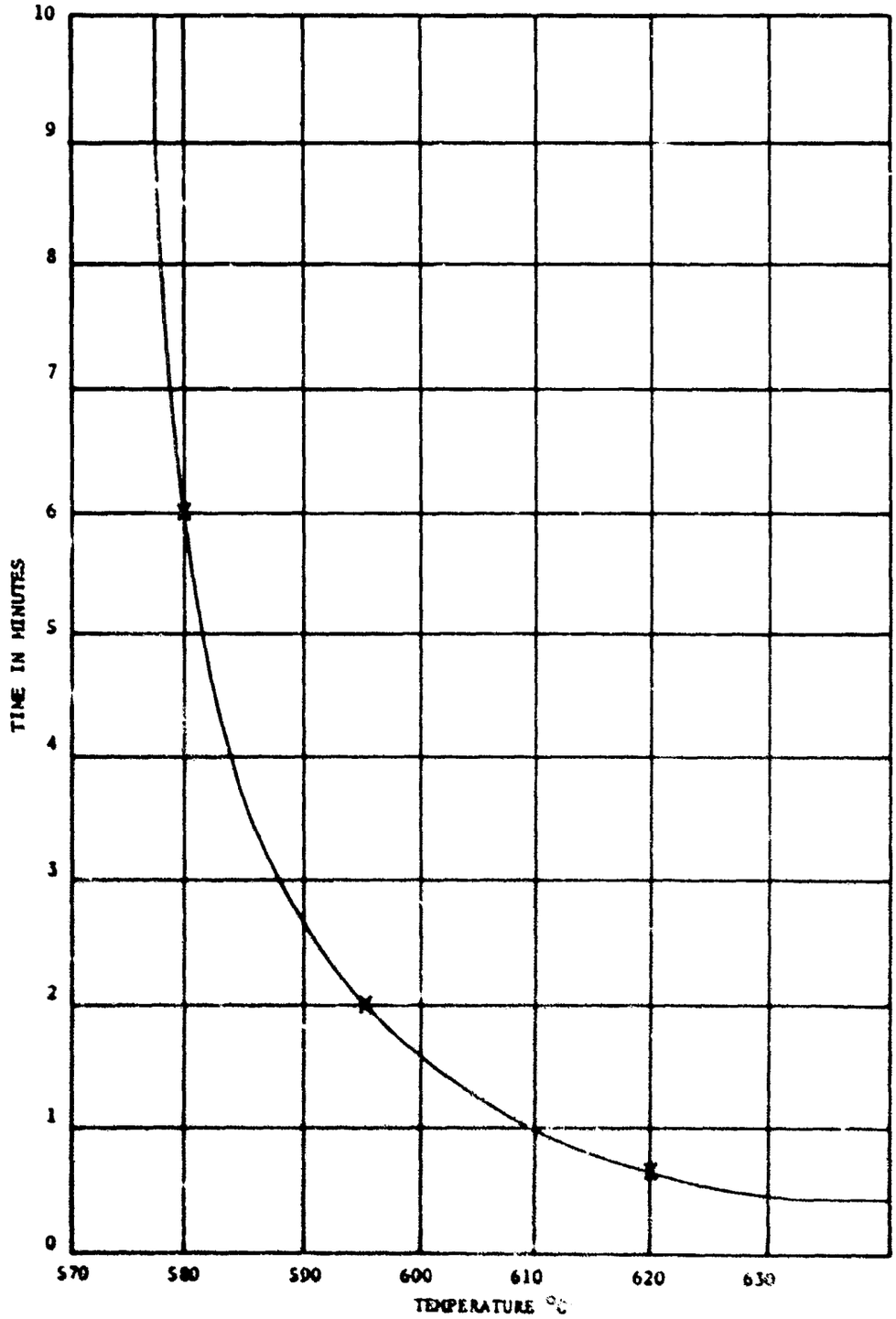

Figure 12

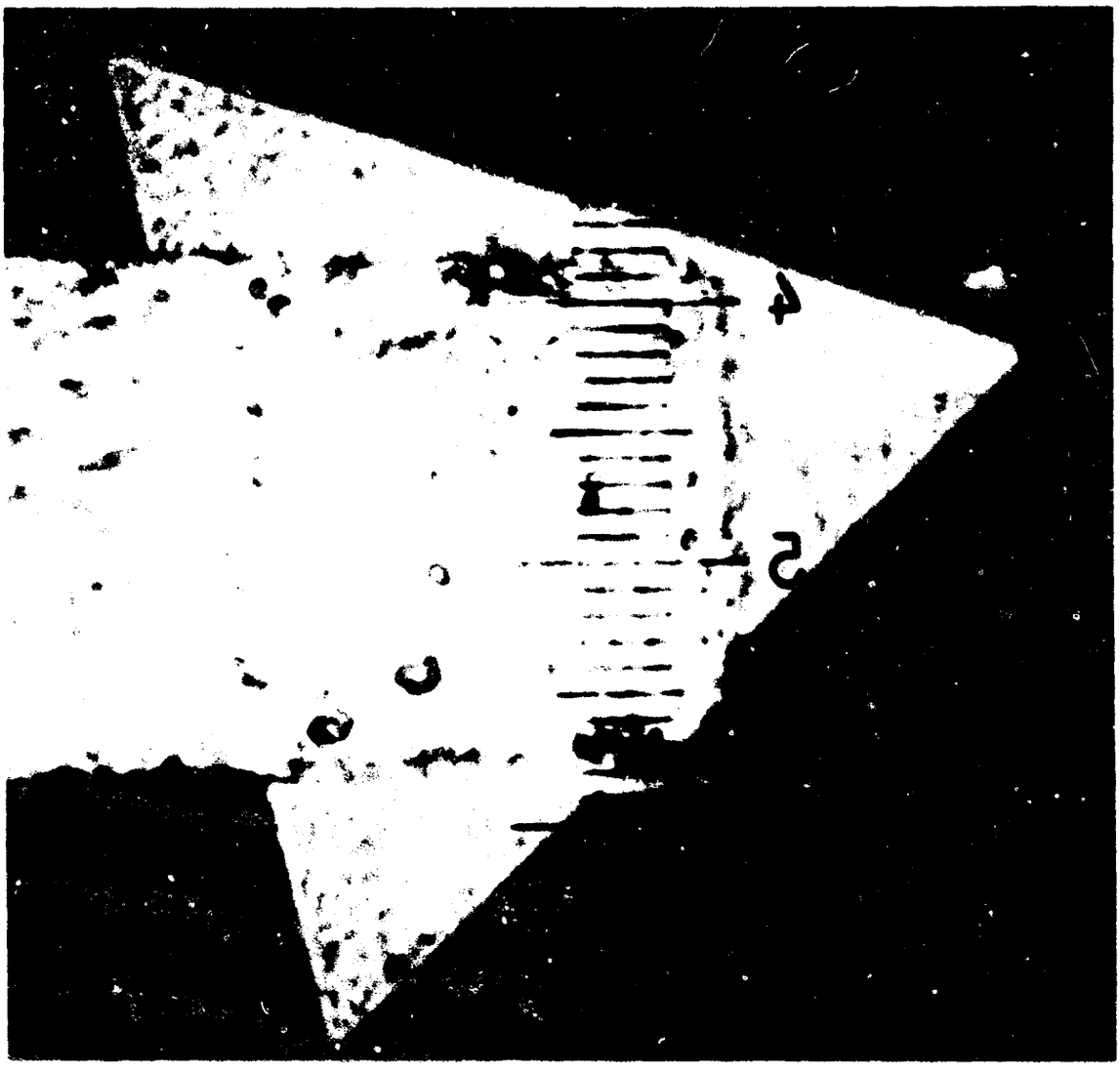

Figure 13

COMPARISON OF THE RADIATION TOLERANCE OF TRANSISTOR TYPES

By

B. Buchanan

R. Dolan

W. Shedd

Solid State Sciences Laboratory
Air Force Cambridge Research Laboratories
Office of Aerospace Research
L.G. Hanscom Field, Bedford, Massachusetts

BIOGRAPHY

Mr. Bobby L. Buchanan received his B.S. in Mathematics and Physics (1953) from Western Kentucky University and his M.S. in Mathematics and Physics (1959) from Northeastern University. He served as a Lieutenant in the U S. Air Force from 1953-57. From 1959-63, he was employed as a physicist with the Advanced Theory Office, Electronic Material Sciences Laboratory. Currently, as a physicist with the Device Physics Branch, Solid State Sciences Laboratory, AFCRL, Mr. Buchanan does research on radiation resistant devices and ion implantation.

Mr. Russell P. Dolan, Jr., received a B.S. from Brown University (1943), and an M.S. from Northeastern University (1958), both in electrical engineering. From 1943 to 1946, he served with the U.S. Army. After discharge, he was employed by the Westinghouse Electric Corp., Bloomfield, New Jersey. Presently, as supervisory research electronic engineer with the Device Physics Branch, Solid State Sciences Laboratory, AFCRL, Mr. Dolan is responsible for the design and fabrication of new semiconductor devices. Emphasis is on radiation resistant solid state devices and ion implantation.

Mr. Walter M. Shedd received his M.S. degree in electrical engineering from M.I.T. in June 1967. From June 1964 to August 1967, Mr. Shedd was an M.I.T. coop student, assigned to AFCRL. Currently he carries out assignments to determine the effects of radiation on semiconductor devices and/or integrated circuits in accordance with established engineering principles. These assignments are to design measuring equipment for the support of research studies relating to new radiation hardened semiconductor device configurations.

339-833 O - 69 - 18

Comparison of the Radiation Tolerance of Transistor Types

ABSTRACT

The radiation tolerance of bipolar and field-effect transistors is compared. Analytical expressions are derived from empirical data relating the basic physical device parameters to the radiation dose. To put in perspective and justify the approach taken, the overall problem and methods of attempted solution of radiation damage to transistors in a missile or satellite environment are briefly examined. The main emphasis is on a new criteria for neutron radiation hardness and the device design implications resulting from using this criteria. The radiation hardness level or tolerable radiation flux Φ_m is defined to be the integrated flux for which $G = G_o/C$. Where G_o is the measure of the gain parameter before irradiation, G is the measure after irradiation, and C is defined to be the tolerable gain-reduction factor. The value that C may have depends not only on the inherent characteristics of the transistor, but also on the circuit functions and the capabilities of the circuit designer. This definition is combined with simplified gain expressions and empirically derived radiation degradation expressions for bipolar and junction-field-effect transistors (JFET). The resulting simple relations giving the radiation tolerance of bipolars and JFET's are, respectively, $\Phi_m(\tau_o) = K_\tau(C-1)\tau_o$ and $\Phi_m(p_o) = 398\ p_o^{.77}\ \ln C$, where τ_o is the initial minority carrier lifetime, p_o is the initial channel doping, and K_τ is the minority carrier lifetime-damage constant. It should be noted that contrary to other derived criteria, the bipolar hardness relation is approximately independent of injection level and depends mainly

on the initial lifetime rather than the base transit time. It is shown that contrary to previously accepted beliefs, the inherent attainable radiation tolerance of JFET's is at least a factor of 10 greater than that of bipolars. Preliminary experimental results on JFET's designed for maximum radiation tolerance are presented.

1. INTRODUCTION

Using solid state device technology in Air Force electronics systems has increased system reliability and decreased component size, both by orders of magnitude. However, these systems are extremely sensitive to radiation of all kinds, for instance, neutrons, gammas, and X-rays from nuclear explosions, or protons from solar flares and electrons in the Van Allen belts of outer space. This sensitivity causes system malfunction ranging from temporary to permanent failure of the electronics at much lower radiation levels than those which would cause structural damage to a missile or satellite. In the case of nuclear explosions, the malfunction is due entirely to radiation occurring well outside the blast area.

Approaches to this problem included metallic shielding and circuit redesign, both of which resulted in some improvement. The former is limited by weight restrictions, and the latter by the performance compromises that must be made to achieve radiation hardening. These are, in some cases, so great as to seriously limit the operational use of the electronics systems being redesigned. Since the most sensitive of all electronic components is the semiconductor device (transistors, diodes, etc.), the most direct approach is to select and utilize the type or class of transistor that is inherently more resistant to radiation. If this approach is to be immediately useful, the selection should be limited to transistor designs that are within the state of the art of present day solid state technology.

Since the transistor radiation-sensitivity problem has been known for a number of years, it is reasonable to expect that this selection would already have been made. Prior to our study, however, no transistor type had emerged as being superior in a radiation environment to all other transistor types. The reason for this is partly due to advances in the state of the art, and partly due to prior criteria for comparison of junction-field-effect and bipolar transistors.

The three principal categories of transistor radiation damage are displacement, ionization, and thermomechanical. The main cause of displacement damage is fast neutrons, and the main effects that permanently degrade transistor operation are minority carrier lifetime reduction and carrier removal. A second-order effect is mobility reduction. The main cause of ionization damage is gamma radiation, which results in permanent effects due to charge build-up in the oxide and transient effects due to photocurrent generation. The transient effects are usually handled by using circumvention techniques in the electronics system. The extent of the transistor degradation due to displacement and ionization damage depends strongly on the transistor type, whereas the extent of thermomechanical damage does

not depend on the transistor type, but depends mainly on packaging and metallization which are common to all types.

The standard transistor types are categorized in Figure 1 and typical cross-sections are shown in Figure 2. The original reason for designating two classes of transistors was that the unipolar operation depends on only one carrier (majority) and the bipolar operation depends on both minority and majority carriers. The bipolar is then seriously degraded by radiation-induced minority-carrier lifetime reduction, whereas the unipolar or field effect transistor is not. One of the two principle classes of field effect transistors, the junction field effect transistor (JFET), is degraded by radiation induced carrier removal. However, the insulated gate (MIS) is little effected by either carrier removal or lifetime changes, but is virtually eliminated as a radiation-resistant device because of permanent charge build-up in the insulator caused by ionizing radiation.

The bipolar and JFET suffer only minor effects due to charge build-up in the oxide passivation when compared to the MOS (Snow et al, 1967). This is because the active region of the MOS is adjacent to or part of the oxide layer. The other types of transistors are eliminated from consideration either because of their experimental nature or because of electrical instabilities other than those induced by radiation. It is, then, the bipolar and JFET which are potentially resistant to permanent radiation damage. A prior comparison (Gregory and Smite, 1965) of the relative radiation tolerance of JFET's and bipolars concluded that the neutron radiation tolerance of JFET's and bipolars was about equal. Therefore, very little effort has been expended on using the JFET as a radiation-resistant device. Our comparison, which follows, shows that the JFET is at least 10 times more tolerant to permanent radiation damage than bipolar transistors.

2. DERIVATION OF RADIATION TOLERANCE RELATIONS

2.1 Criteria

The bipolar is by far the most widely used transistor type. The usual criteria for hardening bipolar transistors to withstand large changes in minority carrier lifetime, τ, leads to very small base-width devices that have very high gains before irradiation and have relatively small gains after irradiation. Although circuits can be designed to accommodate large decreases in gain by using initially very high gain devices, doing so increases the circuit vulnerability to transient ionizing radiation and imposes other detrimental constraints on the circuit design. The following radiation tolerance criteria is proposed. The radiation tolerance level Φ_m is defined to be the integrated flux for which $\frac{G}{G_o} = \frac{1}{C}$, where G_o is the measure of the gain parameter before irradiation, G is the measure after irradiation, and C is the tolerable gain-reduction factor. The value that C may have depends on the inherent characteristics of the transistor, the circuit functions, and the capabilities of the circuit designer. The measure of the gain for bipolars and JFET's are, respectively, taken to be the common emitter current gain, β, and the transconductance, g_m.

2.2 JFET Relations

If the JFET is operated in the region of maximum transconductance, the g_m is given (Dacey and Ross, 1953) by

$$g_m = \frac{2Nq\mu a}{L}$$

where

N = majority carrier concentration in the channel, either n or p

q = the electronic charge

μ = the mobility

a = the channel width

L = the channel length.

It should be noted that if the JFET is operated in a region other than for maximum g_m, the g_m has a weaker dependence on N than the linear one given by this expression. It is assumed that the relation between the majority carrier concentration in the channel and the integrated neutron flu Φ is given by

$$N = N_o \exp\left(-\frac{\Phi}{K}\right)$$

where N_o is the initial carrier concentration and K is the carrier removal constant. Neglecting the second-order dependence of μ on the integrated flux we have

$$\frac{g_m}{g_{mo}} = \frac{N}{N_o} = \exp\left(-\frac{\Phi}{K}\right)$$

where g_{mo} is the initial transconductance and g_m is the transconductance after a dose of Φ neutron per cm^2. Combining this expression with the definition of Φ_m, the neutron tolerance expression for JFET's is

$$\Phi_m = K \ln C.$$

The values of K for n- and p-type channels can be determined from Stein's (Stein, 1964; Stein and Gereth, 1968) experimentally determined log-log plots of the initial carrier removal rates as a function of channel doping concentration and the fact that from the assumed exponential law

$$-\frac{dN}{d\Phi}\Big|_{\Phi \to o} = \frac{N_o}{K} .$$

After some manipulation, the empirically determined damage constants are, for n- and p-type channels,

$$K_p = 398\ p_o^{.77} \text{ and } K_n = 93\ n_o^{.82}.$$

The method of increasing the radiation tolerance of JFET's is clearly then to heavily dope the channel. This cannot be done without some compromise, since the pinch-off voltage of the JFET must be less than the avalanche breakdown voltage and the pinch-off voltage increases with channel doping while the breakdown voltage decreases. It is fortuitous, however, that satisfying this hardening requirement actually increases the JFET gain.

2.3 Simplified Bipolar Relations

Using the charge control approach, a simplified expression for β can be shown (Gregory and Smits, 1965) to be

$$\beta = \frac{\tau}{t_b},$$

where τ is the minority carrier lifetime in the base and t_b is the base transit time. The base transit time is proportional to the square of the base width. The usual relation between the lifetime before and after a dose of Φ n/cm^2 is assumed:

$$\frac{1}{\tau} = \frac{1}{\tau_o} + \frac{\Phi}{K_\tau},$$

where τ_o is the lifetime before irradiation and K_τ is the lifetime damage constant. From these relations we obtain

$$\frac{\beta}{\beta_o} = \frac{1}{1 + \Phi \tau_o / K_\tau}$$

where β and β_o are, respectively, the gain before and after irradiation. Combining with the definition of Φ_m, the radiation tolerance of the bipolar is

$$\Phi_m(\tau_o) = \frac{K_\tau}{\tau_o}(C_\tau - 1).$$

This result for the radiation tolerance of bipolars indicates that for a fixed C_τ the only way to "harden" against permanent damage is by killing lifetimes prior to circuit implementation. This may seem contradictory to the result ($\Phi_m = K_\tau / t_b$) obtained by Gregory and Smits (1965) which indicates that reducing the base width is the only effective "hardening" technique. Their result, however, is equivalent to the special case of setting

$C_\tau = \frac{\tau_o}{t_b}$ and assuming that $\tau_o >> t_b$. Therefore in their criteria, C_τ was not fixed but increased by the same factor as the radiation tolerance for a reduction in base width.

According to Curtis's data (Curtis, 1966), K_τ is relatively independent of carrier concentration for doping concentrations in the range that is useful for bipolar transistor bases. Curtis's published values of K_τ are for lifetimes in the micro-second region, so our extrapolation to the nano-second region is reasonably open to question. Both K_τ and τ_o are dependent on the injection level. Their ratio should, however, be relatively independent of injection level. In fact, if τ_o has a very small value (which is required for maximum hardness under the proposed criteria) and this value was obtained by prior neutron irradiation (or gold doping), and if the usual assumption that the relation $\frac{1}{\tau} = \frac{1}{\tau_o} + \frac{\Phi}{K_\tau}$ is satisfied (for a given injection level) for one value of K_τ and for all values of Φ and τ_o, then $\frac{K_\tau}{\tau_o}$ and hence $\Phi_m(\tau_o)$ are independent of the injection level.

The bipolar radiation tolerance expression clearly points out the importance of "killing" lifetime to harden against permanent-gain degradation. Fortunately, this is consistent with a reduction in transient effects. A lifetime killing process (gold doping) is utilized to reduce transient photocurrents.

3. COMPARISON OF BIPOLARS AND JFET's

Although circuits can usually be designed to accommodate high values of C by using initially very high gain devices, doing so increases the circuit vulnerability to transient ionizing radiation and imposes other detrimental constraints on the circuit design. It is, therefore, proposed that a value $C = C_i$ be selected, where C_i is defined to be the inherent tolerable gain reduction factor, the reduction in gain that can be tolerated before it is necessary to have special circuit designs and compromises to accommodate the eventual permanent-gain reduction.

It is difficult to make a reasonable judgment as to what the precise value of C_i should be, but it seems reasonable to assume that $C_i \leq e = 2.718$. The radiation tolerance relations for p-channel and p-base transistors are plotted in Figure 3 for comparison purposes, where from Curtis (1966) the low injection value of the p-type lifetime-damage constant $K_\tau = 2.4 \times 10^5$ sec cm^{-2} was used.

JFET's and bipolars are either commercially available or within the state of the art for p_o and τ_o, roughly in the range $10^{14} < p_o < 10^{17}$, $2 \times 10^{-9} < \tau_o < 10^{-4}$. In this range Figure 3 shows that the "hardest" JFET is at least 20 times more radiation-tolerant than the "hardest" bipolar if $C \leq e$, and at least 10 times more tolerant if $C \leq 10$. It is only for the very high values of C, where extrinsic circuit considerations preuominate, that the radiation tolerance of the bipolar becomes comparable to the JFET.

There is no reason to expect that the relative radiation tolerance of JFET's and bipolars will be changed by extension of the state of the art, if equal efforts are expended on both. In addition to other technological problems, the base- and channel-width requirements become stringent, since as p_o is increased the pinch-off voltage (being less than the breakdown voltage) requires channel-width reductions, and decreases in τ_o require base-width reductions if usable gain is to be maintained.

Because of different damage constants for n- and p-type silicon, if the preceding comparison were made for n-type channels and n-type bases, the radiation tolerance of the JFET relative to the bipolar would be increased by more than a factor of 2. An alternate, more readily understood plot of β and g_m degradation is given in Figures 4 and 5 for further comparison. These plots give $\frac{1}{C}$ as a function of neutron dose with lifetime and carrier concentration as parameters.

4. COMPARISON OF THEORY WITH EXPERIMENTS

Experimental points determined from the data of Snow, et al (1968) of Fairchild Semiconductor are plotted in Figure 6. The JFET data points are for an n-channel Fairchild experimental JFET with channel doping of 10^{17}. The data points at 10^{14}, 10^{15}, and 10^{16} n/cm^2 were obtained from experiments at the Sandia reactor. The other data points were obtained from experiments at the Berkeley reactor. Considering the simplicity of the theory, it is seen that the experimental points are surprisingly close to the theoretically calculated curve. Two experimental points for the 2N4251 npn transistors, which were considered to be the most radiation tolerant bipolar devices available, are also plotted in Fibure 6. The initial lifetime was not given, but the two points are a good fit to the theoretical curve for $\tau_o = 2\text{x}10^{-9}$ sec.

5. ASSUMPTIONS DAMAGE CONSTANT DATA AND CONJECTURES

The usual assumption of the exponential law (Gregory and Smits, 1965; Cleland et al,1961) for carrier removal implies that if two samples have the same active carrier concentration and one of the samples has already been irradiated and reduced from a previously higher concentration, then the irradiated sample is less susceptible to carrier removal. In fact, if the exponential law is valid, the susceptibility of the irradiated sample to fractional reduction in carrier concentration is the same as before irradiation. This means that it is theoretically possible to have a low-doped sample that has the same resistance to fractional reduction in carrier concentration as a high-doped sample. To prove this, assume an initial concentration of N_o irradiate to a dose of Φ_1, then

$$N_1 = N_o \exp -\left(\frac{\Phi_1}{K(N_o)}\right).$$

Further irradiate the sample by an additional dose of Φ_2, then

$$N_2 = N_o \exp -\left(\frac{\Phi_1 + \Phi_2}{K(N_o)}\right) = N_1 \exp -\left(\frac{\Phi_2}{K(N_o)}\right).$$

Therefore, for equal initial and second doses, $\Phi = \Phi_1 = \Phi_2$, and

$$\frac{N_1}{N_o} = \frac{N_2}{N_1} = \exp -\left(\frac{\Phi}{K(N_o)}\right).$$

Experiments by Stein (1964; 1968) indicate that the exponential law is not followed for p-type material. A plot of Stein's data is shown in Figure 7. The dashed line is the curve followed by the initial carrier-removal rates. That is, fresh un-irradiated samples with various carrier concentration were used to determine this dashed curve for small changes (10%) in carrier concentration. The data points following the solid line were all taken on the same sample, whose carrier concentration was reduced by neutron irradiation from its initial concentration of 2×10^{16}. The other curve shows the carrier removal rate if the exponential law for an initial carrier concentration of 2×10^{16} were followed. It is seen that for about the first factor-of-10 reduction in carrier concentration the initial carrier-removal-rate curve is followed and then an exponential behavior is exhibited. If this curve is used instead of the exponential, it can be shown by integrating Stein's curves that the relations for p-type channels for the first factor-of-10 reduction in carrier concentration becomes

$$\frac{p}{p_o} = \left[1 - b p_o^{-a} \Phi\right]^{\frac{1}{a}} = \frac{g_m}{g m_o} = \frac{1}{C}$$

$$\Phi_m = b^{-1} p_o^{a} \left[1 - C^{-a}\right], \text{ where } a = .77, b = \frac{a}{398}.$$

This indicates for p-type channels that Φ_m is 35 percent smaller (or less) than Φ_m, using the exponential law if $C \leq e$.

In addition to the comprehensive work on carrier-removal rates by Stein (1964, 1968), considerable work was done by Curtis et al (1965, 1966). The discrepancy between reported initial carrier-removal rates is quite large. For an initial carrier concentration of about 5×10^{15} cm^{-3}, Stein and Curtis obtain, respectively, initial carrier-removal rates of 10 and 3 for doped silicon, whereas Larin (1968) recommends a carrier-removal rate of 1.3 for semiconductor device design purposes. This difference becomes enormous when the exponential law is assumed. Our limited experiments indicate that Stein's carrier removal rates are the closest to the actual.

The facts that lifetime and carrier-removal rates are less in neutron-damaged samples and ion implantation is a damaging process, leads us to conjecture that bipolars and JFET's made by ion-implantation doping would be more radiation-resistant than diffused types.

6. CONCLUSIONS

The radiation resistance to permanent-gain degradation of JFET's is at least an order of magnitude greater than that of bipolars. The method of hardening JFET's, unlike the method of hardening bipolars, leads to higher-gain transistors. More work needs to be done on lifetime-damage and carrier-removal-damage constants. Even though the damage-constant data presently available is very useful in device design, extensions of lifetime-damage-constant data to shorter lifetimes and carrier-removal data on heavily damaged and ion-implanted material is highly desirable.

REFERENCES

Cleland, et al (1961) Radiation Damage in Solids, Princeton, N. J.

Curtis, O. L., Jr. (1966) IEEE Trans. Nuclear Science, Vol. NS-13, pp. 33-40.

Curtis, O. L., Jr., Bass, R. F., and Germano, L. A. (1965) Harry Diamond Laboratories report NARD-65-20R.

Curtis, O. L., Jr., Bass, R. F., and Germano, L. A. (1966) Harry Diamond Laboratories report ARD-66-56R.

Dacey, G. C., and Ross, I. M. (1953) Proc. IRE, August 1953, pp. 970-979.

Gregory, B. L., and Smits, F. M. (1965) IEEE Trans. Electron Devices, Vol. ED-12, pp. 254-258.

Larin, Frank (1968) Radiation Effects in Semiconductor Devices, Wiley & Sons, p. 160.

Snow, E. H., Albus, H. P., Lagnina, S. F , Molozzi, A. R., Fitzgerald, D. J., and Kauffman, W. L. (1968) AFCRL-68-0321, Scientific Report No. 5.

Snow, E. H., Grove, A. S., and Fitzgerald, D. J. (1967) Proc. IEEE, July 1967, pp. 1168-1185.

Stein, H. J., (1964) Sandia Corp., Albuquerque, N. Mex., Rept. SC-R-64-193.

Stein, H. J., and Gereth, R. (1968) J. Appl. Physics, May 1968.

FIGURE CAPTIONS

Figure 1. Classification of Transistor Types

Figure 2. Cross-Sections of Transistor Types

Figure 3. Plot of the Radiation Tolerance $\Phi_m(\tau_o)$, the Flux Required to Reduce the p-Base, Bipolar, Common-Emitter, Current Gain by a Factor of C, and $\Phi_m(p_o)$, the Flux Required to Reduce the p-Channel JFET Transconductance by a Factor of C

Figure 4. Plot of Fractional β Degradation as a Function of Neutron Dose

Figure 5. Plot of Fractional g_m Degradation as a Function of Neutron Dose

Figure 6. Plots Comparing Theoretical and Experimental Gain Degradation

Figure 7. Plots Comparing Stein's Neutron-Compensated Carrier-Removal Rates and the Exponential Law

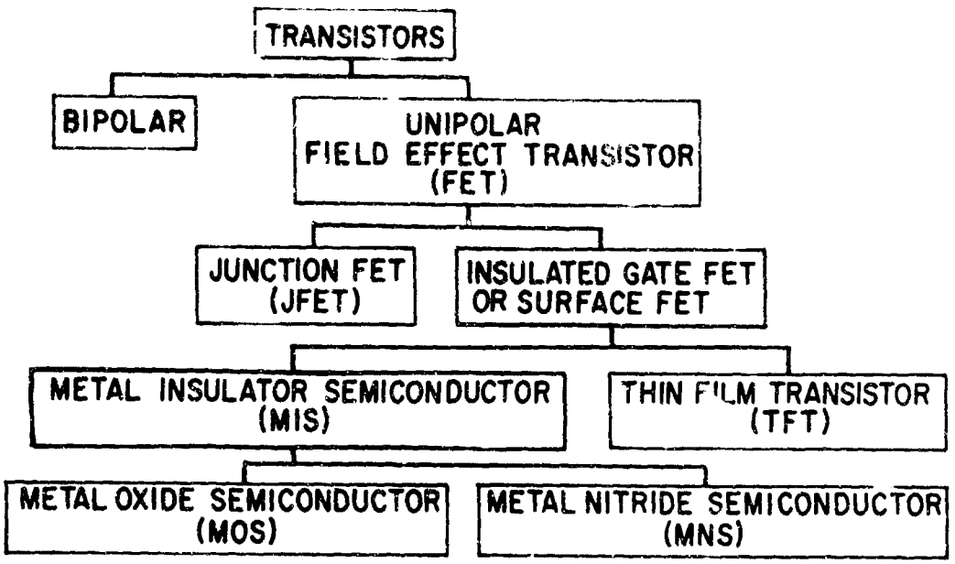

Figure 1

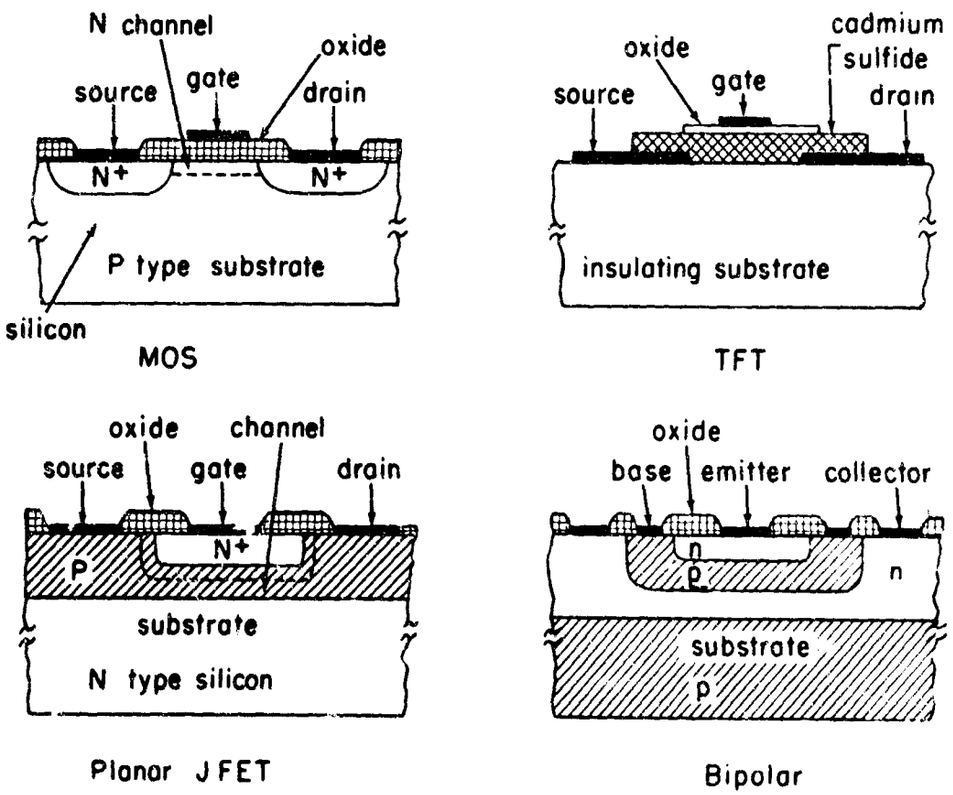

Figure 2

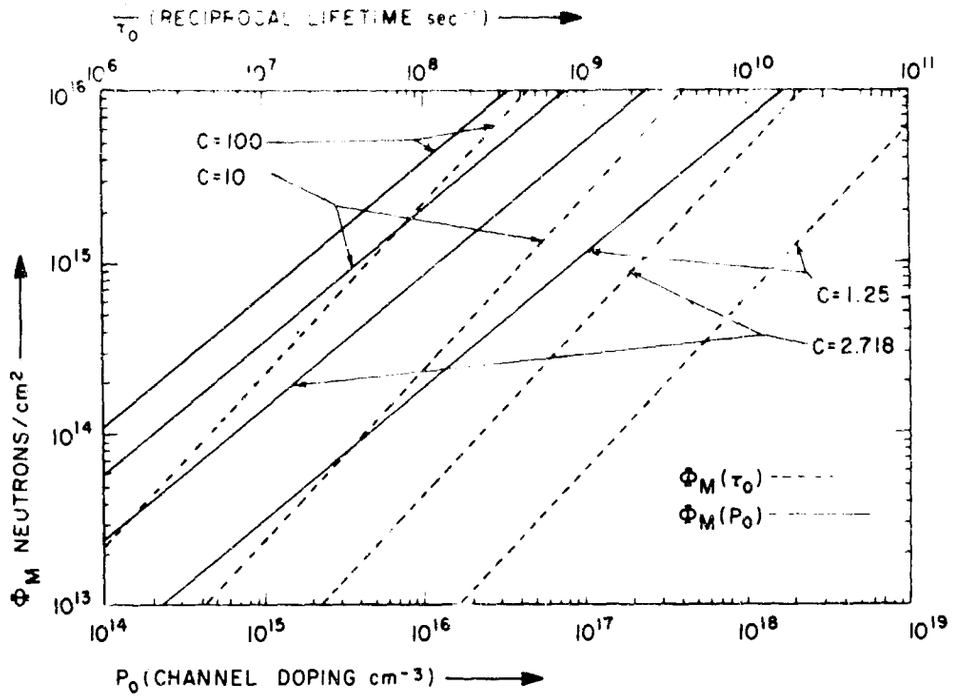

Figure 3

$$\frac{\beta}{\beta_0} = \frac{1}{1+\Phi\frac{\tau_0}{K_\tau}}$$

τ_0 = LOW INJECTION LIFETIME (sec)
K_τ = LOW INJECTION DAMAGE CONSTANT
= 2.4 x 10^5 sec cm^{-2}

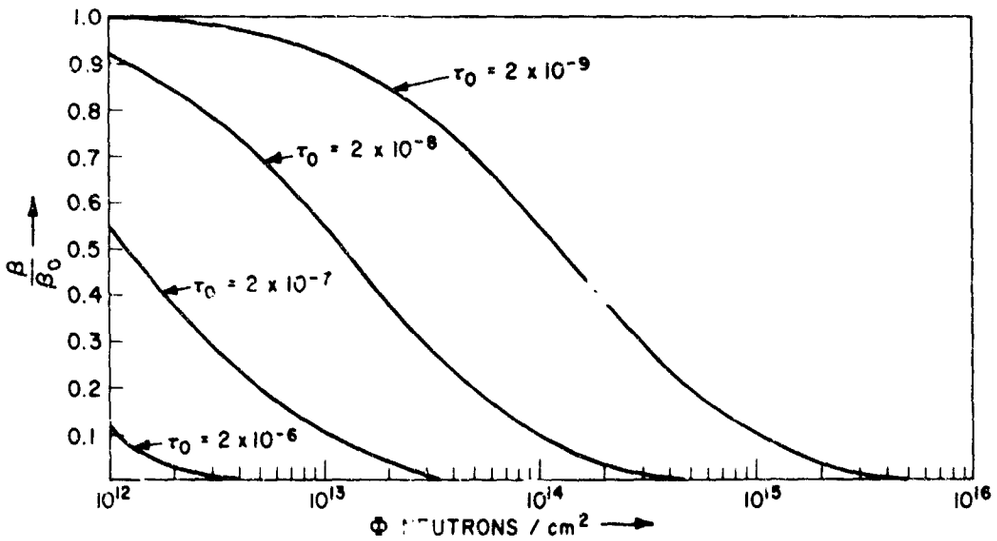

Figure 4

$$\frac{g_m}{g_{mo}} = e^{-\frac{\Phi}{K_P}}$$

$$K_P = 398\, P_0^{.77}$$

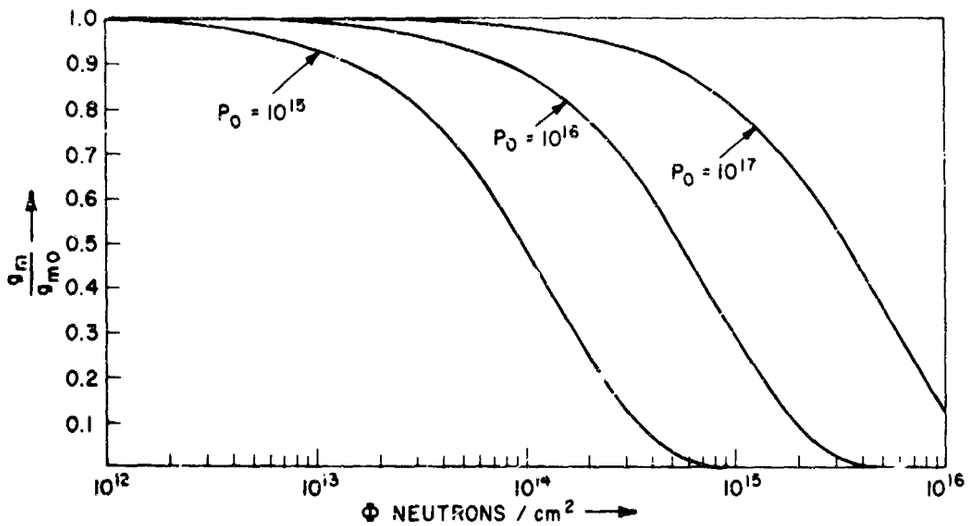

Figure 5

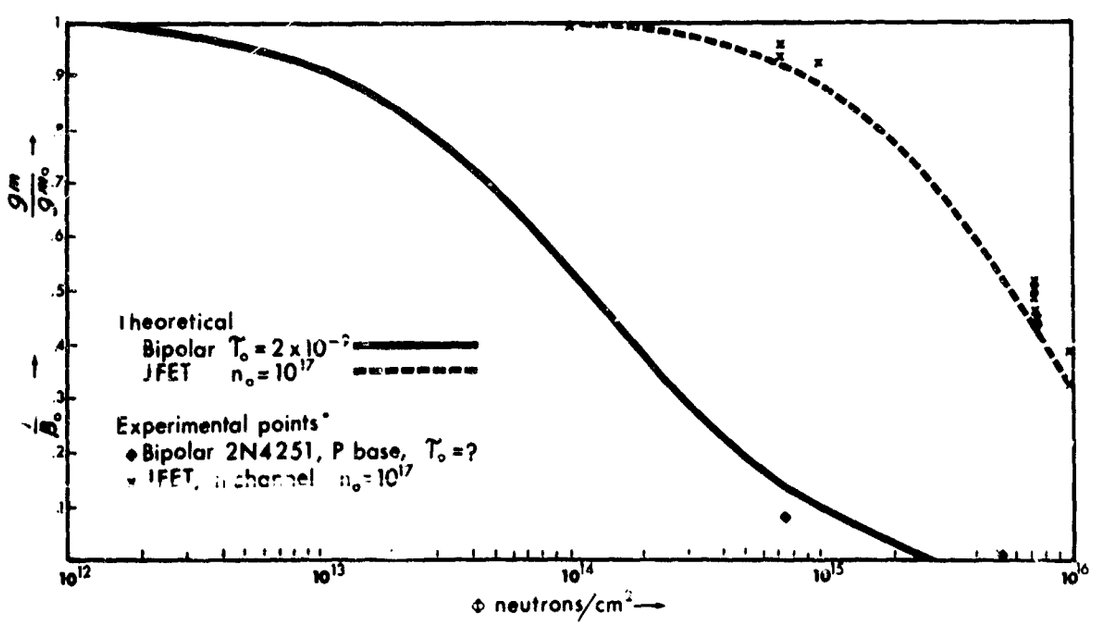

*Experimental points obtained from data of E.H. Snow et al, AFCRL-68-0321

Figure 6

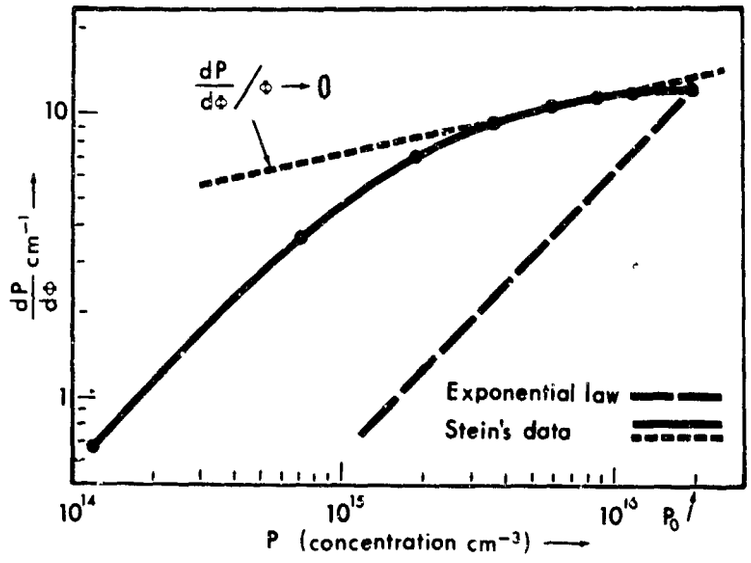
$\frac{dP}{d\Phi}/\Phi \to 0$
10
1
$\frac{dP}{d\Phi}$ cm^{-1} ⟶
Exponential law
Stein's data
10^{14}
10^{15}
10^{16}
P_0
P (concentration cm^{-3}) ⟶

Figure 7

PHYSIOLOGICAL SIGNAL TELEMETRY SYSTEMS AND TELEVISION DATA DISPLAY TECHNIQUES

By

Adolph R. Marko

6570th Aerospace Medical Research Laboratories
Wright-Patterson AFB, Ohio

PHYSIOLOGICAL SIGNAL TELEMETRY SYSTEMS AND TELEVISION DATA DISPLAY TECHNIQUES

Adolph R. Marko

ABSTRACT

Research and development work carried out in the Environmental Medicine Division of the 6570th Aerospace Medical Research Laboratories in the time period from January 1967 to May 1968 produced a 7 channel physiological signal telemetry system and an electronic converter for using television sets in physiological signal monitoring. The telemetry system features rugged construction for field use, one per cent baseline and amplitude stability, plug-in signal and conditioner modules for versatility, low power consumption and a transmitting range up to 1000 feet. The converter may be connected to electrodes, respiration and temperature sensors on a patient and to one or several unmodified television sets. A bar graph display of four vertical bars and two horizontal lines appear on the television screens useful for quick look safety monitoring of patients or volunteers in medical research experiments. In the described model, the vertical bars indicate by their length heart rate, respiration, respiration rate and body temperature, while the horizontal lines are representing the maximum and minimum safety limits. Other

measurements such as blood pressure and environmental factors may be displayed instead or in combination with the above mentioned signals. The developed television techniques may be applied to a variety of signal display problems.

BIOGRAPHY

Mr. Adolf R. Marko was born in Vienna, Austria on 31 December 1913. He studied electrical and electronic engineering and received an Ingeniers Degree from the Institute of Technology in Vienna in the year 1936. Post graduate studies in mathematics, physiology, physics and psychology at the University of Vienna (1946-1950) prepared him for a position as Chief Engineer of Medical Electronic Development at the University Institute of Vienna. In the year 1958, he followed an invitation to the 6570th Aerospace Medical Research Laboratories at Wright-Patterson Air Force Base and became, in 1966, Branch Chief of the Medical Electronics Branch of the Environmental Medicine Division. He holds eight patents (U.S. and Austrian) and is author on 24 publications. Mr. Marko is a member of the Institute of Electrical and Electronic Engineers belonging to the professional groups of "Engineering in Biology and Medicine" and "Engineering Management." He is also a member of the Austrian Society for Electroencephalography.

PHYSIOLOGICAL SIGNAL TELEMETRY SYSTEMS AND TELEVISION DATA DISPLAY TECHNIQUES

Research and development work on television data display techniques and on physiological signal telemetry systems has been carried out in the Environmental Medicine Division of the 6570th Aerospace Medical Research Laboratories at Wright-Patterson Air Force Base under the command of Colonel R. A. Yerg. The Environmental Medicine Division conducts and sponsors research and development pertinent to the performance of man in aerospace systems. This includes research on physiological and performance response to multiple and sequential environmental stresses. Each experiment requires the monitoring of one or several physiological measurements such as heart rate, respiration, blood pressure, body temperature and others for the safety of the volunteer subject involved in the research investigation.

Monitoring of vital signals is usually accomplished in addition to recordings on paper and magnetic tape. Large screen oscilloscopes featuring the display of several measurements simultaneously are employed in advanced facilities but many investigators are still limited to the use of a single or double channel laboratory oscilloscope. The large screen oscilloscope, as shown in Fig. 1, may be considered an ideal tool for monitoring physiological signals because it is easy to read, even at distances up to 30 feet, and it may be adapted to a variety of different display methods. However, these display scopes are expensive, heavy and difficult to move from one location to another. An additional disadvantage lies in the requirement of as many wire lines as there are signals to monitor.

A television receiver can be considered as an extremely well developed portable large screen display equipment that is easily available at less than one tenth of the price for a large screen oscilloscope. Practically any kind of visual information can be displayed on the screen of a television set, without modification of the set itself, by feeding a few millivolts of the proper signal to its antennae terminals. However, one may ask the well justified question: "What does it take to generate these few millivolts of the proper signal?" Well, it takes a multimillion dollar set-up to generate a video signal that will produce the picture sequence of a great movie but it may take only a few hundred dollars for electronic circuits to produce a signal which creates an easy to read display of vital measurements on the screen of an unmodified television set. In other words, the problem is one of optimizing, considering the requirements of effective medical monitoring as well as the television receiver's circuit properties.

Requirements for medical monitoring vary and are dependent on many factors such as kind of patients or volunteers, objective of monitoring, time duration, severity of stress or disease, interference problems, medical and electrical safety considerations and others. Although there are many kinds of physiological measurements known to medical science, only a few are practical for long time monitoring. Heart rate, respiration rate, body temperature and skin temperature are most often used because of their medical significance that is combined with a minimum encumbrance of the subject. Other desirable measurements such as blood pressure, brain waves, pulse amplitude, oxygen consumption, etc., are much more sensitive to artefacts and impose more restrictions on the patient. In order to satisfy a maximum number of these requirements, a versatile prototype converter that accepts four different physiological signals and produces a bar graph display on a television set has been designed and fabricated as an in-house project.

Fig. 2 illustrates the converter model together with a 15 inch portable television set. The screen shows four vertical bars indicating from left to right heart rate, respiration, respiration rate and body temperature. The two horizontal lines may be adjusted to show a low and a high safety limit for each measurement. As an example, the low limit line may signify 40 heartbeats per minute for the heart rate, 5 breaths per minute for the respiration rate and 36° centigrade for the body temperature. The high limit line may be set to indicate 90 heartbeats per minute, 20 breaths per minute and 38° centigrade body temperature. This picture shows the heart rate below the pre set safety line and the temperature close to the upper limit while the respiration rate appears normal. Values for the limit lines and the range of the measurements may be set for a wide variety of needs by the amplitude and position controls on the front panel. A calibrator facilitates the initial adjustments of the bar excursions for heart rate, respiration rate and temperature. On the right side of the control panel is a trigger indicator that flashes with every triggering pulse. This indicator provides easy and fast adjustment of the signal amplifier gain. The left lower part of the control panel shows two rows of input jacks, the upper row labeled DC, 0-5 V inputs and the lower row designated as patient inputs. The lower row is used to connect electrodes, respiration sensor and temperature sensor from the patient direct to the equipment, while the upper row may be used to obtain a graph bar display from signals processed by additional equipment. Blood pressure, skin resistance, environmental factors and other data may be displayed instead or in combination with some of the measurements mentioned above. The converter is connected to one or several television sets using inexpensive twin lead antennae cable. Distances of several hundred feet may be handled without unacceptable loss of picture clarity. For longer distances between converter and television set, coaxial cable and booster amplifiers are necessary.

The next slide, Fig. 3, shows the inside of the converter. Seventeen printed circuit boards contain the circuits for signal conditioning and generating the video signal that modulates a radio frequency oscillator housed in an aluminum enclosure. A regulated power supply is seen in the right upper corner. This laboratory model is not considered a final design because it has been constructed from readily available parts in the laboratory for the purpose of investigating the feasibility and practical usefulness of this approach to physiological monitoring. The application of now available, low cost integrated circuits would reduce components' cost, assembly time, size and weight, significantly.

There are many other aspects to this basic principle of using television techniques that should be investigated in connection with medical monitoring. Future work may investigate the combination of this circuitry with a simplified TV camera for visual monitoring in addition to signal display as well as the addition of oscilloscope trace displays or some alpha numerical information. The technical details of the already accomplished work are outlined in a report with the title "Bio TV" a histogram display system for physiological signal monitoring. This report shall be available by the end of the year 1968 under the designation AMRL-TR-68-2.

The AMRL conducted research and development work on miniature multichannel telemetry systems for monitoring physiological signals since the year 1960. In March 1968, a significant milestone was reached with the completion of a 7 channel pulse duration modulated telemetry unit featuring high baseline stability and low power consumption. The laboratory model shown in Fig. 4 provides 3 channels of electrocardiograms, 1 channel for body temperature and 3 channels that may be used with any transducer delivering signals of 20 millivolts. The bigger box on the left contains the signal conditioners and the 7 channel multiplexer. The smaller box on the right houses the transmitter and the batteries. I would like to demonstrate the application of this in-house built telemetry unit with a 5 minute movie. The film shows research work on oxygen consumption in exercise experiments conducted by Dr. Ray Murray, Professor of Medicine at Indiana University. The telemetry unit transmitted 3 leads of electrocardiogram, oxygen partial pressure, oxygen flow rate and rectal temperature to a nearby receiving and recording station.

(5 minute movie)

The fine overall performance of this laboratory model has been the main reason for procuring miniaturized and mechanically rugged units for field use as seen in the next slide, Fig. 5. Although the same basic system design principles are used in these units, the contractor introduced several additional improvements in circuit design and mechanical construction. The two units are built into sealed nickel-plated aluminum boxes having about one quarter the volume of the prototype model. The box on the left shows the transmitter with a transmitting range of 1000 feet and the two 8, 4 volt batteries that are capable to power the whole system for 20 hours continuously.

The box on the right side contains the multiplexer and seven plug-in modules. Signal conditioner plug-in modules are providing maximum versatility because the transmitting system is not limited to a predetermined set of measurements. The high multiplexer input sensitivity (20 millivolt) simplifies the design of the signal conditioners. Low gain amplifiers for the electrocardiogram are built into the plug-in units but signal conditioner modules for respiration, temperature, pressure and oxygen flow rate contain only an adjustable voltage divider.

Since this telemetry unit operates in the FM band (88-108 mc), inexpensive FM tuners may be used for receiving the signal. In order to separate the multiplexed information channels for recording and display, a pulse duration modulation decoder is used between the receiver and the recorder. The telemetry system uses pulse duration modulation multiplexing with a sampling rate of 200 per second. This limits the highest frequency components of any channel signal to 100 hertz but for practical reasons considering filtering the frequency response of each channel may be defined as zero to 40 hertz. This is similar to the performance of most portable direct writing electrocardiographs. In one experiment, the electrocardiogram was recorded directly from the subject and with the telemetry system using the same direct writing electrocardiograph. There was no distinctive difference in wave shape detected at a paper speed of 50 millimeter per second. Most of our work with telemetry systems is performed on active subjects who are producing muscle action potentials that interfere with the electrocardiogram if the frequency response of the system exceeds 30 hertz. However, the limited frequency response of this system is its main limitation as far as a wide variety of research applications is concerned. Work has been started to investigate different solutions of increasing the channel frequency capabilities without sacrificing stability and low power consumption. The baseline stability of this system is better than one percent over an eight hour period with temperature variations from 40°F to 95°F. Baseline and gain stability are competing very well with precision rack mounted laboratory equipment, allowing high accuracy in remote measurements of temperatures, pressures, oxygen concentration and similar slow varying factors. The power consumption is only about one quarter of the power consumed by a comparable FM-FM system.

I would like to close this presentation with the expression of my gratitude to Colonel R. Yerg, Commander of the AMRL during the reported work period, and to my Division Chiefs, Dr. Alvin Hyde and Dr. McCally for promoting, supporting and encouraging this work. I am also indebted to Dr. Ray Murray at Indiana University for numerous helpful suggestions and to Mr. Erich M. Gienapp and Mr. James Lovin for the outstanding work in laboratory model construction and testing.

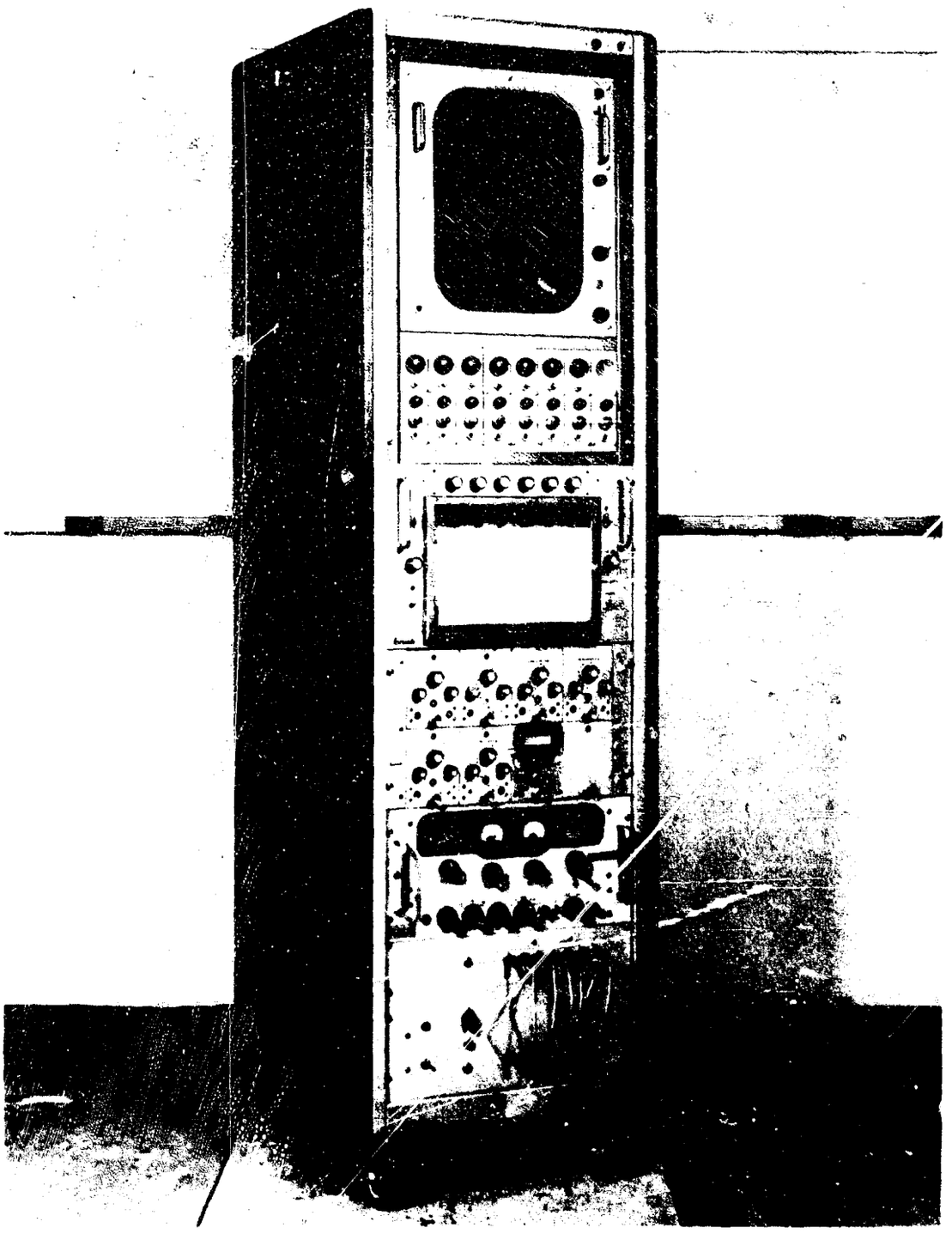

Figure 1. Large screen multichannel monitoring oscilloscope used in telemetry receiving and recording equipment.

Figure 2. TV signal converter with 15" television set.

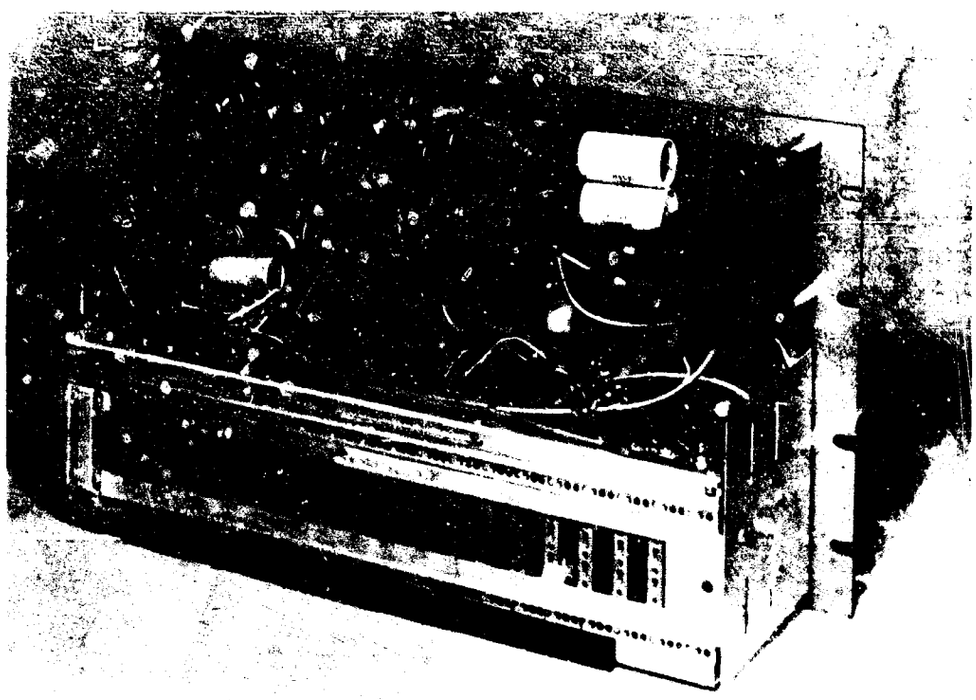

Figure 3. Inside of TV signal converter.

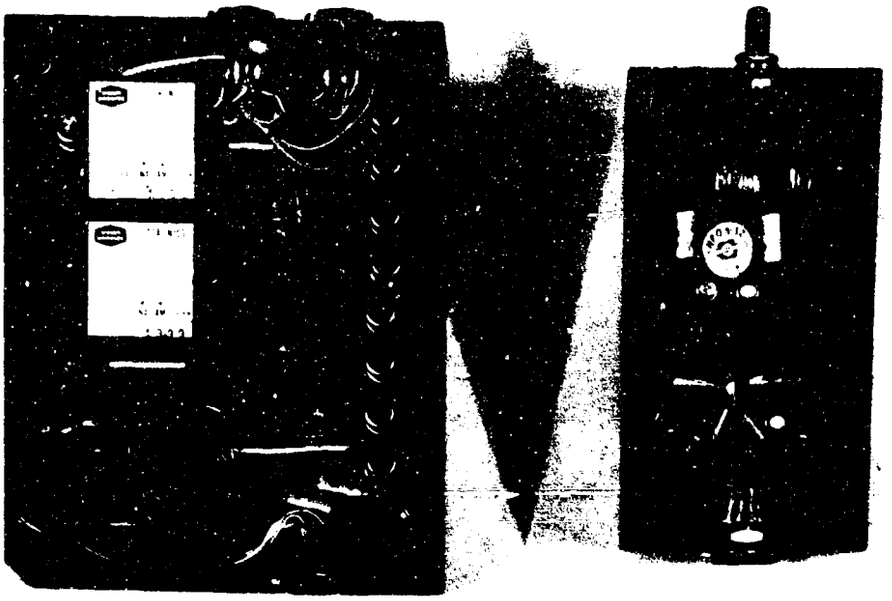

Figure 4. Laboratory model of 7 channel physiological signal telemetry system.

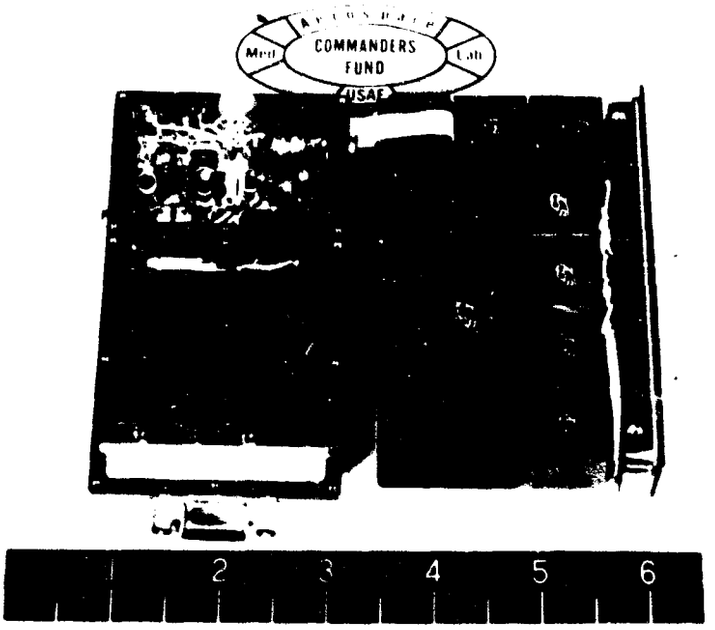

Figure 5. Miniaturized and ruggedized 7 channel telemetry system.

UNCLASSIFIED

Security Classification

DOCUMENT CONTROL DATA - R & D

(Security classification of title, body of abstract and indexing annotation must be entered when the overall report is classified)

1. ORIGINATING ACTIVITY (Corporate author)	2a. REPORT SECURITY CLASSIFICATION
Hq Office of Aerospace Research 1400 Wilson Boulevard Arlington, Va. 22209	UNCLASSIFIED
	2b. GROUP N/A

3. REPORT TITLE

PROCEEDINGS OF THE 1968 AIR FORCE SCIENCE AND ENGINEERING SYMPOSIUM, VOLUME I

4. DESCRIPTIVE NOTES (Type of report and inclusive dates)

Scientific Annual 1968

5. AUTHOR(S) (First name, middle initial, last name) Donald F. Buxton, Robert G. McIver, Walter M. Sellers, Larry L. Fehrenbacher, Gottfried Arnold, Otto F. Maurer, George J. Gauthier, Walter H. Gloor, Daniel J. Jacavanco, A. Howard Hayden, Jr., Richard C. Vanderburgh, L. Keith Norseth, Fritz L. Schuermeyer, John M. Blasingame, Clyde H. Lane, Bobby L. Buchanan, Russell P. Dolan, Jr., Walter M. Shedd, Adolf R. Marko

6. REPORT DATE	7a. TOTAL NO. OF PAGES	7b. NO. OF REFS
March 1969	275	N/A

8a. CONTRACT OR GRANT NO.	N/A	9a. ORIGINATOR'S REPORT NUMBER(S)	
b. PROJECT NO	N/A		N/A
c.	N/A	9b. OTHER REPORT NO(S) (Any other numbers that may be assigned this report)	
d.	N/A		OAR 69-0003 AD 686 100

10. DISTRIBUTION STATEMENT

1. This document has been approved for public release and sale; its distribution is unlimited.

11. SUPPLEMENTARY NOTES	12. SPONSORING MILITARY ACTIVITY
N/A	Hq OAR (RROA) 1400 Wilson Boulevard Arlington, Va. 22209

13. ABSTRACT

This is the first of two volumes containing the unclassified papers presented at the 1968 Air Force Science and Engineering Symposium. The papers in this volume are as follows: "The Production of Restricted Chemical Lesions in the CNS by Chemical Means"; "Development of Hyperbaric Oxygen Therapy for Altitude Decompression Sickness"; "Accelerated Methods and Devices for Diagnosis and Treatment of Infectious Diseases"; "Rare Earth-Zirconia Ceramic Storage Heaters Providing Flight Simulation for Air-Breathing Propulsion Systems"; "Laboratory Simulation of the Service Noise Environment for Sonic-Fatigue Qualification Testing of Aircraft Structures"; "Studies in Organometallic Chemistry - A Novel Synthesis of Ruthenocenes" "Fiber Technology - Spinning and Drawing of a Fused-Ring Polymer"; "Electron Reduction in the Re-Entry Plasma Sheath"; "Vela IV 'Lid' Experiment - Space Evaluation of Lithium Diffused Solar Cells"; "Photoelectric Measurements of Optical Glints from Orbiting Spacecraft"; "Minuteman Ordnance Reliability and Service Life Program"; "Research on Thin-Film Schottky Barriers and Its Application to Devices"; "Stress Effects at the Si-SiO_2 Interface and Its Relationship to Interface States and Metallization Problems in Silicon Devices"; "Comparison of Radiation Tolerance of Transistor Types"; "Physiological Signal Telemetry Systems and Television Data Display Techniques."

DD FORM 1 NOV 65 1473

UNCLASSIFIED

Security Classification

14. KEY WORDS	LINK A		LINK B		LINK C	
	ROLE	WT	ROLE	WT	ROLE	WT
Air Force Science and Engineering Symposium, 1968						
Chemical Lesions in Central Nervous System						
Hyperbaric Oxygen Therapy						
Altitude Decompression Sickness						
Diagnosis and Treatment of Infectious Diseases						
Rare Earth-Zirconia Ceramic Storage Heaters						
Air-Breathing Propulsion Systems						
Sonic-Fatigue Qualification Testing of Aircraft Structures						
Organometallic Chemistry						
Synthesis of Ruthenocenes						
Fiber Technology						
Fused-Ring Polymer						
Electron Reduction						
Re-Entry Plasma Sheath						
Vela IV						
Lithium Diffused Solar Cells						
Photoelectric Measurements						
Optical Glints from Orbiting Spacecraft						
Minuteman Ordnance Reliability and Service Life						
Thin-Film Schottky Barriers						
Stress Effects at the Si-SiO_2 Interface						
Interface States and Metallization Problems						
Silicon Devices						
Radiation Tolerance of Transistor Types						
Physiological Signal Telemetry Systems						
Television Data Display Techniques						